Universitat
de les Illes Balears

TESIS DOCTORAL
2019

NOVEL BIOAVAILABILITY TESTS FOR RISK ASSESSMENT OF ORGANIC EMERGING CONTAMINANTS IN ENVIRONMENTAL SAMPLES AND FOOD COMMODITIES: A HOLISTIC APPROACH

Miguel Oliver Rodríguez

Universitat
de les Illes Balears

TESIS DOCTORAL
2019

Programa de Doctorado en Ciencia y Tecnología Química

NOVEL BIOAVAILABILITY TESTS FOR RISK ASSESSMENT OF ORGANIC EMERGING CONTAMINANTS IN ENVIRONMENTAL SAMPLES AND FOOD COMMODITIES: A HOLISTIC APPROACH

Miguel Oliver Rodríguez

Director/a: Manuel Miró Lladó
Tutor/a: José Manuel Estela Ripoll

Doctor/a por la Universitat de les Illes Balears

Dr. MANUEL MIRÓ LLADÓ, Catedrático de Química Analítica adscrito al Departamento de Química de la UNIVERSITAT DE LES ILLES BALEARS,

DECLARO:

Que la tesis doctoral que lleva por título "*Novel bioavailability tests for risk assessment of organic emerging contaminants in environmental samples and food commodities: A holistic approach",* presentada por MIGUEL OLIVER RODRÍGUEZ para la obtención del título de doctor, ha sido dirigida bajo mi supervisión y que cumple con todos los requisitos científicos y técnicos necesarios para optar al título de Doctor Internacional.

Y para que quede constancia de ello firmo este documento.

Firma

Palma de Mallorca, a veinte de septiembre de dos mil diecinueve.

Agradecimientos

Después de varios años trabajando en este proyecto, es difícil recordar a todos y a cada uno que, de un modo u otro, tanto en lo profesional como en lo personal, han participado y me han ayudado a llegar al final de esta etapa "sano y salvo". Sin ellos, este camino hubiera sido mucho más duro. Vosotros me habéis ayudado a levantarme cada vez que tropecé y animado cada vez que las cosas se ponían feas. Así, quiero agradecer a cada uno de vosotros vuestra implicación y ayuda para que esto haya sido posible.

A mi director de tesis Dr. Manuel Miró, sin su ayuda hoy no estaría aquí. Como en cualquier familia hemos tenido nuestras discusiones pero su energía, su paciencia y su profesionalidad me han hecho mejorar y aprender a lo largo de todos estos años. A María Rosende por ser mi madrina y guiarme en mis primeros pasos como doctorando. A David Cocovi, mi compañero de birras, confidente de alegrías y pesares. A María Trujillo sin ella aún estaría editando el formato de mi tesis y el lab sería un lugar silencioso. A mi colega Javi con el que empecé todo este lío, mi pupilo Marc, y a Julia, miembros del equipo y con los que su compañía el ambiente del lab es más alegre. A todos los visitantes que han pasado por aquí a lo largo de estos años, Ana, Dan, Alejandra, Marta, Mayte, Olivia, Laís, Mook, Wojciech, Tomasz, Carlos, Kateřina, Sol, Rute, Enrique, Isabelle, Richard, Francesca y Ale. Mención especial a Kat, con su esfuerzo y perseverancia logramos nuestro artículo en la revista *Analytical Chemistry*, fruto de un trabajo que estuve a punto de abandonar.

A los profesores visitantes que nos han brindado sus conocimientos, Dr. Burkhard Horstkotte., Dr. Błażej Kudlak, Dr. Dietmar Knopp y Dr. Paul Worsfold por citar algunos. Y a los demás compañeros del departamento de química, Dr. Luis Laglera, Sabrina, Susana, Laura y seguro otros que no recuerdo. Gracias también a los Dr. Antonio Frontera, Dr. Miquel Adrover y Dr. Joaquín Ortega por ayudarme con las distintas técnicas y metodologías experimentales y en la redacción de varios artículos en los que colaboramos con la idea de unificar las distintas ramas de la química. Y a los demás miembros de la ciencia, mi colega de aventuras Miquel Martorell, y a los profesores de bioquímica, Dr. Joan Ribot, Dr. Priam Villalonga, Dra. Marta Monjo y Dra. Joana M. Ramis y a su grupo que me prestaron sus equipos siempre que lo necesité.

Un especial agradecimiento a Pedro González, erudito en el mundo de los liposomas. Con sus conocimientos tuve un punto de partida del cual empezar mi aventura.

Al Dr. Roberto de la Rica que me ha instruido en las artes plasmónicas e inmunoensayos, un claro ejemplo donde la biología y la química van cogidas de la mano.

A la Dra. Marcela A. Segundo que me acogió durante mi estancia en la Universidad de Oporto. Su amabilidad y el buen rollo de su grupo, Margarida, Patrícia, Eduarda, Luisa Sara F., Sara M. y Sandia hicieron que me sintiera como en casa, tanto que repetí una segunda vez, Oporto será mi segundo hogar para siempre. A la Dra. Sofia A. Lima, Ana y Rita que me guiaron en los entresijos de los cultivos celulares. Y para terminar a Inês, mi compañera pero sobretodo amiga, a quien profeso un gran afecto, que cuidó de mí cada día y procuraba que todo me fuera bien dentro y fuera del lab durante mi estancia.

Al Dr. José Benito Quintana (Tito), y a su mujer, la Dra Rosario Rodil (Charo), mis tutores en la Universidad de Santiago de Compostela y a su grupo. Mi estancia fue breve pero muy agradable. Comerse unas castañas recién asadas por el parque de la Alameda en diciembre reconforta y calma la mente.

A los técnicos de los servicios científico-técnicos Joan Cifre, Ferran Hierro, Guillem Ramis y Biel Martorell, y demás personal de la UIB, Sergi, Llorenç y Cati, entre otros, por sus servicios, su ayuda y buena predisposición que facilitan el trabajo en la facultad.

Y fuera del ámbito laboral, a mi familia en general y a mis padres en particular, Toni y Mari. Ellos me han dado todas las comodidades para que haya podido dedicar todo este tiempo a mi pasión sin tener que preocuparme por nada. Nunca me han frenado en ninguna de mis ideas por extravagantes que fueran permitiéndome llegar a lo que hoy soy. A mi hermana Marga, mi amiga y compañera a lo largo de toda mi vida con la que he compartido tantos momentos, buenos y malos. Y de nuevo al resto de miembros de mi familia que de un modo u otro han participado en mi trayectoria científica todos estos años, un fuerte abrazo.

Echando la vista atrás es abrumador la cantidad de personas con las que me he cruzado a lo largo de mi fase de doctorando, a todos, gracias.

Miguel Oliver agradece la concesión de la ayuda por parte de la Conselleria d'Educació, Cultura i Universitats del Gobierno de las Illes Balears y del Fondo Social Europeo por la asignación de la beca predoctoral (no.516 FPI/1681/2014) que ha hecho posible la realización de esta tesis.

La investigación realizada en esta tesis ha sido financiada por el Ministerio de Economía y Competitividad y Agencia Española de Investigación a través de los proyectos CTM2014-56628-C3-3R (MINECO/FEDER) y CTM2017-84763-C3-3R (AEI/FEDER), respectivamente.

A sa meva padrina Margalida

ÍNDICE

Resumen

La exposición a la creciente presencia de contaminantes emergentes en el medioambiente es cada vez más preocupante. Estos contaminantes no solo causan un grave impacto medioambiental a todos los niveles de la cadena trófica, sino que son el motivo, junto a otros parámetros genéticos y socioeconómicos, de la mayoría de enfermedades crónicas.

Para la evaluación del riesgo de los contaminantes de preocupación emergente sobre los organismos, en este trabajo, se ha recurrido a los liposomas, un modelo de membrana. De hecho, el papel de los lípidos en la homeostasis de la membrana va ganando relevancia a medida que se va conociendo como su alteración puede causar cambios en las propiedades fisicoquímicas de la membrana, afectando a varias funciones celulares.

En esta tesis se han estudiado los efectos que causan, directa o indirectamente, distintos contaminantes emergentes, presentes en productos farmacéuticos y de cuidado personal, en diversas propiedades de la membrana, como el orden y empaquetamiento de los fosfolípidos, su fluidez e hidratación. Se estudiaron los efectos membranotrópicos así como la ubicación más probable y la interacción de los contaminantes con los fosfolípidos de membrana mediante una aproximación holística a través de técnicas experimentales y computacionales con el fin obtener una visión global y evitar interpretaciones erróneas. La idea de evaluar la interacción contaminantes-liposoma nos llevó al diseño de un método en flujo completamente automatizado capaz de obtener datos de fluorescencia a tiempo real, su procesado y evaluación, sin intervención humana y con una elevada reproducibilidad. Además, con el fin de investigar la cito/ecotoxicidad de una mezcla binaria de contaminantes, otro capítulo de la tesis se destinó a la realización de una serie de bioensayos usando células, levaduras, bacterias y membranas artificiales.

Los liposomas han demostrado ser una herramienta versátil para la investigación del efecto de contaminantes en bicapas lipídicas, y ofrecen una alternativa in-vitro para evitar la experimentación con seres vivos o pruebas celulares. La facilidad de síntesis y manipulación de estas vesículas lipídicas también permite la automatización de estos ensayos liposomales a través de enfoques fluídicos, lo que simplifica el trabajo experimental y ofrece aplicaciones nuevas en el campo de la exposómica, como el análisis de efecto directo de fracciones biodisponibles de manera no dirigida.

Resum

L'exposició a la creixent presencia de contaminants emergents en el medi ambient és de cada dia més preocupant. Aquests contaminants no només provoquen un greu impacte mediambiental a tots els nivells de la xarxa tròfica sinó que són el motiu, junt a altres paràmetres genètics i socioeconòmics, de la major part de les malalties cròniques.

Per a l'avaluació del risc dels contaminats de preocupació emergent en la biota, en aquest treball, s'han utilitzat liposomes com a model de membrana. De fet, el paper dels lípids en la homeòstasi de la membrana guanya, cada cop, més rellevància a mesura que es coneix com la seva alteració pot provocar canvis en las propietats fisicoquímiques de la membrana afectant a distintes funcions cel·lulars.

En aquesta tesi s'han estudiat els efectes causats, directe o indirectament, per distints contaminants emergents, presents en productes farmacèutics i de cura personal, en diverses propietats de la membrana ja sigui l'ordre i empaquetament dels fosfolípids, la seva fluïdesa o hidratació. Els efectes membranotròpics així com la seva ubicació més probable i la interacció dels contaminants amb els fosfolípids de membrana van ser estudiats en una aproximació holística per mitjà de tècniques experimentals i computacionals amb l'objectiu d'obtenir una visió global i evitar males interpretacions. La idea d'avaluar la interacció contaminant-liposoma ens va dur al disseny d'un mètode en flux completament automatitzat caracteritzat per l'adquisició en temps real de dades de fluorescència, el seu processat i avaluació, sense intervenció humana i amb una alta reproductibilitat. A més, per tal d'investigar la cito/ecotoxicitat d'una mescla binària de contaminants, a un capítol de la tesi es varen realitzat una sèrie de bioassajos fent ús de cèl·lules, llevats, bacteris i membranes artificials.

Els liposomes han demostrat ser una ferramenta versàtil per a la investigació de l'efecte de contaminants sobre la bicapa lipídica i ofereixen una alternativa in-vitro per tal d'evitar l'experimentació amb éssers vius o proves cel·lulars. La facilitat de síntesi i manipulació d'aquestes vesícules lipídiques també permet l'automatització d'aquests assajos liposomals per mitjà de plantejaments fluídics, fet que simplifica el treball experimental i ofereix noves aplicacions en el camp de l'exposòmica, com per exemple, l'anàlisi de l'efecte directe de fraccions biodisponibles de forma no dirigida.

Abstract

Exposure to the increasing occurrence of emerging pollutants in the environment is a topic of major concern. These pollutants do not only cause a serious environmental impact at all levels of the food chain, but they are key contributing along with other genetic and socioeconomic parameters to most chronic diseases.

For the risk assessment of contaminants of emerging concern on organisms, liposomes, as biological membrane surrogates, were employed in this work. In fact, the role of lipids in membrane homeostasis gains steadily relevance, because there is an increasing knowledge on how any alteration can disturb membrane physical-chemical properties thereby affecting several cellular functions.

The main aim of this thesis is to determine direct or indirect effects caused by a selection of emerging contaminants, available in pharmaceutical and personal care products, in several membrane properties, such as phospholipid order and packing, fluidity and hydration. Membranotropic effects as well as the most probable location and interaction of contaminants with the lipid bilayer were studied in a holistic approach through experimental and computational techniques in order to obtain a global view and avoid misleading interpretations. The idea of assessing the actual effect of contaminant species on the structure of liposomes led us to the design of a fully automated flow method that featured real-time acquisition of fluorescence readouts, data processing and feedback in a fully unsupervised mode with a high degree of reproducibility. Further work was also focused on investigating the eco/cytotoxicity of binary mixtures of contaminants by resorting to a suite of bioassays with a diversity of microorganisms, yeasts, cells and artificial membranes.

This thesis serves to demonstrate that lipid vesicles are versatile tools for investigation of the effect of contaminants on lipid bilayers and offer a valuable *in-vitro* alternative to avoid experimentation with living beings or cell testing. The ease of synthesis and manipulation of liposomes also allows the automation of these assays via flow approaches, thus simplifying experimental work and give relevant insight into the field of exposomics, such as effect direct analysis (EDA) of bioavailable fractions in an untargeted fashion.

Listado de publicaciones

La presente tesis doctoral es un compendio de los siguientes artículos de investigación:

1. **Fluorescent lipid nanoparticles as biomembrane models for exploring emerging contaminant bioavailability supported by density functional theory calculations**
   Autores: Miquel Oliver, Antonio Bauzá, Antonio Frontera y Manuel Miró
   Revista: *Environmental Science & Technology (ES&T)*
   Año: **2016**
   Volumen: 50 (13)
   Páginas: 7135-7143
   DOI: 10.1021/acs.est.6b00772
   Índice de impacto (2016): 6.198

2. **A holistic approach for the in-vitro elucidation of the bioaccumulation of organic contaminants of emerging concern in lipid bilayers**
   Autores: Miquel Oliver, Miquel Adrover, Antonio Frontera, Joaquín Ortega-Castro, y Manuel Miró
   Revista: *Science of the Total Environment (STOTEN)*
   Año: **2019**
   Estado: Enviado para su publicación
   Índice de impacto (2018): 5.589

3. **In quest of effect directed analysis at the smart laboratory: Automated system for flow-through evaluation of membranotropic effects of emerging contaminants**
   Autores: Miquel Oliver, Marc Roca-Jiménez, Manuel Miró, y David J. Cocovi-Solberg
   Revista: *Talanta*
   Año: **2020**
   DOI: 10.1016/j.talanta.2019.120600
   Indice de impacto (2018): 4.916

4. **Ecotoxicological equilibria of triclosan in Microtox, XenoScreen YES/YAS, Caco2, HEPG2 and liposomal systems are affected by the occurrence of other pharmaceutical and personal care emerging contaminants**
   Autores: Miquel Oliver, Błażej Kudłak, Monika Wieczerzak, Salette Reis, Sofia Lima, Marcela Segundo, y Manuel Miró
   Revista: *Science of the Total Environment (STOTEN)*
   Año: **2019**
   Estado: Versión revisada (R1) enviada para su publicación

En el anexo se incluye una quinta publicación en *Analytical Chemistry* 91 (2019) 13260 titulada "**Reliable sensing platform for plasmonic Enzyme-Linked Immunosorbent Assays based on Automatic Flow-Based Methodology".**

Capítulo 1. Introducción

1.1. Bioaccesibilidad, biodisponibilidad y bioactividad

Antiguamente la concentración total de un determinado contaminante o xenobiótico (normalmente metal) en una muestra ambiental se usaba para identificar el grado de contaminación y efectos nocivos que podría provocar en la cadena trófica. Esta suposición tiende a sobrevalorar el riesgo potencial de la muestra contaminada en condiciones de exposición real en humanos o biota en general, entendiendo este término como el conjunto de plantas, animales y otros organismos presentes en una zona determinada, ya que el sistema biótico no tiene el poder eluotrópico, las propiedades de desintegración de matriz o la reactividad química de los reactivos químicos usados en metodologías de extracción o análisis para determinar la concentración total del contaminante.

Puesto que el xenobiótico debe cruzar varias interfases y difundir a través de distintos compartimentos ambientales, especialmente en el caso de muestras sólidas, antes de alcanzar su destino final, no toda la masa inicial del compuesto conseguirá llegar al órgano o tejido diana; por el contrario, se distribuirá en todos los compartimentos ecológicos disponibles (figura 1.1). Sin embargo, solo algunas especies presentes en un compartimento dado serán potencialmente tóxicas para la biota. Si bien la especiación química podría parecer la forma más adecuada para cuantificar las especies contaminantes de interés, la interconversión debida al equilibrio dinámico en cada compartimento ambiental y durante el proceso de muestreo hace que las estrategias de fraccionamiento sean más adecuadas para muestras sólidas. De este modo, los ensayos de bioaccesibilidad se han estado usando a lo largo de las últimas décadas para cuantificar la máxima cantidad de xenobiótico capaz de cruzar dichas barreras naturales. Estos ensayos consisten en el estudio de la solubilidad o fracción de compuesto liberada o desorbida de su matriz (ya sea suelo, sedimento, materia particulada, biomasa o incluso alimentos) bajo condiciones de lixiviación biomiméticas y ambientalmente simuladas o bien, determinar la fracción más lábil del contaminante.

1.1.1. Bioaccesibilidad

La primera etapa para que un xenobiótico en una muestra sólida alcance su órgano o tejido diana dentro de un marco ecotoxicológico es pasar desde su reservorio a un medio

acuoso mediante condiciones ecomiméticas de desorción o extracción. Este proceso define la fracción bioaccesible, a veces denominada también lábil. Por tanto, desde un punto de vista alimentario y de salud humana, se puede definir el concepto de bioaccesibilidad como la cantidad o fracción de compuesto de interés que es liberado desde su matriz sólida alimentaria en el tracto gastrointestinal y pasa a ser potencialmente asimilable para su absorción en el endotelio intestinal. Esto incluye pues todos los procesos digestivos y transformaciones que sufre el alimento desde que entra en contacto con la saliva en la boca, pasa por el estómago y hasta que llega al intestino delgado donde interacciona con bilis y jugos duodenales. La bioaccesibilidad de muestras sólidas es normalmente evaluada mediante procesos de digestión *in vitro* simulando los jugos gástricos e intestinales. Numerosos protocolos son usados hoy en día [1,2]. De hecho, las digestiones *in vitro* son una metodología popular y accesible para detectar la bioaccesibilidad potencial, ya que son económicas, rápidas y ofrecen información preliminar relevante para, en caso de necesidad, realizar experimentos *in vivo*. Estos ensayos además permiten la comparación de la matriz alimentaria bruta con la resultante de diferentes tratamientos tecnológicos. La cantidad de lípidos y proteínas de la dieta, cantidad y tipos de sales biliares y la fibra son factores que afectan a la fracción bioaccesible de un xenobiótico de una determinada matriz [3].

Estos protocolos clásicos sin embargo tienen ciertas limitaciones cuando se realizan en modo discontinuo: i) la falta de información en tiempo real de la velocidad de extracción de las especies estudiadas y ii) la ausencia de una eliminación continua de las especies extraídas de la matriz alimentaria así como van siendo desorbidas [4]. Para hacer frente a esos inconvenientes, las tendencias recientes se centran en el desarrollo de metodologías de fraccionamiento en continuo. Estos ensayos de bioaccesibilidad dinámica/cinética permiten una mejora de la simulación de la digestión gastrointestinal fisiológica por medio del paso de jugos a través de una cámara de flujo donde se encuentra la matriz alimentaria a ser estudiada [5].

1.1.2. Biodisponibilidad

La segunda interfase relevante, y de mayor interés en esta disertación, que debe cruzar un xenobiótico con el fin de alcanzar su diana es la membrana externa del organismo

objetivo. Para organismos unicelulares la barrera es la membrana plasmática mientras que para seres más complejos son aquellas membranas derivadas del ectodermo o endodermo en función del tipo de exposición al compuesto de interés (oral, dérmica, inhalatoria, etc…). La fracción de un compuesto dado, o sus metabolitos, capaz de entrar dentro del citoplasma en el caso de organismos simples o de llegar al torrente sanguíneo en seres complejos se conoce con el nombre de fracción biodisponible [6]. Así, a partir de la fracción bioaccesible de un compuesto solo una subfracción podrá cruzar membranas, ser asimilado por el organismo y llevar a cabo su función (tóxica, en el caso de los contaminantes) en el tejido u órgano diana, por lo que se deben realizar pruebas adicionales en la fracción bioaccesible con una partición *in vitro* adicional basada en procesos fisiológicamente relevantes, simulando membranas, como es el caso del uso de liposomas que se describirán más adelante en la introducción y se tratará en los capítulos 3, 4, 5 y 6.

1.1.3. Bioactividad y toxicidad

Una vez que el contaminante ha ingresado en el organismo objetivo, puede afectar varias rutas biológicas, modificándolas o incorporándose al metaboloma del organismo. La bioactividad pues, puede definirse como el efecto especifico después de la exposición a una sustancia, incluyendo la absorción por parte del órgano o tejido y la consecuente respuesta fisiológica [7]. El número exacto de procesos afectados y las consecuencias potencialmente peligrosas solo pueden estudiarse in vivo para cada contaminante, cada organismo y cada modo de exposición. La ISO 17402:2008 define como la fracción biodisponible toxicológicamente activa a la fracción de contaminante capaz de experimentar procesos biológicos, tales como absorción, distribución, metabolismo, excreción o acumulación. Si la sustancia o sus metabolitos son tóxicos para el organismo objetivo, es decir, ponen en peligro su autosustentabilidad a concentraciones relativamente bajas, el foco debe centrarse en el organismo: solo las pruebas ecotoxicológicas pueden evaluar las dosis letales. Si, por el contrario, el analito o sus metabolitos no causan toxicidad aguda, la molécula objetivo podría transformarse o degradarse y, por lo tanto, su concentración disminuye en el organismo objetivo y también en el ecosistema. Esta sería la denominada fracción "biodegradable". Si la molécula objetivo no se metaboliza, entrará y saldrá del organismo objetivo a diferentes

velocidades hasta que se equilibre con el medio (debido a la diferente solubilidad y, por lo tanto, a los coeficientes de partición de la molécula entre el medio y los tejidos del organismo).

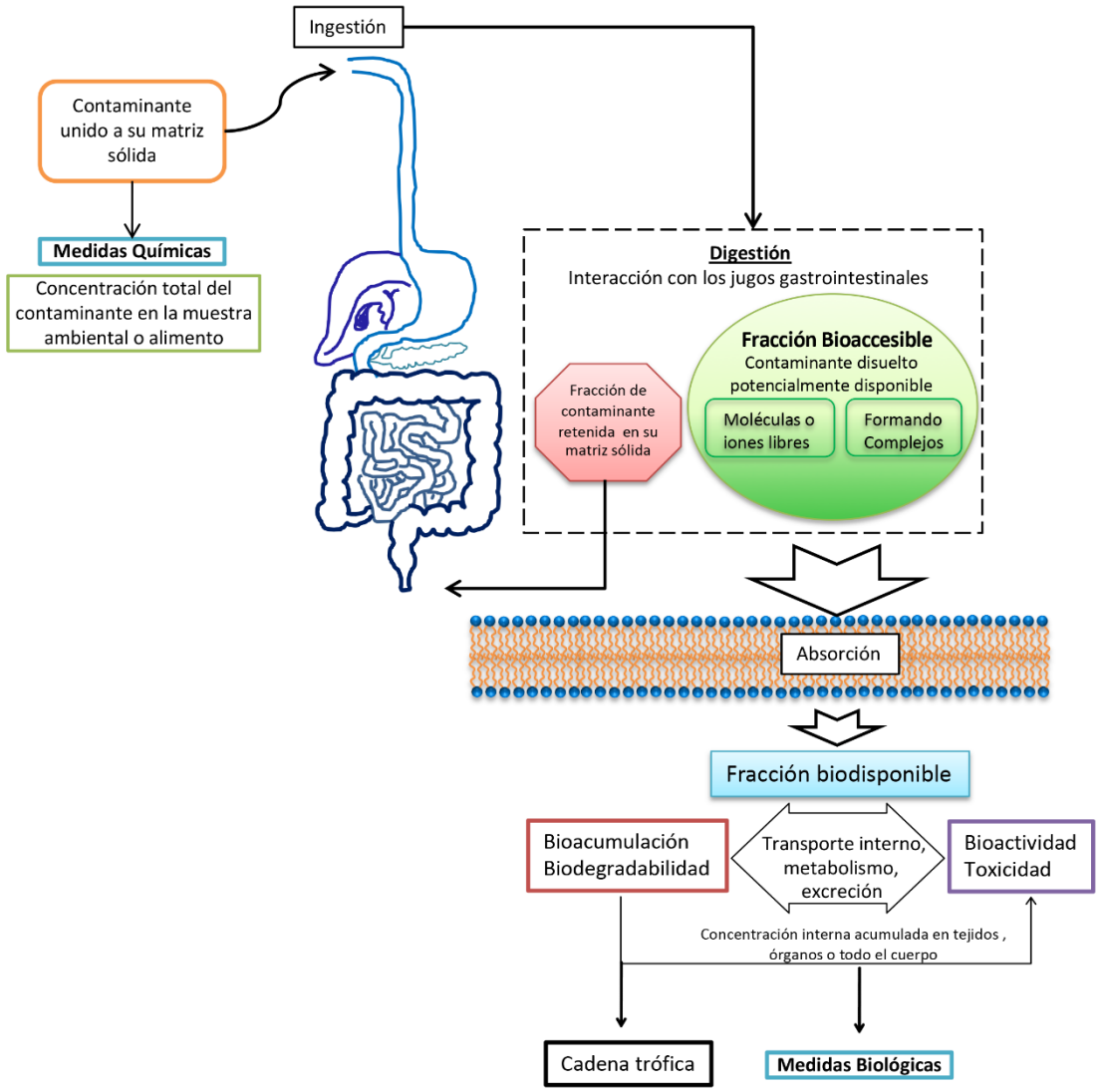

Figura 1.1. Representación esquemática de todos los procesos que sufre un contaminante presente en su matriz sólida desde que es ingerido.

La cantidad de contaminante de una muestra que se retiene en la biota se conoce como fracción "bioacumulable". Cuando un contaminante se acumula en un organismo, conduce a la biomagnificación, es decir, concentraciones crecientes a nivel de cadena

trófica creciente [8]. La toxicidad, la biodegradación y la bioacumulación son procesos de gran interés ambiental y económico y se han llevado a cabo muchos trabajos experimentales para cuantificar la biodegradación y bioacumulación de contaminantes persistentes mediante organismos modelo. Como en el caso de la fracción biodisponible, se ha estudiado la existencia de correlaciones entre fracciones biodegradables y bioacumulables usando pruebas ecotoxicológicas *in vivo* y los resultados de tests de bioaccesibilidad químicos *in vitro* en condiciones operacionalmente definidas, basadas en imitar el medio biótico con extractantes que simulan parámetros químicos de interés fisiológico, como son la capacidad complejante, la constante dieléctrica o la polaridad de fluidos biológicos.

1.2. Membranas, algo más que una pared física

Tal como se ha indicado al inicio de esta disertación, el término biodisponibilidad de un compuesto se refiere a la fracción o porcentaje capaz de atravesar las barreras fisiológicas y llegar a la circulación sistémica del organismo. En los seres vivos, la barrera fisiológica más relevante es la membrana plasmática, es decir, la membrana externa de la célula.

La principal función de las membranas biológicas es el control selectivo del transporte molecular hacia el interior o exterior de las células. La membrana plasmática celular está compuesta básicamente por una estructura en forma de bicapa constituida por dos láminas de fosfolípidos y otros lípidos, como el colesterol, en la cual se encuentran gran diversidad de proteínas. El gran número de estructuras formadas por los lípidos *in vitro* nos da una idea de la variación de las propiedades estructurales que pueden tener lugar en las membranas *in vivo*. Además, los lípidos participan en interacciones entre ellos de forma dinámica lo que permite su movimiento dentro de la membrana, cambios en el grosor de la membrana, del empaquetamiento, fluidez y otras propiedades que veremos a lo largo de este texto y que permiten la formación de dominios cuyas propiedades difieren del resto de la membrana confiriendo características destinadas a funciones concretas. Todo esto demuestra que la membrana no solo compartimenta a la célula actuando de barrera física, sino que juega un papel fundamental en la homeostasis celular mediante la respuesta a estímulos externos y a la comunicación interna [9].

Además, otra característica muy importante y que influye en el comportamiento de la membrana es su asimetría. Las monocapas lipídicas que constituyen la membrana difieren en su composición lo que afecta a varias de las propiedades de la bicapa como su potencial eléctrico, permeabilidad, forma y estabilidad química por lo que la alteración de esta asimetría tiene consecuencias fisiológicas importantes [10].

A pesar de la estabilidad química de la membrana, debe tenerse en cuenta que la interacción entre los lípidos que la componen no está determinada por uniones covalentes sino por un conjunto de fuerzas débiles dominadas por el denominado "Efecto Hidrofóbico".

1.2.1. Efecto hidrofóbico

Es bastante remarcable el hecho de que las membranas sean tan estables sin la presencia de ningún tipo de interacción covalente que las mantengan unidas, de modo que las sutiles fuerzas que permiten la estabilidad de la bicapa deben ser, en su conjunto, fuertes. La principal fuerza implicada se conoce como el Efecto Hidrofóbico, atribuido al aumento de los enlaces de hidrógeno intermoleculares en presencia de moléculas apolares y que ha sido elegantemente discutido por Charles Tanford en su libro: Hydrophobic Effect: Formation of Micelles and Biological Membranes en 1973 y que fue completamente revisado y complementado con nuevos contenidos en 1980 [11].

El Efecto Hidrofóbico podría resumirse como la tendencia a la agregación de moléculas apolares en disolución acuosa con el fin de excluir las moléculas de agua de estos agregados lo máximo posible. Este efecto conlleva un aumento de la entropía. Cualquier estructura y proceso biológico dependen de la participación de interacciones covalentes y no covalentes. Debido a la naturaleza polar del agua, esta compite y debilita las fuerzas electrostáticas y los enlaces de hidrógeno entre moléculas o grupos polares lo que implica que para recurrir a estas fuerzas de carácter débil, las cuales juegan un papel clave en la estabilización de la estructura de muchas macromoléculas biológicas, deben protegerse de su entorno acuoso. Esto se ve reforzado por otra consideración más, esta vez con respecto a las moléculas hidrofóbicas como podrían ser las colas de los fosfolípidos. Las moléculas apolares no pueden participar en el enlace de hidrógeno, tan importante en el agua en estado líquido. Como consecuencia, las moléculas de agua alrededor de esas moléculas apolares se vuelven más ordenadas, es decir, tienen menos

entropía, que las moléculas de agua en el resto de la disolución. Cuando dos de estas moléculas no polares se unen, algunas de sus moléculas de agua circundantes se liberan y pueden regresar a la disolución. Eso hace que las moléculas apolares tengan una tendencia espontánea a preferir ambientes no polares [12]. Como se comentó anteriormente, la agregación de moléculas hidrofóbicas en un entorno acuoso permite la liberación de las moléculas de agua a su alrededor aumentando así la entropía del disolvente y por tanto satisfaciendo la segunda ley de la termodinámica.

Los fosfolípidos son moléculas anfifílicas y como tales forman monocapas espontáneamente en la interfase con el agua, pasando a la formación de bicapas en disolución acuosa, que, a su vez, de forma inherente, se cierran sobre sí mismas con tal de proteger los residuos hidrofóbicos del agua y exponiendo, al mismo tiempo, las cabezas polares hacia el entorno acuoso. De nuevo, la fuerza impulsora de este auto ensamblaje hacia la formación de vesículas es el Efecto Hidrofóbico (figura 1.2.a) y es la base de las membranas biológicas. A parte del efecto mencionado existen otras fuerzas que contribuyen a la estabilización de la membrana [13]. Las fuerzas de Van der Waals (figura 1.2.e) mantienen unido el interior de la membrana a través de interacciones entre dipolos inducidos que se forman instantáneamente entre dos superficies moleculares muy cercanas. Aunque débiles, estas fuerzas aumentan con la longitud de las cadenas siendo de gran importancia por tanto en el centro apolar de la bicapa, estabilizando las cadenas hidrofóbicas. Las cabezas polares, cargadas o no, pueden interaccionar ya sea con otros grupos polares de fosfolípidos adyacentes (figura 1.2.b) o con las moléculas de agua cercanas (figura 1.2.c). Otro fenómeno causante de la formación de la bicapa membranal es aquella relacionada con la movilidad de las colas hidrocarbonadas y que está directamente relacionada con la entropía (figura 1.2.d). Un fosfolípido expuesto al medio acuoso vería su cola apolar rodeada por una rígida red de moléculas de agua que limitarían su libertad de movimiento, reduciendo de este modo la entropía. Al formar parte de la bicapa lipídica, esas colas hidrofóbicas se deshacen de las moléculas de agua que la rodean aumentando su movilidad y, por ende, su entropía aumenta.

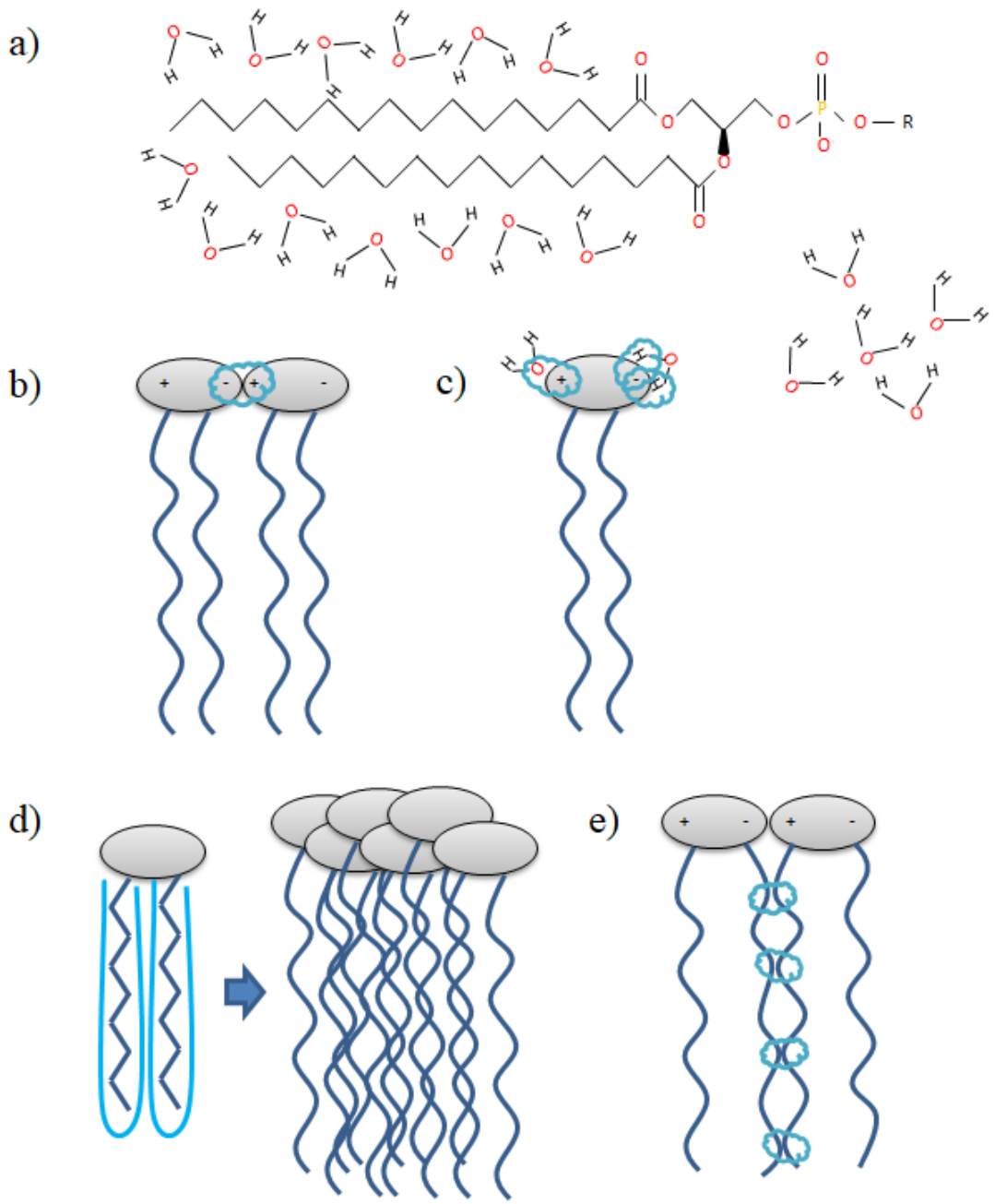

Figura 1.2. Representación de las distintas fuerzas e interacciones involucradas en la estabilidad de la membrana en medio acuoso donde a) es el efecto hidrofóbico, b) son interacciones electrostáticas entre cabezas polares, c) puentes de hidrógeno entre el agua y las cabezas polares, d) movilidad de las colas apolares y e) fuerzas de Van der Waals entre las colas apolares

Podemos concluir por tanto que, aunque son varias las fuerzas e interacciones que permiten la formación y estabilización de la membrana fosfolipídica, el Efecto

Hidrofóbico es el fenómeno más relevante. Dicho efecto solo puede entenderse considerando las particularidades del agua como disolvente, su estructura molecular distintiva y las propiedades cohesivas únicas de ésta. Las fuerzas atractivas entre moléculas hidrofóbicas se generan por el medio acuoso, no de interacciones directas entre estas moléculas apolares, de modo que el Efecto Hidrofóbico es una consecuencia indirecta de las intensas fuerzas direccionales entre las moléculas de agua y su complementariedad. Dicho de otro modo, la estabilización de las membranas se debe, en gran parte, a la propensión del agua a formar puentes de hidrógeno consigo misma la cual es responsable a su vez de su elevada auto-atracción y de otras muchas propiedades.

De hecho, si se considera la entropía de un fosfolípido solo, una dispersión de esta molécula tiene mayor entropía y estabilidad que un agregado de estos. Solamente al considerar la entropía del propio medio acuoso se puede comprender la separación de fases y el plegado tanto de proteínas, fosfolípidos y otras moléculas biológicas en sus formas activas. Esto se debe a que las moléculas de agua adyacentes a una molécula apolar deben recurrir a una disminución de la entropía con tal de mantener interacciones moleculares con otras moléculas de agua debido a la intensa fuerza direccional de esas interacciones. Puesto que la molécula apolar es incapaz de formar puentes de hidrógeno, los puentes de hidrógeno entre moléculas de agua serán en este caso anisotrópicos (direccionales). En cambio, en el seno de la disolución, las moléculas de agua pueden moverse y rotar libremente manteniendo a su vez interacciones entre sus vecinas de modo que estas fuerzas son esencialmente isotrópicas, extendiéndose en todas direcciones y provocando un aumento de la entropía. La tasa de reorientación disminuye drásticamente cerca de las moléculas apolares debido a una disminución sustancial en la movilidad traslacional del agua [14]. Por lo tanto, la red de enlaces de hidrógeno alrededor de los grupos hidrofóbicos no es más rígida o similar al hielo, en comparación con el seno de la disolución, sino que la dinámica de los enlaces de hidrógeno es diferente. Puesto que todo cambio en la entropía debido a cualquier proceso de ordenamiento o estructuración debe ir acompañado de un cambio en la entalpía que lo compense [15] tiene que haber otro factor que contribuya al efecto hidrofóbico. Con el propósito de acomodar una molécula apolar en el medio acuoso se requiere de cierta energía para formar una cavidad en el agua [16]. Este fenómeno implica la rotura o deformación de los

puentes de hidrógeno asociados a una entalpía elevada y positiva que se debe a que las moléculas de agua son pequeñas y los enlaces de hidrógeno entre las moléculas de agua son fuertes; por lo tanto, la densidad de energía cohesiva del agua es alta. Si la molécula introducida fuera hidrofílica podría interaccionar con el agua reduciendo esa entalpía de formación de la cavidad cosa que no ocurre con moléculas hidrofóbicas y que desemboca como consecuencia en una baja solubilidad. Este es por tanto un mecanismo que podría explicar el efecto hidrofóbico aunque tampoco el único [17].

1.2.2. Lípidos

La diferencia más importante entre el modelo de membrana actual y el modelo de mosaico fluido clásico, el cual define a la membrana como una bicapa lipídica fluida con una rápida difusión lateral de lípidos y proteínas distribuidos sin un orden especifico [18], es el elevado orden espacio-temporal prevaleciente en la membrana y dominios presentes en ella [19]. Este orden parece ser esencial para el funcionamiento de las proteínas de membrana. Por tanto, la anticuada idea de proteínas flotando en un mar de lípidos, siendo estos un mero soporte, ha evolucionado, evidenciando el importante papel de la estructura y dinámica de los lípidos que constituyen la membrana en su funcionalidad.

Al igual que las proteínas y los ácidos nucleicos, las propiedades de las membranas lipídicas resultan de la contribución de componentes minoritarios. Los lípidos de membrana tienen diferentes propiedades físicas (a veces incluso dentro de la misma clase), como, por ejemplo, fluidez, área de sección transversal, carga eléctrica, peso molecular y propensión a la fase no lamelar en función de la longitud de la cadena de ácidos grasos, la presencia o no de insaturaciones, etc. Sin embargo, los lípidos no están unidos covalentemente formando las membranas como ya se detalló anteriormente, sino que interactúan dinámicamente para formar disposiciones transitorias cuya estabilidad puede variar [20]. Este fenómeno constituye otra fuente de complejidad para su estudio estructural.

Aunque hay una gran variedad de lípidos de membrana, esta se compone mayoritariamente de 3 tipos: (i) los lípidos basados en el glicerol, (ii) los esteroles y (iii)

los esfingolípidos basados en ceramida. A su vez los lípidos basados en el glicerol se pueden dividir en fosfolípidos y glicosilglicéridos.

1.2.2.1. Fosfolípidos

Los fosfolípidos son los lípidos más abundantes en las membranas. Su estructura consta de 4 partes básicas: uno o más ácidos grasos; un soporte donde se anclan las cadenas de ácidos grasos; un grupo fosfato, y un grupo alcohol unido al fosfato. En el caso que el soporte donde se anclan los ácidos grasos sea el glicerol, un polialcohol de 3 carbonos, se denominan fosfoglicéridos o glicerofosfolípido, aunque se les suele denominar comúnmente fosfolípidos (figura 1.3).

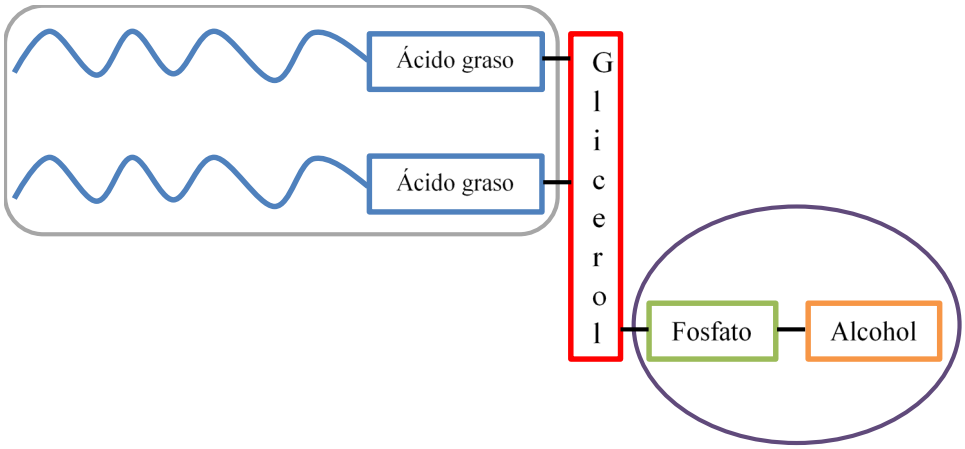

Figura 1.3. Representación de la estructura básica de un fosfolípido.

Los dos ácidos grasos, o uno solo en el caso de hidrólisis parcial, unidos a los carbonos C1 y C2 del glicerol constituyen la cola apolar o hidrofóbica del fosfolípido, mientras que el resto, esterificado al C3 del glicerol mediante un ácido fosfórico, se conoce como cabeza polar o hidrofílica.

En función del alcohol unido al fosfato por un enlace éster se derivan los distintos fosfolípidos o fosfoglicéridos. Los grupos más comunes son: colina, serina, etanolamina, inositol y glicerol (figura 1.4). Según el grupo polar tendremos pues,

fosfatidilcolina (PC), fosfatidilserina (PS), fosfatidiletanolamina (PE), fosfatidilinositol (PI) o fosfatidilglicerol (PG), y en el caso de que se forme una estructura dimérica donde un grupo glicerol actúa de puente a dos fosfoglicéridos, el fosfolípido es entonces un difosfatidilglicerol (cardiolipina) [21].

Además, estos grupos polares confieren ciertas características al fosfolípido, ya sea el volumen que determinará su forma, por ejemplo cilíndrica en el caso de PC al ser un grupo voluminoso, o cónica truncada en el caso de PE caracterizada por un grupo polar pequeño respecto al área de sección transversal de la cola apolar [9]; o su carga neta siendo por ejemplo neutra o zwitteriónica en la PC y PE, y negativas en la PS, PG y PI.

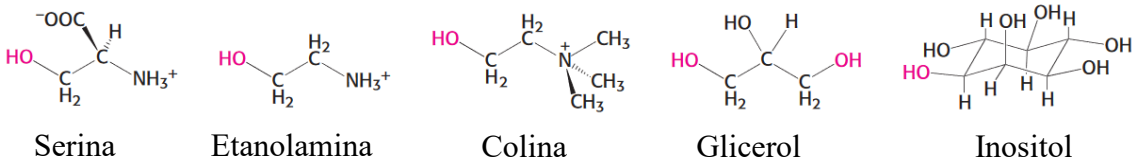

Figura 1.4. Distintos alcoholes que contituyen el grupo polar en los fosfolípidos.

Las fuentes más comunes para la obtención de fosfolípidos naturales son los tejidos animales, como el cerebro bovino, o la yema de huevo y aceites vegetales como la soja, maíz, algodón, girasol y colza. Entre estos, la soja y la yema de huevo son los más usados, siendo la fosfatidilcolina (PC) extraída de la soja (figura 1.5) el fosfolípido usado en todos nuestros trabajos de esta tesis para la síntesis de liposomas.

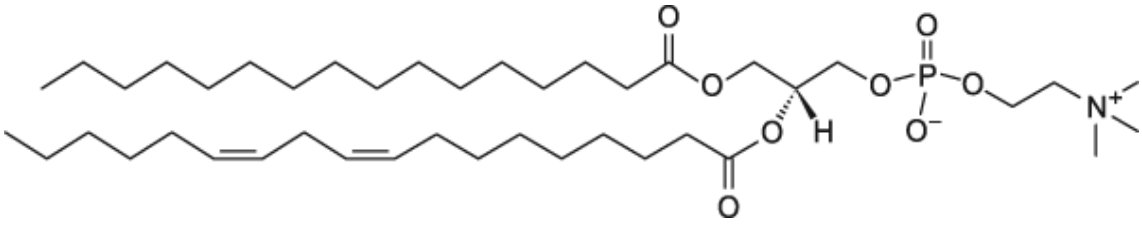

Figura 1.5. Estructura más común de la fosfatidilcolina (PC) de soja formada por un fosfolípido mixto con el grupo polar colina y las colas C16 y C18:2.

La PC de soja se caracteriza por una concentración en ácidos grasos insaturados mayor del 50% (figura 1.6) siendo el mayoritario el ácido linoleico (59-70%) perteneciente a la serie omega 6, con 18 carbonos y dos insaturaciones, seguido por el ácido palmítico (12-17%), con una cadena saturada de 16 carbonos, y el ácido oleico (7-12%), un ácido graso monoinsaturado de 18 carbonos de la serie omega 9.

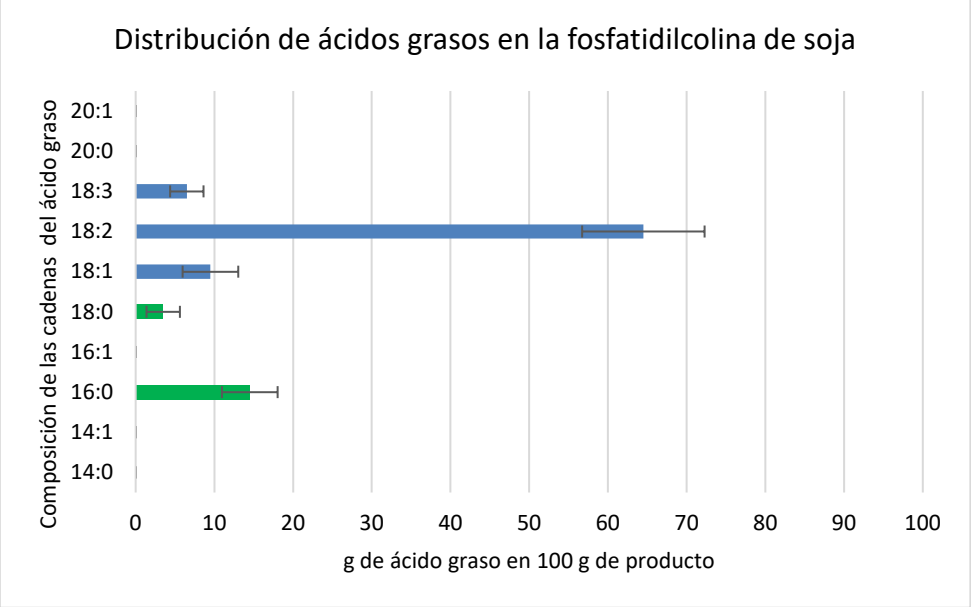

Figura 1.6. Distribución de los ácidos grasos en la fosfatidilcolina (PC) de soja. En azul se muestran los ácidos grasos insaturados y en verde los ácidos grasos saturados.

La esfingomielina es un tipo especial de fosfolípido ya que, aunque contenga un grupo fosfato, el esqueleto de glicerol es sustituido por esfingosina, un aminoalcohol, por lo que también se engloba dentro de los llamados esfingolípidos. La esfingosina se une por el grupo amino a un ácido graso mediante un enlace amida lo que constituye la ceramida. Cuando al hidroxilo primario de la ceramida se une la fosfocolina o fosfoetanolamina al conjunto se le conoce como esfingomielina. Recientemente se ha hecho evidente que los esfingolípidos están involucrados en muchas enfermedades humanas, incluyendo diabetes, cánceres, síndromes neurológicos, infecciones y enfermedades de los sistemas cardiovascular y respiratorio [22].

1.2.2.2. Glucolípidos

En el caso de que el grupo unido a la ceramida sea uno o más glúcidos, en lugar del grupo fosfato con la colina o etanolamina, la molécula se conoce como glucolípido. El cerebrósido es el glucolípido más simple, en el que la ceramida se une a un único residuo, glucosa o galactosa, mediante un enlace β-glucosídico. Los glucolípidos, por tanto, no son fosfolípidos. Dentro de la categoría de glucolípidos se pueden incluir también los derivados del glicerol que contienen azúcares. En los glicosilglicéridos, el C3 del glicerol es esterificado a un azúcar en lugar de un fosfato y alcohol. Estas moléculas abundan en sistemas fotosintéticos, ya sea en bacterias, algas o plantas aunque también pueden aparecer en animales [23].

1.2.2.3. Esteroles

Los esteroles son esteroides, moléculas formadas por 4 anillos insaturados unidos, 3 de ellos de seis carbonos y uno de cinco. En los esteroles, a este grupo de anillos se le añade un grupo hidroxilo en un extremo capaz de interaccionar con la parte polar de los fosfolípidos, y una cadena hidrocarbonada en el otro extremo que facilita el anclaje dentro de la membrana. El colesterol es el esterol más importante en las células animales y juega un papel clave en el control de las propiedades de la membrana como veremos más adelante.

Para concluir este apartado cabe indicar que una característica importante de las membranas biológicas es la existencia de asimetrías transversales y laterales. Por un lado, la monocapa citosólica o interna contiene altos niveles de fosfatidilserina y fosfatidiletanolamina, mientras que la monocapa extracelular es rica en fosfatidilcolina y esfingomielina (simetría de sección transversal). Por otro lado, varios tipos de células están altamente polarizadas (asimetría lateral). Por lo tanto, las células epiteliales y endoteliales, además de ciertas células glandulares, tienen membranas basales, laterales y apicales bien definidas con composiciones lipídicas y proteicas específicas [24]. Cuando estas regiones, que difieren en su composición del resto de la membrana, son pequeñas en comparación con las áreas circundantes (como una isla en el mar), se le denomina dominio de membrana.

1.2.3. Estructuras de los fosfolípidos en la membrana

Los lípidos de membrana son polimórficos, es decir, pueden existir en una gran variedad de distintas estructuras secundarias supramoleculares organizadas mayor que la que pueden presentar las proteínas y ácidos nucleicos.

A nula o baja hidratación y/o baja temperatura, la mayoría de los lípidos forman una estructura o fase cristalina verdadera en sus tres dimensiones (L_c) [25]. En el caso de algunos fosfolípidos (como la fosfatidilcolina) al ser incubados en un medio acuoso a baja temperatura adoptan la denominada fase subgel ($L_{c'}$) con las cadenas hidrocarbonadas inclinadas. Esta fase consiste en capas cristalinas apiladas de forma irregular, considerada pues un cristal bidimensional.

Cuando los lípidos, y en particular los fosfolípidos, se hidratan estos se reorganizan en más de un tipo estructura o fase (figura 1.7) incluso en el caso de un solo lípido puro. La forma predominante dependerá de parámetros tales como la concentración, temperatura, presión, fuerza iónica y pH. Las fases más comunes son:

- Fase lamelar líquido cristalina o fase fluida (L_α). Se caracteriza por un considerable desorden de las cadenas alifáticas. Esta fase aparece a altas temperaturas y es la más abundante en membranas biológicas.

- Fase lamelar gel (L_β). Se forma a bajas temperaturas. Los lípidos están fuertemente empaquetados entre si y las cadenas apolares se encuentran muy ordenadas. Al encontrarse extendidas al máximo las cadenas, todas en configuración *trans*, el grosor de la bicapa en fase gel es mayor que en fase líquido-cristalina y su densidad también es ligeramente mayor. En el caso de la fosfatidilcolina u otros lípidos con grupos polares voluminosos, las cadenas alifáticas están inclinadas respecto a la normal de la bicapa. Esta forma con las cadenas inclinadas se conoce como fase $L_{\beta'}$. A partir de cierto nivel de inclinación, el empaquetamiento se estabiliza mediante la interdigitación de las cadenas (no inclinadas) de distintas capas. En esta fase gel interdigitada ($L_{\beta I}$) el grosor de la bicapa es mucho menor que otras fases [26]. Por otro lado, la fase $L_{\beta'}$ puede experimentar una modulación periódica que resulta en una fase ondulada ($P_{\beta'}$), un intermediario entre la fase $L_{\beta'}$ y L_α.

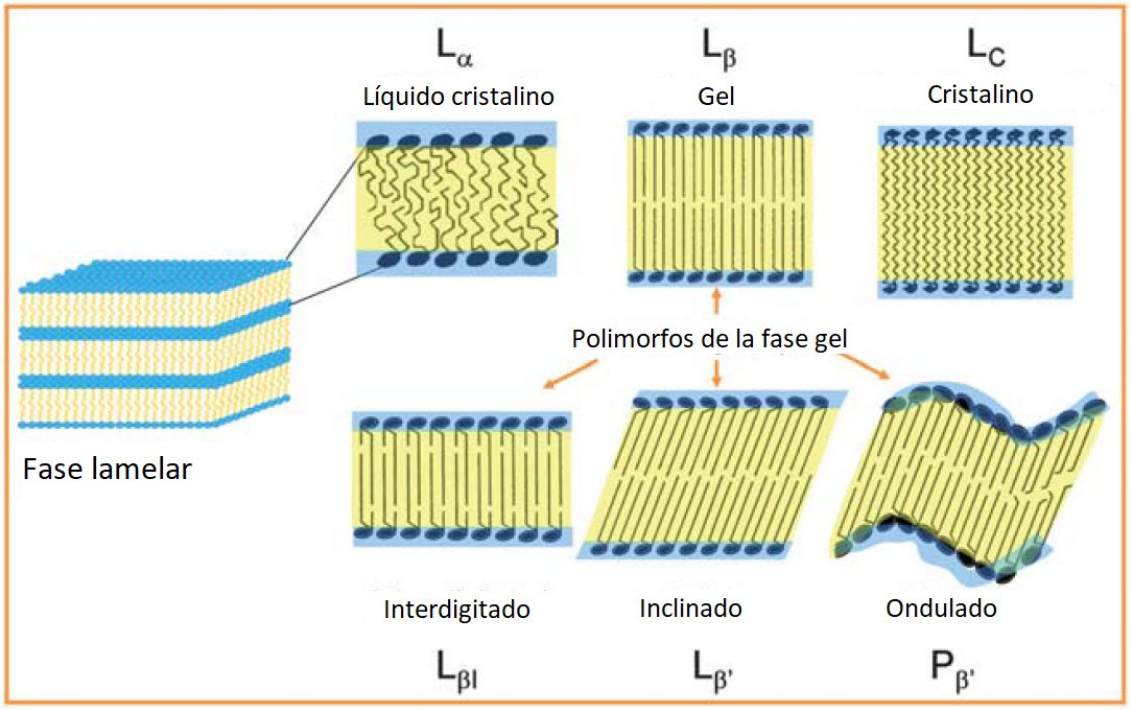

Figura 1.7. Representación de las distintas fases lamelares de las membranas [25]

A pesar de que las fases lamelares son las estructuras más prevalentes en las células, existen otras muchas fases no lamelares [27] entre las que destacan por ejemplo las fases hexagonales (H), micelar (M) y varias formas tridimensionales cúbicas representadas por la letra Q:

- Fase hexagonal I (H_I). Los lípidos se organizan formando micelas en forma de cilindros empaquetados en un modelo hexagonal con las cabezas polares orientadas hacia el exterior en contacto con el medio acuoso.

- Fase hexagonal II (H_{II}). La organización de los lípidos es en forma de cilindros con un empaquetamiento hexagonal, pero en este caso las cabezas polares se encuentran dirigidas hacia el interior. Esta fase es muy común en la fosfatidiletanolamina (PE) caracterizada por una cabeza polar débilmente hidratada e interacciones atractivas entre los grupos polares de PE vecinas.

- Fase micelar (M). Para que se dé esa morfología es necesario que el lípido tenga forma de cono invertido donde la cabeza polar es mucho más voluminosa que la cola apolar como ocurre en los lisofosfolípidos constituidos por una sola cola.

- Fase cúbica (Q). Se caracteriza por ser estructuras periódicas en tres dimensiones bicontinuas o discontinuas.

Aunque normalmente se clasifica la transición entre fases en función de la temperatura como veremos en la siguiente sección, también se puede clasificar una transición de fases en función del contenido de agua [28], desde micelas invertidas y fase H_{II} cuando el contenido de agua es bajo, pasando por las distintas fases lamelares hasta llegar a H_I, micelas y por último monómeros.

1.2.4. Temperatura de transición de los fosfolípidos

No se debe considerar a la bicapa lipídica como un sólido o un fluido similar al agua sino más bien como lo que se observaría al derretir manteca siendo el estado gel un sólido blando mientras que la fase líquido-cristalina es un fluido viscoso. Pero la cuestión es, ¿por qué se derriten las cadenas grasas alifáticas?

Al calentar un lípido, tienen lugar rotaciones de todos los carbonos de la cadena, entre los enlaces C-C. La configuración *trans* tiene el nivel menos energético ya que en esta forma, los grupos más grandes están lo más alejados posible entre ellos, evitando al máximo el impedimento estérico. En la figura 1.8.a se muestra un fragmento de ácido graso saturado no fundido, en estado *trans.* La rotación de los enlaces conduce a un estado eclipsado de elevada energía debido a un alto impedimento de los grupos (figura 1.8.b). La rotación adicional relaja parte de ese estrés estérico que resulta en otra disposición de menor energía denominada *gauche* pero más energética que el estado *trans*. En el estado *gauche* se crea un pliegue de la cadena (figura 1.8.c) que, tras varios pliegues, lleva a la fusión del lípido [29]. Esas torceduras se desplazan rápidamente por la cadena hacia los extremos de las colas en el interior de la bicapa lo que explica que la cadena sea más fluida en su extremo omega que en el extremo cercano al grupo polar.

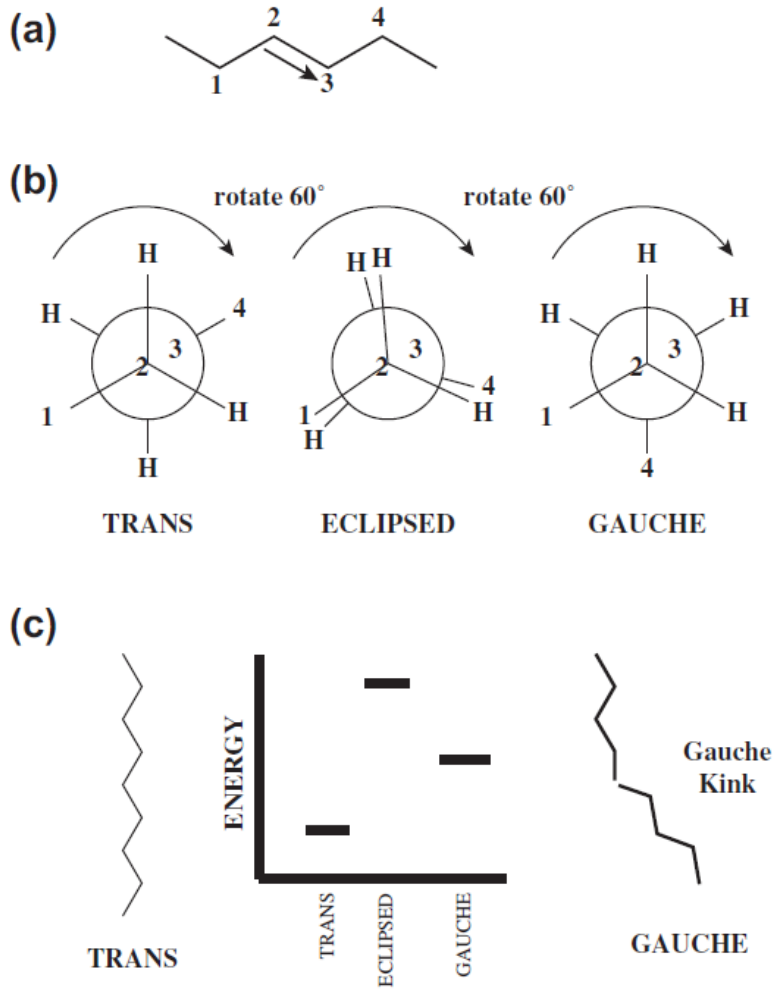

Figura 1.8. Esquema de la fusión de una cadena saturada. a) Representación de un fragmento de 4C en estado no fundido, estado *trans*. b) Proyecciones de Newman para los 4 carbonos secuenciales mostrados en a) donde se demuestra que, al calentar la cadena, se da una rotación alrededor de los carbonos 2 y 3 dando lugar a nuevos estados, eclipsado y *gauche*. En c) se muestran los distintos niveles energéticos de los 3 estados y la formación de los pliegues *gauche*.[29]

Centrándonos en las fosfatidilcolinas, existen distintas temperaturas de transición de fase:

- Temperatura de sub-transición (T_s): es aquella en la que se pasa de una fase cristalina o subgel a fase gel (en cualquiera de sus variantes ya sea normal, inclinada o interdigitada). $L_c/L_{c'} \rightarrow L_\beta/ L_{\beta'}/ L_{\beta I}$

- Temperatura de pre-transición (T_p): corresponde al paso de fase gel a fase periódica ondulada. L_β/ $L_{\beta'}$/ $L_{\beta I} \rightarrow P_\beta$ [30].

- Temperatura de transición de fase principal (T_m): es aquella a la que los fosfolípidos pasan de estado gel con ondulación periódica a líquido cristalino ($P_\beta \rightarrow L_\alpha$). Se la denomina también temperatura de fusión y es la que implica un mayor cambio de entalpía y una alteración significativa en el orden y fluidez de la membrana. Hay varios factores que afectan a la T_m:

    - La naturaleza del grupo polar. Por ejemplo, PE con las mismas cadenas apolares presenta una mayor T_m que PC o PG debido a una interacción más fuerte de la cabeza polar.

    - La longitud de las cadenas hidrocarbonadas. Cuanto mayor es la cola apolar mayor es la T_m.

    - El grado de saturación de las cadenas alifáticas. Fosfolípidos con la misma cabeza polar y longitud de cola apolar, aquellos con insaturaciones presentan una menor T_m.

    - Pureza. Cuanto menor sea la pureza del fosfolípido más amplio será el rango de la T_m, debido a la mezcla de distintas longitudes de las cadenas alifáticas y distintos grados de saturación.

La pre-transición y la transición de fase principal son parte de la transición de fusión de las cadenas de fosfolípidos como las fosfatidilcolinas y la división en dos transiciones es la consecuencia de cambios simultáneos en el orden de los fosfolípidos y la curvatura de la membrana. Como la fase ondulada P_β aparece antes de la fusión de la cadena principal, debe corresponder a una fase lipídica parcialmente desordenada [31]. Por esta razón, se supone que las ondulaciones observadas en la parte superior de las bicapas lipídicas surgen de disposiciones periódicas de dominios lipídicos ordenados lineales y dominios desordenados.

Cambios del pH también puede modular el comportamiento de la fase lipídica como consecuencia de la protonación/desprotonación de los grupos polares [32] alterando la carga superficial de la membrana, la polaridad y su hidratación que determinan en última estancia la temperatura de fusión.

Debido al alto grado de insaturaciones y a la presencia de diversas cadenas de ácidos grasos, la fosfatidilcolina de soja no tiene una temperatura de fusión fija o puntual sino un amplio espectro, desde alrededor de -28ºC hasta unos 5ºC (figura 1.9) lo que dificulta la observación de la fase de pretransición, aun así, durante el calentamiento (curva azul de la figura 1.9) se intuyen dos picos, uno alrededor de -20ºC que podría ser la pretransición y otro pico a -4.5ºC. Esto hace que a temperatura fisiológica la PC se encuentre completamente en fase líquido-cristalina (L_α).

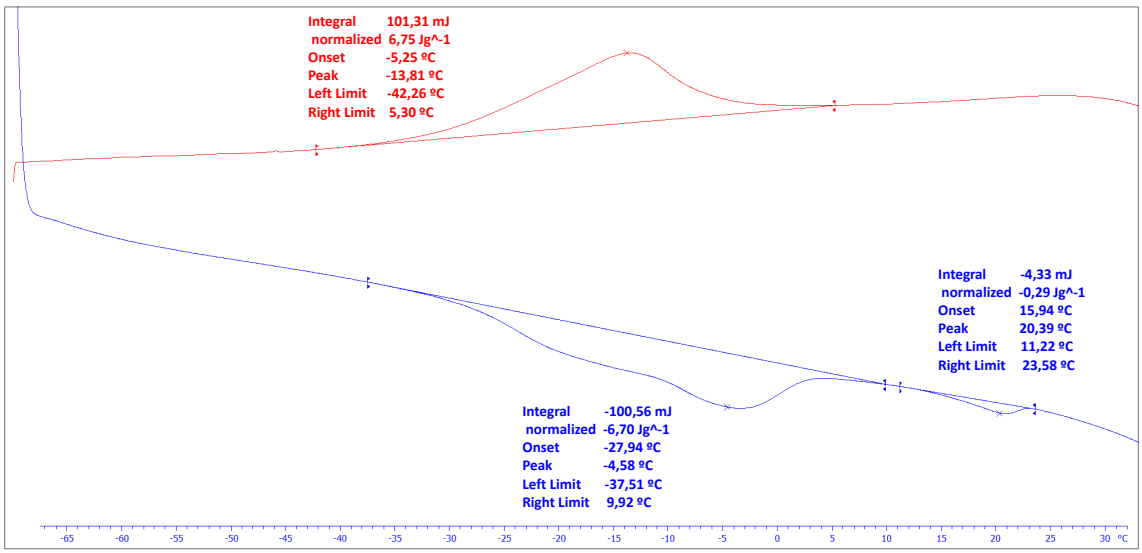

Figura 1.9. Estudio por calorimetría diferencial de barrido (DSC) de la fosfatidilcolina de soja. La muestra encapsulada en un recipiente de aluminio de 40 µL sellado se sometió a un rango de temperatura de -70ºC a 35ºC con un ratio de 2ºC/min. La curva roja representa el enfriamiento mientras que la curva azul es el calentamiento y por tanto la fusión.

1.2.5. Fluidez de las membranas

Las transiciones de fase descritas en el apartado anterior y que ocurren dentro de la membrana se pueden considerar como fenómenos integradores de la organización dinámica molecular de las membranas, las cuales se puede dividir en movimientos conformacionales (relacionados con los movimientos intramoleculares y el orden del empaquetamiento lipídico de largo alcance) y los movimientos de traslación (que indican la posición lateral de la molécula en el plano de la bicapa y están relacionadas

con el orden a corto alcance del empaquetamiento de los lípidos).[33] Por lo tanto, se puede considerar que el término de fluidez de membrana utilizado comúnmente, engloba tanto dinámicas conformacionales (microviscosidad) como traslacionales (difusión lateral).

Sin entrar en mucho detalle ni en ecuaciones matemáticas podemos definir varios parámetros físicos asociados a la fluidez de la membrana (figura 1.10) que nos permiten entender mejor su dinámica:

- Constantes de difusión. La difusión es el movimiento aleatorio de una partícula debido al intercambio de energía térmica con su entorno. En los movimientos de difusión se engloban los de rotación sobre el eje principal del propio fosfolípido y de traslación o lateral en el plano de la membrana [34].

- *Flip-flop.* Este movimiento hace referencia al intercambio o translocación del lípido entre las dos monocapas de la membrana y se caracteriza por ser un proceso muy lento. Se le conoce también como difusión transversal.

- La rotación axial, como se ha descrito anteriormente, consiste en la rotación de los enlaces C-C de las colas apolares y lleva a la formación de pliegues durante la fusión de los fosfolípidos.

- Las cadenas también experimentan movimientos de flexión.

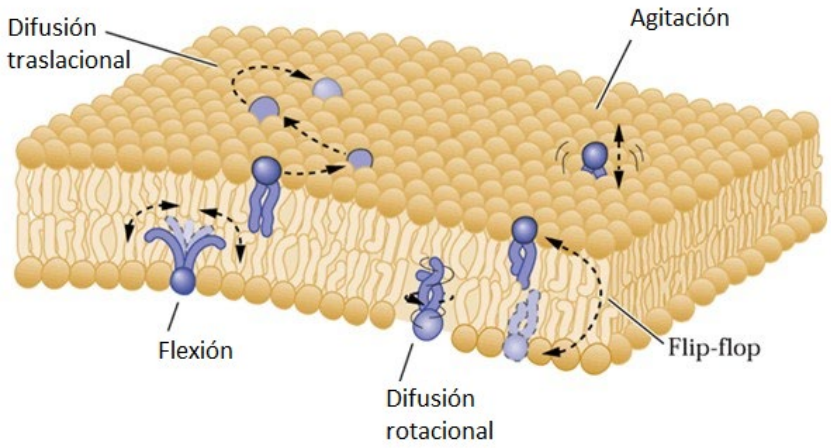

Figura 1.10. Representación esquemática de los distintos movimientos de los fosfolípidos en la membrana y que definen el grado de fluidez. Modificado de [39]

Existen otros parámetros ligados a la fluidez de membrana [35] aunque no impliquen de forma directa movimientos de los lípidos:

- Orden. Este parámetro se relaciona con la orientación de las moléculas lipídicas, siendo por defecto perpendicular al plano de la membrana. A mayor desorden mayor es el ángulo entre el eje longitudinal del lípido y la normal de la membrana hasta 90ºC en el que el lípido se encontraría paralelo al plano de la membrana. El orden además está ligado con el empaquetamiento de los lípidos y se divide en un orden traslacional y uno conformacional.

- Permeabilidad. Para la mayoría de las moléculas apolares externas, la principal vía de penetración a través de la membrana es una combinación entre difusión y partición las cuales dependen en parte de la fluidez de la membrana. Por otra parte, en el caso de, por ejemplo, moléculas cargadas, el paso a través de la membrana se da a través de poros transitorios generados por fluctuaciones termales.

- Microviscosidad. Este parámetro hace referencia a la facilidad y velocidad a la que se producen los movimientos anisotrópicos de los lípidos dentro de la membrana, es decir, la difusión traslacional y rotacional. Habrá por tanto un gradiente de fluidez desde la superficie hacia el centro de la bicapa donde se localizan las colas debido al hecho que las cabezas presentan una velocidad rotacional menor que los extremos hidrofóbicos.

La fluidez es también responsable de la flexibilidad de la membrana que le permite adoptar distintas formas y experimentar multitud de cambios morfológicos entre esas formas. Estas transformaciones se rigen por deformaciones de flexión, que cambian la curvatura de la membrana evitando su ruptura y dependen principalmente de dos parámetros elástico-fluidos [36]: la curvatura espontánea de la membrana, que describe la asimetría entre las dos caras de la bicapa y que puede ser alterada por la inclusión de iones, xenobióticos o proteínas, y su rigidez a la flexión, que se define como la resistencia de la membrana a doblarse de su curvatura preferida. La fluidez de la membrana también implica la formación de compartimentos intramembrana, mediante mecanismos de segmentación y de formación de dominios [37], a través de la posibilidad de cambios en la composición local a través de la difusión lateral de sus componentes.

Diversos factores pueden afectar a la fluidez de la membrana, por ejemplo, los propios fosfolípidos que la componen. Aquellos con colas insaturadas pueden perturbar el empaquetamiento lipídico, aumentando la fluidez de la membrana al impedir que los fosfolípidos saturados se alineen correctamente. La presencia de colas insaturadas pues, aumenta el desorden de la membrana que a su vez implica un mayor espaciado entre las cabezas polares y un debilitamiento de la red de puentes de hidrógenos de moléculas de agua del medio provocando un aumento de la elasticidad de la membrana [38]. A su vez, aumenta la velocidad de hidratación de la membrana comparada con la red perfectamente organizada presente en una membrana bien ordenada.

La presencia de colesterol también es una pieza clave en la dinámica de la membrana. El papel de este esterol es el de ajustar la fluidez de la membrana y por tanto participa en la denominada adaptación homeoviscosa de numerosos seres vivos [40]. De hecho, el colesterol influye de forma significativa en la naturaleza de la fase lipídica. En presencia de esta molécula, la bicapa lipídica adquiere una fase lamelar extra conocida como fase líquido-ordenada (L_o) la cual comparte características entre las fases gel y fluida [41]. Cuando el colesterol se incorpora en una fase gel, ordenada y compacta, el esterol perturba su empaquetamiento y por tanto reduce el orden lipídico. Por el contrario, al intercalarse en una membrana en fase lamelar fluida desordenada, (L_α o también conocida como L_d), la rígida estructura del colesterol favorece la conformación *trans* de las cadenas lipídicas. Así, la nueva fase L_o presenta una difusión rotacional y lateral similar a la de la fase fluida (L_α) pero un orden conformacional típico de una fase gel [42].

1.2.6. Efectos membranotrópicos de xenobióticos

Las distintas fases de los fosfolípidos no solo pueden ser alteradas por el nivel de hidratación de la membrana y la temperatura, y en menor extensión por el tipo de lípido, pH o fuerza iónica sino también por las interacciones lípido-lípido y lípido-péptido que ocurren en la membrana e incluso por la perturbación generada cuando una molécula externa o xenobiótico interacciona con la bicapa lipídica ya sea superficialmente o en su interior. La presencia de estos compuestos puede causar diversos efectos en la biofísica, dinámica y estructura de membrana los cuales a su vez son responsables de cambios relevantes en la actividad celular, así como en la función de proteínas de membrana o en

la transducción o recepción de señales. Los xenobióticos pueden, por ejemplo, alterar la microviscosidad de la membrana, el orden, la formación de dominios, o su curvatura e indirectamente alterar el funcionamiento de enzimas que requieren un entorno muy bien definido para su correcta actividad. El grado de perturbación en la bicapa vendrá dado por la estructura del xenobiótico, sus propiedades fisicoquímicas y los lípidos implicados en la interacción [43]. Los efectos en las membranas que pueden surgir de la interacción xenobiótico-membrana se resumen en la figura 1.11.

La partición o distribución de los xenobióticos (ya sean contaminantes o medicamentos) en las membranas biológicas desempeña un papel importante en su biodisponibilidad, absorción, transporte y distribución. Si consideramos la vía oral como la entrada principal de los xenobióticos debemos evaluar su capacidad de transporte a través del epitelio intestinal, una monocapa de células que recubren el interior del intestino, al ser la barrera que deben cruzar para llegar a la circulación sistémica. Así pues, para una absorción eficiente del tracto gastrointestinal, un compuesto debe atravesar la membrana plasmática de los enterocitos que recubren la luz intestinal, lo que determinará su biodisponibilidad, para bien o para mal. La mayoría de los compuestos atraviesan la membrana plasmática por difusión pasiva a través de la bicapa lipídica [44] por lo que los principales determinantes de la absorción son las interacciones entre el compuesto de interés y los lípidos de membrana.

Por tanto, entender la interacción de fármacos o contaminantes con la membrana es de gran interés para conocer realmente hasta qué punto un compuesto puede alterar nuestro organismo. Eso se debe a que en el pasado solo se consideraba la interacción entre xenobiótico y molécula diana asumiendo que la membrana era una barrera que actuaba solo de forma pasiva pero, actualmente, se sabe que los fosfolípidos pueden interaccionar con los xenobióticos de forma activa.

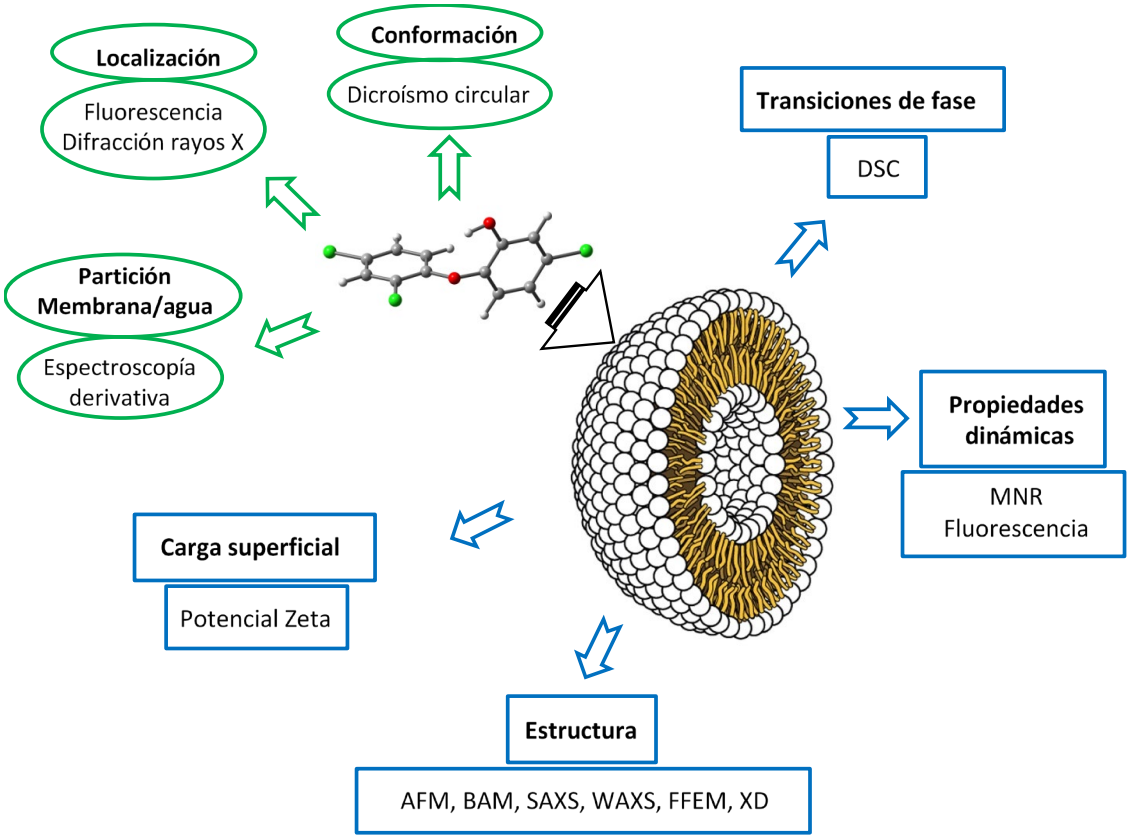

Figura 1.11. Representación esquemática de las técnicas analíticas disponibles para la evaluación de los posibles efectos de los xenobióticos sobre membranas (efectos sobre la estructura de la membrana, la carga superficial, las propiedades dinámicas y la transición de fase) y los efectos de la membrana sobre las moléculas del fármaco o contaminante (efectos sobre la partición del compuesto entre la fase acuosa y la fase lipídica, localización y orientación de la molécula en la membrana, y su conformación). Las técnicas analíticas son las siguientes: Espectroscopia de resonancia magnética nuclear (NMR), difracción de rayos X (XD), microscopía de fuerza atómica (AFM), calorimetría diferencial de barrido (DSC), microscopía de ángulo de Brewster (BAM), dispersión de rayos X de ángulo reducido (SAXS) y de ángulo amplio (WAXS) y microscopía electrónica de criofractura (FFEM).

1.3. Liposomas, modelo mimético de membrana

1.3.1. Breve historia de los liposomas, un accidente fortuito

A inicios de la década de los sesenta, en pleno apogeo de la historia de las biomembranas y su estudio a través del microscopio electrónico, un descubrimiento afortunado tuvo lugar desencadenando lo que sería el surgir de una subdisciplina completamente nueva en el campo de las ciencias farmacéuticas basado en la tecnología de los liposomas y el concepto de nano transportadores de fármacos [45] [46].

En 1962 mientras Alex Bangham se dedicaba al estudio del papel de las membranas biológicas, en particular fosfolípidos, en el proceso de la coagulación de la sangre, observó algo que le dejó fascinado. En sus propias palabras, estaba jugando con frotis (fina película de muestra) de lecitina de huevo en un portaobjetos del microscopio y contempló asombrado la forma en que reaccionaban con el agua para formar frondas móviles de estructura delicada e intrincada [47]. Con ayuda de su compañero Horne observaron esas dispersiones lipídicas con tinción negativa con la ayuda del microscopio electrónico y tras varias sesiones tuvieron la clara evidencia de que los fosfolípidos en agua formaban estructuras tipo bolsa que se ajustaban mucho a lo que habían previsto [48]. Lo único que debían hacer era agitar fosfolípidos en agua y la solvatación y la entropía asegurarían la formación espontánea de sistemas de membrana cerrada, refiriéndose a ellos como mesofases esmécticas multilamelares o esférulas fosfolipídicas [49]. Más tarde las llamarían coloquialmente como Bangasomas o liposomas, término propuesto por Gerald Weissmann [50] y como se les conoce hoy día, definidos como vesículas microscópicas compuestas de una o más bicapas lipídicas.

En los años siguientes, Bangham siguió trabajando y mostrando la utilidad de los liposomas como modelo sintético de membrana [51] para estudiar propiedades fundamentales de las membranas biológicas como la permeación, adhesión y fusión [52–54]. La primera aplicación de Bangham fue el estudio de los mecanismos de acción de anestésicos locales demostrando que los liposomas expuestos a estos fármacos mostraban una mayor permeabilidad a solutos iónicos [55,56]. Otras de sus aplicaciones fue en el tratamiento de la insuficiencia respiratoria en niños recién nacidos mediante un fármaco liposomal constituido por una mezcla de dos fosfolípidos al que bautizó como

ALEC ("artificial lung expanding compound"), de su nombre en inglés [57]. Un año antes de su muerte, y como único autor a sus 88 años, publicó el que sería su último artículo en 2009 [58] con la idea de que las mezclas de materiales volátiles, a los que denominó *bouquet* (aroma en francés), podrían afectar a la respuesta inmune al alterar la carga superficial de las membranas.

Desde los primeros estudios de Bangham, los liposomas siguen siendo un modelo esencial y básico para el estudio de cualquier fenómeno biológico, bioquímico, biofísico, farmacológico o farmacéutico que de una forma u otra involucra a las membranas constituidas por fosfolípidos.

1.3.2. Liposomas

Los liposomas son nanopartículas a base de lípidos compuestas principalmente por fosfolípidos, especialmente fosfatidilcolina (PC), el fosfolípido más abundante en la naturaleza. En medio acuoso, los fosfolípidos se agregan, tal como se ha detallado anteriormente mediante la descripción del Efecto Hidrofóbico, y disponen en estructuras de bicapa, simple o múltiple, formando vesículas esféricas con las colas hidrofóbicas enfrentadas, y las cabezas polares orientadas hacia el núcleo acuoso y la disolución extravesicular [59].

Los liposomas se han usado y siguen usándose ampliamente debido a su biocompatibilidad, biodegradabilidad y baja toxicidad en las industrias cosmética y farmacéutica como vehículos para la administración de medicamentos. Diferentes compuestos pueden ser agregados para cambiar las características de estas nanopartículas lipídicas, como su permeabilidad a un compuesto dado, la carga superficial, el tamaño, la afinidad por un tejido o señal bioquímica actuando como sondas [60]. La adición de colesterol, por ejemplo, puede controlar el orden y la fluidez de la membrana [61] y, por lo tanto, la solubilidad de los medicamentos seleccionados. Los tensioactivos, por otra parte, forman parte de la membrana de los llamados transferomas [62], lo que aumenta su flexibilidad, deformabilidad y, por lo tanto, su facilidad de penetración en la piel, mejorando de este modo la asimilación del medicamento por vía tópica; los ethosomas [63], en cambio incluyen altas concentraciones de etanol en sus formulaciones aumentando también su permeabilidad a través del estrato córneo,

mejorando por tanto la acumulación de fármacos en la piel. Los liposomas sigilosos o furtivos (del inglés "stealth") tienen la superficie recubierta con polietilenglicol (PEG), lo que mejora la estabilidad de estas vesículas en el torrente sanguíneo prologando su tiempo de residencia, haciéndolos más biodisponibles al organismo. Por otro lado, los proteoliposomas [64,65] son aquellas vesículas que contienen tanto fosfolípidos como proteínas, o los magnetoliposomas, con un núcleo magnético, que son utilizados en aplicaciones de fototermia [66], ofrecen un nivel adicional de complejidad. El uso de fosfolípidos de extractos de bacterias (p. Ej., Escheriosoma [67]) o eritrocitos [68,69] son otras formas de obtener liposomas mucho más elaborados y biomiméticos. Los liposomas se usan ampliamente en aplicaciones biomédicas, como nanotransportadores de fármacos [70], sistemas de modelo de membrana celular, biosensores, en imágenes médicas, o adyuvantes en vacunas (virosomas) [71,72] potenciando tanto la inmunidad medida por células como la humoral.

Entre las aplicaciones mencionadas anteriormente, el uso de liposomas como modelo minimalista de membrana celular es una herramienta útil como primera aproximación para el estudio del efecto de compuestos en membranas, ya sean fármacos o contaminantes. Dado que las membranas plasmáticas son demasiado complejas para ser caracterizadas en términos fisicoquímicos simples, el estudio cuantitativo de cuestiones tales como la interacción de estas con fármacos o contaminantes suele realizarse por medio de sistemas modelo. Por lo tanto, para comprender las funciones básicas de las membranas, o los mecanismos por los cuales se someten a transiciones específicas y su dinámica es alterada, se utilizan modelos in *vitro* simples que generalmente consisten en uno o dos componentes. Los liposomas nos permiten estudiar un coeficiente de partición de fármacos más realista en la membrana biológica que el clásico logaritmo de partición octanol-agua (log K_{OW}) [73–76]. Los efectos membranotrópicos causados por los xenobióticos también se investigan ampliamente utilizando liposomas como membranas biomiméticas. Esos fenómenos implican cambios en la bicapa lipídica, como el orden, la fluidez y la permeabilidad que se pueden estudiar a través de diferentes técnicas [77–79] detalladas en la fig. 1.11. La fluorescencia es una técnica de bajo costo, no invasiva y más simple pero indirecta para explorar las alteraciones de la membrana. Para este propósito, en la mayoría de los casos se deben emplear sondas fluorescentes de membrana [80,81].

Hay que tener en cuenta que, al ser los liposomas un modelo simplificado de la membrana plasmática, constituidos solo por la fracción lipídica, los fenómenos de transporte en la bicapa, si los hubiera, serán únicamente por difusión pasiva simple, puesto que, para difusión facilitada y transporte activo, con requerimiento de energía en forma de adenosín trifosfato (ATP), se requiere de la presencia de proteínas [82]. De todos modos, este hecho no es una gran desventaja puesto que como se ha indicado anteriormente, la mayoría de los compuestos atraviesan la membrana por difusión simple.

1.3.3. Clasificación morfológica de los liposomas

Una forma de clasificar los liposomas es en función de su morfología considerando características como su tamaño y número de bicapas.

Los liposomas formados por el método clásico de hidratación del film lipídico, explicado en la siguiente sección, genera como resultado vesículas multilamelares (MLV) con un tamaño alrededor de varios micrómetros. Estos liposomas están formados por bicapas lipídicas concéntricas separadas entre ellas por una capa acuosa. Debido a su formación espontánea son difíciles de controlar por lo que las vesículas originadas son muy heterogéneas tanto en tamaño como en número de bicapas. Son muy usadas a nivel industrial debido a su fácil producción a gran escala por ejemplo en el encapsulado de fármacos [83]. Un post procesado de las MLV nos permite la obtención de vesículas de menor tamaño y formadas por una sola bicapa o lamela como los SUV (*small unilamelar vesicles*), liposomas de entre 25 y 50 nm con una elevada tensión debido a su curvatura, o los LUV (*large unilamelar vesicles*), de un mayor tamaño comprendido entre 100 y 1000 nm. Otros métodos de síntesis dan lugar a liposomas mucho mayores que los LUV, denominados GUV (*giant unilamelar vesicles*), vesículas gigantes mayores de 1 µm. En función del objetivo del estudio se eligen un tipo u otro de liposoma por ejemplo los SUV se usan para explorar parámetros de superficie [84]; los LUV sin embargo son los más usados en el laboratorio como modelos minimalistas de la membrana plasmática en el estudio de, por ejemplo, factores de partición de fármacos o la interacción de xenobióticos con la membrana y sus efectos sobre las propiedades de membrana. Por otro lado, los GUV son ideales para el estudio de transportadores de

membrana mediante la inclusión de proteínas gracias a su elevado volumen interno que permite la entrada de una gran cantidad de moléculas antes de que éstas inhiban el transporte [85].

Otros liposomas menos utilizados son las vesículas oligolamelares (OLV) o multivesiculares (MVV) que implica la presencia de diversas vesículas unilamelares dentro de otra de mayor tamaño y que han sido usadas por ejemplo en el ensamblaje de nanoreactores [86]. Los distintos tipos de liposomas descritos en función de su morfología se detallan en la figura 1.12.

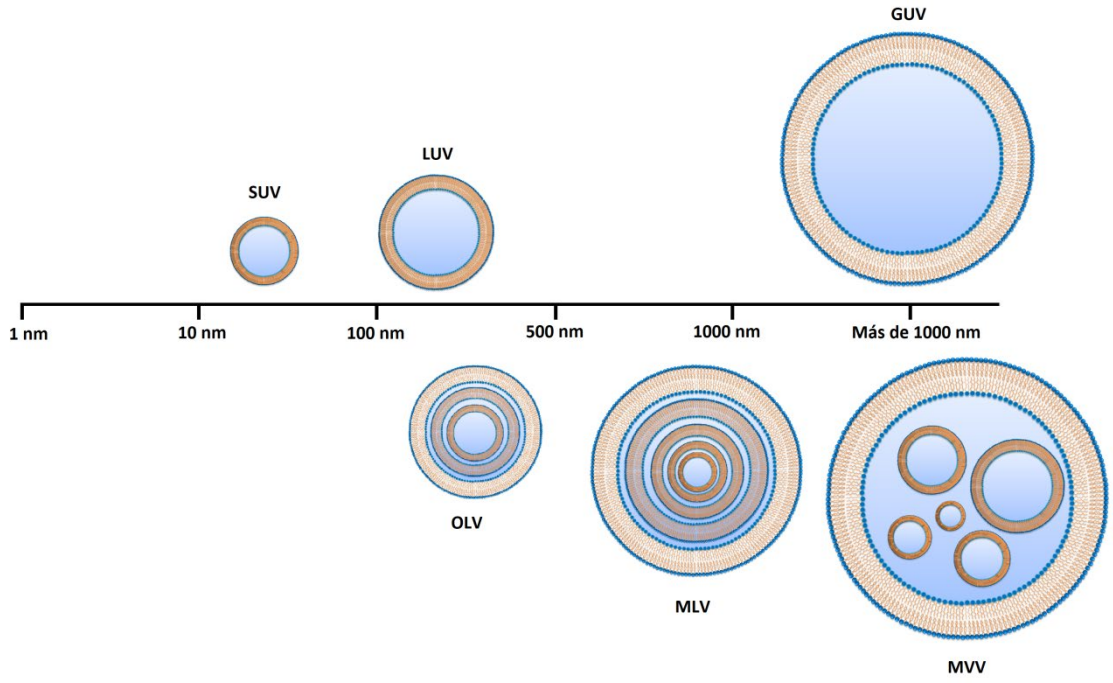

Figura 1.12. Clasificación estructural de los liposomas.

De todas formas, con los avances actuales ya no tiene mucho sentido relacionar la clasificación estructural de los liposomas con su aplicación puesto que a lo largo de estas últimas décadas los liposomas, tal como se ha comentado anteriormente, se han ido perfeccionando y modificando con la adición de otros componentes no lipídicos que mejoran unas u otras características en función del uso que se les va a dar; sobre todo en el campo de la farmacología y medicina.

1.3.4. Métodos de preparación de los liposomas

La preparación de liposomas se puede llevar a cabo mediante diversas técnicas en función del producto final deseado. Una forma de clasificar los distintos métodos de síntesis de liposomas es la siguiente: sonicación, evaporación del disolvente, inyección del disolvente, evaporación de fase inversa y solubilización por surfactante (detergente), los cuales se detallarán a continuación.

1.3.4.1. Sonicación

Mediante agitación mecánica y fenómenos de cavitación los lípidos son directamente solubilizados en el medio acuoso, siendo probablemente el método más usado en la generación de SUVs aunque presenta una serie de desventajas ya sea contaminación metálica en el caso de usar una sonda de ultrasonidos, y degradación de los fosfolípidos o compuestos que vayan a ser encapsulados causado por las elevadas temperaturas locales alcanzadas. La principal ventaja de la sonicación es la prescindencia del uso de disolventes orgánicos. A parte de la sonda de ultrasonidos la cual requiere cierto volumen de muestra y libera una enorme cantidad de energía, también puede hacerse uso de un baño de ultrasonidos. Este segundo método es más versátil ya que permite un control más exacto de la temperatura de la disolución liposomal, se evita la contaminación por metales, se puede trabajar con volúmenes más pequeños de muestra y permite la aplicación de una atmósfera inerte.

1.3.4.2. Evaporación del disolvente

El segundo método se basa en la formación de una fina película de fosfolípidos por la evaporación del disolvente orgánico en el que estaban disueltos y posterior hidratación en un medio acuoso, normalmente un tampón a pH y fuerza iónica controlada descrito por Bangham [54]. Al ser este método el usado a lo largo del presente trabajo, a continuación, se detallan las distintas etapas del mismo:

1. Inicialmente se procede a la preparación de MLVs una vez elegida la composición lipídica (en nuestro caso fosfatidilcolina de soja, LIPOID S100) y

el medio acuoso a utilizar de acuerdo con el objetivo del trabajo. La primera etapa consiste en la disolución de los lípidos. Los lípidos seleccionados se disuelven en un disolvente orgánico y suficientemente volátil, normalmente cloroformo o una mezcla de cloroformo-metanol para aquellos lípidos con carácter más polar, con el fin de obtener una disolución homogénea de los componentes que constituirán la membrana de los liposomas. Normalmente la concentración de lípidos es de 10-100 mg lípido/mL disolvente orgánico. En el caso de la PC de soja, este fosfolípido a temperatura ambiente tiene una textura blanda y muy viscosa lo que dificulta su manipulación.

2. Una vez preparada la disolución lipídica se procede a la formación de una fina película lipídica por evaporación del disolvente. Para ello, un volumen adecuado se adiciona a un matraz de fondo redondo y seguidamente se adapta a un rotavapor. La presión se reduce hasta alrededor de 300 mbar, para favorecer la evaporación del disolvente, pero sin que este llegue a hervir. La temperatura del baño de agua donde se mantiene en todo momento el matraz con la disolución lipídica se ajusta a 30ºC; incrementando la temperatura se acelera el proceso de secado, pero a su vez se favorece la oxidación de los fosfolípidos. Otro factor que influye a la degradación de los lípidos es la radiación solar, para ello procuraremos de algún modo evitar la exposición lumínica de la disolución. En este trabajo se ha optado por envolver el recipiente con papel de aluminio. El rotavapor es clave para la formación de la película lipídica en las paredes del matraz, cuanto mayor sea el matraz mayor será la superficie de evaporación y más fina será la capa de lípidos. Tras un par de horas en el rotavapor el matraz con la pared cubierta por la película de lípidos se acopla a una bomba de vacío para eliminar las trazas de disolvente restantes.

Existen ligeras variaciones en la formación del film lipídico. Para volúmenes pequeños, por debajo de 1 mL, el disolvente orgánico se puede evaporar usando un vial y en campana extractora mediante la corriente de algún gas inerte como el nitrógeno o argón. Otra opción es el uso de un disolvente orgánico con un punto de fusión cercano a la temperatura ambiente como el ciclohexano o terbutanol. La disolución lipídica preparada en uno de estos disolventes se congela mediante un baño de hielo seco y a continuación se liofiliza en bomba de vacío hasta su secado.

3. La siguiente etapa es la hidratación de la película lipídica. Para ello se adiciona el volumen deseado de la disolución acuosa seleccionada que consistirá en una disolución tampón a pH y fuerza iónica fisiológicos. En el caso de usar fosfolípidos con temperaturas de transición de fase de gel a líquido cristalino (T_m) por encima de la temperatura ambiental se debe calentar la disolución acuosa por encima de esta. Si se usa una mezcla de fosfolípidos se trabajará siempre sobre la temperatura del fosfolípido con la mayor T_m. Para favorecer la hidratación se usa agitación por vortex o baño de ultrasonidos hasta que todos los lípidos se desprendan de las paredes del matraz y se hayan incorporado a la disolución. Este proceso suele durar alrededor de 1h. En todo momento la mezcla se mantendrá por encima de la T_m. En este momento la disolución acuosa habrá adquirido un aspecto lechoso, de color blanquecino y con cierta turbidez. Se recomienda dejar reposar la disolución para que los liposomas formados, en su estado líquido cristalino, se terminen de hidratar y estabilizar, para ello se suele dejar la disolución liposomal toda la noche en nevera. Esta etapa de envejecimiento o maduración hace que el siguiente paso de dimensionado sea más fácil y mejore la homogeneidad de la distribución de tamaños. Los liposomas formados son de gran tamaño, por encima de 1 μm, y multilamelares (MLVs) con una estructura análoga a la cebolla, es decir, vesículas con varias bicapas cada una de ellas separada de las demás por una capa acuosa (ver fig. 1.12). Si la hidratación del film lipídico se realiza de forma natural a lo largo de varios días se obtienen liposomas gigantes (GUV) de hasta 10 μm [87]. Los GUV también se pueden obtener por electroformación aplicando un campo eléctrico e hidratando el film lipídico durante varias horas [88–90].

Procesado secundario de los liposomas para el ajuste de tamaño

Una vez los MLVs se han hidratado y estabilizado, se requiere un post procesado para la obtención de liposomas de menor tamaño y unilamelares (LUVs o SUVs) [91], en el caso de necesitarlo, puesto que para la mayoría de supuestos, los MLVs son demasiado grandes y heterogéneos. Este procesado secundario se consigue con varias técnicas siendo la extrusión o la ultrasonicación las más frecuentes, tal como se describen a continuación.

Extrusión

La extrusión mediante la prensa francesa implica el paso de liposomas a través de un pequeño orificio a elevada presión, unos 20000 psi. El método es simple, rápido, reproducible y permite el manejo delicado de muestras inestables. La membrana porosa consiste normalmente en un filtro de policarbonato de poro controlado (desde 0.03 a 1 μm) que permite elegir el tamaño final de los liposomas. La extrusión suele usarse para la generación de LUVs, siendo un método más preciso que la sonicación en la obtención de vesículas con un bajo índice de polidispersión. La extrusión de por sí no es una técnica de preparación de liposomas, sino que previamente deben haber sido sintetizados con otros métodos tal como se ha comentado anteriormente.

En nuestros experimentos, para la obtención de LUVs se ha utilizado un miniextrusor de membrana de la casa comercial Avanti Lipids. Este pequeño instrumento de uso manual consiste en:

- Bloque metálico de alta conductividad térmica, permite la síntesis de liposomas cuyos fosfolípidos tengan una T_m por encima de la temperatura ambiental.
- Dos jeringas de cristal de 1mL.
- Mini-extrusor de acero inoxidable y teflón el cual se divide en una serie de componentes detallados en la figura 1.13.

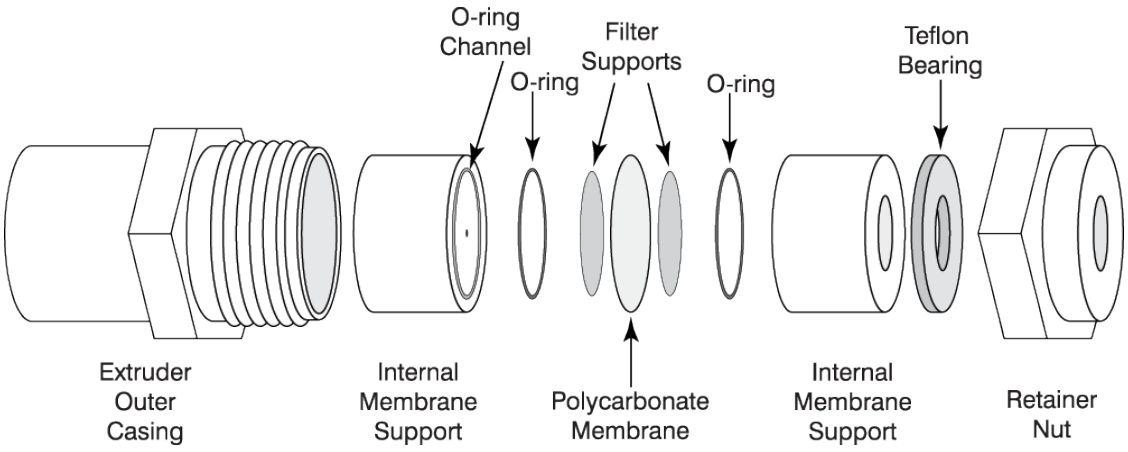

Figura 1.13. Diagrama de las distintas partes del extrusor. Extraído de avantilipids.com/.

Se debe tener en cuenta que para la extrusión de liposomas se necesitan una serie de pases a través del filtro del tamaño de poro elegido para obtener liposomas de baja polidispersión y de la medida deseada. En la figura 1.14 se puede observar que antes de pasar por el extrusor con una membrana de 100 nm, los liposomas miden más de 1000 nm y que un solo pase por el filtro ya desplaza la distribución por debajo de los 1000 nm, aunque a su vez la polidispersión se hace mayor tal como indica el mayor ancho de banda. Tras 3 pases por el extrusor el máximo del pico cada vez se desplaza a tamaños menores y la amplitud de banda se reduce. Al cabo de 29 pases la pequeña banda situada entre los 1000 y 10000 nm ha desaparecido, habiendo un solo pico de gran intensidad y baja amplitud de banda situada cerca de los 100 nm. Hay que tener en cuenta que las medidas obtenidas mediante DLS (*dynamic light scattering*) toman en consideración el radio hidrodinámico, es decir, la esfera de solvatación que envuelve a los liposomas de modo que ese tamaño siempre es ligeramente superior al que tendría el liposoma propiamente dicho y del que se obtendría mediante microscopía de transmisión. De todos modos, el diámetro medio de los liposomas siempre será levemente mayor a la del tamaño del poro del filtro usado, debido a la flexibilidad de la membrana lipídica.

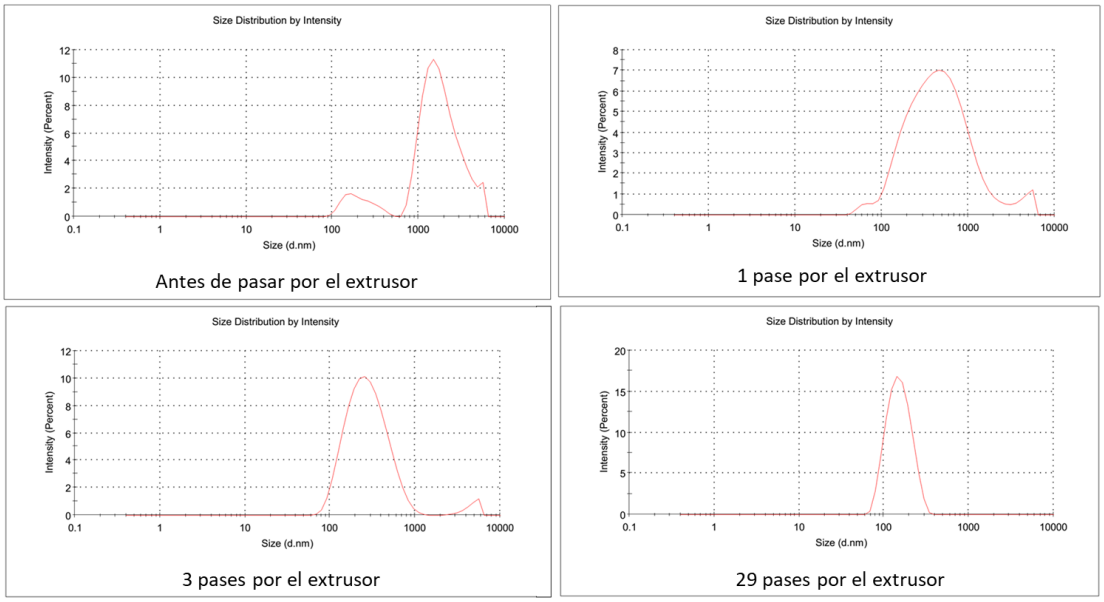

Figura 1.14. Diagramas de distribución de medidas por intensidad mediante DLS con distinto número de pasos por el extrusor.

Sonicación

Mediante la aplicación de ultrasonidos durante unos 5-10 min por encima de la T_m, se consiguen SUVs de alrededor de 15-50 nm de diámetro a través del quebrantamiento de los MLVs. Se puede usar tanto un baño como una sonda de ultrasonidos. El primero suele usarse para soluciones liposomales diluidas mientras que el uso de la sonda es necesario para suspensiones de fosfolípidos concentradas que requieren un gran aporte de energía. Tal como se indicó anteriormente, la sonda puede provocar contaminaciones por desprendimiento de trazas de metal en la disolución y degradación del producto debido a la elevada temperatura que adquiere la muestra durante el tratamiento de sonicación. Otro problema de la sonicación es la baja reproducibilidad, lo que conlleva la obtención de liposomas de distintos tamaños entre lotes debido a la dificultad de reproducir exactamente las mismas condiciones del proceso. La generación de SUVs se verifica por el aclaramiento de la suspensión de lípidos obteniéndose una mezcla más transparente. La turbidez se debe a la dispersión de la luz provocada por los MLVs en suspensión residuales. Se puede realizar una etapa de centrifugado para separar esas partículas de mayor tamaño y obtener una suspensión clara de SUVs. Un inconveniente de estos liposomas de reducido diámetro es su elevado grado de curvatura siendo por tanto inherentemente inestables. Si se mantienen por debajo de su T_m, los SUVs tienden a fusionarse de forma espontánea para formar vesículas de mayor tamaño.

1.3.4.3. Inyección o dispersión de disolvente

En los métodos de síntesis por dispersión de disolvente, los lípidos son disueltos en un disolvente orgánico. La disolución lipídica es entonces puesta en contacto con la disolución acuosa. Los lípidos se reorganizan en la interfase entre los dos disolventes en forma de monocapa siendo este el primer paso para la formación de la bicapa de los liposomas, de modo que las colas apolares están en contacto con el disolvente orgánico y las cabezas polares con el medio acuoso. Dentro de esta categoría podemos distinguir 3 metodologías en función de los disolventes usados y sus proporciones ya sea (i) el uso de un disolvente orgánico miscible en la fase acuosa, (ii) un disolvente orgánico inmiscible en el medio acuoso el cual se encuentra en exceso, o bien (iii) un disolvente orgánico inmiscible en exceso en el medio acuoso. Las más usadas son:

Inyección de etanol

En el primer caso descrito en el apartado previo una disolución de lípidos en etanol es rápidamente inyectada mediante una fina aguja en un medio acuoso, normalmente una disolución tampón de pH fisiológico, en exceso. De ese modo, los lípidos se dispersan uniformemente en todo el medio. A medida que el etanol se diluye llega a una concentración crítica que fuerza a los fosfolípidos a auto-ensamblarse en la fase acuosa y se forman espontáneamente SUVs [92]. La desventaja de este método es la baja solubilidad de los lípidos en etanol lo que a su vez implica que los liposomas se encuentren muy diluidos. Otro problema es la formación de una mezcla azeotrópica del etanol con el agua, lo que dificulta la eliminación total del primero.

Inyección de éter

En la inyección de éter, la disolución de lípidos en la fase orgánica se inyecta lentamente en el medio acuoso en exceso a una temperatura suficientemente alta, o a baja presión, de modo que el disolvente se vaya evaporando durante el proceso de mezcla [93]. Los liposomas obtenidos en este caso son mayores que con la inyección de etanol, pero el hecho de que el éter se evapore a la vez que es inyectado permite soluciones lipídicas de elevada concentración.

1.3.4.4. Evaporación de fase inversa

La metodología denominada evaporación de fase inversa implica la formación de micelas invertidas [94] y podría englobarse dentro de la metodología (iii) de la categoría anterior. Se inicia el proceso con la formación de una emulsión, con ayuda de una breve etapa de sonicación, de la fase acuosa en un exceso de fase orgánica con los lípidos disueltos originando las mencionadas micelas invertidas. El disolvente orgánico se elimina lentamente a baja presión provocando el colapso de las micelas a un estado de gel viscoso y finalmente a una suspensión acuosa. Los liposomas se forman en un punto crítico en el que ese estado gel colapsa y algunas de las micelas se desintegran. El exceso de fosfolípidos en el medio conforma bicapas alrededor de las micelas restantes en el medio, lo que resulta en la formación de liposomas LUVs y MLVs.

1.3.4.5. Solubilización por surfactante

Para finalizar, la solubilización por surfactante consiste en que la mezcla lipídica se incorpora en el medio acuoso con ayuda de micelas de detergente. De este modo se forman micelas mixtas que, a medida que se elimina el surfactante por distintos medios (normalmente diálisis [95,96]), se enriquecen en fosfolípidos hasta que se combinan para formar liposomas, normalmente LUVs.

A parte de todas esas técnicas clásicas descritas, la gama de métodos de preparación de liposomas se ha visto ampliado mediante nuevas técnicas para adaptarse a la producción a escala industrial [97], puesto que los métodos clásicos consumen grandes cantidades de disolventes orgánicos y constan de diversas etapas para su homogeneización que consume demasiada energía para su síntesis a gran escala. Además estos últimos años se han propuesto mejoras en los procesos convencionales y llevado a cabo el desarrollo de nuevas rutas para la síntesis de liposomas con la idea de, por ejemplo, reducir el uso de disolventes orgánicos [98] como los métodos microfluidicos [99] o basados en el uso de fluidos supercríticos [100].

1.4. Técnicas para la determinación de parámetros de membrana

1.4.1. Técnicas fluorimétricas

Las técnicas fluorimétricas más empleadas para determinar párametros de membrana son la polarización generalizada y anisotropía, las cuales se detallan a continuación.

1.4.1.1. Polarización generalizada

Los distintos parámetros que determinan el estado de la membrana, como son el orden, el empaquetamiento o la fluidez de la membrana generalmente se miden por resonancia de espín electrónico, resonancia magnética nuclear, y difusión de moléculas de membrana, por citar algunas. Una forma indirecta, pero simple y sencilla, de inferir las

características de las membranas es utilizar sondas sensibles a la polaridad cuyos espectros de emisión cambian con la polaridad del medio que les rodea. La polaridad en las membranas biológicas generalmente representa el nivel de hidratación de la bicapa, por lo que existe una relación entre ambos conceptos. En los capítulos 3, 4, 5 y 6 de esta tesis se utilizarán las sondas denominadas Laurdan y Prodan.

Dentro de la membrana, en ambientes no polares, el fluoróforo naftaleno, presente en las sondas Laurdan y Prodan, experimenta un máximo de intensidad de longitud de onda de emisión centrado a 440 nm. Sin embargo, al incrementarse la polaridad de la membrana alrededor de la sonda, se observa un desplazamiento batocrómico (hacia el rojo) continuo del espectro de emisión debido a la hidratación de la membrana la cual es un indicador de la perturbación de las vesículas lipídicas. La entrada de agua conlleva una pérdida de orden y empaquetamiento de los fosfolípidos que puede medirse de forma semicuantitativa e indirecta mediante medidas fluorimétricas de las sondas de membrana mencionadas. Este comportamiento característico del grupo naftaleno es debido a las moléculas de disolvente que rodean al fluoróforo formando dipolos y alineándose a lo largo de este al ser excitado. La reorientación de los dipolos de disolvente en las inmediaciones de la sonda requiere energía lo que provoca, por tanto, una disminución de energía del estado excitado del naftaleno. Este fenómeno se conoce como relajación dipolar y es el causante del desplazamiento del máximo de emisión de la sonda hacia valores alrededor de 490 nm, debido a la formación de un estado excitado de transferencia de carga estabilizado por el proceso de reorientación de los dipolos de las moléculas de agua [101,102]. Cuanto mayor sea el proceso de relajación del agua acontecido en el entorno de la sonda, más notable es el efecto membranotrópico. Dicho de otro modo, cuanto mayor sea la cantidad de moléculas de agua (u otro disolvente polar) alrededor del fluoróforo, mayor es el desplazamiento hacia el rojo del máximo del espectro de emisión de la sonda. Para medir este efecto se recurre a la técnica denominada polarización generalizada (GP) definida por la ecuación 1.1:

$$GP = \frac{I_B - I_R}{I_B + I_R} \qquad Ecuación\ 1.1$$

Donde I_B y I_R se refieren a las intensidades de fluorescencia del máximo de emisión de la sonda en sus componentes espectrales azul y rojo respectivamente, eso es a 440 nm y 490 nm; estos valores a su vez se corresponden al máximo de emisión de la sonda en

fase gel (sobre 440 nm) y líquido cristalino (sobre 490 nm) [103] respectivamente, aunque los valores pueden variar ligeramente en función de los fosfolípidos de la membrana. Los valores otorgados por esa ecuación se relacionan con el orden y empaquetamiento de los lípidos dentro de la membrana y también de su hidratación. Todos estos parámetros a su vez son característicos de la fase/estado de la membrana. Una membrana en fase gel cuyos fosfolípidos presentan un alto grado de empaquetamiento da como resultado valores de GP positivos, pero nunca mayores de +1; mientras que una fase líquido cristalina, caracterizada por una membrana más desordenada e hidratada da valores de GP negativos hasta -1.

En este trabajo la selección de las sondas hidrofóbicas, Prodan y Laurdan para el estudio de GP es debido a que ambas son capaces de detectar cambios en el empaquetamiento y orden lipídico como consecuencia de su fuerte sensibilidad a la polaridad del medio que las rodea. Mientras que Prodan nos informa de cambios e interacciones a la altura de la cabeza polar de los fosfolípidos, la sonda Laurdan caracterizada por una cola hidrofóbica 4 veces más larga (3 carbonos en el caso de Prodan y 12 en el caso de Laurdan) se sitúa ligeramente a mayor profundidad, a la altura del glicerol, es decir, en la interfase hidrofílica-hidrofóbica de la membrana con su cola de ácido láurico fuertemente anclada entre las colas de los fosfolípidos mediante fuerzas de Van der Waals. A lo largo de los experimentos realizados durante este trabajo se ha observado de hecho que la sonda Prodan presenta una gran movilidad dentro de la membrana cuando esta se encuentra en fase líquido-cristalina y que su posición dentro de la membrana es difícil de predecir. Este comportamiento errático del fluoróforo dentro de la fase hidrofílica de los fosfolípidos, dificulta los cálculos de GP. Teniendo en cuenta la estructura de ambas sondas es fácil entender que la mayor movilidad del Prodan es debido a su cola apolar de ácido propanoico mucho más corta que la de Laurdan lo que hace que el Prodan sea también parcialmente soluble en agua. Otro punto importante a tener en cuenta es que, debido a su localización mucho más superficial en la membrana, y por tanto en un ambiente más polar, la sonda Prodan es más sensible a la rotación de los dipolos de agua que se mueven más libremente en la interfase membrana/medio acuoso. Si se analiza el desplazamiento del máximo de emisión de ambas sondas por debajo y sobre la temperatura de transición en liposomas sintetizados con un mismo

fosfolípido se observa otra diferencia clave entre Laurdan y Prodan: la segunda nos permite detectar claramente la pre-transición a la altura de las cabezas polares.

Laurdan y Prodan fueron por primera vez diseñadas y sintetizadas por Gregorio Weber con el propósito de estudiar el fenómeno de la relajación dipolar [104,105]. El residuo fluorescente de naftaleno presente en estas sondas posee un momento dipolar debido a la separación parcial de cargas entre los grupos 2-dimetilamino y 6-carbonil. Este momento dipolar experimenta un incremento al ser excitado siendo capaz de causar el reordenamiento de las moléculas de disolvente cercanas. Cabe remarcar que el fenómeno de relajación dipolar solo se da en medios polares, y que el desplazamiento batocrómico gradual del espectro de emisión tiene lugar por encima de la temperatura de transición, mientras que por debajo de este punto, en la fase gel, caracterizada por un alto grado de empaquetamiento, no hay una relación entre temperatura y desplazamiento del máximo de emisión de la sonda, por lo que la relajación dipolar acontece solamente cuando los fosfolípidos se encuentran en fase líquido cristalina. Esta particularidad nos permite determinar la temperatura de transición de fase de los fosfolípidos que se corresponde al punto de inflexión de la curva obtenida al representar los valores de GP frente a temperatura ya que la GP a esa temperatura experimenta un cambio abrupto. No solo eso sino que experimentos previos [103] revelan que la relajación dipolar es independiente del grupo polar y de la carga de los fosfolípidos y también del pH en un rango de 4 a 10, de modo que este fenómeno se debe únicamente al estado de fase de la membrana. La concentración y la dinámica molecular de las moléculas de agua integradas dentro de la membrana varían en función de la fase de los fosfolípidos.

Tal como se ha comentado anteriormente, la medida de GP nos permite conocer la velocidad y magnitud del proceso de relajación dipolar, pero además, la sonda Laurdan nos permite el estudio de la posible coexistencia de fases y su interconversión [106,107]. Eso es debido a que el espectro de excitación de la sonda Laurdan en fase líquido-cristalina experimenta una disminución de intensidad a longitudes de onda más largas respecto al espectro de excitación en fase gel. En la fase líquido-cristalina pura, a elevada temperatura, el valor de GP es más alto excitando a una longitud de onda baja cerca a los 320 nm y va disminuyendo gradualmente hasta un mínimo alrededor de los 410 nm. Durante la transición de fase de los fosfolípidos se observa el fenómeno contrario, tiene lugar un aumento progresivo de la GP hacia longitudes de onda de

excitación más largas. En cambio, cuando los fosfolípidos se encuentran en fase gel, el valor de GP es independiente de la longitud de onda de excitación usada.

El fenómeno de la polarización generalizada es muy complejo e incluso todavía ahora aún se presentan nuevas perspectivas en cuanto a los espectro de emisión de Prodan y Laurdan [108,109] y en este trabajo solamente se detallan varios puntos básicos para su entendimiento y aplicación haciendo uso de un modelo simplificado y de fluorescencia en estado estacionario. Sin embargo, la comprensión incompleta de los detalles de la fotofísica de la sonda Laurdan no impide su uso para la determinación del grado de relajación dipolar ni de la coexistencia de las distintas fases en la membrana. Para una lectura y comprensión mucho más profunda y completa se debe recurrir a estudios de espectroscopía de fluorescencia resuelta en el tiempo la cual se aleja de los experimentos de este trabajo. Por favor, si es de su interés, haga uso de las diversas citas que acompañan al texto.

1.4.1.2. Anisotropía

La anisotropía de fluorescencia se basa en el principio de que el grado de anisotropía de una molécula en disolución, en este caso un fluoróforo, en unas condiciones de temperatura y viscosidad constantes, está relacionado inversamente con su rotación molecular y directamente con su peso molecular aparente que cambiará en el caso de formación de complejos. En este trabajo, el objetivo no es buscar la formación del complejo y sus respectivas constantes de formación-disociación sino estudiar los cambios de fluidez, y por tanto de viscosidad, que acontecen en la membrana tras la adición de distintos compuestos, ya que el valor de anisotropía variará en función de la microviscosidad del entorno donde se encuentre nuestra sonda fluorescente dentro de la bicapa lipídica.

La anisotropía (r) se usa para caracterizar el grado de polarización lineal de la emisión de fluorescencia resultante de la fotoselección de una muestra ópticamente isotrópica, es decir, que sus propiedades son iguales en todas direcciones. Manteniendo la excitación polarizada verticalmente se puede observar la intensidad de fluorescencia de un fluoróforo a través de la orientación paralela (vertical) o perpendicular (horizontal) del

filtro polarizador de emisión, I_{VV} y I_{VH}, respectivamente. En el caso de una excitación continuada la anisotropía en estado estacionario se define con la ecuación 1.2.

$$r_{ss} = \frac{I_{VV} - I_{VH}}{I_{VV} + 2I_{VH}} \qquad Ecuación\ 1.2$$

El denominador se considera equivalente a la intensidad total, es independiente de la polarización y se define como la suma de los tres componentes de emisión mutuamente ortogonales entre sí [110].

Existen diferentes fuentes de errores e incertidumbres a tener en cuenta al determinar la anisotropía de fluorescencia, por lo que los valores de anisotropía obtenidos experimentalmente suelen precisar de una corrección de errores y efectos sistemáticos causados por el propio instrumento o por las propiedades de la muestra.

La respuesta de los elementos ópticos y el detector de radiación electromagnética pueden ser muy diferentes para los componentes verticales y horizontales de la emisión de fluorescencia polarizada. La transmisión de monocromadores de rejilla, por ejemplo, es particularmente sensible a la orientación lineal de polarización del haz entrante, un efecto que también puede ser muy dependiente de la longitud de onda. Esta sensibilidad diferencial del canal de detección puede corregirse (en cada longitud de onda de emisión, λ_{em}) por el factor G, que representa la relación de la sensibilidad del sistema de detección para la luz polarizada vertical frente a la polarizada horizontalmente [111], de acuerdo a la ecuación 1.3:

$$G = \frac{I_{HV}}{I_{HH}} \qquad Ecuación\ 1.3$$

De modo que la ecuación de anisotropía con el factor de corrección G queda definida por la ecuación 1.4:

$$r_{ss} = \frac{I_{VV} - GI_{VH}}{I_{VV} + 2\mathrm{G}I_{VH}} \qquad Ecuación\ 1.4$$

En un entorno viscoso (figura 1.15.a) como puede ser el caso de una membrana en estado gel, las moléculas de fluoróforo al estar en un ambiente restrictivo estarán con el dipolo orientado de forma paralela a la luz polarizada de excitación vertical dando un valor de anisotropía elevado. En el caso contrario, cuando el fluoróforo se encuentra en

un ambiente fluido donde puede rotar libremente (figura 1.15.b), las moléculas estarán orientadas de forma aleatoria dentro de la membrana de modo que al incidir la luz polarizada solo serán excitadas aquellas con el dipolo orientado paralelamente al haz de excitación vertical provocando que la emisión polarizada sea solo parcial dándose el fenómeno de fotoselección. Por tanto, la anisotropía nos permite medir la rigidez de un entorno molecular haciendo uso de fluoróforos cuya localización dentro de la membrana es conocida.

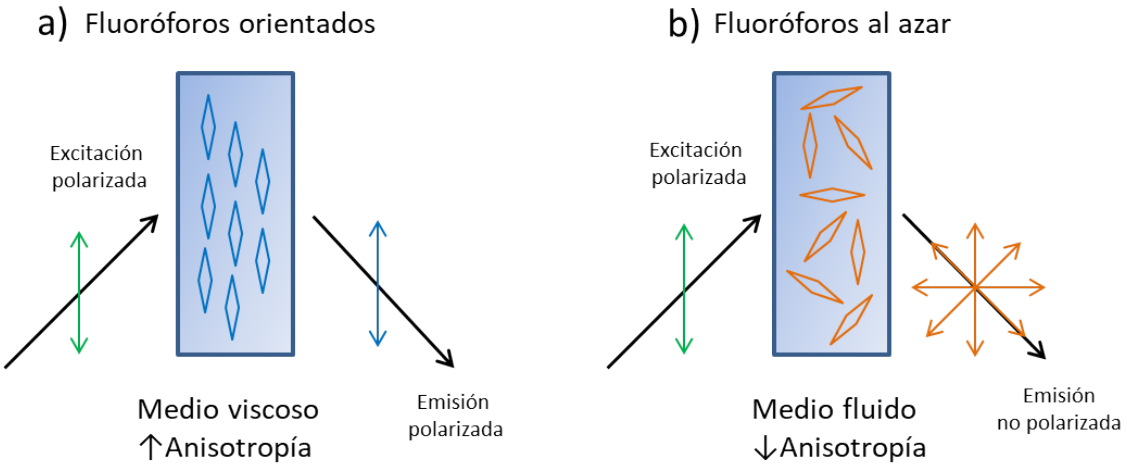

Figura 1.15. Efectos de la excitación polarizada y la difusión rotacional en la polarización o anisotropía de la emisión de un determinado fluoróforo en a) un medio viscoso y b) un medio fluido. Modificado de [102].

1.4.2. Otras técnicas de análisis de membrana

Aunque el valor de GP se obtiene fácilmente y es muy útil para demostrar cambios relativos en el empaquetamiento, polaridad y orden de los fosfolípidos de la membrana, este parámetro puede pasar por alto varios aspectos fisicoquímicos de la membrana. Una razón para esta limitación es la falta de conocimiento de los mecanismos exactos que acontecen tras los cambios espectrales en la emisión de fluorescencia de las sondas de membrana. Por lo tanto, dichos mecanismos deben abordarse a fondo antes de interpretar con precisión cualquier valor empírico obtenido mediante el uso de estas sondas y los valores de GP.

El uso de otras técnicas en conjunto con la fluorescencia nos permite un entendimiento mucho más amplio y específico de los fenómenos acontecidos en la membrana tras la interacción de los contaminantes de interés, eso es, los efectos membranotrópicos. Así, un estudio holístico de la interacción contaminante-membrana nos da una visión mucho más real del fenómeno al abordarlo desde distintos puntos de vista.

En el capítulo 3 se detallan los estudios realizados por cálculos de la teoría del funcional de la densidad (DFT) basados en mecánica cuántica a los que se han recurrido, con la colaboración de los miembros del grupo de química supramolecular (SUPRAMOL) de la UIB, para investigar complejos no covalentes 1:1 de las sondas fluorescentes y contaminantes emergentes con dipalmitoilfosfatidilcolina, como un modelo minimalista de un liposoma, para evaluar tanto las energías de interacción como las geometrías de los complejos.

En el capítulo 4 se exploran las interacciones de los contaminantes con la membrana liposomal mediante i) estudios por espectroscopía de resonancia magnética nuclear de protón (^{1}H-RMN), que nos permite conocer a nivel atómico la arquitectura específica de las interacciones de los compuestos de interés con los fosfolípidos de los liposomas y ii) simulaciones por medio de cálculos computacionales de dinámica molecular (basados en cálculos de mecánica clásica) tomando como modelo de estudio un fragmento de la bicapa constituido por 128 fosfolípidos que nos permite un mayor conocimiento de las localizaciones más probables de los distintos contaminantes estudiados dentro de la bicapa lipídica. Estos experimentos se han llevado a cabo con la ayuda del grupo de reactividad molecular y diseño de fármacos (REACMOL) de la UIB.

1.5. Toxicidad, evaluación del daño provocado por los xenobióticos en modelos biológicos

La disminución de la contaminación de fuentes puntuales y la prohibición de algunos productos químicos persistentes de acuerdo a normativas internacionales y europeas como el caso del REACH han tenido efectos positivos en el nivel de contaminación ambiental en las últimas décadas. Sin embargo, al mismo tiempo, el desarrollo industrial se ha dedicado al diseño y síntesis de nuevos productos que afectan nuestra vida diaria.

Para mejorar su tiempo de vida útil, se han introducido en el mercado compuestos orgánicos con determinadas propiedades fisicoquímicas, como antimicrobianos, retardantes de llama, conservantes, nanomateriales, plastificantes y aditivos, para reemplazar, a su vez, los productos prohibidos, lo que ha generado preocupaciones medioambientales debido a su alta tasa de producción y uso generalizado. Otros productos como fármacos (antiinflamatorios, antidiabéticos, antibióticos) y productos para el cuidado personal, que incluyen cosméticos, protectores solares UV y fragancias [112], se llevan utilizando desde hace tiempo. Estudios recientes han demostrado que todas estas especies son sustancias químicas ambientalmente persistentes y, en algunos casos, eliminadas de forma incompleta por las plantas de tratamiento de aguas residuales o procesos de biodegradación [113,114]. Además, estos compuestos pueden tener efectos adversos en el funcionamiento de los ecosistemas y la calidad de los entornos acuáticos [115]. Por todo ello se debe identificar los posibles efectos nocivos sobre la salud humana y ecológica para el uso seguro de estos productos químicos.

El término "contaminantes de preocupación emergente" o "contaminantes emergentes" se refiere a las clases de compuestos que actualmente se sabe que son persistentes en el medio ambiente debido a la introducción ininterrumpida como resultado de actividades antropogénicas, provocando un impacto ecológico y en la cadena trófica, pero que aún no están regulados [116,117]. La Comisión Europea es consciente de la aparición de cantidades crecientes de estas especies con posibles efectos nocivos para la fauna y flora silvestre y, por lo tanto, ha publicado recientemente dos Listas de Vigilancia (Watch Lists): (i) Commission implementing decision (EU) 2015/495 of 20 March 2015 establishing a watch list of substances for Union-wide monitoring in the field of water policy pursuant to Directive 2008/105/EC of the European Parliament and of the Council, *Off. J. Eur.* L 78 (2015) 40-42 y (ii) Commission Implementing Decision (EU) 2018/840 of 5 June 2018 establishing a watch list of substances for Union-wide monitoring in the field of water policy pursuant to Directive 2008/105/EC of the European Parliament and of the Council, *Off. J. Eur.* L 141 (2018) 9-12. La Watch List de 2018 añade nuevas sustancias que deben ser monitorizadas en toda la Unión en el ámbito de la política de aguas de conformidad con la Directiva 2008/105/ CE [UE 2015/495]. Las sustancias presentes en esta lista se seleccionan entre aquellas para las cuales la información actual disponible indica que pueden representar un riesgo

significativo para la biota y la salud humana a través del medio acuático, y aquellas que se identifican como contaminantes emergentes potenciales para los que existen una falta de datos de monitoreo. La exposición/evaluación de riesgo apropiada de esas especies está asociada a los llamados estudios exposómicos [118,119]. Dentro de la evaluación del riesgo de los contaminantes se engloban los ensayos de toxicidad a distintos niveles, ya sea en células individuales, microorganismos unicelulares, pluricelulares u organismos avanzados.

1.5.1. Ensayos de citotoxicidad

Los ensayos de citotoxicidad con células de mamíferos resultan ser de gran utilidad para la detección de los posibles efectos adversos de xenobióticos sobre la salud humana. Existen un gran número de líneas celulares y protocolos para evaluar la acción de un fármaco o contaminante sobre la viabilidad celular. Entre ellas destaca el uso de líneas inmortales o tumorales.

A pesar de las limitaciones a la hora de extrapolar las observaciones de ensayos *in vitro* a *in vivo* [120], la citotoxicidad que pueda provocar un compuesto de interés de forma individual o junto a otros compuestos en la función celular es de especial relevancia para evaluar efectos sobre el ciclo de proliferación. Además, estas perturbaciones suelen aparecer antes de un posible daño en el ADN (efecto genotóxico) de modo que el efecto citotóxico de un xenobiótico es de utilidad como indicador temprano de daño celular con posibles consecuencias a mayor escala o en relación a efectos crónicos [121].

La viabilidad celular se define como la cantidad de células sanas en una muestra. La proliferación celular es un indicador esencial para la comprensión de los mecanismos de acción de ciertos genes, proteínas y rutas de acción involucradas en la supervivencia o muerte celular después de la exposición a sustancias potencialmente tóxicas. Los ensayos usados para la determinación de la viabilidad celular son también útiles para detectar su proliferación y estado de salud. La medida de la viabilidad es a veces el objetivo principal del experimento mientras que en otras ocasiones este parámetro es de utilidad para correlacionar la cantidad de células con un determinado comportamiento celular. Existen diversas metodologías basadas en distintas funciones celulares como la actividad enzimática y metabólica o la permeabilidad de la membrana por citar algunas

[122]. Estos ensayos se pueden dividir en i) tintes de exclusión, ii) colorimétricos, iii) fluorímetricos y iv) luminométricos [123]. En este trabajo se han usado dos ensayos colorimétricos: MTT, basado en el uso de bromuro de 3-(4,5-dimetiltiazol-2-il)-2,5-difeniltetrazolio, y LDH mediante el uso del enzima lactato deshidrogenasa.

1.5.1.1. Ensayos basados en actividad metabólica: MTT

Uno de los ensayos más conocidos en el estudio de citotoxicidad aguda (exposiciones del xenobitótico de 24 a 96 horas) es el ensayo MTT. En este ensayo se mide la disminución de la viabilidad celular como medida directa de citotoxicidad a través del estudio de la función mitocondrial, siendo pues un ensayo de actividad metabólica. El compuesto MTT, perteneciente a las sales de tetrazolio de color amarillento y soluble en agua, es reducido a cristales de formazano, de color violeta intenso e insoluble, por acción principalmente de la enzima mitocondrial succinato deshidrogenasa siendo pues la cantidad de formazano producida proporcional al nivel metabólico energético de la célula [124]. Los cristales de formazano formados se solubilizan con DMSO y el color se detecta por espectrofotometría.

Sin embargo, este ensayo no puede discernir entre efectos citotóxicos o citostáticos (que interrumpe el ciclo celular) lo que puede llevar a casos de sobreestimación del efecto tóxico relacionado con la muerte celular del compuesto estudiado. En otros casos ocurre que la célula está dañada o muriendo pero aún es capaz de expresar cierta actividad deshidrogenasa dando lugar a una sobreestimación de la viabilidad celular [125]. Además, el ensayo MTT asume que la capacidad de las células para reducir el MTT permanece constante a lo largo de todo el periodo del cultivo celular [126]. Por tanto, con este ensayo y variaciones del mismo se debe tener en cuenta que las células metabólicamente inactivas también pueden detectarse como células muertas, aunque no todas las células inactivas estén muertas. Esto puede considerarse como una desventaja de estos ensayos basados en el metabolismo. De todas formas, el rol exclusivo de la mitocondria y de la succinato deshidrogenasa en la reducción del MTT en células intactas es cuestionable [127]. Aunque las mitocondrias son una fuente importante de la coenzima nicotin adenin dinucleótido en su forma reducida (NADH), el agente reductor intracelular más relevante, este coenzima se puede generar en otros orgánulos y regiones de la célula. De

hecho, parece ser que la reducción del MTT al formazano está principalmente ligada a la cantidad de NADH producido en la glucólisis, en vez de la respiración celular, de modo que este ensayo debería verse más bien como una medida de la tasa de producción de NAD(P)H glucolítico [128]. Diversas evidencias a raíz de un estudio [129] sugieren que el MTT entra a las células por endocitosis, es reducido en compartimentos endosomales/lisosomales y el formazano producido es excretado al exterior celular por exocitosis donde se acumula en forma de agujas cristalinas. Así, el ensayo MTT mediría la endocitosis, un rasgo fundamental de la mayoría de las células activas siendo por tanto válida aún la asunción del uso del ensayo MTT para el estudio de la viabilidad celular. Otros estudios sin embargo indican que la formación de cristales extracelulares podría ser debido a la reducción del propio medio de cultivo [130] o la actividad de determinadas enzimas ligadas a la membrana plasmática [131].

En este tipo de ensayos se deben planificar cuidadosamente los periodos de tiempo con el fin de evitar que las células alcancen un nivel de confluencia excesiva lo que implicaría un agotamiento del medio de cultivo y por tanto una menor viabilidad celular. Si las células alcanzan la fase estacionaria o la absorbancia no es lineal, el ensayo debería reducirse o cambiar la concentración de células de partida. En el caso de que las células paren de dividirse durante el ensayo debido a la elevada densidad celular del cultivo los valores de absorbancia serían erróneos, eso es debido al apiñamiento de las células que ven su superficie de expansión reducida, lo que resulta en un cambio de morfología y disminución del factor de crecimiento [132]. Por tanto, un factor clave es la densidad en la siembra que, para las células con una tasa de proliferación rápida, como los fibroblastos, debe ser baja. Es crucial que las células no alcancen la confluencia antes del punto final del ensayo; de lo contrario, se retiran del ciclo celular o incluso mueren [133].

A pesar de las incongruencias e inconvenientes, tomando una serie de precauciones necesarias, el ensayo MTT sigue siendo a día de hoy un test rápido, económico y de fácil uso para evaluar de forma fiable la actividad metabólica de los cultivos celulares y por tanto su viabilidad celular, características de crecimiento y valores de IC_{50} [134] (concentración de xenobiótico inhibitoria del 50% de viabilidad celular)

1.5.1.2. Ensayos basados en permeabilidad de la membrana: LDH

La determinación de la enzima lactato deshidrogenasa (LDH) liberada en el medio extracelular nos permite conocer la cantidad de células muertas o células con la membrana plasmática dañada, siendo por tanto un test de citotoxicidad basado en la permeabilidad de la membrana [135]. La actividad LDH se realiza a través de una reacción enzimática de dos etapas representadas en la figura 1.16:

1. Reducción de NAD^+ a NADH y H^+ catalizada por LDH mediante la oxidación de lactato a piruvato.

2. La enzima diaforasa usa la coenzima NADH y H^+ para reducir la sal de tetrazolio de color amarillo a un formazano de color rojo con un máximo de absorción alrededor de 500 nm.

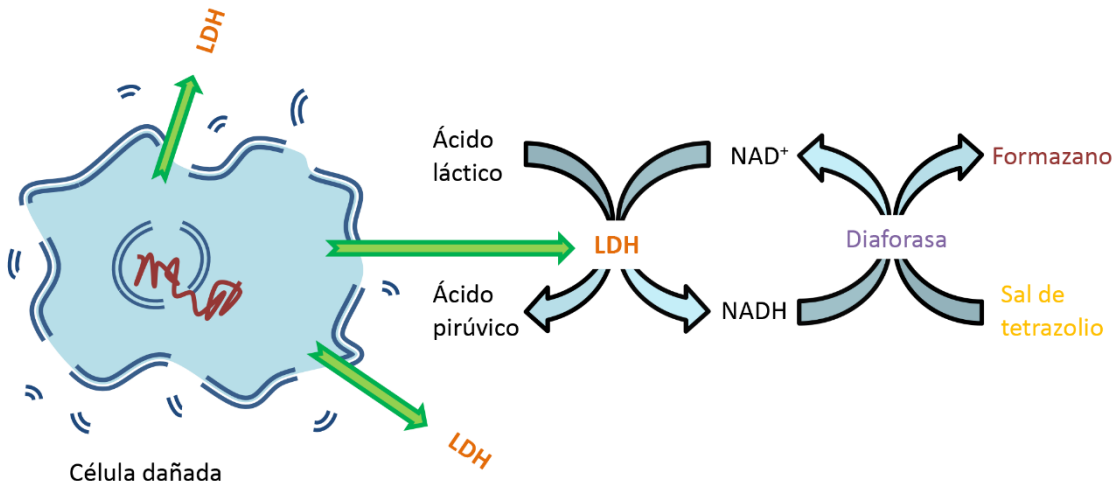

Figura 1.16. Representación esquemática del ensayo LDH en una célula con la membrana plasmática dañada.

En esencia, la absorbancia del formazano es directamente proporcional al número de células dañadas a diferencias del ensayo MTT donde la mayor cantidad de color violeta era indicativo de una mayor cantidad de células viables.

En este ensayo como control positivo suele usarse algún surfactante como el detergente Triton X-100 que provocará la lisis total de la membrana plasmática permitiendo evaluar la liberación máxima de LDH en el sobrenadante.

Uno de los inconvenientes de los ensayos basados en la integridad de la membrana es que los daños causados por la mayoría de los agentes tóxicos son inicialmente intracelulares. Así, una célula podría estar irreversiblemente dañada aun manteniendo la membrana plasmática intacta infravalorando pues el daño citotóxico del compuesto estudiado [136]. De hecho, comparando los ensayos de MTT y LDH, el primero es más sensible cuando se estudian efectos a agentes tóxicos a corto plazo, por debajo de las 8 h, lo que confirma que el daño por un xenobiótico suele iniciarse en el interior de la célula antes de que la membrana se vea alterada [137]. Por eso debe tenerse en cuenta que, para evitar la sobreestimación o la subestimación de la toxicidad de una sustancia, se requieren incubaciones con varias concentraciones de la sustancia tóxica a distintos tiempos para poder distinguir entre los efectos en orgánulos específicos o citotoxicidad general. Además, se recomienda el uso de más de un ensayo para determinar la viabilidad celular en estudios *in vitro*, ya que esto aumenta la fiabilidad de los resultados y permite una mayor comprensión del efecto citotóxico del xenobiótico estudiado.

1.5.2. Ensayos de ecotoxicidad

Los ensayos de ecotoxicidad por otro lado son útiles para la evaluación preliminar y biomonitoreo de los efectos de posibles contaminantes en la salud medioambiental, sobre todo en los ecosistemas acuáticos, centrándose en el funcionamiento de la cadena trófica y no en el individuo en particular. Los modelos biológicos más usados como bioindicadores en estos ensayos suelen ser *Daphnia magna,* un pequeño crustáceo planctónico de agua dulce también conocido con el nombre de pulga de agua, y *Chironomus tentans,* la larva de una especie de mosquito. Ambos organismos desempeñan un papel importante en la cadena trófica y son sensibles a gran diversidad de contaminantes. Su facilidad de cultivo y ciclo de vida corto les hace un buen candidato para los ensayos de ecotoxicidad, proporcionando un cierto grado de

conocimiento de los posibles efectos adversos e impacto de los químicos potencialmente peligrosos persistentes en el medio acuático [138].

1.5.2.1. Microtox® con bacterias

La bacteria bioluminiscente *Vibrio fisheri* es también un recurrente en los ensayos de ecotoxicidad, específicamente en el conocido como test de toxicidad aguda Microtox®. Este bioensayo utilizado en el capítulo 6 se basa en la reducción de luminiscencia natural de la bacteria marina mencionada en presencia de agentes contaminantes, relacionándose con una inhibición de su metabolismo, pero sin que ello implique su muerte. La metodología y descripción de este ensayo figura en la guía internacional ISO 11348-1. Una de las mayores ventajas del Microtox® es que la bacteria se encuentra en viales liofilizada al vacío de modo que no precisa de un cultivo previo, facilitando mucho su manipulación. Tampoco requiere de métodos asépticos debido al corto periodo de incubación del ensayo y su uso es inmediato, emitiendo luminiscencia en el instante en que se hidrata [139]. A pesar de ser un ensayo relativamente antiguo se sigue usando a día de hoy ya sea para el análisis en agua subterránea contaminada por alquilfenoles de cadena corta e hidrocarburos aromáticos heterocíclicos [140], para el estudio de extractos de suelos industriales contaminados por hidrocarburos aromáticos policíclicos) [141], nanopartículas metálicas en agua dulce [142] y pesticidas [143].

1.5.2.2. XenoScreen YES/YAS con levaduras

Los disruptores endocrinos (EDC, de sus siglas en inglés), según el informe de la OMS titulado “State of the Science of Endocrine Disrupting Chemicals—2012” son aquellos compuestos exógenos capaces de alterar el equilibrio hormonal provocando cambios en el funcionamiento del sistema endocrino y por tanto causando efectos adversos para la salud en los organismos expuestos a esos xenobióticos, su progenie o (sub) poblaciones. La alteración del sistema endocrino puede tener lugar a través de distintos mecanismos, ya sea bloqueando receptores hormonales debido a la similitud del compuesto disruptor con la hormona diana o interfiriendo en la síntesis, transporte o metabolismo de las hormonas [144,145].

Los EDCs pueden interactuar con los receptores de membrana de distintas formas según su naturaleza: los compuestos agonistas son capaces de mimetizar las propiedades de las hormonas endógenas y pueden unirse a los receptores hormonales y activar la respuesta, sin embargo su acción no necesariamente implica la misma cadena de eventos moleculares que la de la hormona; por otro lado, los EDCs pueden actuar como antagonistas, bloqueando el receptor hormonal y por tanto bloqueando la transcripción genética ligada a esa señal. Por tanto, lo disruptores endocrinos son capaces tanto de mejorar como de reducir o incluso bloquear la eficiencia de diversos procesos biológicos afectando al desarrollo y a la salud reproductiva [146]. Para el estudio de las propiedades (anti) estrogénicas y (anti) androgénicas de compuestos químicos por medio de su actividad agonista o antagonista se usa el ensayo XenoScreen YES/YAS (del inglés Yeast Estrogen/Androgen Screen) en el cual la levadura *Saccharomyces cerevisiae* es usada como organismo modelo. En este ensayo, usado en el capítulo 6, la levadura es modificada genéticamente con la secuencia de ADN de los receptores humanos hormonales hERα (YES) o hAR (YAS) y como controles positivos se usan el 17-β estradiol para el test YES y 5α-dihidrotestosterona para YAS. Además, las células también contienen un plásmido de expresión que porta el gen reportero lacZ que codifica la enzima β-galactosidasa y los elementos de respuesta a estrógeno (YES) o andrógenos (YAS). Brevemente, lo que ocurre, al unirse un ligando a los receptores hERα o hAR estos interaccionan con los elementos de respuesta presentes en el plásmido y modulan la transcripción del reportero lacZ. La enzima β-galactosidasa expresada provoca la conversión del sustrato amarillo clorofenol rojo-β-D-galactopiranósido (CPRG) a clorofenol rojo que se mide de forma cuantitativa con un espectrofotómetro [147]. Así pues, el escaneo de sustancias exógenas con posibles efectos en el sistema endocrino es otro tipo de ensayo de ecotoxicidad que nos permite conocer aquellos xenobióticos que pueden alterar al organismo desde un punto de vista hormonal.

1.6. Referencias

(1) Rodriguez-Amaya, D. B. Quantitative Analysis, in Vitro Assessment of Bioavailability and Antioxidant Activity of Food Carotenoids—A Review. *J. Food Compos. Anal.* **2010**, *23* (7), 726–740. https://doi.org/10.1016/j.jfca.2010.03.008.

(2) Quintana, J. B.; Rosende, M.; Montes, R.; Rodríguez-Álvarez, T.; Rodil, R.; Cela, R.; Miró, M. In-Vitro Estimation of Bioaccessibility of Chlorinated Organophosphate Flame Retardants in Indoor Dust by Fasting and Fed Physiologically Relevant Extraction Tests. *Sci. Total Environ.* **2017**, *580*, 540–549. https://doi.org/10.1016/j.scitotenv.2016.11.210.

(3) Courraud, J.; Berger, J.; Cristol, J.-P.; Avallone, S. Stability and Bioaccessibility of Different Forms of Carotenoids and Vitamin A during in Vitro Digestion. *Food Chem.* **2013**, *136* (2), 871–877. https://doi.org/10.1016/j.foodchem.2012.08.076.

(4) Rosende, M.; Prieto, A.; Etxebarria, N.; Martorell, G.; Miró, M. Automatic Mesofluidic System Combining Dynamic Gastrointestinal Bioaccessibility with Lab-on-Valve-Based Sorptive Microextraction for Risk Exposure of Organic Emerging Contaminants in Filter-Feeding Organisms. *Anal. Chem.* **2019**, *91* (9), 5739–5746. https://doi.org/10.1021/acs.analchem.8b05870.

(5) Herrera, M. A.; Rosende, M.; Arruda, M. A. Z.; Miró, M. On-Line Coupling of Physiologically Relevant Bioaccessibility Testing to Inductively Coupled Plasma Spectrometry: Proof of Concept for Fast Assessment of Gastrointestinal Bioaccessibility of Micronutrients from Soybeans. *Anal. Chim. Acta* **2016**, *939*, 1–9. https://doi.org/10.1016/j.aca.2016.07.030.

(6) Holst, B.; Williamson, G. Nutrients and Phytochemicals: From Bioavailability to Bioefficacy beyond Antioxidants. *Curr. Opin. Biotechnol.* **2008**, *19* (2), 73–82. https://doi.org/10.1016/j.copbio.2008.03.003.

(7) Carbonell-Capella, J. M.; Buniowska, M.; Barba, F. J.; Esteve, M. J.; Frígola, A. Analytical Methods for Determining Bioavailability and Bioaccessibility of Bioactive Compounds from Fruits and Vegetables: A Review. *Compr. Rev. Food*

Sci. Food Saf. **2014**, *13* (2), 155–171. https://doi.org/10.1111/1541-4337.12049.

(8) Council, N. R. *Bioavailability of Contaminants in Soils and Sediments: Processes, Tools, and Applications*; The National Academies Press: Washington, DC, 2003. https://doi.org/10.17226/10523.

(9) Escribá, P. V.; González-Ros, J. M.; Goñi, F. M.; Kinnunen, P. K. J.; Vigh, L.; Sánchez-Magraner, L.; Fernández, A. M.; Busquets, X.; Horváth, I.; Barceló-Coblijn, G. Membranes: A Meeting Point for Lipids, Proteins and Therapies. *J. Cell. Mol. Med.* **2008**, *12* (3), 829–875. https://doi.org/10.1111/j.1582-4934.2008.00281.x.

(10) Marquardt, D.; Geier, B.; Pabst, G. Asymmetric Lipid Membranes: Towards More Realistic Model Systems. *Membranes (Basel).* **2015**, *5* (2), 180–196. https://doi.org/10.3390/membranes5020180.

(11) Tanford, C. *The Hydrophobic Effect : Formation of Micelles and Biological Membranes*, 2d ed.; Wiley, Ed.; New York, 1980.

(12) Crichton, R. Structural and Molecular Biology for Chemists. In *Biological Inorganic Chemistry*; John Fedor, 2019; pp 35–79. https://doi.org/10.1016/B978-0-12-811741-5.00003-5.

(13) Stillwell, W. Water and the Hydrophobic Effect. In *An Introduction to Biological Membranes*; Elsevier, 2013; pp 29–41. https://doi.org/10.1016/B978-0-444-52153-8.00003-9.

(14) Homsi Brandeburgo, W.; van der Post, S. T.; Meijer, E. J.; Ensing, B. On the Slowdown Mechanism of Water Dynamics around Small Amphiphiles. *Phys. Chem. Chem. Phys.* **2015**, *17* (38), 24968–24977. https://doi.org/10.1039/C5CP03486H.

(15) Patterson, D.; Barbe, M. Enthalpy-Entropy Compensation and Order in Alkane and Aqueous Systems. *J. Phys. Chem.* **1976**, *80* (21), 2435–2436. https://doi.org/10.1021/j100562a026.

(16) Kronberg, B. The Hydrophobic Effect. *Curr. Opin. Colloid Interface Sci.* **2016**, *22*, 14–22. https://doi.org/10.1016/j.cocis.2016.02.001.

(17) Fisicaro, E.; Compari, C.; Braibanti, A. Hydrophobic Hydration Processes. General Thermodynamic Model by Thermal Equivalent Dilution Determinations. *Biophys. Chem.* **2010**, *151* (3), 119–138. https://doi.org/10.1016/j.bpc.2010.06.001.

(18) Singer, S. J.; Nicolson, G. L. The Fluid Mosaic Model of the Structure of Cell Membranes. *Science (80-.).* **1972**, *175* (4023), 720 LP – 731. https://doi.org/10.1126/science.175.4023.720.

(19) Vereb, G.; Szöllősi, J.; Matkó, J.; Nagy, P.; Farkas, T.; Vígh, L.; Mátyus, L.; Waldmann, T. A.; Damjanovich, S. Dynamic, yet Structured: The Cell Membrane Three Decades after the Singer–Nicolson Model. *Proc. Natl. Acad. Sci.* **2003**, *100* (14), 8053 LP – 8058. https://doi.org/10.1073/pnas.1332550100.

(20) Escribá, P. V. Membrane-Lipid Therapy: A New Approach in Molecular Medicine. *Trends Mol. Med.* **2006**, *12* (1), 34–43. https://doi.org/10.1016/j.molmed.2005.11.004.

(21) Berg, J. M.; Tymoczko, J. L.; Stryer, L. *Biochemistry*, 7th ed.; W. H. Freeman and Company, Ed.; Kate Ahr Parker: New York, 2012.

(22) Zheng, W.; Kollmeyer, J.; Symolon, H.; Momin, A.; Munter, E.; Wang, E.; Kelly, S.; Allegood, J. C.; Liu, Y.; Peng, Q.; et al. Ceramides and Other Bioactive Sphingolipid Backbones in Health and Disease: Lipidomic Analysis, Metabolism and Roles in Membrane Structure, Dynamics, Signaling and Autophagy. *Biochim. Biophys. Acta - Biomembr.* **2006**, *1758* (12), 1864–1884. https://doi.org/10.1016/j.bbamem.2006.08.009.

(23) Guschina, I. A.; Harwood, J. L. Lipids: Chemical Diversity. *Wiley Encyclopedia of Chemical Biology*. Wiley May 15, 2008, pp 1–14. https://doi.org/doi:10.1002/9780470048672.wecb292.

(24) Baumgart, T.; Hess, S. T.; Webb, W. W. Imaging Coexisting Fluid Domains in Biomembrane Models Coupling Curvature and Line Tension. *Nature* **2003**, *425* (6960), 821–824. https://doi.org/10.1038/nature02013.

(25) Kulkarni, C. V. Lipid Crystallization: From Self-Assembly to Hierarchical and Biological Ordering. *Nanoscale* **2012**, *4* (19), 5779–5791.

https://doi.org/10.1039/C2NR31465G.

(26) A.Smith, E.; K.Dea, P. Differential Scanning Calorimetry Studies of Phospholipid Membranes: The Interdigitated Gel Phase. In *Applications of Calorimetry in a Wide Context - Differential Scanning Calorimetry, Isothermal Titration Calorimetry and Microcalorimetry*; Amal Ali Elkordy, Ed.; IntechOpen, 2013; p 38. https://doi.org/10.5772/51882.

(27) Koynova, R.; Tenchov, B. Transitions between Lamellar and Nonlamellar Phases in Membrane Lipids and Their Physiological Roles. *OA Biochem.* **2013**, *1* (1), 9. https://doi.org/10.13172/2052-9651-1-1-602.

(28) Seddon, J. M. Structure of the Inverted Hexagonal (HII) Phase, and Non-Lamellar Phase Transitions of Lipids. *BBA - Rev. Biomembr.* **1990**, *1031* (1), 1–69. https://doi.org/10.1016/0304-4157(90)90002-T.

(29) Stillwell, W. *An Introduction to Biological Membranes : From Bilayers to Rafts*; Newnes, Ed.; Elsevier Science, 2013.

(30) Janiak, M. J.; Small, D. M.; Shipley, G. G. Temperature and Compositional Dependence of the Structure of Hydrated Dimyristoyl Lecithin. *J. Biol. Chem.* **1979**, *254* (13), 6068–6078.

(31) Heimburg, T. A Model for the Lipid Pretransition: Coupling of Ripple Formation with the Chain-Melting Transition. *Biophys. J.* **2000**, *78* (3), 1154–1165. https://doi.org/10.1016/S0006-3495(00)76673-2.

(32) Koynova, R.; Tenchov, B. Lipids: Phase Transitions. *Wiley Encyclopedia of Chemical Biology*. May 15, 2008, pp 1–15. https://doi.org/doi:10.1002/9780470048672.wecb287.

(33) Mouritsen, O. G.; Kinnunen, P. K. J. Role of Lipid Organization and Dynamics for Membrane Functionality. In *Biological Membranes*; Kenneth M. MerzJr., Roux, B., Eds.; Birkhäuser Boston: Boston, MA, 1996; pp 463–502. https://doi.org/10.1007/978-1-4684-8580-6_14.

(34) Seu, K. J.; Cambrea, L. R.; Everly, R. M.; Hovis, J. S. Influence of Lipid Chemistry on Membrane Fluidity: Tail and Headgroup Interactions. *Biophys. J.*

2006, *91* (10), 3727–3735. https://doi.org/10.1529/biophysj.106.084590.

(35) Dzikovski, B.; Freed, J. H. Fluidity of Membranes. In *Wiley Encyclopedia of Chemical Biology*; Begley, T. P., Ed.; Major Reference Works; John Wiley & Sons, Inc.: Hoboken, NJ, USA, 2008; pp 1–14. https://doi.org/doi:10.1002/9780470048672.wecb313.

(36) Helfrich, W. Elastic Properties of Lipid Bilayers: Theory and Possible Experiments. *Z. Naturforsch. C.* **1973**, *28* (11), 693–703.

(37) Lipowsky, R. Remodeling of Membrane Compartments: Some Consequences of Membrane Fluidity. *Biol. Chem.* **2014**, *395* (3), 253–274. https://doi.org/10.1515/hsz-2013-0244.

(38) Mondal, D.; Dutta, R.; Banerjee, P.; Mukherjee, D.; Kumar Maiti, T.; Sarkar, N. Modulation of Membrane Fluidity Performed on Model Phospholipid Membrane and Live Cell Membrane: Revealing through Spatiotemporal Approaches of FLIM, FAIM, and TRFS. *Anal. Chem.* **2019**, *91* (7), 4337–4345. https://doi.org/10.1021/acs.analchem.8b04044.

(39) Membrane Structure 1.Creation of the first cell and membrane The two most important elements of cellular life—the boundary that separates the "inside" https://slideplayer.com/slide/5004394/ (accessed Sep 19, 2019).

(40) Stillwell, W. Long-Range Membrane Properties. In *An Introduction to Biological Membranes*; Elsevier, 2013; pp 215–237. https://doi.org/10.1016/B978-0-444-52153-8.00011-8.

(41) Marsh, D. Cholesterol-Induced Fluid Membrane Domains: A Compendium of Lipid-Raft Ternary Phase Diagrams. *Biochim. Biophys. Acta - Biomembr.* **2009**, *1788* (10), 2114–2123. https://doi.org/10.1016/j.bbamem.2009.08.004.

(42) Eeman, M.; Deleu, M. From Biological Membranes to Biomimetic Model Membranes. *Biotechnol. Agron. Société Environ.* **2012**, *14* (4), 719–736.

(43) Lúcio, M.; Lima, J. L. F. C.; Reis, S. Drug-Membrane Interactions: Molecular Mechanisms Underlying Therapeutic and Toxic Effects of Drugs. In *Ideas in Chemistry and Molecular Sciences*; Prof. Bruno Pignataro, Ed.; Wiley-VCH

Verlag GmbH & Co. KGaA: Weinheim, Germany, 2010; pp 191–214. https://doi.org/10.1002/9783527630516.ch8.

(44) Kansy, M.; Fischer, H.; Kratzat, K.; Senner, F.; Wagner, B.; Parrilla, I. High-Throughput Artificial Membrane Permeability Studies in Early Lead Discovery and Development. In *Pharmacokinetic Optimization in Drug Research*; Prof. Bernard Testa Dr. Han van de Waterbeemd, Prof. Gerd Folkers Prof. Richard Guy, Eds.; Verlag Helvetica Chimica Acta: Zürich, 2001; pp 447–464. https://doi.org/10.1002/9783906390437.ch24.

(45) Sessa, G.; Weissmann, G. Incorporation of Lysozyme into Liposomes. A Model for Structure-Linked Latency. *J. Biol. Chem.* **1970**, *245* (13), 3295–3301.

(46) Gregoriadis, G.; Ryman, B. E. Liposomes as Carriers of Enzymes or Drugs: A New Approach to the Treatment of Storage Diseases. *Biochem. J.* **1971**, *124* (5), 58P. https://doi.org/10.1042/bj1240058P.

(47) Weissig, V. Liposomes Came First: The Early History of Liposomology. In *Liposomes: Methods and Protocols*; D'Souza, G. G. M., Ed.; Humana Press: New York, NY, 2017; pp 1–15. https://doi.org/10.1007/978-1-4939-6591-5_1.

(48) Bangham, A. D.; Horne, R. W. Negative Staining of Phospholipids and Their Structural Modification by Surface-Active Agents as Observed in the Electron Microscope. *J. Mol. Biol.* **1964**, *8* (5), 660–668. https://doi.org/10.1016/S0022-2836(64)80115-7.

(49) Bangham, A. D. Liposomes: The Babraham Connection. *Chem. Phys. Lipids* **1993**, *64* (1–3), 275–285. https://doi.org/10.1016/0009-3084(93)90071-A.

(50) Sessa, G.; Weissmann, G. Phospholipid Spherules (Liposomes) as a Model for Biological Membranes. *J. Lipid Res.* **1968**, *9* (3), 310–318.

(51) Bangham, A. D.; Hill, M. W.; Miller, N. G. A. Preparation and Use of Liposomes as Models of Biological Membranes. In *Methods in Membrane Biology*; Edward D. Korn, Ed.; Springer US: Boston, MA, 1974; pp 1–68. https://doi.org/10.1007/978-1-4615-7422-4_1.

(52) Bangham, A. D.; Standish, M. M.; Watkins, J. C. Diffusion of Univalent Ions

across the Lamellae of Swollen Phospholipids. *J. Mol. Biol.* **1965**, *13* (1), 238–252. https://doi.org/10.1016/S0022-2836(65)80093-6.

(53) Bangham, A. D.; Standish, M. M.; Weissmann, G. The Action of Steroids and Streptolysin S on the Permeability of Phospholipid Structures to Cations. *J. Mol. Biol.* **1965**, *13* (1), 253–259. https://doi.org/10.1016/S0022-2836(65)80094-8.

(54) Bangham, A. D.; De Gier, J.; Greville, G. D. Osmotic Properties and Water Permeability of Phospholipid Liquid Crystals. *Chem. Phys. Lipids* **1967**, *1* (3), 225–246. https://doi.org/10.1016/0009-3084(67)90030-8.

(55) Johnson, S. M.; Miller, K. W.; Bangham, A. D. The Opposing Effects of Pressure and General Anaesthetics on the Cation Permeability of Liposomes of Varying Lipid Composition. *Biochim. Biophys. Acta - Biomembr.* **1973**, *307* (1), 42–57. https://doi.org/10.1016/0005-2736(73)90023-0.

(56) Bangham, A. D. Liposomes and the Physico-Chemical Basis of Unconsciousness. *FASEB J.* **2005**, *19* (13), 1766–1768. https://doi.org/10.1096/fj.05-1103ufm.

(57) Bangham, A. D.; Miller, N. G. A.; Davies, R. J.; Greenough, A.; Morley, C. J. Introductory Remarks about Artificial Lung Expanding Compounds (ALEC). *Colloids and Surfaces* **1984**, *10*, 337–341. https://doi.org/10.1016/0166-6622(84)80034-7.

(58) Bangham, A. The Physical Chemistry of Self/Non-Self: Jigsaws, Transplants and Fetuses. *FASEB J.* **2009**, *23* (11), 3644–3646. https://doi.org/10.1096/fj.09-1102ufm.

(59) Akbarzadeh, A.; Rezaei-Sadabady, R.; Davaran, S.; Joo, S. W.; Zarghami, N.; Hanifehpour, Y.; Samiei, M.; Kouhi, M.; Nejati-Koshki, K. Liposome: Classification, Preparation, and Applications. *Nanoscale Res. Lett.* **2013**, *8* (1), 102. https://doi.org/10.1186/1556-276X-8-102.

(60) García-Pinel, B.; Porras-Alcalá, C.; Ortega-Rodríguez, A.; Sarabia, F.; Prados, J.; Melguizo, C.; López-Romero, J. M. Lipid-Based Nanoparticles: Application and Recent Advances in Cancer Treatment. *Nanomaterials* **2019**, *9* (4), 638. https://doi.org/10.3390/nano9040638.

(61) Islam Shishir, M. R.; Karim, N.; Gowd, V.; Zheng, X.; Chen, W. Liposomal Delivery of Natural Product: A Promising Approach in Health Research. *Trends Food Sci. Technol.* **2019**, *85*, 177–200. https://doi.org/10.1016/j.tifs.2019.01.013.

(62) Rai, S.; Pandey, V.; Rai, G. Transfersomes as Versatile and Flexible Nano-Vesicular Carriers in Skin Cancer Therapy: The State of the Art. *Nano Rev. Exp.* **2017**, *8* (1), 19. https://doi.org/10.1080/20022727.2017.1325708.

(63) Maestrelli, F.; Capasso, G.; González-Rodríguez, M. L.; Rabasco, A. M.; Ghelardini, C.; Mura, P. Effect of Preparation Technique on the Properties and in Vivo Efficacy of Benzocaine-Loaded Ethosomes. *J. Liposome Res.* **2009**, *19* (4), 253–260. https://doi.org/10.3109/08982100902788408.

(64) Yakushi, T.; Masuda, K.; Narita, S.; Matsuyama, S.; Tokuda, H. A New ABC Transporter Mediating the Detachment of Lipid-Modified Proteins from Membranes. *Nat. Cell Biol.* **2000**, *2* (4), 212–218. https://doi.org/10.1038/35008635.

(65) Sherman, D. J.; Xie, R.; Taylor, R. J.; George, A. H.; Okuda, S.; Foster, P. J.; Needleman, D. J.; Kahne, D. Lipopolysaccharide Is Transported to the Cell Surface by a Membrane-to-Membrane Protein Bridge. *Science (80-.).* **2018**, *359* (6377), 798–801. https://doi.org/10.1126/science.aar1886.

(66) Rodrigues, A.; Matos, J.; Nova Dias, A.; Almeida, B.; Pires, A.; Pereira, A.; Araújo, J.; Queiroz, M.-J.; Castanheira, E.; Coutinho, P. Development of Multifunctional Liposomes Containing Magnetic/Plasmonic MnFe2O4/Au Core/Shell Nanoparticles. *Pharmaceutics* **2019**, *11* (1), 10. https://doi.org/10.3390/pharmaceutics11010010.

(67) Khan, A. A.; Jabeen, M.; Khan, A. A.; Owais, M. Anticancer Efficacy of a Novel Propofol–Linoleic Acid-Loaded Escheriosomal Formulation against Murine Hepatocellular Carcinoma. *Nanomedicine* **2013**, *8* (8), 1281–1294. https://doi.org/10.2217/nnm.12.166.

(68) Kuo, Y.-C.; Wu, H.-C.; Hoang, D.; Bentley, W. E.; D'Souza, W. D.; Raghavan, S. R. Colloidal Properties of Nanoerythrosomes Derived from Bovine Red Blood Cells. *Langmuir* **2016**, *32* (1), 171–179.

https://doi.org/10.1021/acs.langmuir.5b03014.

(69) Ruokonen, S.-K.; Duša, F.; Rantamäki, A. H.; Robciuc, A.; Holma, P.; Holopainen, J. M.; Abdel-Rehim, M.; Wiedmer, S. K. Distribution of Local Anesthetics between Aqueous and Liposome Phases. *J. Chromatogr. A* **2017**, *1479*, 194–203. https://doi.org/10.1016/j.chroma.2016.12.005.

(70) Alavi, M.; Karimi, N.; Safaei, M. Application of Various Types of Liposomes in Drug Delivery Systems. *Adv. Pharm. Bull.* **2017**, *7* (1), 3–9. https://doi.org/10.15171/apb.2017.002.

(71) Schwendener, R. A. Liposomes as Vaccine Delivery Systems: A Review of the Recent Advances. *Ther. Adv. Vaccines* **2014**, *2* (6), 159–182. https://doi.org/10.1177/2051013614541440.

(72) Li, M.; Du, C.; Guo, N.; Teng, Y.; Meng, X.; Sun, H.; Li, S.; Yu, P.; Galons, H. Composition Design and Medical Application of Liposomes. *Eur. J. Med. Chem.* **2019**, *164*, 640–653. https://doi.org/10.1016/j.ejmech.2019.01.007.

(73) Lopes-de-Campos, D.; Nunes, C.; Sarmento, B.; Jakobtorweihen, S.; Reis, S. Metronidazole within Phosphatidylcholine Lipid Membranes: New Insights to Improve the Design of Imidazole Derivatives. *Eur. J. Pharm. Biopharm.* **2018**, *129*, 204–214. https://doi.org/10.1016/j.ejpb.2018.05.036.

(74) Fitzgerald, N. J. M.; Wargenau, A.; Sorenson, C.; Pedersen, J.; Tufenkji, N.; Novak, P. J.; Simcik, M. F. Partitioning and Accumulation of Perfluoroalkyl Substances in Model Lipid Bilayers and Bacteria. *Environ. Sci. Technol.* **2018**, *52* (18), 10433–10440. https://doi.org/10.1021/acs.est.8b02912.

(75) di Cagno, M. P.; Stein, P. C. Studying the Effect of Solubilizing Agents on Drug Diffusion through the Unstirred Water Layer (UWL) by Localized Spectroscopy. *Eur. J. Pharm. Biopharm.* **2019**, *139*, 205–212. https://doi.org/10.1016/j.ejpb.2019.04.005.

(76) Lin, S.; Yang, X.; Liu, H. Development of Liposome/Water Partition Coefficients Predictive Models for Neutral and Ionogenic Organic Chemicals. *Ecotoxicol. Environ. Saf.* **2019**, *179*, 40–49. https://doi.org/10.1016/j.ecoenv.2019.04.036.

(77) Pires, F.; Geraldo, V. P. N.; Rodrigues, B.; Granada-Flor, A. de; de Almeida, R. F. M.; Oliveira, O. N.; Victor, B. L.; Machuqueiro, M.; Raposo, M. Evaluation of EGCG Loading Capacity in DMPC Membranes. *Langmuir* **2019**, *35* (20), 6771–6781. https://doi.org/10.1021/acs.langmuir.9b00372.

(78) Oliva, R.; Emendato, A.; Vitiello, G.; De Santis, A.; Grimaldi, M.; D'Ursi, A. M.; Busi, E.; Del Vecchio, P.; Petraccone, L.; D'Errico, G. On the Microscopic and Mesoscopic Perturbations of Lipid Bilayers upon Interaction with the MPER Domain of the HIV Glycoprotein Gp41. *Biochim. Biophys. Acta - Biomembr.* **2016**, *1858* (8), 1904–1913. https://doi.org/10.1016/j.bbamem.2016.05.007.

(79) Gonzalez, S.; Gallier, F.; Kellouche, S.; Carreiras, F.; Novellino, E.; Carotenuto, A.; Chassaing, G.; Rovero, P.; Uziel, J.; Lubin-Germain, N. Studies of Membranotropic and Fusogenic Activity of Two Putative HCV Fusion Peptides. *Biochim. Biophys. Acta - Biomembr.* **2019**, *1861* (1), 50–61. https://doi.org/10.1016/j.bbamem.2018.10.011.

(80) Faggiano, S.; Ronda, L.; Raboni, S.; Sartor, F.; Cavatorta, V.; Sgarbi, E.; Caivano, G.; Pertile, M.; Mozzarelli, A. Phospholipid Components of the Synthetic Pulmonary Surfactant CHF5633 Probed by Fluorescence Spectroscopy. *Int. J. Pharm.* **2018**, *553* (1–2), 290–297. https://doi.org/10.1016/j.ijpharm.2018.10.045.

(81) Widomska, J.; Welc, R.; Gruszecki, W. I. The Effect of Carotenoids on the Concentration of Singlet Oxygen in Lipid Membranes. *Biochim. Biophys. Acta - Biomembr.* **2019**, *1861* (4), 845–851. https://doi.org/10.1016/j.bbamem.2019.01.012.

(82) Stillwell, W. Membrane Transport. In *An Introduction to Biological Membranes*; Stillwell, W. B. T.-A. I. to B. M., Ed.; Elsevier: San Diego, 2013; pp 305–337. https://doi.org/https://doi.org/10.1016/B978-0-444-52153-8.00014-3.

(83) Jesorka, A.; Orwar, O. Liposomes: Technologies and Analytical Applications. *Annu. Rev. Anal. Chem.* **2008**, *1* (1), 801–832. https://doi.org/10.1146/annurev.anchem.1.031207.112747.

(84) Sorkin, R.; Kampf, N.; Zhu, L.; Klein, J. Hydration Lubrication and Shear-

Induced Self-Healing of Lipid Bilayer Boundary Lubricants in Phosphatidylcholine Dispersions. *Soft Matter* **2016**, *12* (10), 2773–2784. https://doi.org/10.1039/C5SM02475G.

(85) Bian, T.; Autry, J. M.; Casemore, D.; Li, J.; Thomas, D. D.; He, G.; Xing, C. Direct Detection of SERCA Calcium Transport and Small-Molecule Inhibition in Giant Unilamellar Vesicles. *Biochem. Biophys. Res. Commun.* **2016**, *481* (3–4), 206–211. https://doi.org/10.1016/j.bbrc.2016.10.096.

(86) Bolinger, P.-Y.; Stamou, D.; Vogel, H. Integrated Nanoreactor Systems: Triggering the Release and Mixing of Compounds Inside Single Vesicles. *J. Am. Chem. Soc.* **2004**, *126* (28), 8594–8595. https://doi.org/10.1021/ja049023u.

(87) Reeves, J. P.; Dowben, R. M. Formation and Properties of Thin-Walled Phospholipid Vesicles. *J. Cell. Physiol.* **1969**, *73* (1), 49–60. https://doi.org/10.1002/jcp.1040730108.

(88) Angelova, M. I.; Dimitrov, D. S. Liposome Electroformation. *Faraday Discuss. Chem. Soc.* **1986**, *81*, 303–311. https://doi.org/10.1039/dc9868100303.

(89) Dimitrov, D. S.; Angelova, M. I. Lipid Swelling and Liposome Formation Mediated by Electric Fields. *J. Electroanal. Chem. Interfacial Electrochem.* **1988**, *253* (2), 323–336. https://doi.org/10.1016/0022-0728(88)87069-4.

(90) Rodriguez, N.; Pincet, F.; Cribier, S. Giant Vesicles Formed by Gentle Hydration and Electroformation: A Comparison by Fluorescence Microscopy. *Colloids Surfaces B Biointerfaces* **2005**, *42* (2), 125–130. https://doi.org/10.1016/j.colsurfb.2005.01.010.

(91) Ahmed, K. S.; Hussein, S. A.; Ali, A. H.; Korma, S. A.; Lipeng, Q.; Jinghua, C. Liposome: Composition, Characterisation, Preparation, and Recent Innovation in Clinical Applications. *J. Drug Target.* **2019**, *27* (7), 742–761. https://doi.org/10.1080/1061186X.2018.1527337.

(92) Kremer, J. M. H.; Van der Esker, M. W.; Pathmamanoharan, C.; Wiersema, P. H. Vesicles of Variable Diameter Prepared by a Modified Injection Method. *Biochemistry* **1977**, *16* (17), 3932–3935. https://doi.org/10.1021/bi00636a033.

(93) Deamer, D.; Bangham, A. D. Large Volume Liposomes by an Ether Vaporization Method. *Biochim. Biophys. Acta - Nucleic Acids Protein Synth.* **1976**, *443* (3), 629–634. https://doi.org/10.1016/0005-2787(76)90527-X.

(94) Szoka, F.; Papahadjopoulos, D. Procedure for Preparation of Liposomes with Large Internal Aqueous Space and High Capture by Reverse-Phase Evaporation. *Proc. Natl. Acad. Sci. U. S. A.* **1978**, *75* (9), 4194–4198. https://doi.org/10.1073/pnas.75.9.4194.

(95) Alpes, H.; Allmann, K.; Plattner, H.; Reichert, J.; Rick, R.; Schulz, S. Formation of Large Unilamellar Vesicles Using Alkyl Maltoside Detergents. *Biochim. Biophys. Acta - Biomembr.* **1986**, *862* (2), 294–302. https://doi.org/10.1016/0005-2736(86)90231-2.

(96) Milsmann, M. H. W.; Schwendener, R. A.; Weder, H.-G. The Preparation of Large Single Bilayer Liposomes by a Fast and Controlled Dialysis. *Biochim. Biophys. Acta - Biomembr.* **1978**, *512* (1), 147–155. https://doi.org/10.1016/0005-2736(78)90225-0.

(97) Laouini, A.; Jaafar-Maalej, C.; Limayem-Blouza, I.; Sfar, S.; Charcosset, C.; Fessi, H. Preparation, Characterization and Applications of Liposomes: State of the Art. *J. Colloid Sci. Biotechnol.* **2012**, *1* (2), 147–168. https://doi.org/10.1166/jcsb.2012.1020.

(98) Patil, Y. P.; Jadhav, S. Novel Methods for Liposome Preparation. *Chem. Phys. Lipids* **2014**, *177*, 8–18. https://doi.org/10.1016/j.chemphyslip.2013.10.011.

(99) van Swaay, D.; deMello, A. Microfluidic Methods for Forming Liposomes. *Lab Chip* **2013**, *13* (5), 752–767. https://doi.org/10.1039/c2lc41121k.

(100) Meure, L. A.; Foster, N. R.; Dehghani, F. Conventional and Dense Gas Techniques for the Production of Liposomes: A Review. *AAPS PharmSciTech* **2008**, *9* (3), 798–809. https://doi.org/10.1208/s12249-008-9097-x.

(101) Viard, M.; Gallay, J.; Vincent, M.; Meyer, O.; Robert, B.; Paternostre, M. Laurdan Solvatochromism: Solvent Dielectric Relaxation and Intramolecular Excited-State Reaction. *Biophys. J.* **1997**, *73* (4), 2221–2234. https://doi.org/10.1016/S0006-3495(97)78253-5.

(102) Lakowicz, J. R.; Masters, B. R. Principles of Fluorescence Spectroscopy, Third Edition. *J. Biomed. Opt.* **2008**, *13* (2), 029901. https://doi.org/10.1117/1.2904580.

(103) Parasassi, T.; De Stasio, G.; Ravagnan, G.; Rusch, R. M.; Gratton, E. Quantitation of Lipid Phases in Phospholipid Vesicles by the Generalized Polarization of Laurdan Fluorescence. *Biophys. J.* **1991**, *60* (1), 179–189. https://doi.org/10.1016/S0006-3495(91)82041-0.

(104) Weber, G.; Farris, F. J. Synthesis and Spectral Properties of a Hydrophobic Fluorescent Probe: 6-Propionyl-2-(Dimethylamino)Naphthalene. *Biochemistry* **1979**, *18* (14), 3075–3078. https://doi.org/10.1021/bi00581a025.

(105) Macgregor, R. B.; Weber, G. Fluorophores in Polar Media: Spectral Effects of the Langevin Distribution of Electrostatic Interactions. *Ann. N. Y. Acad. Sci.* **1981**, *366* (1), 140–154. https://doi.org/10.1111/j.1749-6632.1981.tb20751.x.

(106) Parasassi, T.; De Stasio, G.; d'Ubaldo, a; Gratton, E. Phase Fluctuation in Phospholipid Membranes Revealed by Laurdan Fluorescence. *Biophys. J.* **1990**, *57* (6), 1179–1186. https://doi.org/10.1016/S0006-3495(90)82637-0.

(107) Lúcio, A. D.; Vequi-Suplicy, C. C.; Fernandez, R. M.; Lamy, M. T. Laurdan Spectrum Decomposition as a Tool for the Analysis of Surface Bilayer Structure and Polarity: A Study with DMPG, Peptides and Cholesterol. *J. Fluoresc.* **2010**, *20* (2), 473–482. https://doi.org/10.1007/s10895-009-0569-5.

(108) Vequi-Suplicy, C. C.; Coutinho, K.; Lamy, M. T. New Insights on the Fluorescent Emission Spectra of Prodan and Laurdan. *J. Fluoresc.* **2015**, *25* (3), 621–629. https://doi.org/10.1007/s10895-015-1545-x.

(109) Pérez, H. A.; Disalvo, A.; Frías, M. de los Á. Effect of Cholesterol on the Surface Polarity and Hydration of Lipid Interphases as Measured by Laurdan Fluorescence: New Insights. *Colloids Surfaces B Biointerfaces* **2019**, *178*, 346–351. https://doi.org/10.1016/j.colsurfb.2019.03.022.

(110) Vinegoni, C.; Feruglio, P. F.; Gryczynski, I.; Mazitschek, R.; Weissleder, R. Fluorescence Anisotropy Imaging in Drug Discovery. *Adv. Drug Deliv. Rev.* **2018**, S0169-409X(18)30027-9. https://doi.org/10.1016/j.addr.2018.01.019.

(111) Ameloot, M.; vandeVen, M.; Acuña, A. U.; Valeur, B. Fluorescence Anisotropy Measurements in Solution: Methods and Reference Materials (IUPAC Technical Report). *Pure Appl. Chem.* **2013**, *85* (3), 589–608. https://doi.org/10.1351/PAC-REP-11-11-12.

(112) Ebele, A. J.; Abou-Elwafa Abdallah, M.; Harrad, S. Pharmaceuticals and Personal Care Products (PPCPs) in the Freshwater Aquatic Environment. *Emerg. Contam.* **2017**, *3* (1), 1–16. https://doi.org/10.1016/j.emcom.2016.12.004.

(113) Fairbairn, D. J.; Arnold, W. A.; Barber, B. L.; Kaufenberg, E. F.; Koskinen, W. C.; Novak, P. J.; Rice, P. J.; Swackhamer, D. L. Contaminants of Emerging Concern: Mass Balance and Comparison of Wastewater Effluent and Upstream Sources in a Mixed-Use Watershed. *Environ. Sci. Technol.* **2016**, *50* (1), 36–45. https://doi.org/10.1021/acs.est.5b03109.

(114) Reemtsma, T.; Berger, U.; Arp, H. P. H.; Gallard, H.; Knepper, T. P.; Neumann, M.; Quintana, J. B.; Voogt, P. de. Mind the Gap: Persistent and Mobile Organic Compounds-Water Contaminants That Slip Through. *Environ. Sci. Technol.* **2016**, *50* (19), 10308–10315. https://doi.org/10.1021/acs.est.6b03338.

(115) Lohmann, R.; Muir, D.; Zeng, E. Y.; Bao, L.-J.; Allan, I. J.; Arinaitwe, K.; Booij, K.; Helm, P.; Kaserzon, S.; Mueller, J. F.; et al. Aquatic Global Passive Sampling (AQUA-GAPS) Revisited: First Steps toward a Network of Networks for Monitoring Organic Contaminants in the Aquatic Environment. *Environ. Sci. Technol.* **2017**, *51* (3), 1060–1067. https://doi.org/10.1021/acs.est.6b05159.

(116) Schnoor, J. L. Re-Emergence of Emerging Contaminants. *Environ. Sci. Technol.* **2014**, *48* (19), 11019–11020. https://doi.org/10.1021/es504256j.

(117) Richardson, S. D.; Ternes, T. A. Water Analysis: Emerging Contaminants and Current Issues. *Anal. Chem.* **2018**, *90* (1), 398–428. https://doi.org/10.1021/acs.analchem.7b04577.

(118) Wild, C. P. Complementing the Genome with an "Exposome": The Outstanding Challenge of Environmental Exposure Measurement in Molecular Epidemiology. *Cancer Epidemiol. Biomarkers Prev.* **2005**, *14* (8), 1847–1850. https://doi.org/10.1158/1055-9965.EPI-05-0456.

(119) Vrijheid, M. The Exposome: A New Paradigm to Study the Impact of Environment on Health. *Thorax* **2014**, *69* (9), 876–878. https://doi.org/10.1136/thoraxjnl-2013-204949.

(120) Rehberger, K.; Kropf, C.; Segner, H. In Vitro or Not in Vitro: A Short Journey through a Long History. *Environ. Sci. Eur.* **2018**, *30* (23), 12. https://doi.org/10.1186/s12302-018-0151-3.

(121) Ekwall, B. Screening of Toxic Compounds in Mammalian Cell Cultures. *Ann. N. Y. Acad. Sci.* **1983**, *407* (1), 64–77. https://doi.org/10.1111/j.1749-6632.1983.tb47814.x.

(122) Adan, A.; Kiraz, Y.; Baran, Y. Cell Proliferation and Cytotoxicity Assays. *Curr. Pharm. Biotechnol.* **2016**, *17* (14), 1213–1221. https://doi.org/10.2174/1389201017666160808160513.

(123) Aslantürk, Ö. S. In Vitro Cytotoxicity and Cell Viability Assays: Principles, Advantages, and Disadvantages. In *Genotoxicity - A Predictable Risk to Our Actual World*; Marcelo L. Larramendy and Sonia Soloneski, Ed.; InTech, 2018. https://doi.org/10.5772/intechopen.71923.

(124) Mosmann, T. Rapid Colorimetric Assay for Cellular Growth and Survival: Application to Proliferation and Cytotoxicity Assays. *J. Immunol. Methods* **1983**, *65* (1–2), 55–63. https://doi.org/10.1016/0022-1759(83)90303-4.

(125) Ulukaya, E.; Ozdikicioglu, F.; Oral, A. Y.; Demirci, M. The MTT Assay Yields a Relatively Lower Result of Growth Inhibition than the ATP Assay Depending on the Chemotherapeutic Drugs Tested. *Toxicol. In Vitro* **2008**, *22* (1), 232—239. https://doi.org/10.1016/j.tiv.2007.08.006.

(126) Petty, R. D.; Sutherland, L. A.; Hunter, E. M.; Cree, I. A. Comparison of MTT and ATP-Based Assays for the Measurement of Viable Cell Number. *J. Biolumin. Chemilumin.* **1995**, *10* (1), 29–34. https://doi.org/10.1002/bio.1170100105.

(127) Stockert, J. C.; Horobin, R. W.; Colombo, L. L.; Blázquez-Castro, A. Tetrazolium Salts and Formazan Products in Cell Biology: Viability Assessment, Fluorescence Imaging, and Labeling Perspectives. *Acta Histochem.* **2018**, *120*

(3), 159–167. https://doi.org/10.1016/j.acthis.2018.02.005.

(128) Stockert, J. C.; Blázquez-Castro, A.; Cañete, M.; Horobin, R. W.; Villanueva, Á. MTT Assay for Cell Viability: Intracellular Localization of the Formazan Product Is in Lipid Droplets. *Acta Histochem.* **2012**, *114* (8), 785–796. https://doi.org/10.1016/j.acthis.2012.01.006.

(129) Liu, Y.; Peterson, D. A.; Kimura, H.; Schubert, D. Mechanism of Cellular 3-(4,5-Dimethylthiazol-2-Yl)-2,5-Diphenyltetrazolium Bromide (MTT) Reduction. *J. Neurochem.* **1997**, *69* (2), 581–593. https://doi.org/10.1046/j.1471-4159.1997.69020581.x.

(130) Young, F. M.; Phungtamdet, W.; Sanderson, B. J. S. Modification of MTT Assay Conditions to Examine the Cytotoxic Effects of Amitraz on the Human Lymphoblastoid Cell Line, WIL2NS. *Toxicol. Vitr.* **2005**, *19* (8), 1051–1059. https://doi.org/10.1016/j.tiv.2005.05.001.

(131) Honoré, S.; Kovacic, H.; Pichard, V.; Briand, C.; Rognoni, J.-B. A2β1-Integrin Signaling by Itself Controls G1/S Transition in a Human Adenocarcinoma Cell Line (Caco-2): Implication of NADPH Oxidase-Dependent Production of ROS. *Exp. Cell Res.* **2003**, *285* (1), 59–71. https://doi.org/10.1016/S0014-4827(02)00038-1.

(132) Freshney, R. I. *Culture of Animal Cells*; John Wiley & Sons, Inc.: Hoboken, NJ, USA, 2010. https://doi.org/10.1002/9780470649367.

(133) Gasque, K. C. da S.; Al-Ahj, L. P.; Oliveira, R. C.; Magalhães, A. C. Cell Density and Solvent Are Critical Parameters Affecting Formazan Evaluation in MTT Assay. *Brazilian Arch. Biol. Technol.* **2014**, *57* (3), 381–385. https://doi.org/10.1590/S1516-89132014005000007.

(134) Sieuwerts, A. M.; Klijn, J. G. M.; Peters, H. A.; Foekens, J. A. The MTT Tetrazolium Salt Assay Scrutinized: How to Use This Assay Reliably to Measure Metabolie Activity of Cell Cultures in Vitro for the Assessment of Growth Characteristics, IC_{50}-Values and Cell Survival. *Clin. Chem. Lab. Med.* **1995**, *33* (11), 813–824. https://doi.org/10.1515/cclm.1995.33.11.813.

(135) Decker, T.; Lohmann-Matthes, M.-L. A Quick and Simple Method for the

Quantitation of Lactate Dehydrogenase Release in Measurements of Cellular Cytotoxicity and Tumor Necrosis Factor (TNF) Activity. *J. Immunol. Methods* **1988**, *115* (1), 61–69. https://doi.org/10.1016/0022-1759(88)90310-9.

(136) Sumantran, V. N. Cellular Chemosensitivity Assays: An Overview. In *Cancer Cell Culture: Methods and Protocols*; Cree, I. A., Ed.; Humana Press: Totowa, NJ, 2011; pp 219–236. https://doi.org/10.1007/978-1-61779-080-5_19.

(137) Fotakis, G.; Timbrell, J. A. In Vitro Cytotoxicity Assays: Comparison of LDH, Neutral Red, MTT and Protein Assay in Hepatoma Cell Lines Following Exposure to Cadmium Chloride. *Toxicol. Lett.* **2006**, *160* (2), 171–177. https://doi.org/10.1016/j.toxlet.2005.07.001.

(138) Park, S. Y.; Choi, J. Cytotoxicity, Genotoxicity and Ecotoxicity Assay Using Human Cell and Environmental Species for the Screening of the Risk from Pollutant Exposure. *Environ. Int.* **2007**, *33* (6), 817–822. https://doi.org/10.1016/j.envint.2007.03.014.

(139) Johnson, B. T. Microtox® Acute Toxicity Test. In *Small-scale Freshwater Toxicity Investigations: Toxicity Test Methods*; Blaise, C., Férard, J.-F., Eds.; Springer Netherlands: Dordrecht, 2005; pp 69–105. https://doi.org/10.1007/1-4020-3120-3_2.

(140) Brinkmann, M.; Schneider, A.-L.; Bluhm, K.; Schiwy, S.; Lehmann, G.; Deutschmann, B.; Müller, A.; Tiehm, A.; Hollert, H. Ecotoxicity of Nitrogen, Sulfur, or Oxygen Heterocycles and Short-Chained Alkyl Phenols Commonly Detected in Contaminated Groundwater. *Environ. Toxicol. Chem.* **2019**, *38* (6), 1343–1355. https://doi.org/10.1002/etc.4423.

(141) Madrid, F.; Rubio-Bellido, M.; Villaverde, J.; Peña, A.; Morillo, E. Natural and Assisted Dissipation of Polycyclic Aromatic Hydrocarbons in a Long-Term Co-Contaminated Soil with Creosote and Potentially Toxic Elements. *Sci. Total Environ.* **2019**, *660*, 705–714. https://doi.org/10.1016/j.scitotenv.2018.12.376.

(142) Fajardo, C.; Costa, G.; Nande, M.; Martín, C.; Martín, M.; Sánchez-Fortún, S. Heavy Metals Immobilization Capability of Two Iron-Based Nanoparticles (NZVI and Fe3O4): Soil and Freshwater Bioassays to Assess Ecotoxicological

Impact. *Sci. Total Environ.* **2019**, *656*, 421–432. https://doi.org/10.1016/j.scitotenv.2018.11.323.

(143) Bustos, N.; Cruz-Alcalde, A.; Iriel, A.; Fernández Cirelli, A.; Sans, C. Sunlight and UVC-254 Irradiation Induced Photodegradation of Organophosphorus Pesticide Dichlorvos in Aqueous Matrices. *Sci. Total Environ.* **2019**, *649*, 592–600. https://doi.org/10.1016/j.scitotenv.2018.08.254.

(144) Henley, D. V; Korach, K. S. Endocrine-Disrupting Chemicals Use Distinct Mechanisms of Action to Modulate Endocrine System Function. *Endocrinology* **2006**, *147* (6), s25–s32. https://doi.org/10.1210/en.2005-1117.

(145) Shanle, E. K.; Xu, W. Endocrine Disrupting Chemicals Targeting Estrogen Receptor Signaling: Identification and Mechanisms of Action. *Chem. Res. Toxicol.* **2011**, *24* (1), 6–19. https://doi.org/10.1021/tx100231n.

(146) Earl Gray Jr, L.; Wilson, V. S.; Stoker, T.; Lambright, C.; Furr, J.; Noriega, N.; Howdeshell, K.; Ankley, G. T.; Guillette, L. Adverse Effects of Environmental Antiandrogens and Androgens on Reproductive Development in Mammals. *Int. J. Androl.* **2006**, *29* (1), 96–104. https://doi.org/10.1111/j.1365-2605.2005.00636.x.

(147) Czernych, R.; Chraniuk, M.; Zagożdżon, P.; Wolska, L. Characterization of Estrogenic and Androgenic Activity of Phthalates by the XenoScreen YES/YAS in Vitro Assay. *Environ. Toxicol. Pharmacol.* **2017**, *53*, 95–104. https://doi.org/10.1016/j.etap.2017.05.010.

CAPÍTULO 2. OBJETIVOS

Esta tesis consta de 3 objetivos principales donde el hilo conductor se basa siempre en el modelo liposomal de lecitina de soja como membrana sintética natural para el estudio de interacciones de compuestos orgánicos y su distribución en membrana así como metodologías de biodisponibilidad y toxicidad aplicadas a un grupo de contaminantes emergentes seleccionados pertenecientes a diversas categorías, todos ellos incluidos dentro de los denominados productos farmacéuticos y de cuidado personal (PPCPs).

En relación a los contaminantes evaluados en esta tesis y su categoría destacamos:

- Triclosán (TCS o T), agente antiséptico con propiedades antifúngicas y antibacterianas usado en cosméticos (dentífricos, colutorios, desodorantes, etc) y productos de higiene hospitalarios.

- Parabenos (metil y butilparabeno), conservantes utilizados en la industria cosmética y farmacéutica, incluso usados como aditivos alimentarios.

- Diclofenaco (DCF), fármaco de la familia de los antinflamatorios no esteroideos. Se usa para reducir inflamaciones y como analgésico.

- Bisfenol A (BPA), aditivo usado en la fabricación de distintos plásticos que pueden estar en contacto con los alimentos y conocido disruptor endocrino.

- Clorpirifós, plaguicida insecticida. Este compuesto a pesar de no estar incluido dentro de la categoría de PPCP puede estar presente en productos agroalimentarios como frutas, verduras y hortalizas, y cuencas fluviales debido a su uso excesivo en control de plagas de insectos en cosechas.

Los objetivos de la tesis se detallan a continuación:

1. Estudio de los efectos membranotrópicos que puedan causar los contaminantes de preocupación emergente en liposomas constituidos por fosfatidilcolina de soja. Se recurrirá a diversas metodologías para abarcar de una forma holística los procesos de interacción entre xenobiótico y fosfolípido de membrana tanto por técnicas experimentales (fluorescencia y RMN) como computacionales (FDT y DM). Con los resultados obtenidos podremos conocer la alteración en los

parámetros de la bicapa como la polaridad o la fluidez, la interacción del compuesto con regiones específicas de los fosfolípidos junto con sus energías de interacción y geometría de los complejos, y la posición más probable del contaminante dentro de la membrana. Toda esta información nos permitirá entender los mecanismos de interacción contaminante-membrana, evaluar el posible grado de penetración a través de la membrana, así como la alteración que puede provocar dentro de la membrana celular.

2. Desarrollo de un método en flujo inteligente para el monitoreo no supervisado y la investigación de cinéticas de permeación de contaminantes en liposomas constituidos por más de un lípido, como por ejemplo aquellos con distintas concentraciones de colesterol, lo que a su vez condiciona la fluidez y empaquetamiento de los fosfolípidos de la membrana. La finalidad de este sistema basado en la adquisición y procesado de datos por el software CocoSoft es el análisis de múltiples muestras de forma completamente automatizada, desde la toma de la muestra hasta la limpieza del sistema sin intervención del investigador, mejorando así la fiabilidad del método analítico. Los resultados de medidas fluorimétricas usando sondas de membrana nos darán información tanto de los tiempos de estabilización necesarios para llegar a un equilibrio, para la sonda y contaminantes, entre la membrana y el medio acuoso, así como del mayor o menor grado de alteración en la membrana liposomal causados por los contaminantes de interés.

3. Realización de ensayos de citotoxicidad y ecotoxicidad con mezclas binarias de contaminantes. Los primeros se realizarán en células eucariotas de origen humano tanto de colon como de hígado (ambos órganos implicados en el metabolismo de los xenobióticos), mientras que los ensayos de ecotoxicidad se llevarán a cabo en organismos vivos incluyendo bacterias y levaduras. Los resultados obtenidos nos darán una idea de como un compuesto por debajo de su concentración de toxicidad mínima puede afectar a la toxicidad de otro en términos de sinergismo y antagonismo. Estos ensayos se compararán además con experimentos de polarización generalizada en liposomas en busca de una relación entre toxicidad *in vivo* y efectos membranotrópicos *in vitro* con el fin de reducir dentro de lo posible toda manipulación de organismos vivos en pruebas de toxicidad ambiental.

2.1. Objetivos adicionales

Para evaluar la bioaccesibilidad de contaminantes emergentes en muestras ambientales, se llevará a cabo la optimización de un ensayo por inmunoabsorción ligado a enzimas (ELISA) competitivo combinado con un método automático en flujo para la generación *in situ* de nanopartículas de oro (AuNP). La nucleación, crecimiento y distribución de tamaño de las AuNP será monitoreado a tiempo real con el fin de determinar la concentración de diclofenaco (DCF) en agua de mar, sin tratamiento previo, mediante resonancia plasmónica de superficie localizada (LSPR).

En el **anexo I** se incluye un breve resumen del fenómeno de LSPR y su aplicación en ELISA seguido del artículo original titulado "A reliable sensing platform for plasmonic ELISA based on automatic flow-based methodology" donde se detalla todo el proceso de optimización tanto del inmunoensayo como del sistema fluídico.

A pesar de no formar parte del trabajo principal al no incluir los liposomas, este estudio se engloba dentro de la temática de bioaccesibilidad de contaminantes emergentes en muestras ambientales y por tanto tiene cabida dentro de la presente disertación.

Capítulo 3. Estudios Membranotrópicos de Fluorescencia y su Correlación con la Teoría del Funcional de la Densidad

3.1. Resumen

En este trabajo, se han combinado el empleo de sensores y métodos *in silico* para estudiar la biodisponibilidad de contaminantes medioambientales a través de nanopartículas lipídicas (liposomas), las cuales pueden imitar el comportamiento de las membranas biológicas. Se han utilizado dos sondas fluorescentes de membrana (Prodan y Lauran) para el estudio *in vitro* de los efectos membranotrópicos del metilparabeno, butilparabeno y triclosán a distintas temperaturas. Para la monitorización del comportamiento de estos compuestos en la membrana, se han utilizado técnicas de anisotropía de fluorescencia, dispersión de luz y medidas de polarización generalizada. Además, se han aplicado cálculos basados en la teoría del funcional de la densidad (DFT, RI-BP86-D3/def2-SVP) para estudiar las energías de interacción y las geometrías de complejos 1:1 no covalentes formados entre las sondas fluorescentes y los contaminantes emergentes con dipalmitoilfosfatidilcolina como modelo simple de liposoma. Esta información se puede relacionar con el grado de penetración de contaminantes a través de la bicapa lipídica. Los resultados experimentales obtenidos, apoyados por los cálculos DFT y los datos ecotoxicológicos, permiten concluir que las medidas analíticas de fluorescencia de los cambios de empaquetamiento, permeabilidad y fluidez de la membrana son apropiadas para predecir la potencial biodisponibilidad y la toxicidad de contaminantes emergentes.

3.2. Artículo original

A continuación, se adjunta el artículo original "Fluorescent lipid nanoparticles as biomembrane models for exploring emerging contaminant bioavailability supported by density functional theory calculations", de Miquel Oliver, Antonio Bauzá, Antonio Frontera y Manuel Miró, publicado el 31 de mayo de 2016 en la revista *Environmental Science & Technology*.

Environmental Science & Technology

Article

pubs.acs.org/est

Fluorescent Lipid Nanoparticles as Biomembrane Models for Exploring Emerging Contaminant Bioavailability Supported by Density Functional Theory Calculations

Miquel Oliver, Antonio Bauzá, Antonio Frontera,* and Manuel Miró*

Department of Chemistry, University of the Balearic Islands, Carretera de Valldemossa km 7.5, 07122 Palma de Mallorca, Illes Balears Spain

Supporting Information

ABSTRACT: Experimental sensing schemes and thermodynamic in-silico studies are combined holistically in this manuscript so as to give new insights into the bioavailability of environmental contaminants via permeation across lipid nanoparticles (liposomes) as a mimicry of biological membranes. Using Prodan and Laurdan as fluorescent membrane probes, phosphatidylcholine-based unilamellar liposomes are harnessed to investigate membranotropic effects of alkyl esters of p-hydroxybenzoic acid and triclosan in vitro on the basis of steady-state fluorescence anisotropy, light scattering, and generalized polarization measurements. The feasibility of the analytical responses to ascertain differences in temperature-dependent contaminant bioavailability is investigated in detail. High level density functional theory (DFT) calculations (RI-BP86-D3/def2-SVP) have been resorted to investigate noncovalent 1:1 complexes of the fluorescent probes and emerging contaminants with dipalmitoylphosphatidylcholine, as a minimalist model of a lipid nanoparticle, to evaluate both the interaction energies and the geometries of the complexes. This information can be related to the degree of penetration of the guest across the lipid bilayer. Our experimental results supported by in-silico DFT calculations and ecotoxicological data let us to conclude that simple analytical measurements of liposomal changes in lipid packaging, permeability, and fluidity are appropriate to foresee the potential bioavailability and toxicity of emerging contaminants.

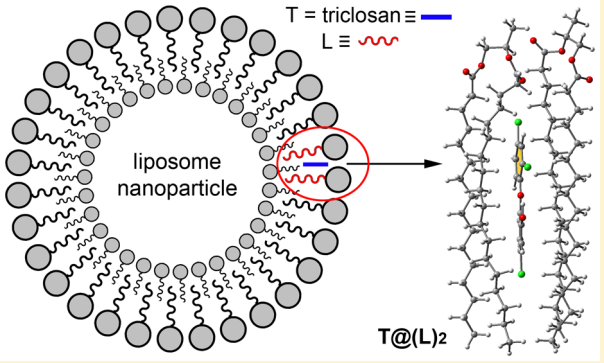

INTRODUCTION

Risk assessment of potentially contaminated environmental compartments usually aims at holistically exploring the potential exposure of exogenic compounds to biota[1−4] or the cause-effect relationships in untargeted assays capitalizing upon effect-directed analysis.[5,6] The broad concept of contaminant bioavailability might encompass up to three steps: (i) solubility or bioaccessibility studies, (ii) environmental bioavailability, and finally (iii) toxicological biovailability as endorsed by ISO 17402:2008.[7] A bioavailable compound might be defined as that which is freely available, and thus bioaccessible, to cross an organism's cellular membrane from the medium the organism inhabits.[2,8] Once transfer across the membrane has occurred, investigation of toxicokinetics in the organism including internal transport, metabolism, and excretion constitutes the last step of human health risk assessments.[9] A battery of toxicological assays at a target receptor or more advanced (bio)analytical approaches involving (i) environmental metabolomics, for identification of endogenous metabolites as biomarkers of contaminant exposure at sublethal levels,[10] and (ii) partition-based dosing techniques, using contaminant-loaded sorbent matrixes in combination with biota for identifying observable effects of toxicants from the simplified sample matrix,[11] might nicely embrace the holistic view of bioavailability. However, in vivo testing methods and the use of experimental organisms are not recommended by REACH guidelines because of ethical considerations,[12] rather the exploration of nonbiota based viable alternatives as a proxy for contaminant bioavailability by a given living organism or the human body. Partitioning based approaches using a variety of deployable passive dosimeters, including (i) semipermeable membrane devices (SPMD)[13−16] and (ii) solid-phase microextraction based devices,[17,18] furnished with varied membranes of hydrophobic nature (e.g., polydimethylsiloxane,[19] low-density polyethylene or composite materials) have been resorted for many years (also allied to the effect-directed analysis concept[5]) to the uptake of freely dissolved concentrations of organic pollutants occurring in environmental aquatic compartments. The aim behind is to shed light on bioavailable fractions under conservative scenarios. In fact, SPMD and related approaches might bias priorization of

Received: February 13, 2016
Revised: May 4, 2016
Accepted: May 31, 2016
Published: May 31, 2016

DOI: 10.1021/acs.est.6b00772
Environ. Sci. Technol. 2016, 50, 7135−7143

bioavailable and thus hazardous compounds toward lipophilic fractions, which in many instances are in good agreement with the octanol−water (K_{ow}) partition coefficients. This indicates the quest for novel in vitro methods for better simulation of the potential permeation through biological membranes as is contemplated in the bioavailability concept.

Bearing in mind the amphiphilic nature of phospholipids constituting cellular membranes, interactions of target species with cell components other than hydrophobic partitioning with the acyl chains of the lipids including dipole−dipole and hydrogen bonding with the polar heads of the lipids need to be explored for ascertainment of membranotropic effects and the extent of permeability of those exogenous species across the lipid bilayer.[20,21] In the mimicry of physiologically based processes, lipids nanoparticles or vesicles, also termed liposomes, are deemed most appropriate minimal biologically relevant models of cell membranes.[22,23] Phosphatidylcholine (PC) is the major membrane phospholipid in eukaryotic cells along with the major structural component of cellular membranes.[20,21] To this end, biologically derived PC-based liposomes are promising nanometer-scale particles to ascertain potential in vitro bioavailability via membrane perturbation effects across a range of organic pollutants through natural lipid membranes. In fact, liposomes prepared from natural PC serve to mimic the heterogeneous composition of the biological cell membranes.

In this work, PC-based large unilamellar liposomal nanoparticles tailored with two distinct polarity-sensitive membrane probes with the naphthalene backbone as fluorophore, namely, Prodan and Laurdan,[24−26] were harnessed for discrimination of membranotropic effects at the polar head and acyl chains of PC, respectively, so as to indicate the actual risk of pollutant bioavailability. The idea behind is to identify the extent of permeation of moderately polar emerging contaminants (EC) with log K_{ow} spanning from 1.96 to 4.76 and solubilities from 10 to 2500 mg/L (namely, triclosan, butylparaben, and methylparaben), taken as model compounds, across lipid bilayers. The motivation of this research is linked to recent amendments of EU regulation 1223/2009 on cosmetic products for preservatives with compliance from 30 October of 2014 (Commission Regulation (EU) No. 358/2014)[27] and 16 April of 2015 (Commission Regulation (EU) No. 1004/2014),[28] respectively, in which esters of 4-hydroxybenzoic acids (including methylparaben) are restricted to a maximum concentration of 0.4% but butylparaben down to 0.14%;[28] and triclosan to 0.2% in mouthwashers and 0.3% in the remainder of cosmetic products.[27]

Polarization fluorescence spectroscopy and fluorescence anisotropy are harnessed as detection techniques to explore the magnitude of temperature-dependent changes in lipid arrangement, and membrane fluidity,[29−32] as advantageous measures to account for EC bioavailability. Light scattering is also evaluated as a detection technique to elucidate alterations in liposome size and topography. Although liposomal nanoparticles have been used in research for many years to investigate biophysical responses of membranes to external stimuli[26,29,33] and biological activity of water-soluble drug formulations,[34−36] the feasibility of fluorophore-bearing liposomal nanoparticles as markers for in vitro elucidation of the degree of penetration of ECs into biomembrane models has not been described as of yet. Qualitative or semiquantitative information afforded by fluorescent liposomal systems is usually capitalized on binary (yes/no) response or trial and error observations. For further insight into the permeation of ECs across PC environments, the physicochemical nature and structure of the target species need to be contemplated. Hereto, thermodynamic high level density functional theory (DFT) calculations relying upon quantum mechanics have been adopted in this work to quantify the interaction energies and the geometries of noncovalent adducts between organic exogenous species and the amphiphilic domain of dipalmitoylphosphatidylcholine (C16:0), taken as a model of well-ordered phospholipid structure. To the best of our knowledge, a holistic approach combining liposome based fluorescence spectroscopic data with in silico DFT theoretical studies is presented for first time herein for expedient assessment of the impact of emerging environmental xenobiotics onto biomembrane models on the basis of their bioavailability in risk assessment scenarios.

EXPERIMENTAL SECTION

Reagents, Analytes, and Instrumental Detection Techniques. Large unilamellar hollow lipid nanoparticles, obtained by mechanical dispersion of lipids in aqueous medium with the aid of rotating knives, were kindly provided by ENOC Solutions (PC2 liposomes, Port d'Andratx, Balearic Islands, Spain, http://www.transtechnics.com/), and used as received. A stock solution of liposomal nanoscale particles was made of soybean lecithin containing ≥94% phosphatidylcholine (PC) with a concentration of 100 mg/mL and average molecular weight of 787g/mol. The major fatty acid components of soybean PC consist of acyl moieties of 18:2, 16:0, and 18:1 with nominal percentages of 63%, 14.9%, and 11.4% respectively. It also contains ≤4% lysophosphatidylcholine (lyso-PC) and ≤3% of nonpolar lipids as minor ingredients. The intensity weighted mean hydrodynamic size of vesicles (Z average) was 159 ± 2 nm with a polydispersity index of 0.105 as calculated by Quasi Elastic Light Scattering (QELS) using the NanoBrook 90Plus Particle Size Analyzer (Brookhaven, Holtsville, New York). A transmission electron micrograph of hollow liposome nanoparticles at the 4 mg/mL PC level is shown in Figure S1 (Supporting Information, SI). The transition phase temperature interval from the gel to liquid crystalline phase as determined by differential scanning calorimetry (DSC 3+, Mettler-Toledo, Barcelona, Spain) ranged from −28 to 5 °C as a consequence of the heterogeneity in the composition of fatty acids and the occurrence of a small percentage of lyso-PC. In fact, no sharp phase transition is reported in membranes having a complex chemical composition.[35,37] In our case, a phase pretransition temperature is identified at ca. −20 °C with a second transition at −4.5 °C (see Figure S2). Working standard solutions of 50 μmol/L PC bearing liposomes were prepared—by serial dilution—in 10 mmol/L HEPES buffer at pH 7.4 containing 0.1 mol/L NaCl. This concentration was selected aimed at affording a clear suspension of lipid nanoparticles to prevent light scattering within the range of 350−500 nm. Turbidity might cause fluorescence depolarization, which decreases the anisotropy linearly with the solution optical density.[38,39] Under the above experimental conditions, the optical density at 440 nm (anisotropy detection wavelength) was merely 0.015 AU.

The fluorescent membrane probes, viz., 6-dodecanoyl-2-dimethylaminonaphthalene (Laurdan) and 6-propionyl-2-dimethylaminonaphthalene (Prodan), and emerging contaminants (EC), viz., methyl paraben, butyl paraben, and triclosan (see Scheme S1) were purchased from Sigma-Aldrich, Madrid, Spain. Stock solutions of probes and EC were prepared at concentration levels of 10 mmol/L in dimethyl sulfoxide and 10

DOI: 10.1021/acs.est.6b00772
Environ. Sci. Technol. 2016, 50, 7135−7143

g/L in methanol, respectively. Working solutions of both probes were fixed to 2 μmol/L throughout while bioavailability test assays of EC were carried out at the 10 μg/mL level. The concentration level of target species was set two decades below the maximum allowed concentration in cosmetics as endorsed in current EU legislation frameworks.[27] The Laurdan/PC concentration ratio was set to 1:25 throughout, according to previous authors,[26] so as to ameliorate method's sensitivity in fluorescence generalized polarization (GP) and membrane anisotropy measurements.

Probe anisotropy fluorescence and GP spectroscopic measurements were performed by a Varian Cary Eclipse fluorescence spectrometer (Agilent technologies, Mulgrave, Victoria) equipped with a Xenon flash lamp and a thermostated quartz cell with an inner volume of 1.4 mL and 10 mm-path length using the Cary Eclipse manufacturer's software for spectra recording and data processing. A Peltier 4-position multicell holder accessory that permits fluorescence measurements on up to four samples, while precisely controlling the temperature and rate of stirring, was selected for fast sequential experiments. Dynamic light scattering measurements for investigation of the size and internal complexity of liposomal PC nanoparticles were effected with Beckman Coulter's Epics XL-MCL flow cytometer (Beckman Coulter Ltd., Brea, CA) equipped with the WinMDI 2.9 software.

Analytical Procedure. *Fluorescence Measurements.* A solution of 5.0 mL of 50 μmol/L PC-bearing liposomal nanoparticles was incubated in an amber vial with either 2 μmol/L Laurdan for 75 min or 2 μmol/L Prodan for 10 min at room temperature and in the dark with gentle agitation every 5 min. A further incubation with the biocides at the 10 μg/mL level was undertaken for 15 min under identical experimental conditions as for probes with nanoscale liposomes. Anisotropy fluorescence and GP readouts were recorded in quadruplicate for probe-bearing liposomes in EC containing or EC-free solution at 3 °C, 10 °C, 25 °C, and 37 °C for repeatability studies, with a delay of 5 min prior to effecting the reading at a preset temperature. Magnetic agitation with 2.5 mm diameter PTFE magnetic stirring bar (BRAND, Sigma-Aldrich, Madrid, Spain) was used throughout.

Fluorescence Generalized Polarization. Laurdan and Prodan fluorescence emission spectra are blue-shifted with a maximum signal at around 440 nm (I_B) in nonpolar media and, red-shifted spectrum with maximum fluorescence intensity at 490 nm (I_R) in aqueous media. GP values were calculated using the following equation:

$$GP = \frac{I_B - I_R}{I_B + I_R}$$

The penetration of water into the liposomal bilayer leads to a decrease of probe's excited state energy for reorientation of solvent molecules in the so-called dipolar relaxation phenomenon, which is reflected in a continuous bathochromic shift of the probe's emission spectrum. The bathochromic shift does not depend on the polar head and its charge,[24] merely on the phase state of the lipid bilayer.[40] In the gel phase, the values of GP are high and positive, whereas the liquid-crystalline phase features low and normally negative values. GP varies in all cases between −1 and +1. In this article, the fluorescence excitation wavelength was set to 360 nm for both probes, with 5 nm slits widths and a 650 V photomultiplier (PTM) detector voltage. Fluorescence emission spectra were registered from 400 to 600 nm at 10 Hz with a 10 nm/s scan rate (1 nm-resolution) for every sample and temperature assayed.

Steady-State Fluorescence Anisotropy. Fluorescence anisotropic measurements (r_{ss}) were performed for Laurdan with polarized excitation light in L-format (single emission channel) with 10 nm slit widths and a 600 V PMT detector voltage. Fluorescence emission intensities at 440 nm, with excitation at 350 nm, were recorded for the excitation and the emission polarizers mounted vertically (I_{VV}) and for the excitation and the emission polarizers in vertical and horizontal orientation, respectively (I_{VH}), using the *Advanced Reads* module, as per the equation below:[41]

$$r_{SS} = \frac{I_{VV} - GI_{VH}}{I_{VV} + 2GI_{VH}}$$

The instrument-related G factor is estimated as the ratio of the sensitivities of the polarizer for vertically (I_{HV}) and horizontally polarized emission (I_{HH}) using horizontally polarized excitation. This parameter offsets the contribution of the measurement pathway to the observed total polarization, and is calculated as follows:

$$G = \frac{I_{HV}}{I_{HH}}$$

In our case, the G factor within the temperature range of 3−37 °C is estimated as 1.47 ± 0.01.

THEORY

Computational Methods. The geometries of the complexes and interaction energies were computed using the BP86 functional couple with Grimme's latest available correction of dispersion (D3).[42] The def2-SVP basis set was used for optimization. Solvent effects were taken into account using discrete water molecules in the polar head level of the phospholipid and also a polarizable continuum model (COSMO)[43] implemented in the TURBOMOLE 7.0 software.[44] No symmetry constrains were imposed in the course of the study of the interaction of water molecules with the C16:0 PC model (denoted as **P** in Figure 1, see also Scheme S1). The idea behind is to select the most abundant saturated fatty acid in soybean lecithin for which the strongest hydrophobic interactions are to occur with the aliphatic chains of probes and ECs. The 1:1 complexes between the phospholipid molecule and the probes (Prodan (**p**) and Laurdan (**l**)) or contaminants (triclosan (**T**), methylparaben (**M**), and butylparaben (**B**)) were first optimized keeping the PC frozen as a first stage followed by allowing 13 discrete water molecules to reorganize. Diagrammatic descriptions of the PC phospholipid used as a minimalist model of liposome along with several complexes with the fluorescent probes are illustrated in Figure 1. The BP86-D3/def2-SVP level of theory is a good compromise between the accuracy of the results and the size of the system. We have used electronic energies without zero point energy correction due to the size of the systems evaluated. The BP86-D3 method has been previously used to successfully analyze a variety of noncovalent interactions including those studied herein.[45]

Underlying Principles of Anisotropy and Fluorescence Generalized Polarization in Liposome Based Bioavailability Testing Supported by DFT Calculations. Steady-state fluorescence emission spectra and Stokes shifts of the fluorophore-bearing Laurdan and Prodan probes are good

DOI: 10.1021/acs.est.6b00772
Environ. Sci. Technol. 2016, 50, 7135−7143

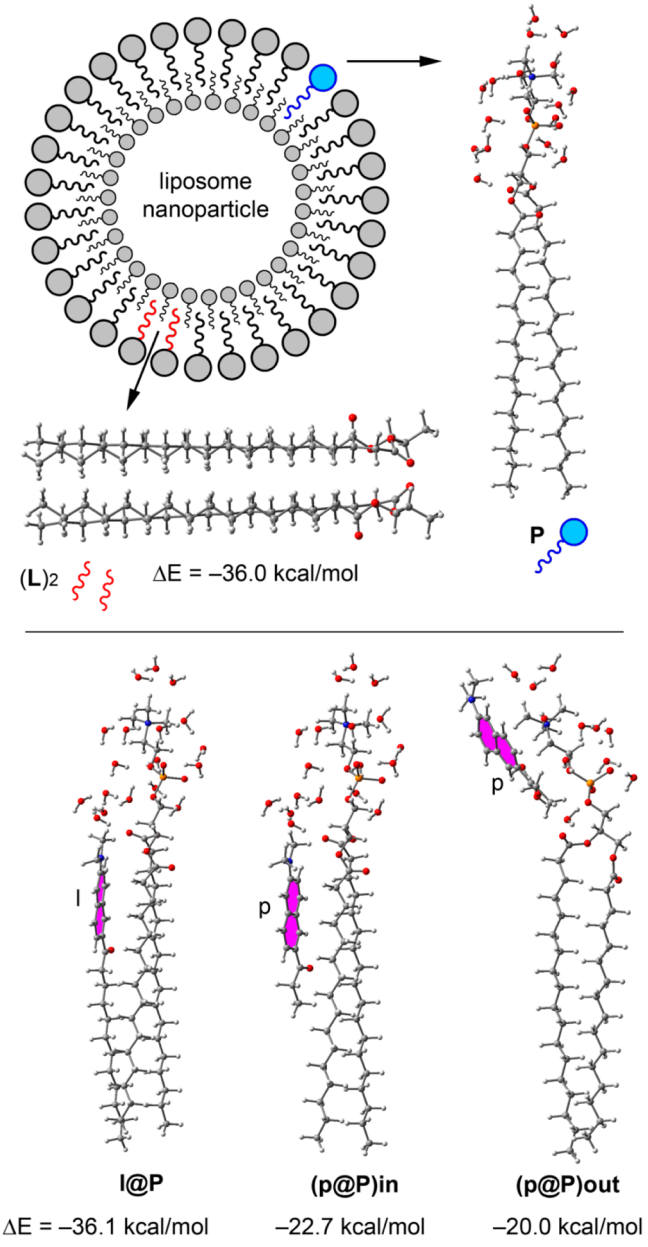

Figure 1. Schematic representation of the liposomal nanoparticle, the in-silico DFT model of solvated phospholipid (**P**) and its complexes with Laurdan (**l**) and Prodan (**p**). A dimer $(\mathbf{L})_2$ of the hydrophobic acyl chain region of **P** is also illustrated.

indicators of structural and dynamic alterations of liposome lipid bilayers. Notwithstanding the fact that the two probes are supposedly probing distinct depths of the lipid membrane phase, no thermodynamic predictions are found in the literature reporting interaction energies of the two probes at the hydrophilic−hydrophobic interface of the liposomal nanoparticle. Insights are here provided for the first time by quantum mechanics. Whenever inserted into the PC liposome, we have demonstrated (see Figure 1) that the Laurdan lauric tail aligns with the phospholipid acyl chain region and the $N(CH_3)_2$ moiety attached to the fluorophore naphthalene ring (highlighted in fuchsia in Figure 1) locates at the phospholipid glycerol backbone. The computed interaction energy of the **l@P** complex is ΔE = −36.1 kcal/mol. Using Laurdan one can thus employ its spectral sensitivity to measure variations in a deep stratum of the membrane in the presence of contaminants. Permeation of a given contaminant might lead to a loose and disordered liposome structure and allows more water to partition into the hydrophilic−hydrophobic interface. Conversely, higher ordering of the lipid chains might be also triggered by the contaminant thus resulting in a less polar microenvironment for Laurdan. To quantify the above effects, Laurdan's fluorescence emission intensities at the blue (nonpolar environment) and the red (polar environment) edges of the spectrum were taken to measure the probe's fluorescence GP along with its temperature dependence relative to the phase behavior of the lipid molecules surrounding the probe.

Using in-silico DFT data for Prodan, two **p@P** complexes (in and out, see Figure 1) with similar binding energies (ΔE = −22.7 and −20.0 kcal/mol, respectively) are encountered. At this point, several considerations should be made. First, the probe in the liposome is expected to develop at least two concurrent interactions with two phospholipid molecules. Assuming that the binding is additive, the interaction energies will be approximately −72.2 kcal/mol and −45.4 kcal/mol for Laurdan and Prodan, respectively. Second, the long acyl chains of **P** are interacting with adjacent molecules in the liposome, therefore for the probe to penetrate into the liposomal nanoparticle two **P** chains must be at least separated. We have also computed the interaction energy of two pair of acyl chains in the hydrophobic core of the liposome, denoted as $(\mathbf{L})_2$ in Figure 1. The resulting interaction energy is ΔE = −36.0 kcal/mol. Consequently, the incorporation of the probe is only favored when surpassing the energy to separate the acyl chains. This is the case of Laurdan, since the interaction with two phospholipid chains (ΔE = −72.2 kcal/mol) is favorable against the energy for breaking $(\mathbf{L})_2$. However, the balance for Prodan is only −9.4 kcal/mol, which is deemed insufficient to compensate the interaction energy of the outer arrangement (ΔE = −20.0 kcal/mol, see **(p@P)out** in Figure 1) without the energy penalty to separate the chains. This preliminary study agrees well with experimental evidence reported in the literature,[24,25] suggesting that Laurdan interacts with the interior part of the liposome while Prodan is more dynamic and remains in the polar head region. Further theoretical considerations of the role of solvent dipolar relaxation upon GP measurements are available in the SI.

Bioavailability of target species across lipid membranes can also be explored in vitro via steady-state fluorescence anisotropy based on the principle of photoselective excitation of Laurdan's naphthalene moiety by polarized light, which is sensitive to rotational diffusion of the fluorophore.[41] Probe's fluorescence anisotropy is related to lipid bilayer microviscosity, hence inversely correlated with its fluidity. When the membrane is rigid the fluorescent dye cannot rotate so the emission polarized light is high. On the contrary, membranotropic effects increasing PC mobility and membrane fluidity (e.g., supramolecular interactions with exogenic species) lead to suppression of fluorescence anisotropy. Brownian rotation of the fluorophore-bearing liposomes causes in our case negligible depolarization inasmuch as the rotational rate is much slower than the rate of fluorescence emission. In this work, the magnitude of the permeation and insertion of ECs into the liposomal nanoparticle might be thus evaluated semiquantitatively by the variation of Laurdan's fluorescence anisotropic measurements whereby the larger the variation the greater the potential bioavailability of the contaminant becomes.

DOI: 10.1021/acs.est.6b00772
Environ. Sci. Technol. 2016, 50, 7135−7143

RESULTS AND DISCUSSION

Optical Scattering Results. Preliminary experimental explorations of EC bioavailability using biomembrane mimetic systems were conducted via flow cytometric measurements (see SI). Notwithstanding the fact that the particle size distribution of large unilamellar vesicles lies at the bottom end of the particle size requirements for detection of scattered light in flow cytometry optical scattering maps are deemed useful screening tools for qualitative exploration of membranotropic effects by external agents as illustrated in Figure S3. The 2D bivariate dot plots of forward-scattered (FS) versus side-scattered (SS) light foster the visualization of potential differences between empty lipid nanoparticles populations and those in the presence of target species. A broader dispersion of SS data is observed for triclosan against the two parabens and empty liposomes, while no significant changes in liposome sizes as identified by FS are observed in any case. Bearing in mind that SS data are proportional to surface topography and internal complexity of the nanoscale liposomes, greater membrane permeability and thus potential bioavailability is identified for triclosan, which is in good agreement with GP and fluorescence anisotropy results and thermodynamic calculations. For quantitative assessment of membranotropic effects the ratio of SS events at half peak maximum (M1, see Figure S4) to the total number of effective events (MT) is compiled in Table S1. Note that MT is variable and much lower that the nominal number of events (set in our case to 10 000) because of size particle limitations in flow cytometry and the fact that more than one liposome might move through the laser beam at a given moment. Light scattering results with M1/MT ranging from 0.47 to 0.49 indicated that no significant differences between empty liposomes and those with methylparaben and butylparaben at the 10 μg/mL level are observed, yet the internal complexity of the liposomes significantly increased and was greatly variable with triclosan (wider SS peak) at the same concentration level with an M1/MT ratio as high as 0.60.

Bioavailability Tests Based on Fluorescence Generalized Polarization Spectroscopy. On the basis of the scarcity of investigations in previous communications dealing with fluorescence GP measurements, preliminary experiments were undertaken so as to set the incubation times of PC liposomes with the fluorescent membrane probes with and without the addition of EC until steady-state fluorescence readouts were obtained. Experimental results revealed that Prodan GP reached steady-state measurements in about 10 min as expected for more shallowly located probes in contrast to Laurdan for which GP values stabilized after 75 min as a consequence of probe penetration into deeper regions of the lipid bilayer. Laurdan's time-dependent batochromic shift is attributed to the progressive membrane hydration at the level of PC glycerol backbone to which Laurdan's fluorophore is aligned (see Figure 1). As for incubation of probe-loaded liposomes with the ECs steady-state GP responses were afforded in 15 min with a slight variation by 1.5% in GP values until 35 min. Several previous authors reported incubation times for Laurdan in PC liposomes of a mere 5 min,[35] 15 min,[31,33] or 30 min.[46] Insufficient probe stabilization times would in turn jeopardize the interpretation of the liposome membranotropic effects by the action of ECs.

Below in Figure 2 and Table S2 are given the experimental Laurdan's GP results for the probe alone as compared with those obtained in the presence of individual biocides (methylparaben, butylparaben and triclosan) at the concentration levels set in Experimental at 3 °C, 10 °C, 25 °C, and 37 °C. Statistical *t*-tests of comparison of experimental means (α = 0.05) were preceded by the evaluation of potential outliers using the Grubbs' test and the comparison of sample variances via *F*-test.

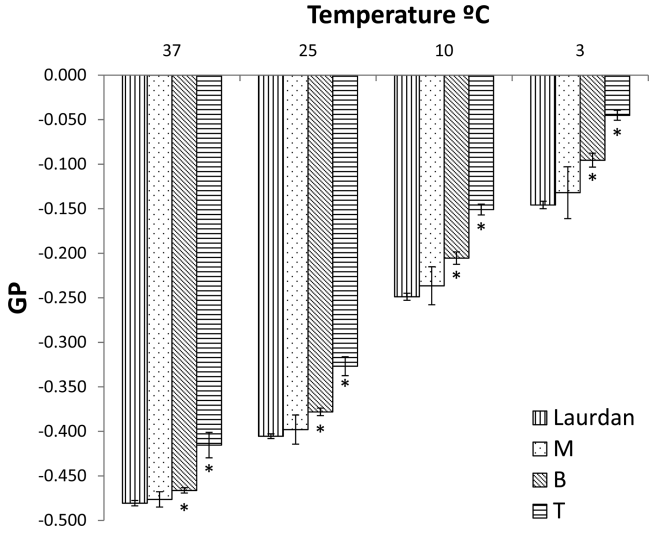

Figure 2. Laurdan's fluorescence Generalized Polarization (GP) data of PC liposomes with EC or EC-free solution in bioavailability testing. Experimental data are obtained at four temperatures (3 °C, 10 °C, 25 °C, and 37 °C). Statistically significant differences between control (Laurdan-embedded PC) or experimental (Laurdan-embedded PC with ECs) solutions are indicated with an asterisk.

Regardless of the incubation temperature, Laurdan's fluorescence GP values for the probe alone were in all instances negative within the range of −0.481 to −0.146, indicative of the liquid-crystalline phase of soybean lecithin based vesicles. This also holds true for the bioavailability tests in the presence of biocides. Experimental results with relative standard deviations (RSD) ≤ 13% compiled in Table S2 suggested that a temperature-dependent variation of GP occurred for triclosan and butylparaben with statistically significant increase upon decreasing the temperature from 37 °C to 3 °C. The GP increase (hypsochromic shift) for butylparaben and triclosan suggests enhanced lipid packing and ordering at the glycerol level with concomitant membrane dehydration. This effect is less remarkable at temperatures ≥25 °C inasmuch as the bioavailability tests are conducted at temperatures far above the lipid main phase transition temperature. Triclosan with half as much molar concentration (viz., 34.5 μM **T** against 65.7 μM **M**) modified Laurdan's GP values to a greater extent than parabens with a GP increase from ca. 14 to 69% as compared to Laurdan alone (see Table S3), which is indicative of a greater penetration into lipid membranes. As for butylparaben, a 3-fold increase of GP against methyparaben is observed regardless of the temperature to which the bioavailability test is performed. Examples of the time-resolved emission spectra and hypsochromic shift of Laurdan embedded PC liposomal nanoparticles with triclosan against triclosan-free solution at 3 and 37 °C are depicted in Figure S5.

Experimental GP values of Prodan, with RSD ≤ 11% (see Figure S6 and Tables S4 and S5), are slightly lower than those of Laurdan, which is in good agreement with observations by Först et al.[34] This is a consequence of the fact that Prodan is located more shallowly in the lipid bilayer, as demonstrated by

DOI: 10.1021/acs.est.6b00772
Environ. Sci. Technol. 2016, 50, 7135−7143

DFT calculations (see Figure 1).Our findings in Figure S6 and Tables S4 and S5 indicate that Prodan in PC liposomes was affected by the presence of biocides to a much lesser extent than for Laurdan, and thus supramolecular interactions with the polar moieties of the membrane phase are deemed weaker, especially for both 4-hydroxybenzoate derivatives. A bathochromic shift is however induced by triclosan at two temperatures. This is attributed to the reorganization of Prodan at the membrane phase−water interface triggered by vesicle ordering at the phospholipid acyl chain region as a result of which the probe is pulled out and partition into the aqueous medium increases. Previous authors exploring interaction of antioxidant species with liposomes as biomembrane model systems speculated that short-tailed probes might be pulled toward the outer polar region in the course of penetration of a lipophilic compound.[47] Using computational modeling, this assumption has been demonstrated on the basis of the similar binding energies of the outer and inner Prodan arrangements with ΔE = −22.7 and −20.0 kcal/mol, respectively. Hence, the variation of Prodan GP values might be regarded as a false positive inasmuch as no significant modification of the domain structure at the polar head moieties is likely to occur.

As a result of the membranotropic effects indicated above and distinct behavior between Laurdan and Prodan supported by significant differences in GP values, triclosan is expected to penetrate deeper into the lipid bilayer and alter by supramolecular interactions the packing of phospholipids stronger. Of the three EC studied triclosan is therefore deemed the most bioavailable species, followed by butylparaben. Negligible effects by methylparaben on Prodan and Laurdan GP data suggested that methylparaben is prone to remain in the aqueous phase.

Bioavailability Tests Based on Fluorescence Anisotropy. As is the case with bioavailability tests relying upon GP measurements, triclosan afforded the largest variation in liposome steady-state anisotropy fluorescence as compared to Laurdan alone (control), increasing up to 22% (see Figure 3 and Tables S6 and S7) against variations down to 5% for the other two parabens. On the contrary, fluorescence anisotropy of liposomal Laurdan in the presence of triclosan shows greater variation as the temperature increases. As a result of the looser structure of the phospholipid bilayer at higher temperatures, triclosan seems to penetrate deeper (c.f.r. next section) and becomes confined in a hydrophobic environment at physiological temperature (37 °C). This is attributed to the stiffening effect by the hydrophobic interactions between the aromatic rings of triclosan and the acyl chains with the subsequent enhancement of liposomal microviscosity. Identical observations have been reported by independent researchers exploring biophysical effects of natural antioxidants (viz., resveratrol and curcumin) on PC-based liposomes.[48,49]

This accounts for the fact that Laurdan's GP for triclosan is less changeable at higher temperatures as compared to the control system (probe alone) because of increased bioavailability of triclosan, which locates in a deeper stratum of the lipid bilayer as compared to Laurdan.

In-Silico DFT Calculations for Prediction of Membranotropic Effects. The DFT optimized structures of methylparaben (**M**), butylparaben (**B**), and triclosan (**T**) are shown in Figure 4 along with their 1:1 complexes with **P** and their corresponding binding energies. From the inspection of the computational results, several interesting considerations can be made. First, **M** and **B** are basically planar molecules and,

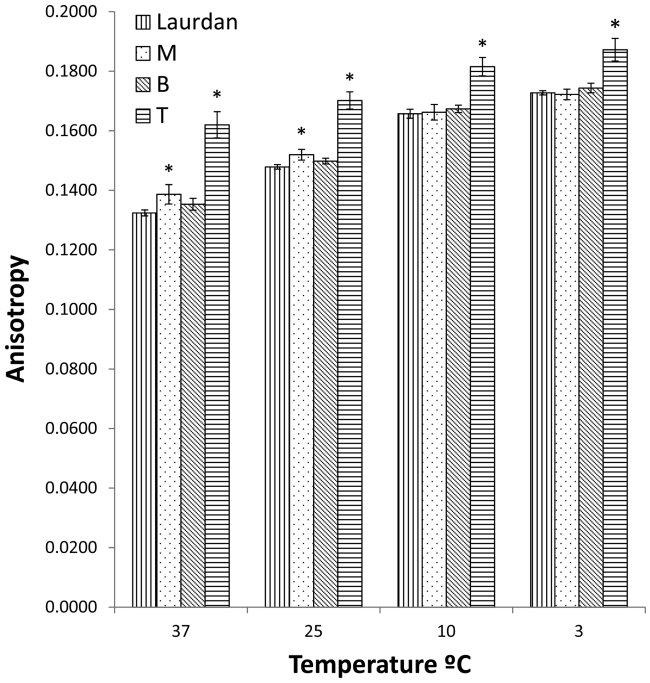

Figure 3. Fluorescence anisotropy measurements for Laurdan-embedded PC liposomes with EC or EC-free solution in bioavailability testing. Experimental data are obtained at four temperatures (3 °C, 10 °C, 25 °C, and 37 °C). Statistically significant differences between control (Laurdan-embedded PC) or experimental (Laurdan-embedded PC with ECs) solutions are indicated with an asterisk.

conversely, **T** is nonplanar. Therefore, the diffusion of **T** across the lipid bilayer compared to the other contaminants and probes is expected to be sterically more difficult. We have, however, the energetic difference between the minimum energy geometry (nonplanar) and an imposed planar conformation (denoted as **T′**), which is 3.8 kcal/mol. Second, **B** complexed to **P** either at the hydrophobic region **(B@P)in** or at the polar head level **(B@P)out** presents similar interaction energies (ΔE = −27.8 and −27.0 kcal/mol, respectively). Therefore, the computational model indicates that the contaminant would remain in the outer shell of the liposomal nanoparticle, inasmuch as the energy cost to separate the chains of two contiguous phospolipids is ΔE = −36.0 kcal/mol (see Figure 1). Third, **M** has even a higher tendency to remain outside the nanoparticle as the interaction with the polar moieties of the phospolipid (ΔE = −31.1 kcal/mol) is more favorable than that with the acyl chains of **P** (ΔE = −22.2 kcal/mol). Finally, **T** bears a totally different behavior. The noncovalent complex with the polar moieties is less favorable (ΔE = −9.8 kcal/mol) than that with the nonpolar chains (ΔE = −22.2 kcal/mol). An interesting issue is that the interaction with the chains induces a coplanarity of the aromatic rings in **T**, thus facilitating the permeability across the lipid membrane. For this contaminant with the strongest ability to penetrate across PC lipid layers, based on DFT calculations, we have also computed a ternary complex where **T** is sandwiched between two phospholipids (hydrophobic part), denoted as $\mathbf{T@(L)_2}$ that affords a very large interaction energy (ΔE = −65.8 kcal/mol). Interestingly, the geometry adopted by **T** in the ternary complex is totally planar (see $\mathbf{T@(L)_2}$ in Figure 4). This large interaction energy is able to compensate the energy (−36.0 kcal/mol) required to separate the chains of two contiguous phospholipids, thus

DOI: 10.1021/acs.est.6b00772
Environ. Sci. Technol. 2016, 50, 7135−7143

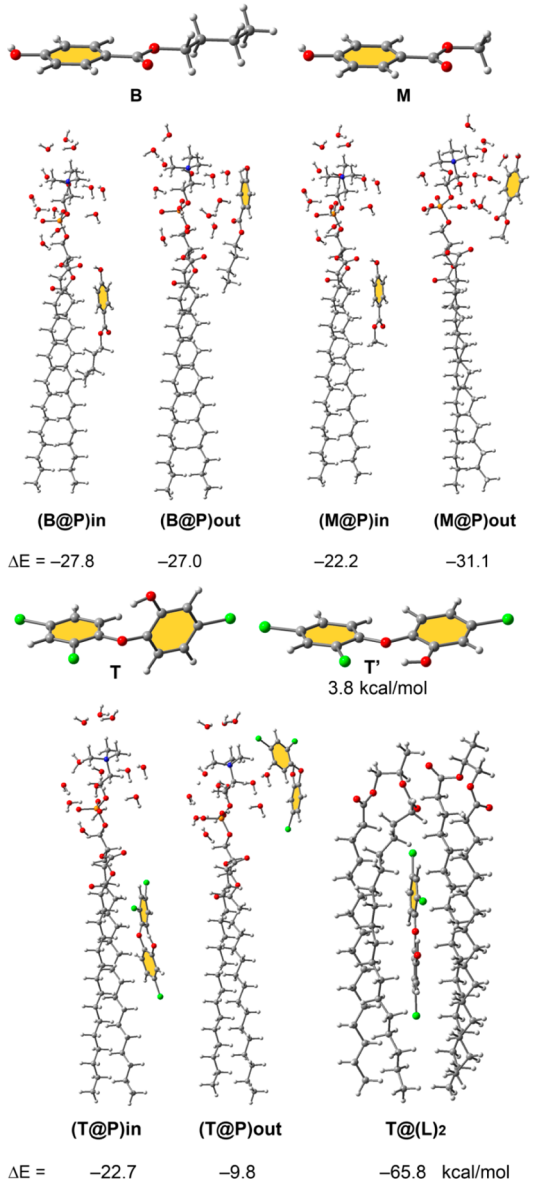

Figure 4. In-silico DFT optimized geometries of the three ECs and their noncovalent 1:1 complexes with **P** at two depths (polar head and glycerol region) and $(\mathbf{L})_2$. Binding energies are also indicated.

indicating a facile diffusion process of this contaminant toward the core of the liposomal nanoparticle.

We have further analyzed the ability of triclosan to diffuse across the lipid bilayer by computing several binary complexes locating **T** at different liposomal depths (see Figure 5). Computational results suggested that the initial position where the triclosan is close to the glycerol moiety presents slightly lower interaction energy than the other two positions where the triclosan is either in the midst or at the hydrophobic end of the aliphatic chains. This clearly indicates that triclosan can move freely through the fatty acid region of the bilayer phase.

Critical Evaluation of Computational and Experimental Bioavailability Results with Ecotoxicological Data. Experimental results with nanoscale lipid nanoparticles using naturally occurring phospholipids and in-silico DFT calculations were contrasted with ecotoxicological information by acute toxicity tests in a variety of trophic groups including bacteria (viz., *Vibrio fisheri*),[50−55] invertebrates (*Daphnia*

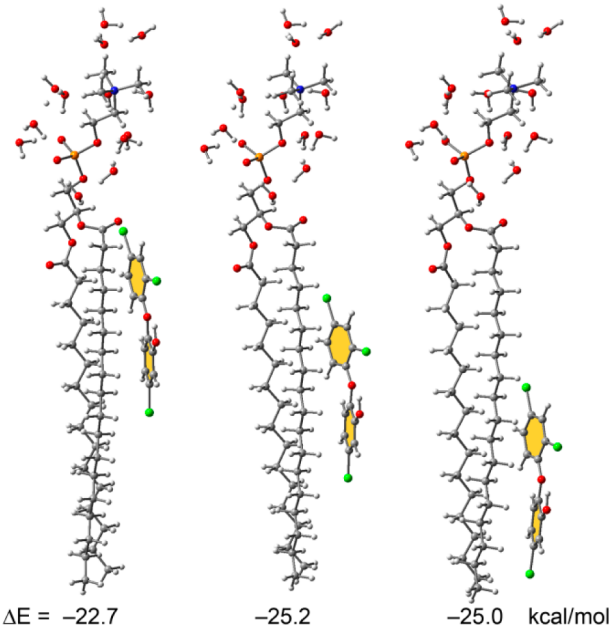

Figure 5. In-silico DFT optimized geometries and interaction energies of several complexes of triclosan (T) with the acyl region of the solvated phospholipid (P) at three different membrane depths.

magna),[55,56] and freshwater fish (*Pimephales promelas*).[56] Median effective concentrations (EC50) of the three target ECS exposed to bioluminescent bacteria and median lethal concentrations (LC50) for the animal groups at a given time frame are listed in Table S8. Regardless of the tested biota, the lowest EC50 and LC50 values for triclosan[50,53,56] signaled a superior toxicity as compared to 4-hydroxybenzoate derivatives, from which butyparaben shows significantly higher lethal and noxious effects on biota.[54−56] Bioconcentration factors (BCF) in fish[57] are on a par with LC50 ecotoxicological data and indicate that triclosan is largely bioaccumulable. Most importantly, our simple, fast and cost-effective in vitro method based on fluorescence GP or anisotropy measurements for bioavailability testing of ECs using PC liposomes offers a suitable proxy for end points of concern, such as toxicity and bioaccumulation, with no need of laborious and time-consuming in vivo testing protocols.

■ ASSOCIATED CONTENT

Supporting Information

The Supporting Information is available free of charge on the ACS Publications website at DOI: 10.1021/acs.est.6b00772.

Additional experimental data and information includes (i) the description of solvent dipolar relaxation phenomenon; (ii) optical scattering, TEM, and DSC results; (iii) Prodan's and Laurdan's GP fluorescence and anisotropy measurements for PC liposomes; and (iv) toxicological data for the target preservatives (PDF)

■ AUTHOR INFORMATION

Corresponding Authors

*Tel: +34-971173498; fax: +34-971173426; e-mail: toni.frontera@uib.es (A.F.).
*Tel: +34-971172746; fax: +34-971173426; e-mail: manuel.miro@uib.es (M.M.).

DOI: 10.1021/acs.est.6b00772
Environ. Sci. Technol. 2016, 50, 7135−7143

Notes

The authors declare no competing financial interest.

■ ACKNOWLEDGMENTS

M.M and M.O. acknowledge financial support from the Spanish Ministry of Economy and Competitiveness (MINECO) through projects CTM2014-56628-C3-3-R and CTM2014-61553-EXP. M.O. extends his appreciation to the Government of the Balearic Islands, Conselleria d'Educació, Cultura i Universitats, and the European Social Fund for PhD fellowship allocation (no. FPI/1681/2014). A.B. and A.F. acknowledge financial support from MINECO through projects CTQ2014-57393-C2-1-P and CONSOLIDER INGENIO 2010 CSD2010-00065 (FEDER funds). The authors are grateful to Dr. Pedro González and Mr. Jaume Cuart from Enoc Solutions for fruitful discussions and skilled technical assistance in the characterization of PC vesicles. Mr. Joan Cifre and Dr. Priam Villalonga at UIB are greatly acknowledged for assistance in differential scanning calorimetry and flow cytometry measurements, respectively. We also thank CTI from UIB for free allocation of computer time.

■ REFERENCES

(1) Collins, C. D.; Craggs, M.; Garcia-Alcega, S.; Kademoglou, K.; Lowe, S. Towards a unified approach for the determination of the bioaccessibility of organic pollutants. *Environ. Int.* **2015**, *78* (5), 24−31.

(2) Fedotov, P. S.; Kördel, W.; Miró, M.; Peijnenburg, W. J. G. M.; Wennrich, R.; Huang, P.-M. *Crit. Rev. Environ. Sci. Technol.* **2012**, *42* (11), 1117−1171.

(3) Koch, I.; Reimer, K. Bioaccessibility Extractions for Contaminant Risk Assessment. In *Comprehensive Sampling and Sample Preparation*; Pawliszyn, J., Ed.; Academic Press: Oxford, 2012; ch. 3.24, pp 487−507.

(4) Bacon, J. R.; Davidson, C. M. Is there a future for sequential chemical extraction? *Analyst* **2008**, *133* (1), 25−46.

(5) Brack, W.; Bandow, N.; Schwab, K.; Schulze, T.; Streck, G. Bioavailability in effect-directed analysis of organic toxicants in sediments. *TrAC, Trends Anal. Chem.* **2009**, *28* (5), 543−549.

(6) Simon, E.; Lamoree, M. H.; Hamers, T.; de Boer, J. Challenges in effect-directed analysis with a focus on biological samples. *TrAC, Trends Anal. Chem.* **2015**, *67* (4), 179−191.

(7) International Organization for Standardization. *Soil Quality-Requirements and Guidance for the Selection and Application of Methods for the Assessment of Bioavailability of Contaminants in Soil and Soil Materials*; ISO/TS 17402:2008; Geneva, Switzerland, 2008.

(8) Semple, K. T.; Doick, K. J.; Burauel, P.; Craven, A.; Harms, H. Defining bioavailability and bioaccessibility of contaminated soil and sediment is complicated. *Environ. Sci. Technol.* **2004**, *38* (12), 228A−231A.

(9) Tsaioun, K.; Kates, S. A., Eds. *Absorption, Distribution, Metabolism, Excretion, Toxicity (ADMET) for Medical Chemists*; John Wiley & Sons, Inc.: Hoboken, NJ, 2011.

(10) Simpson, M. J.; McKelvie, J. R. Environmental metabolomics: new insights into earthworm ecotoxicity and contaminant bioavailability in soil. *Anal. Bioanal. Chem.* **2009**, *394* (1), 137−149.

(11) Bandow, N.; Altenburger, R.; Lübcke-von Varel, U.; Paschke, A.; Streck, G.; Brack, W. Partitioning-based dosing: an approach to include bioavailability in the effect-directed analysis of contaminated sediment samples. *Environ. Sci. Technol.* **2009**, *43* (10), 3891−3896.

(12) Schoeters, G. The REACH perspective: toward a new concept of toxicity testing. *J. Toxicol. Environ. Health, Part B* **2010**, *13* (2−4), 232−241.

(13) Zabiegała, B.; Kot-Wasik, A.; Urbanowicz, M.; Namieśnik, J. Passive sampling as a tool for obtaining reliable analytical information in environmental quality monitoring. *Anal. Bioanal. Chem.* **2010**, *396* (1), 273−296.

(14) Esteve-Turrillas, F. A.; Yusà, Y.; Pastor, A.; de la Guardia, M. New perspectives in the use of semipermeable membrane devices as passive samplers. *Talanta* **2008**, *74* (4), 443−457.

(15) Greenwood, R.; Mills, G. A.; Vrana, B. Potential applications of passive sampling for monitoring non-polar industrial pollutants in the aqueous environment in support of REACH. *J. Chromatogr. A* **2009**, *1216* (3), 631−639.

(16) Lissalde, S.; Charriau, A.; Poulier, G.; Mazzella, N.; Buzier, R.; Guibaud, G. Overview of the Chemcatcher(®) for the passive sampling of various pollutants in aquatic environments Part B: Field handling and environmental applications for the monitoring of pollutants and their biological effects. *Talanta* **2016**, *148*, 572−582.

(17) Silva, E. A. S.; Risticevic, S.; Pawliszyn, J. Recent trends in SPME concerning sorbent materials, configurations and in vivo applications. *TrAC, Trends Anal. Chem.* **2013**, *43*, 24−36.

(18) Bojko, B.; Cudjoe, E.; Gómez-Ríos, G. A.; Gorynski, K.; Jiang, R.; Reyes-Garcés, N.; Risticevic, S.; Silva, E. A. S.; Togunde, O.; Vuckovic, D.; Pawliszyn, J. SPME-quo vadis? *Anal. Chim. Acta* **2012**, *750*, 132−151.

(19) Seethapathy, S.; Górecki, T. Applications of polydimethylsiloxane in analytical chemistry: A review. *Anal. Chim. Acta* **2012**, *750*, 48−62.

(20) Escribá, P. V.; González-Ros, J. M.; Goñi, F. M.; Kinnunen, P. K. J.; Vigh, L.; Sánchez-Magraner, L.; Fernández, A. M.; Busquets, X.; Horváth, I.; Barceló-Coblijn, G. Membranes: a meeting point for lipids, proteins and therapies. *J. Cell. Mol. Med.* **2008**, *12* (3), 829−875.

(21) Dowhan, W.; Bogdanov, M. Functional roles of lipids in membranes. In *Biochemistry of Lipids, Lipoproteins and Membranes*, 4th ed.; Vance, D. E., Vance, J. E., Eds.; Elsevier: The Netherlands, 2002.

(22) Lasic, D. D.; Barenholz, Y., Eds. *Handbook of Nonmedical Applications of Liposomes*; CRC Press: Boca Raton, FL, 1996.

(23) Janoff, A. S., Ed. *Liposomes: Rational Design*; Marcel Dekker: New York, 1999.

(24) Parasassi, T.; Krasnowska, E. K.; Bagatolli, L.; Gratton, E. Laurdan and Prodan as Polarity-Sensitive Fluorescent Membrane Probes. *J. Fluoresc.* **1998**, *8* (4), 365−373.

(25) Chong, P. L-G. Effects of hydrostatic pressure on the location of PRODAN in lipid bilayers and cellular membranes. *Biochemistry* **1988**, *27* (1), 399−404.

(26) Harris, F. M.; Best, K. B.; Bell, J. D. Use of laurdan fluorescence intensity and polarization to distinguish between changes in membrane fluidity and phospholipid order. *Biochim. Biophys. Acta, Biomembr.* **2002**, *1565* (1), 123−128.

(27) Official Journal of the European Union, Commission Regulation (EU) No. 358/2014 of 9 April 2014 amending Annexes II and V to Regulation (EC) No. 1223/2009 of the European Parliament and of the Council on cosmetic products, L 107/5−9, Brussels, 2014.

(28) Official Journal of the European Union, Commission Regulation (EU) No 1004/2014 of 18 September 2014 amending Annex V to Regulation (EC) No 1223/2009 of the European Parliament and of the Council on cosmetic products, L 282/5−8, Brussels, 2014.

(29) Ehrlich, N.; Christensen, A. L.; Stamou, D. Fluorescence anisotropy based single liposome assay to measure molecule-membrane interactions. *Anal. Chem.* **2011**, *83* (21), 8169−8176.

(30) Ghazaryan, N. A.; Ghulikyan, L.; Kishmiryan, A.; Andreeva, T. V.; Utkin, Y. N.; Tsetlin, V. I.; Lomonte, B.; Ayvazyan, N. M. Phospholipases a2 from Viperidae snakes: Differences in membranotropic activity between enzymatically active toxin and its inactive isoforms. *Biochim. Biophys. Acta, Biomembr.* **2015**, *1848* (2), 463−468.

(31) Wesołowska, O.; Gasiorowska, J.; Petrus, J.; Czarnik-Matusewicz, B.; Michalak, K. Interaction of prenylated chalcones and flavanones from common hop with phosphatidylcholine model membranes. *Biochim. Biophys. Acta, Biomembr.* **2014**, *1838* (1), 173−184.

(32) Wesołowska, O.; Kuzdzał, M.; Štrancar, J.; Michalak, K. Interaction of the chemopreventive agent resveratrol and its metabolite, piceatannol, with model membranes. *Biochim. Biophys. Acta, Biomembr.* **2009**, *1788* (9), 1851−1860.

DOI: 10.1021/acs.est.6b00772
Environ. Sci. Technol. 2016, 50, 7135−7143

(33) Pruchnik, H.; Bonarska-Kujawa, D.; Kleszczyńska, H. Effect of chlorogenic acid on the phase transition in phospholipid and phospholipid/cholesterol membranes. *J. Therm. Anal. Calorim.* **2014**, *118* (2), 943−950.
(34) Först, G.; Cwiklik, L.; Jurkiewicz, P.; Schubert, R.; Hof, M. Interactions of beta-blockers with model lipid membranes: molecular view of the interaction of acebutolol, oxprenolol, and propranolol with phosphatidylcholine vesicles by time-dependent fluorescence shift and molecular dynamics simulations. *Eur. J. Pharm. Biopharm.* **2014**, *87* (3), 559−569.
(35) Kovács, E.; Savopol, T.; Iordache, M. M.; Săplăcan, L.; Sobaru, I.; Istrate, C.; Mingeot-Leclercq, M. P.; Moisescu, M. G. Interaction of gentamicin polycation with model and cell membranes. *Bioelectrochemistry* **2012**, *87*, 230−235.
(36) Pereira-Leite, C.; Nunes, C.; Lima, J. L. F. C.; Reis, S.; Lúcio, M. Interaction of celecoxib with membranes: the role of membrane biophysics on its therapeutic and toxic effects. *J. Phys. Chem. B* **2012**, *116* (46), 13608−13617.
(37) Ostro, M. J., Ed. *Liposomes*; Marcel Dekker: New York, 1983.
(38) Lentz, B. R.; Moore, B. M.; Barrow, D. A. Light-scattering effects in the measurement of membrane microviscosity with diphenylhexatriene. *Biophys. J.* **1979**, *25* (3), 489−494.
(39) Ghosh, N.; Majumder, S. K.; Gupta, P. K. Fluorescence depolarization in a scattering medium: effect of size parameter of a scatterer. *Phys. Rev. E: Stat. Phys., Plasmas, Fluids, Relat. Interdiscip. Top.* **2002**, *65* (2), 026608.
(40) Parasassi, T.; De Stasio, G.; Ravagnan, G.; Rusch, R. M.; Gratton, E. Quantitation of lipid phases in phospholipid vesicles by the generalized polarization of Laurdan fluorescence. *Biophys. J.* **1991**, *60* (1), 179−189.
(41) Lakowicz, J.R., Ed. *Principles of Fluorescence Spectroscopy*, 3rd ed.; Springer Science+Business Media: Heidelberg, 2006.
(42) Grimme, S.; Antony, J.; Ehrlich, S.; Krieg, H. A consistent and accurate ab initio parametrization of density functional dispersion correction (DFT-D) for the 94 elements H-Pu. *J. Chem. Phys.* **2010**, *132* (15), 154104−19.
(43) Klampt, A. The COSMO and COSMO-RS solvation models. *WIREs Comput. Mol. Sci.* **2011**, *1* (5), 699−709.
(44) Ahlrichs, R.; Bär, M.; Hacer, M.; Horn, H.; Kömel, C. Electronic structure calculations on workstation computers: The program system turbomole. *Chem. Phys. Lett.* **1989**, *162* (3), 165−169.
(45) Mirzaei, M.; Nikpour, M.; Bauzá, A.; Frontera, A. On the Importance of C-H/π and C-H···H-C Interactions in the Solid State Structure of 15-Lipoxygenase Inhibitors Based on Eugenol Derivatives. *ChemPhysChem* **2015**, *16* (10), 2260−2266.
(46) Cieślik-Boczula, K.; Petrus, R. M.; Köhler, G.; Lis, T.; Koll, A. Interaction of piperidin derivative of Mannich base with DPPC liposomes. *J. Phys. Chem. B* **2013**, *117* (10), 2938−2946.
(47) Kużdżał, M.; Wesołowska, O.; Strancar, J.; Michalak, K. Fluorescence and ESR spectroscopy studies on the interaction of isoflavone genistein with biological and model membranes. *Chem. Phys. Lipids* **2011**, *164* (4), 283−291.
(48) Neves, A. R.; Nunes, C.; Reis, S. New Insights on the Biophysical Interaction of Resveratrol with Biomembrane Models: Relevance for Its Biological Effects. *J. Phys. Chem. B* **2015**, *119* (35), 11664−11672.
(49) Niu, Y.-M.; Wang, X.-Y.; Chai, S.-H.; Chen, Z.-Y.; An, X.-Q.; Shen, W.-G. Effects of curcumin concentration and temperature on the spectroscopic properties of liposomal curcumin. *J. Agric. Food Chem.* **2012**, *60* (7), 1865−1870.
(50) Rosal, R.; Rodea-Palomares, I.; Boltes, K.; Fernández-Piñas, F.; Leganés, F.; Petre, A. Ecotoxicological assessment of surfactants in the aquatic environment: combined toxicity of docusate sodium with chlorinated pollutants. *Chemosphere* **2010**, *81* (2), 288−293.
(51) Farré, M.; Asperger, D.; Kantiani, L.; González, S.; Petrovic, M.; Barceló, D. Assessment of the acute toxicity of triclosan and methyl triclosan in wastewater based on the bioluminescence inhibition of Vibrio fischeri. *Anal. Bioanal. Chem.* **2008**, *390* (8), 1999−2007.
(52) Tatarazako, N.; Ishibashi, H.; Teshima, K.; Kishi, K.; Arizono, K. Effects of triclosan on various aquatic organisms. *Environ. Sci.* **2004**, *11* (2), 133−140.
(53) Lopez-Roldan, R.; Kazlauskaite, L.; Ribo, J.; Riva, M. C.; González, S.; Cortina, J. L. Evaluation of an automated luminescent bacteria assay for in situ aquatic toxicity determination. *Sci. Total Environ.* **2012**, *440*, 307−313.
(54) Bazin, I, Gadal, A, Touraud, E, Roig, B. Hydroxy benzoate preservatives (parabens) in the environment: data for environmental toxicity assessment. In *Xenobiotics in the Urban Water Cycle: Mass Flows, Environmental Process, Mitigation and Treatment Strategies, Environmental Pollution*; Fatta-Kassinos, D., Bester, K., Kümmerer, K., Eds.; Springer Science+Business Media B.V: Heidelberg, 2010, Vol *16*; ch. 14, pp 245−257.
(55) Terasaki, M.; Makino, M.; Tatarazako, N. Acute toxicity of parabens and their chlorinated by-products with Daphnia magna and Vibrio fischeri bioassays. *J. Appl. Toxicol.* **2009**, *29* (3), 242−247.
(56) Brausch, J. M.; Rand, G. M. A review of personal care products in the aquatic environment: environmental concentrations and toxicity. *Chemosphere* **2011**, *82* (11), 1518−1532.
(57) United States Environmental Protection Agency, *Estimation Programs Interface Suite for Microsoft Windows*, US EPA, Washington, DC, 2015. Available at: http://www.epa.gov/tsca-screening-tools/epi-suitetm-estimation-program-interface.

DOI: 10.1021/acs.est.6b00772
Environ. Sci. Technol. 2016, 50, 7135−7143

3.2.1. Información suplementaria (supplementary information)

A continuación, se detalla la información relativa al artículo original publicado.

SUPPORTING DATA INFORMATION

Fluorescent lipid nanoparticles as biomembrane models for exploring emerging contaminant bioavailability supported by density functional theory calculations

Miquel Oliver, Antonio Bauzá, Antonio Frontera* and Manuel Miró*

Department of Chemistry, University of the Balearic Islands, Carretera de Valldemossa km 7.5, 07122 Palma de Mallorca, Illes Balears, Spain

Corresponding authors:

Antonio Frontera. Department of Chemistry, University of the Balearic Islands, Carretera de Valldemossa km 7.5, 07122 Palma de Mallorca, Illes Balears, Spain.

E-mail: toni.frontera@uib.es. Tel: +34-971173498. FAX: +34-971173426.

Manuel Miró. FI-TRACE group, Department of Chemistry, University of the Balearic Islands, Carretera de Valldemossa km 7.5, 07122 Palma de Mallorca, Illes Balears, Spain.

E-mail: manuel.miro@uib.es. Tel: +34-971172746. FAX: +34-971173426.

Number of pages: 20

Number of schemes: 1

Number of figures: 6

Number of tables: 8

Relationship between Generalized fluorescence measurements and solvent polar relaxation

In non-polar membrane environments, the naphthalene fluorophore features a maximum-intensity wavelength in the fluorescence emission spectrum centred at 440 nm. However, a bathochromic Stokes (red) shift is observed upon increasing of membrane phase polarity, that is, membrane hydration, which is an indicator of the perturbation of the lipid nanoscale vesicles rendering a looser and disordered structure that might be measured semi-quantitatively by the decrease in GP values. This characteristic behaviour is a consequence of solvent molecules surrounding the probe's fluorophore moiety to form dipole states and to reorientate along the fluorophore's dipole moment upon its excitation. This phenomenon is known as solvent dipolar relaxation and results in a red-shifted emission towards 490 nm as a result of the formation of a charge transfer excited state, stabilized by the water dipole reorientation process (1,2). The more acute is the water relaxation process occurring in the vicinity of the probe the more significant the membranotropic effects are. Prodan serves to signal interactions on the polar moieties of PC while Laurdan does at the hydrophilic-hydrophobic interface of the lipid bilayer. The latter is harnessed in this work as a marker of enhanced contaminant penetration across the liposomal bilayer and thus indicates *in-vitro* bioavailability with potential in-vivo absorption by the systemic circulation. It should be also noted that exogenic compounds might also participate in supramolecular interactions leading to improved lipid packing as identified by hypsochromic (blue) shift towards 440 nm, with the subsequent increase in Laurdan GP, for which the liposomal nanoparticle behaviour resembles the gel phase more closely and the solvent dipolar relaxation process is lessened to a large extent.

Flow cytometry measurements

Working solutions of 50 µmol/L PC liposomes in buffer (10 mmol/L HEPES, 0.1 mol/L NaCl, pH 7.4) with and without the addition of a given concentration of EC were analyzed by flow cytometry. To this end, the liposomal nanoparticles were mixed and incubated with 10 µg/mL biocide (one at a time) for 1 h in the dark and room temperature. In each measurement, a nominal number of 10,000 events were recorded. Two dynamic scattering parameters were determined in every individual sample: the forward laser light scattering (FS) and the side laser light scattering (SS). The former gives insight into the vesicle size distribution and the latter relates to inner vesicle composition and complexity. Semi-quantitative population data were obtained with WinMDI 2.9 software.

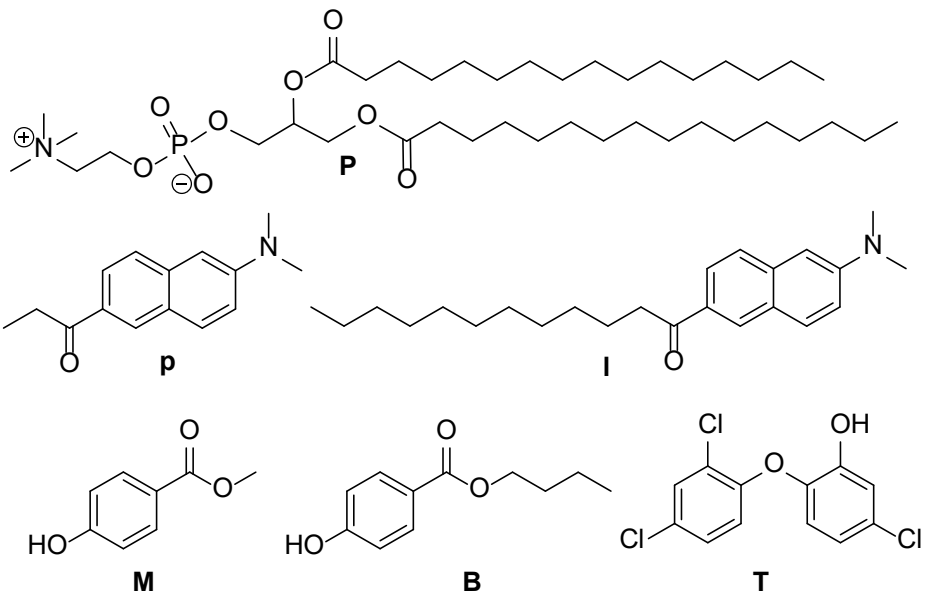

Scheme S1. Chemical structure of the phospholipid (16:0) PC model, fluorescent membrane probes and target contaminants explored in this work. **P**: Phosphatidylcholine. **p**: Prodan. **l**: Laurdan. **M**: Methylparaben. **B**: Butylparaben. **T**: Triclosan.

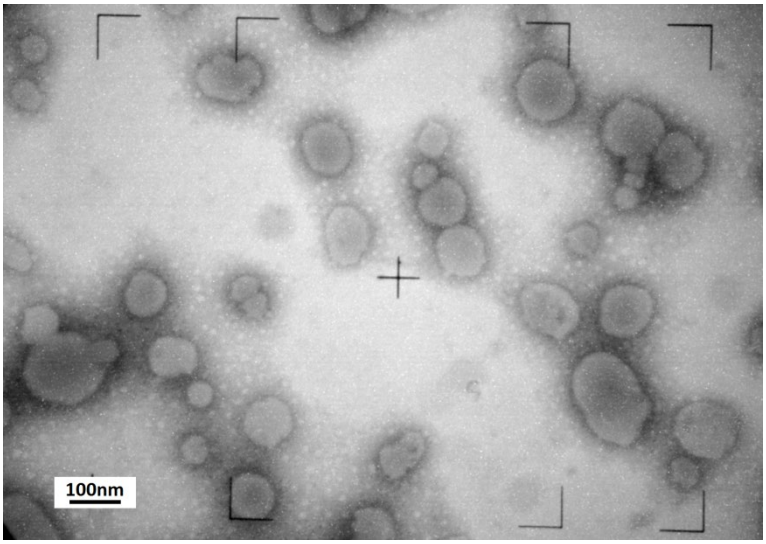

Figure S1. Transmission electron micrograph of soybean PC liposomes at the 4mg PC/mL level with a 80K magnification

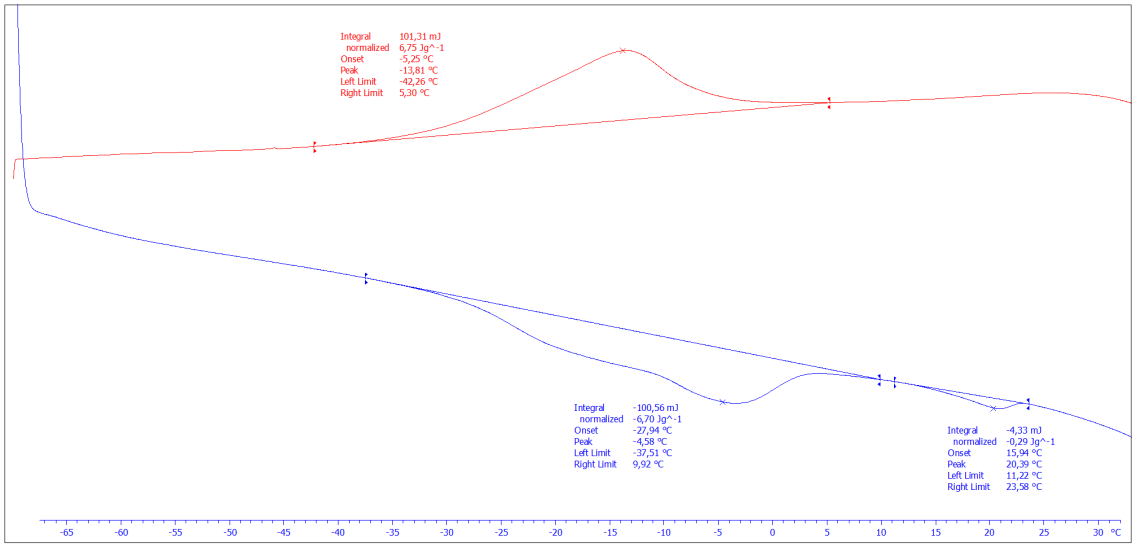

Figure S2. Differential scanning calorimetric (DSC) explorations of changes in soybean PC phase transition temperatures. DSC graph is obtained with a heating rate of 2.0 ºC/min within the -70 to 35 ºC range using 40µL aluminium sample vials.

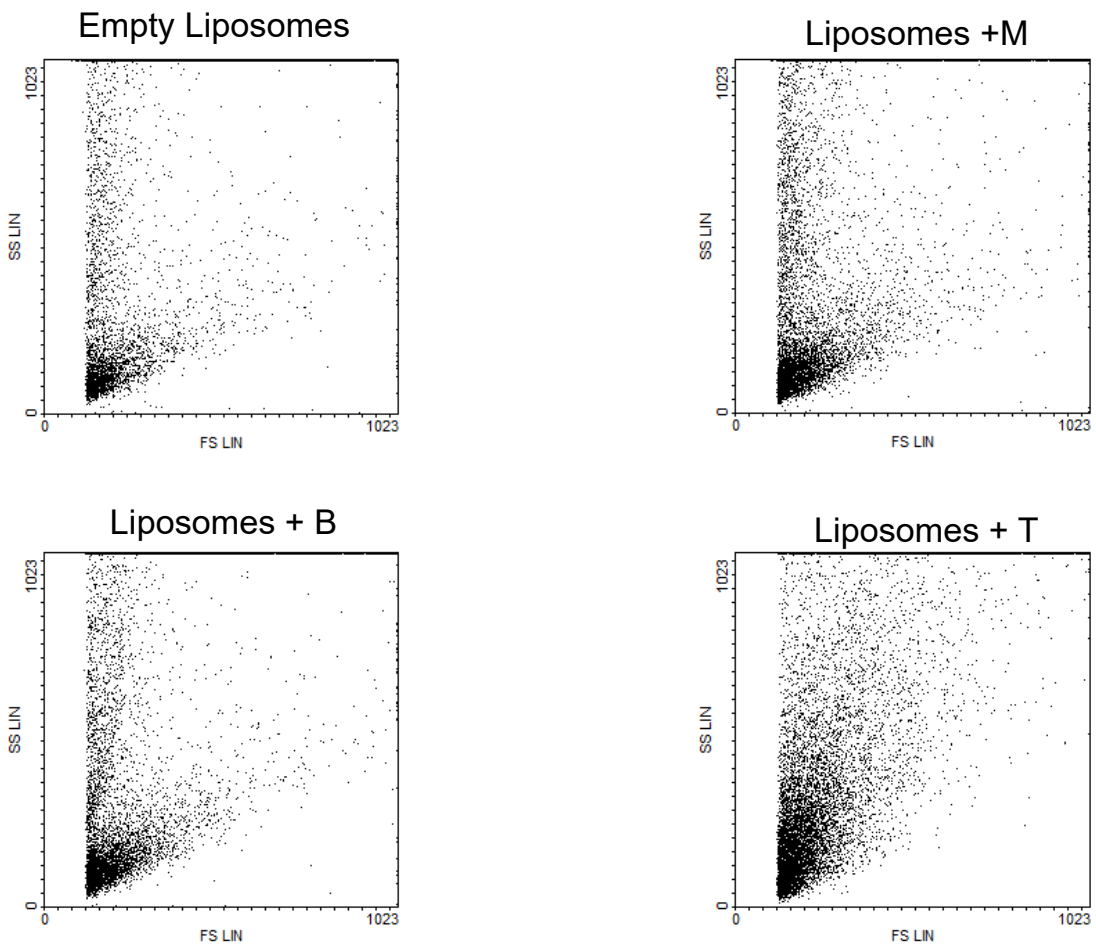

Figure S3. 2D optical scattering plots for empty PC liposomes against PC liposomes in the presence of methylparaben (M), butylparaben (B) and triclosan (T).

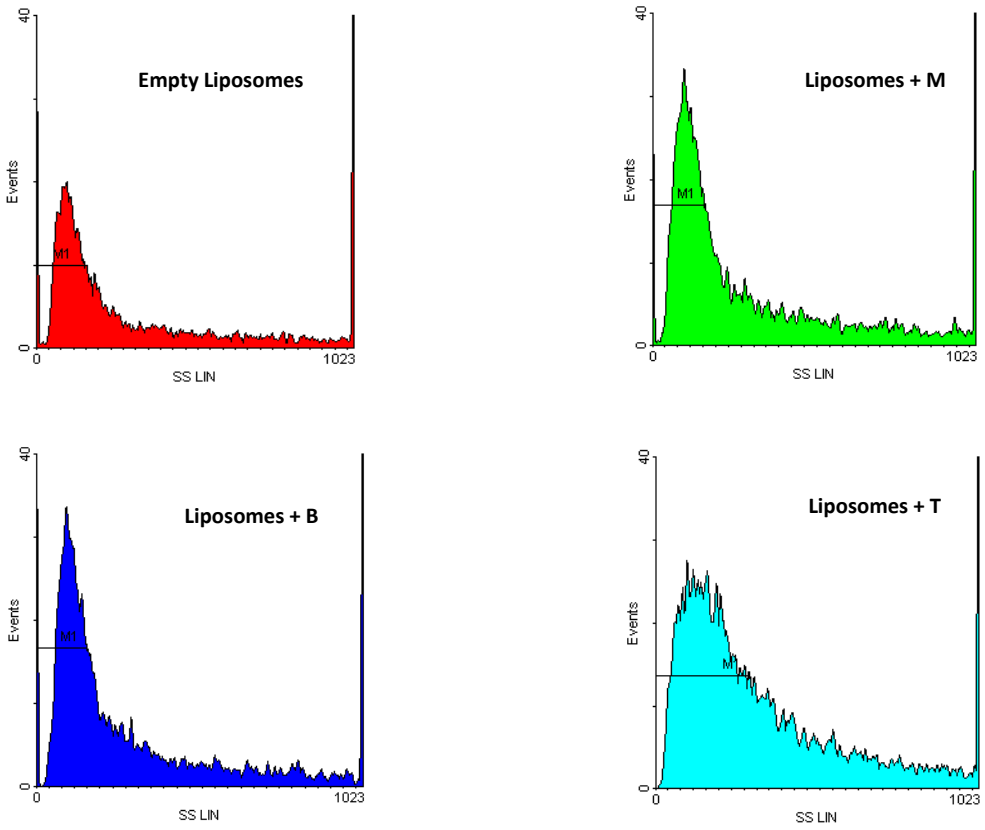

Figure S4. Side-scattered light profiles for empty PC liposomes against PC liposomes in the presence of methylparaben (M), butylparaben (B) and triclosan (T)

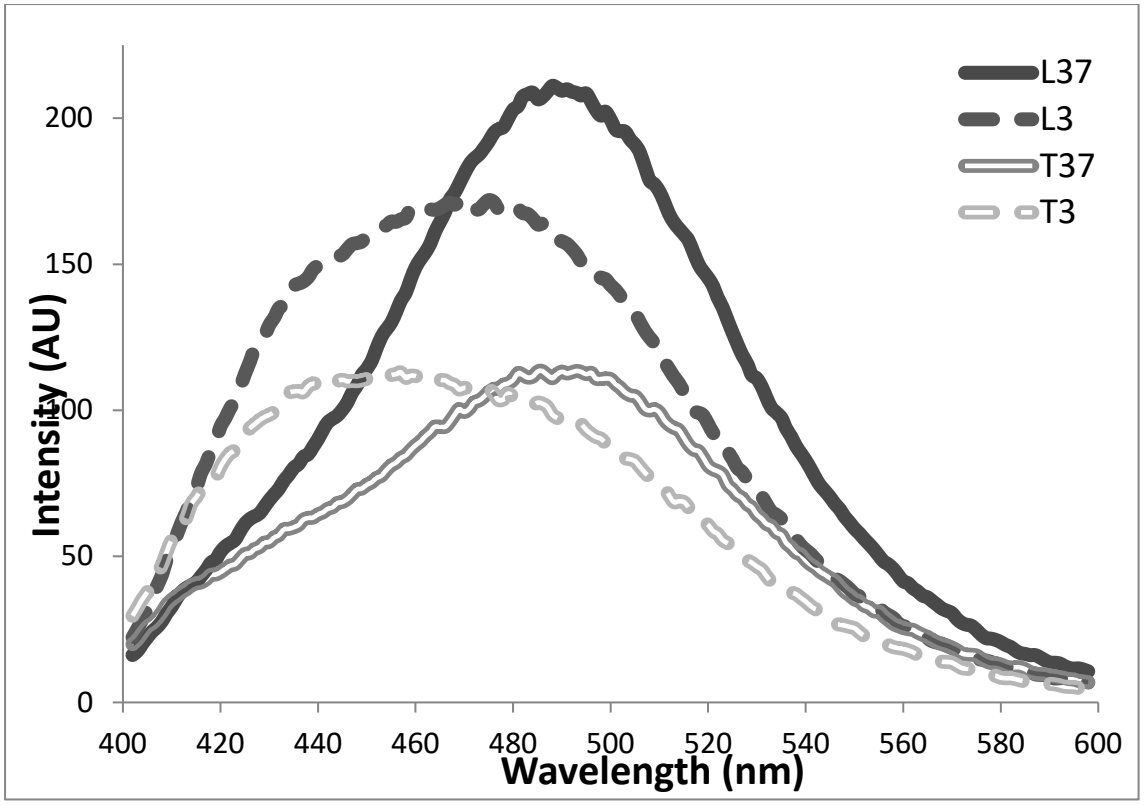

Figure S5. Steady-state fluorescence emission spectra of Laurdan-embedded PC liposomes with (T) and without (L) triclosan at 3 and 37ºC. Hypsochromic (blue) shifts and quenching effects of triclosan at the 10 µg/mL level are identified.

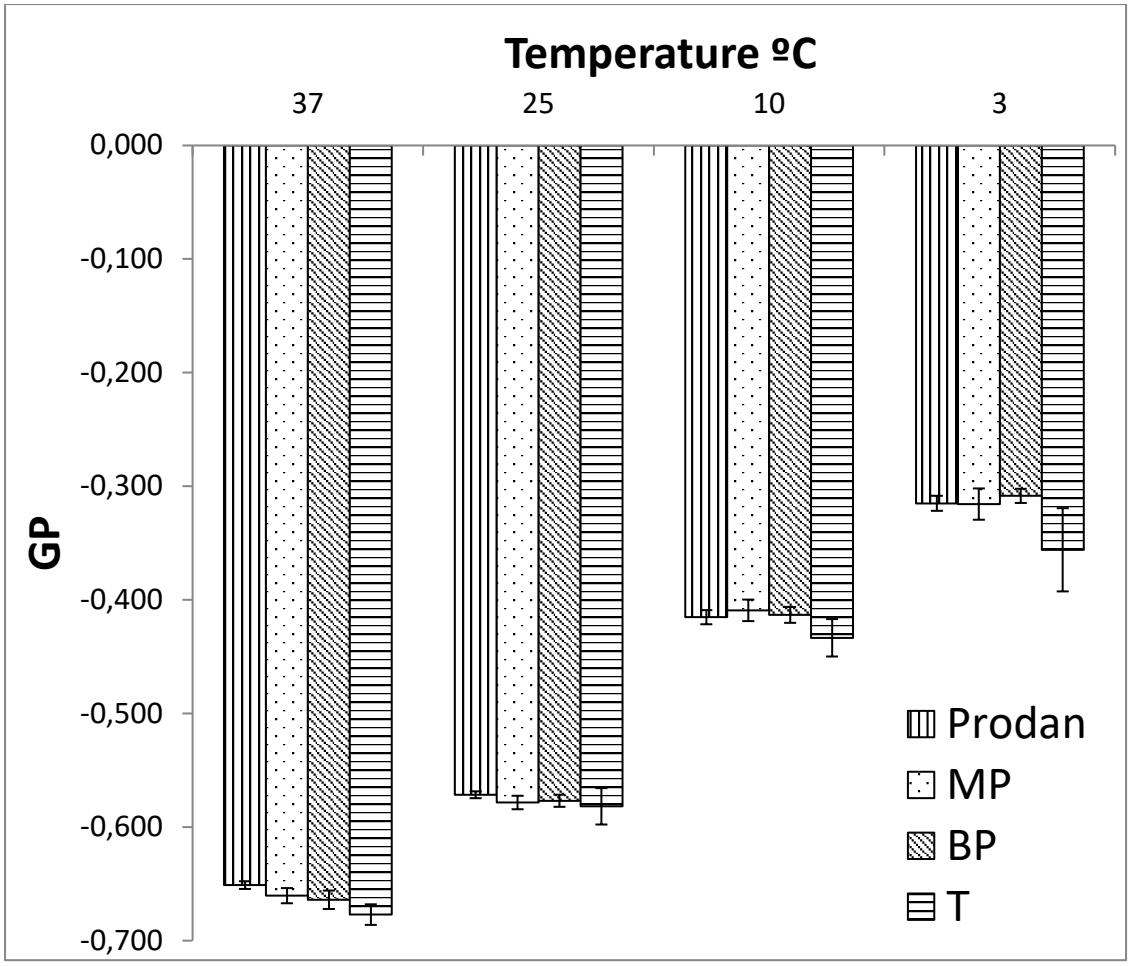

Figure S6. Prodan's GP fluorescence data of PC liposomes in the presence or absence of emerging contaminants in bioavailability testing. Experimental data are obtained at four different temperatures (3 ºC, 10ºC, 25ºC and 37ºC).

Table S1. Quantitative evaluation of EC permeability through PC liposomes by light scattering.

Compound	**MT**	**M1**	**M1/MT**
Liposome	3,449	1,623	0.47
Methylparaben	5,856	2,815	0.48
Butylparaben	5,495	2,674	0.49
Triclosan	8,474	5,090	0.60

Table S2. Laurdan's GP fluorescence data for the investigated contaminants on the basis of the incubation temperature.

	Laurdan	**Methylparaben**		**Butylparaben**		**Triclosan**	
T (ºC)	**GP±SD**	**GP±SD**	t_{exp}	**GP±SDsd**	t_{exp}	**GP±SD**	t_{exp}
37	-0.481±0.003	-0.476±0.009	1.319^{a}	-0.466±0.003	9.577^{f}	-0.42±0.01	12.644^{c}
25	-0.405±0.003	-0.40±0.02	1.271^{b}	-0.378±0.004	15.520^{f}	-0.33±0.01	20.388^{d}
10	-0.249±0.004	-0.24±0.02	1.601^{b}	-0.205±0.007	15.302^{f}	-0.151±0.006	36.579^{e}
3	-0.146±0.004	-0.13±0.03	1.329^{b}	-0.095±0.008	15.982^{f}	-0.045±0.006	38.407^{e}

Note: The superscripts refer to the following critical *t*-values: a = 2.262, b= 2.365, c = 2.306, d = 2.571, e = 2.179 and f = 2.145

Table S3: Increase of Laurdan's GP fluorescence data for soybean PC liposomes in the presence of emerging contaminants in bioavailability testing at varied temperatures.

	% GP Increase			
Temperature(ºC)	**37**	**25**	**10**	**3**
Methylparaben	0.9	1.8	4.9	9.5
Butylparaben	3.0	6.7	17.4	34.5
Triclosan	13.6	19.4	39.3	69.1

Experimental conditions. PC concentration: 50μM, Laurdan concentration: 2 μM, EC concentration: 10 μg/mL

Table S4. Prodan's GP fluorescence data for the investigated contaminants on the basis of the incubation temperature

	Prodan	**Methylparaben**		**Butyparaben**		**Triclosan**	
T (ºC)	**GP±SD**	**GP±SD**	t_{exp}	**GP±SD**	t_{exp}	**GP±SD**	t_{exp}
37	-0.651±0.003	-0.660±0.007	2.491[a]	-0.664±0.008	2.545[a]	-0.677±0.009	5.438[b]
25	-0.572±0.003	-0.578±0.006	2.049[a]	-0.577±0.005	1.494[a]	-0.58±0.02	1.735[c]
10	-0.415±0.006	-0.409±0.009	1.061[a]	-0.413±0.007	0.376[a]	-0.43±0.02	2.087[b]
3	-0.315±0.007	-0.32±0.01	0.089[a]	-0.308±0.006	1.250[a]	-0.36±0.04	3.060[c]

Note: The superscripts refer to the following critical *t*-values: a = 2.447, b = 2.228 and c = 2.306

Table S5: Variation of Prodan's GP fluorescence data for soybean PC liposomes in the presence of emerging contaminants in bioavailability testing at varied temperatures

	% GP variation			
Temperature(ºC)	**37**	**25**	**10**	**3**
Methylparaben	-1.4	-1.2	1.4	-0.2
Butylparaben	-2.0	-0.9	0.5	2.1
Triclosan	-4.0	-1.8	-4.4	-13.0

Experimental conditions. PC concentration: 50µM, Prodan concentration: 2 µM, EC concentration: 10 µg/mL

Table S6. Fluorescence anisotropic measurements (r_{ss}) for the investigated contaminants on the basis of the incubation temperature

	Laurdan	**Methylparaben**		**Butylparaben**		**Triclosan**	
Temperature (°C)	**r_{ss}±SD**	**r_{ss} ±SD**	***t*exp**	**r_{ss} ±SD**	***t*exp**	**r_{ss} ±SD**	***t*exp**
37	0.132±0.001	0.139±0.003	3.658[a]	0.135±0.002	1.191[a]	0.162±0.004	13.059[c]
25	0.1479±0.0008	0.152±0.002	4.184[a]	0.1498±0.0009	1.904[b]	0.170±0.003	14.945[a]
10	0.166±0.002	0.166±0.003	0.321[a]	0.167±0.001	1.059[a]	0.181±0.003	9.196[a]
3	0.1728±0.0007	0.172±0.002	0.581[a]	0.174±0.002	0.816[a]	0.187±0.004	7.511[c]

Note: The superscripts refer to the following critical *t*-values: a = 2.447, b = 2.571, c = 3.182

Table S7: Variation of fluorescence anisotropy data for soybean PC liposomes in the presence of emerging contaminants in bioavailability testing at varied temperatures

	% Variation of fluorescence anisotropy			
Temperature (ºC)	**37**	**25**	**10**	**3**
Methylparaben	4.7	2.8	0.3	-0.3
Butylparaben	2.2	1.3	1.0	0.9
Triclosan	22.3	15.1	9.5	8.4

Experimental conditions. PC concentration: 50µM, Laurdan concentration: 2 µM, EC concentration: 10 µg/mL

Table S8. Ecotoxicological and bioaccumulation data of target species

Target compound	***Vibrio fisheri* EC50 (15min)**	***Daphnia magna* LC50 (48h)**	***Pimephales promelas* LC50 (48h)**	**Bioconcentration factor (BCF*)* (3)**
Triclosan	0.15-0.95 µg/mL (4-7)	0.39 µg/mL (8)	0.27 µg/mL (8)	368
Butylparaben	1.2-2.5 µg/mL (9,10)	5.3-9.2 µg/mL (8,10)	4.2 µg/mL (8)	112
Methylparaben	5.9-9.6 µg/mL (9,10)	24.6-62 µg/mL (8,10)	No effects found at concentrations exceeding water solubility (> 2.5 g/L) (8)	6.4

Supporting information references

(1) Lakowicz J.R. (Ed.). *Principles of Fluorescence Spectroscopy, 3rd Edition*; Springer Science+Business Media: New York, 2006; chap. 6 and 7.

(2) Viard, M.; Gallay, J.; Vincent, M.; Meyer, O.; Robert, B.; Paternostre, M. Laurdan solvatochromism: solvent dielectric relaxation and intramolecular excited-state reaction. *Biophys. J.* **1997**, *73* (4), 2221–2234.

(3) United States Environmental Protection Agency, *Estimation Programs Interface Suite™ for Microsoft® Windows*, US EPA, Washington, DC, USA, 2015. Available at: http://www.epa.gov/tsca-screening-tools/epi-suitetm-estimation-program-interface

(4) Rosal, R.; Rodea-Palomares, I.; Boltes, K.; Fernández-Piñas, F.; Leganés, F.; Petre, A. Ecotoxicological assessment of surfactants in the aquatic environment: combined toxicity of docusate sodium with chlorinated pollutants. *Chemosphere* **2010,** *81*(2), 288-293.

(5) Farré, M.; Asperger, D.; Kantiani, L.; González, S.; Petrovic, M.; Barceló, D. Assessment of the acute toxicity of triclosan and methyl triclosan in wastewater based on the bioluminescence inhibition of Vibrio fischeri. *Anal. Bioanal. Chem.* **2008**, *390* (8), 1999–2007.

(6) Tatarazako, N.; Ishibashi, H.; Teshima, K.; Kishi, K.; Arizono, K. Effects of triclosan on various aquatic organisms. *Environ Sci.* **2004**, 11(2), 133-140.

(7) Lopez-Roldan, R.; Kazlauskaite, L.; Ribo, J.; Riva, M.C.; González, S.; Cortina, J.L. Evaluation of an automated luminescent bacteria assay for in situ aquatic toxicity determination. *Sci. Total Environ.* **2012**, *440*, 307-313.

(8) Brausch, J.M.; Rand, G.M. A review of personal care products in the aquatic environment: environmental concentrations and toxicity. *Chemosphere* **2011**, *82* (11), 1518- 1532.

(9) Bazin I, Gadal A, Touraud E, Roig B. Hydroxy benzoate preservatives (parabens) in the environment: data for environmental toxicity assessment. *In Xenobiotics in the Urban Water Cycle: Mass Flows, Environmental Process, Mitigation and Treatment Strategies*; Fatta-Kassinos, D.; Bester, K.; Kümmerer, K. (Eds); Environmental Pollution, Vol 16, Springer Science+Business Media B.V: Heidelberg, 2010, ch. 14, pp. 245-257.

(10) Terasaki, M.; Makino, M.; Tatarazako, N. Acute toxicity of parabens and their chlorinated by-products with Daphnia magna and Vibrio fischeri bioassays. *J. Appl. Toxicol*. **2009**, *29* (3), 242–247.

Capítulo 4. Estudios Membranotrópicos de Fluorescencia Combinados con ^{1}H-RMN y Dinámica Molecular

4.1. Resumen

Este trabajo se basa en el empleo de liposomas y en la combinación de diferentes técnicas, incluyendo (i) anisotropía de fluorescencia y polarización generalizada usando sondas fluorescentes de membrana (Laurdan y Prodan), (ii) medidas de ^{1}H-NMR y (iii) simulaciones de dinámica molecular para el estudio de la interacción entre contaminantes y la membrana lipídica. Se han seleccionado diferentes compuestos modelo con diversas propiedades fisicoquímicas y que son representativos de tres clases de contaminantes emergentes presentes en el medioambiente: (i) diclofenaco como modelo de fármaco antiinflamatorio, (ii) triclosán como agente antimicrobiano, y (iii) bisfenol A como aditivo plástico, en comparación con clorpirifós, como insecticida. Las conclusiones derivadas de las medidas anisotrópicas empleando Laurdan se encuentran de acuerdo con los datos obtenidos con ^{1}H-NMR y señalan que tanto triclosán como clorpirifós se bioacumulan en las membranas. Además, los estudios de dinámica molecular indicaron que la difusión lateral de la bicapa lipídica es mucho más lenta cuando triclosán o clorpirifós se incorporan a la bicapa. Estos resultados sugieren la idea de la necesidad de un enfoque holístico que sea capaz de abordar la complejidad de las bicapas lipídicas que imitan las membranas celulares eucariotas para explorar la distribución de contaminantes y la bioacumulación a través de las membranas.

4.2. Artículo original

A continuación, se adjunta el artículo original "A holistic approach for the in-vitro elucidation of the bioaccumulation of organic contaminants of emerging concern in lipid bilayers"de Miquel Oliver, Miquel Adrover, Antonio Frontera, Joaquín Ortega-Castro, y Manuel Miró, enviado el 20 de septiembre de 2019 para su publicación en *Science of the Total Environment*.

Elsevier Editorial System(tm) for Science of the Total Environment

Manuscript Draft

Manuscript Number:

Title: A holistic approach for the in-vitro elucidation of the bioaccumulation of organic contaminants of emerging concern in lipid bilayers

Article Type: Research Paper

Keywords: bioaccumulation; bioavailability; liposome; lipid bilayer; emerging contaminants; holistic approach

Corresponding Author: Professor Manuel Miro, PhD

Corresponding Author's Institution: University of Balearic Islands

First Author: Manuel Miro, PhD

Order of Authors: Manuel Miro, PhD; Miquel Oliver; Miquel Adrover; Antonio Frontera; Joaquin Ortega-Castro

Abstract: A holistic semi-quantitative analytical approach based on high-resolution and low-resolution empirical techniques, and theoretical quantum mechanics is herein presented for the in-vitro investigation of the distribution and potential bioavailability of emerging contaminants via passive diffusion across lipid bilayers. Phosphatidylcholine (PC) liposomes are selected as membrane surrogates, and contaminant effects are explored by (i) fluorescence anisotropy and generalized polarization assays using membrane fluorescence probes (laurdan and prodan), (ii) 1H NMR measurements to ascertain interactions with PC and (iii) molecular dynamics simulations. In particular, model compounds with distinct physico-chemical properties that are representative of three different classes of emerging contaminants in environmental compartments are chosen in this study: (i) diclofenac as a model of anti-inflammatory drug; (ii) triclosan as an anti-microbial agent; and (iii) bisphenol A as a plastic additive, and compared with chlorpyrifos as a legacy insecticide. Laurdan anisotropic measurements are in good agreement with 1H NMR data and pinpoint that triclosan and chlorpyrifos are highly bioaccumulable in membranes. Molecular dynamic studies also indicate that the lateral diffusion of the lipid bilayer is much lower with the incorporation of either triclosan and chlorpyrifos into the bilayer. Our findings suggest that laurdan anisotropy using PC-based liposomes serves as a fast and cost-effective approach, notwithstanding its low resolution features, for risk assessment of emerging contaminants.

Suggested Reviewers: Mark Cave
British Geological Survey
mrca@bgs.ac.uk
Expert on bioaccessibility assays

Dimosthenis Giokas
Ionannina University

A holistic approach for the *in-vitro* elucidation of the bioaccumulation of organic emerging contaminants in lipid bilayers

Miquel Oliver[a], Miquel Adrover[b], Antonio Frontera[c], Joaquín Ortega-Castro[b], Manuel Miró[a]

[a] *FI-TRACE group, Department of Chemistry, University of the Balearic Islands, Carretera de Valldemossa km 7,5, E-07122 Palma de Mallorca, Spain.*

[b] *REACMOL group, Department of Chemistry, University of the Balearic Islands, Carretera de Valldemossa km 7,5, E-07122 Palma de Mallorca, Spain.*

[c]*SUPRAMOL group, Department of Chemistry, University of the Balearic Islands, Carretera de Valldemossa km 7,5, E-07122 Palma de Mallorca, Spain.*

Abstract

A holistic semi-quantitative analytical approach based on high-resolution and low-resolution empirical techniques, and theoretical quantum mechanics is herein presented for the *in-vitro* investigation of the distribution and potential bioavailability of emerging contaminants via passive diffusion across lipid bilayers. Phosphatidylcholine (PC) liposomes are selected as membrane surrogates, and contaminant effects are explored by (i) fluorescence anisotropy and generalized polarization assays using membrane fluorescence probes (laurdan and prodan), (ii) ^{1}H NMR measurements to ascertain interactions with PC and (iii) molecular dynamics simulations. In particular, model compounds with distinct physico-chemical properties that are representative of three different classes of emerging contaminants in environmental compartments are chosen in this study: (i) diclofenac as a model of anti-inflammatory drug; (ii) triclosan as an anti-microbial agent; and (iii) bisphenol A as a plastic additive, and compared with chlorpyrifos as a legacy insecticide. Laurdan anisotropic measurements are in good agreement with ^{1}H NMR data and pinpoint that triclosan and chlorpyrifos are highly bioaccumulable in membranes. Molecular dynamic studies also indicate that the lateral diffusion of the lipid bilayer is much lower with the incorporation of either triclosan and chlorpyrifos into the bilayer. Our findings suggest that laurdan anisotropy using PC-

based liposomes serves as a fast and cost-effective approach, notwithstanding its low resolution features, for risk assessment of emerging contaminants.

Keywords: bioaccumulation, liposome, lipid bilayer, emerging contaminants, holistic approach

INTRODUCTION

Industrial developments are linked to the launching of novel objects that impact our daily life. To ameliorate their shelf time, organic chemicals with given physicochemical properties, such as anti-microbials, preservatives, nanomaterials, and additives have been introduced in the market, in some instances, for replacing banned compounds. Other chemicals such as pharmaceuticals and personal care products including anti-inflammatory drugs, anti-diabetics, antibiotics, cosmetics, UV-sunscreens and fragrances[1] have been continuously used since decades to serve for human well-being. Recent studies have however demonstrated that most of these compounds are environmentally persistent chemicals, and in some cases, inefficiently removed by wastewater treatment plants or biodegradation processes.[2,3] Also, they might have adverse effects against the ecosystem services and the quality of aquatic biota.[4]

The term '*contaminants of emerging concern*' or '*emerging contaminants*' is actually coined to refer to those compound classes that are currently encountered in environmental compartments and have impacted the wildlife and trophic chain, yet they are still unregulated.[5,6] The European Commission fully aware of this fact has already launched the first and second "Watch List"[7,8] that refer to those substances or family classes for which Union-wide monitoring data ought to be gathered for the purpose of human risk exposure and assessment.

Appropriate risk exposure of those compounds is associated to the so-called exposomic studies. Exposomics refers to the combination of exposures to a number of chemical and physical stressors along with human genetics that might account for chronic human diseases.[9] The main challenge of the exposomics workflow is to explore and identify as many as possible exposures via epidemiological studies of an individual in a holistic format, including those related to the environment, diet, and endogenous processes.[10] To tackle this challenge, environmental metabolomics has become an emerging discipline

in the field of exposomics, and is based on the use of model animals (e.g., earthworms) to identify a number of endogenous metabolites as potential biomarkers of contaminant exposure.[11]

It should be however noted that the REACH (Registration, Evaluation, Authorisation and restriction of CHemicals) regulation of the European Union is currently promoting alternative methods to *in-vivo* assays for the hazard assessment of substances in order to reduce the number of tests on animals.[12] *In-vitro* assays seem to fulfil EU demands, yet method development to get insight into potential toxicity effects on biota is not straightforward. In fact, a pivotal issue of *in-vitro* testing is to elucidate mechanisms at the molecular level for inferring contaminant distribution and accumulation in membranes within the broad concept of bioavailability,[13,14] as defined by ISO 17402:2008.[15] To this end, biorelevant membrane surrogates of eukaryotic cells as a proxy of lipid bilayers are called for. Lipid-based nanoparticles, also termed liposomes,[16-18] have been consolidated as mock cellular membranes for the *in-vitro* exploration of interactions of chemical compounds with the phospholipids integrating biological membranes.[19,20] Because phosphatidylcholine (PC) is the most abundant phospholipid in eukaryotic membrane cells *in-situ* synthesized large unilamelar vesicles/liposomes (LUV) from natural sources of PC containing both saturated and unsaturated chains has been herein selected as a model of biological membranes.

This work proposes a new multidisciplinary approach involving a holistic exploration of qualitative and semi-quantitative membranotropic effects on liposomes caused by three model compounds, representative of three different classes of emerging contaminants[1], namely diclofenac (DCF) as a model of anti-inflammatory drug that was included in the first EU Watch List, triclosan (TCS) as anti-microbial agent, and bisphenol A (BPA) as a plastic additive, and compared against a legacy insecticide, *viz*, clorpyrifos (CPF), endorsed by the current EU Water Framework Directive.[21] The model analytes are characterized by varying physicochemical properties, including acid-base behavior (pK_a values), log $P_{oct/water}$ values, van der Waals volumes and dipole moments, the last two calculated using Density Functional Theory calculations, and also EC50/LC50 values for distinct trophic levels that are estimated on the basis of impairment/mortality of zebrafish (*Danio rerio*) embryos, immobility/mortality of *Daphnia sp.* and luminescence inhibition of *Vibrio fisheri* (see Table 1).

Table 1. Physicochemical properties of the target compounds.

Compound/ Chemical structure	**μ_D[b]**	**vdW volume[b]**	**logP[c]**	**pKa**	**Microtox toxicity *(Vibrio fischeri)***	**Water flea toxicity (*Daphnia sp.*)**	**Zebrafish toxicity *(Danio rerio)***
Diclofenac[a] 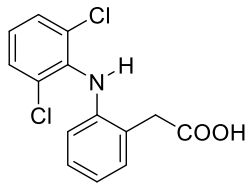	0.39 D (11.46 D)	323.4 Å^3 (324.3 Å^3)	4.51 (log D = 1.7)	4.15	73 µM IC_{50}[d] at 15min *Environ. Pollut.* 237 (2018) 549 54 µM IC_{50} at 15 min *Environ. Toxicol. Chem.* 36 (2017) 807	61 µM LC_{50}[e] at 48h *Bull. Environ. Contam. Toxicol. 97 (*2016) 84	39 µM LC_{50} at 48 hpf[f] *Sci. Total Environ. 666 (2019) 1273*
Triclosan 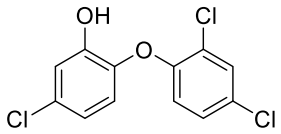	1.25 D	295.2 Å^3	4.76	7.9	2.5 µM IC_{50} at 15 min *Chemosphere* 108 (2014) 239	1.1 µM LC_{50} at 48h *Ecotoxicol.* 22 (2013) 1384 2.1 µM LC_{50} at 48h *Environ. Sci. Pollut. Res. 26* (2019) *16289*	2.2 µM LC_{50} at 48 hpf *Environ. Sci. Technol.* 53 (2019) 11988 3.9 µM LC_{50} at 48 hpf *Sci. Total Environ. 666 (2019) 1273*

Table 1. *(continued)*

Compound/ Chemical structure	**μ_D[b]**	**vdW volume[b]**	**logP[c]**	**pKa**	**Microtox toxicity *(Vibrio fischeri)***	**Water flea toxicity (*Daphnia sp.*)**	**Zebrafish toxicity *(Danio rerio)***
Bisphenol A 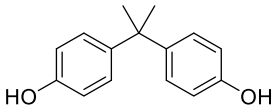	1.24 D	296.5 Å^3	3.32	9.6	27 μM IC_{50} at 15min *Comp. Biochem. Physiol. C*, 152 (2010) 407 38 μM IC_{50} at 30min *Molecules* 23 (2018) 3226	64 μM LC_{50} at 48h *Environ. Sci. Pollut. Res. 24 (*2017) 23872 56 μM LC_{50} at 48h. *J. Health Sci. 50 (*2004) 97	63 μM LC_{50} at 48 hpf *Sci. Total Environ. 666 (2019) 1273*
Chlorpyrifos 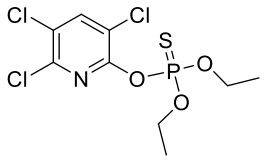	2.19 D	357.7 Å^3	4.96	-	0.76 μM IC_{50} at 15min *J. Hazard. Mat. B103* (2003) 93	2.3×10^{-4} μM LC_{50} at 48h. *Environ. Toxicol. Chem.* 15 (1996) 1133 2.6×10^{-4} μM LC_{50} at 48h. *Ecotox. Environ. Safety 71 (*2008) 219 1.4×10^{-3} μM LC_{50} at 48h *Ecotox. Environ. Safety 64* (2006) 207	16 μM LC_{50} at 5 dpf[g] *Environ. Toxicol. Chem.* 33 (2014) 1337 3.4 μM LC_{50} at 99 hpf *J. Hazard. Mater.* 334 (2017) 121 2.0 μM LC_{50} at 96 h in adult. *Environ. Toxicol. Pharmacol*. 43 (2016) 166

[a] Values in parenthesis correspond to the anionic form of the carboxylic group.
[b] The dipole moment and the van der Waals (vdW) volume values were estimated using density functional theory (DFT) calculations at the B3LYP/6-31G* level of theory using the Spartan'10 v.1.0 program (Wavefunction INC. 18401 von Karman Ave., Irvine, CA 92612. www.wavefun.com).
[c] Logarithm of the octanol/water partition coefficient, experimental values (www.chemspider.com)
[d] IC_{50}: median inhibition concentration
[e] LC_{50}: median lethal concentration
[f] hpf (hours post fertilization)
[g] dpf (days post fertilization)

Both empirical and theoretical *in-silico* studies have been selected to mechanistically infer molecular interactions of the above compounds and potential accumulation within lipid bilayers via passive diffusion. Two fluorescent membrane probes bearing naphthalene moieties (*viz.*, 6-propionyl-2-dimethylaminonaphthalene (prodan) and 6-dodecanoyl-2-dimethylaminonaphthalene (laurdan) have been chosen to ascertain low-resolution changes in bilayer organization by generalized polarization (GP) or fluorescence anisotropic (r_{ss}) measurements that serve to indicate alterations in lipid ordering and liposome fluidity, respectively.[22-25] The results arising from this low-resolution technique have been complemented by high-resolution NMR spectroscopy. The use of diffusion-ordered NMR spectroscopy (DOSY) experiments allows elucidating whether or not the contaminants are bound to the vesicles. In addition, 2D ^{1}H,^{1}H-ROESY and ^{1}H,^{1}H-NOESY experiments,[26] together with potential ^{1}H chemical shift perturbations in the course of vesicle titration assays would provide relevant insights on the favorable interaction/s occurring at atomic resolution. This holistic empirical approach is expected to elucidate the extent of binding of targets to biomembrane surrogates, along with their potential accumulation within lipid bilayers, and thus enable identification of potentially hazardous chemical compounds. Empirical data are to be supplemented by theoretical calculations based on Molecular Dynamics (MD) simulations using a realistic model of lipid bilayer that might offer invaluable information at the molecular level of the equilibrium distribution of each contaminant across the hydrophilic and hydrophobic regions of phospholipids.[27,28]

MATERIALS AND METHODS

Detailed information and description of (i) reagents and target compounds, (ii) synthesis of liposomes, (iii) generalized polarization and anisotropic analysis using fluorescent membrane probes, (iv) Assignment of ^{1}H NMR signals to liposomes, (v) interaction of contaminants with liposomes elucidated by ^{1}H NMR, and (vi) theoretical molecular dynamic studies is available as supporting information (SI).

In brief, the synthesis of the large unilamellar vesicles (LUV) made of phosphatidylcholine (PC) was performed from multilamellar vesicles (see SI) by multiple extrusion through a 100 nm pore size polycarbonate filter. The potential alteration of phospholipid packing and ordering at distinct regions of LUVs in the

presence of contaminants was investigated by fluorescent membrane probes (laurdan and prodan) at 37ºC. Preliminary control experiments were undertaken to demonstrate that the structural integrity of the liposomes was not jeopardized with the maximum percentage of methanol from the standards of the target compounds added to the liposomal solution (≤ 0.4% methanol). Contaminant-dependent alteration of the fluidity of the membrane was also investigated by laurdan anisotropic measurements. The NMR assignment of the signals of PC liposomes was carried out using 1D-^{1}H, 2D-^{1}H,^{1}H-NOESY and 2D-^{1}H,^{1}H-ROESY experiments. NOESY and ROESY are NMR experiments that allow establishing correlations between different ^{1}H that are physically close to each other regardless they are bonded or not. Typically, ^{1}H,^{1}H-ROESY experiments are used for molecules of relatively low molecular weight (<1k Da) because their NOE effects are too weak to be detectable. In our work, 1D-^{1}H, 2D-^{1}H,^{1}H-NOESY and 2D-^{1}H,^{1}H-ROESY assays were also used to study the interactions between the different contaminants and the PC liposomes, which were performed by titration experiments. 1D-^{1}H, 2D-^{1}H,^{1}H-NOESY and 2D-^{1}H,^{1}H-ROESY experiments were acquired by using a water suppression pulse sequence. The potential formation of a complex between PC liposomes and the various contaminants was assessed by using diffusion-ordered NMR spectroscopy (DOSY), which is able to provide insights on the diffusion coefficients of the different molecules in solution, and thus on the hydrodynamic radius of the molecule. Finally, the molecular dynamics (MD) simulations were performed by using the united-atom approximation and conducted on a fully hydrated palmitoyl-linoleylphosphatidylcholine (C18:2/C16:0, PLPC) topology that was arranged in a bilayer of 64 lipid molecules per leaflet.

RESULTS AND DISCUSION

Decoding the membranotropic features of environmental contaminants using fluorescent probes

A strong hypsochromic Stock (blue) shift of the $\lambda_{em,max}$ of laurdan (Figure S1) is observed by increasing TCS concentrations, thus suggesting a perturbation of the probe microenvironment polarity as a result of TCS addition. This might occur as a consequence of a membrane dehydration process occurring at the probe surrounding, which is located at the hydrophilic-hydrophobic interface of the lipid bilayer.[29] This

effect was also observed when LUVs were titrated with BPA, DCF or CPF, but to a much lesser extent (Figures S2-S4). In addition, the titration of LUVs with BPA afforded two clearly distinguishable fluorescence bands (Figure S2). The addition of BPA most likely drives laurdan to exhibit two different but notably populated environments and implies that only a part of the hydrophilic-hydrophobic liposome interface is hydrated. However, fluorescent phenomena other than solvent dipolar relaxation might also occur.[30]

The increase of laurdan's Generalized Polarization (GP) values is indicative of the packed structure of the lipid bilayer in the presence of the xenobiotic as well as of the membrane dehydration level. Figure 1A (illustrating the addition of contaminant at 50 μM) revealed that a maximum GP increase -as compared to laurdan alone- occurs for BPA, followed by TCS, CPF and DCF (see Figures S1-S4 for visualization of spectral shifts and SI for the equation of GP). In fact, the *t*-tests of comparison of means revealed the existence of significant differences at α=0.05 between the GP value of the probe alone and those obtained in the presence of individual compounds. However, DCF seems to be the pollutant with the lesser PC membranotropic effect. This is in good agreement with previous results by Suwalsky *et al.*[31] who reported mild variations of Laurdan GP up to 2 mM DCF. In addition, the trends of GP values are highly concentration dependent (Figure 1B), because e.g. TCS and CPF induce an enhanced lipid ordering and compact structural assembly at concentrations above 100 μM.

The GP values obtained for prodan as a probe revealed that the four contaminants follow the same trend than that observed for laurdan (Figure 1C), with statistically significant GP differences in all cases against prodan alone. Again, the influence of bisphenol A on GP was stronger than that of the other pollutants. However, a smaller variation of average prodan GP data is measured for all of the targets when compared to the probe alone. This observation can be attributed to the ability of prodan to move out and into the LUVs[32] as corroborated by the more negative GP values compared to those of laurdan. Consequently, the polarity of the medium around prodan is much less affected by the contaminants. In fact, *in-silico* DFT calculations indicate that the binding energy of prodan at the polar head of the phospholipid is akin to that at the glycerol region,**¡Error! Marcador no definido.** yet its intercalation into the lipid molecules would require the separation of the acyl chains. Our conclusion is that the shallow prodan

probe might not serve as a good indicator of the interaction of xenobiotics with lipid bilayers.

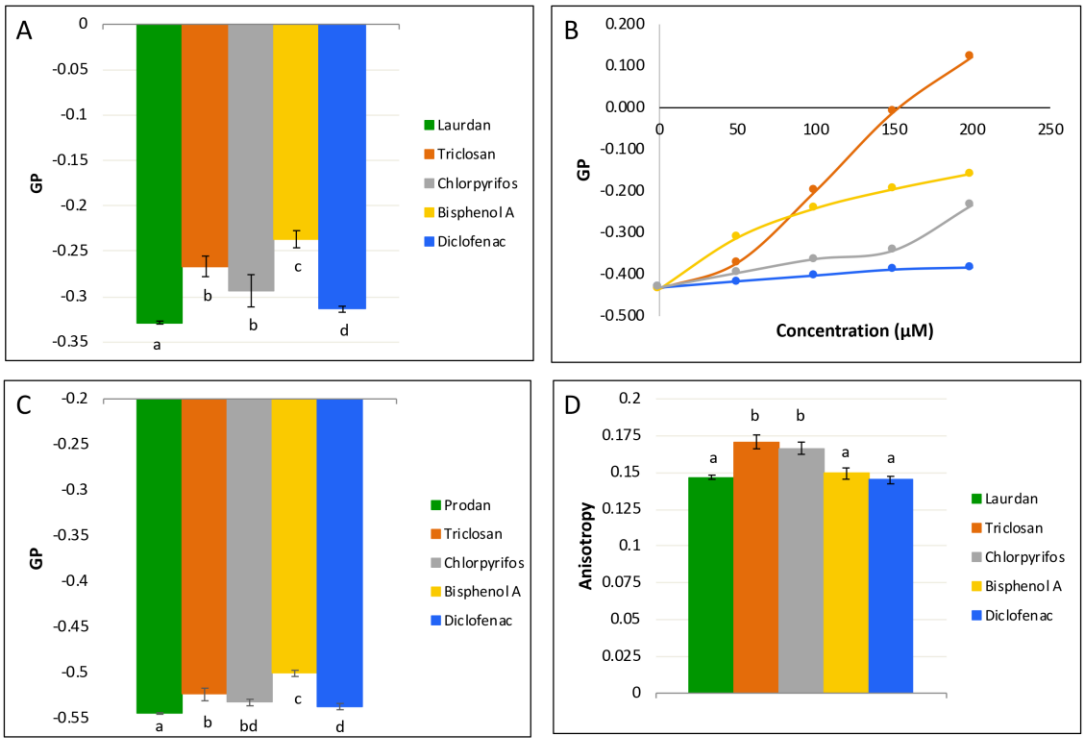

Figure 1. Fluorescence studies of soy PC LUVs at 37ºC using laurdan and prodan as membrane probes. (A) Laurdan's GP values obtained with PC LUVs in the presence of various organic contaminants at a concentration level of 50 µM. (B) Laurdan's GP values obtained for PC LUVs at different concentration levels of each studied contaminant (50, 100, 150 and 200 µM). Data corresponding to TCS is shown in *orange*, that corresponding to CPF is shown in *grey*, that corresponding to BPA is shown in *yellow* and data for DCF is shown in *blue.* (C) Prodan's GP values obtained with PC LUVs in the presence of various organic contaminants at a concentration level of 50 µM (D) Fluorescence anisotropy measurements for laurdan-embedded PC liposomes with various individual contaminants at a concentration level of 50 µM. Statistical tests were based on *t*-tests of comparison of means at a significance level (α) of 0.05.

Fluorescence spectroscopy was also used to explore anisotropic effects (r_{ss} equation is given in SI). Laurdan anisotropy was only affected, in a statistically significant manner (α=0.05), by TCS and CPF (Figure 1D). The increase of the r_{ss} values from ~0.15 to ~0.17 suggests that the liposomal microviscosity is enhanced by the above contaminants, whereas the fluidity of the phospholipid bilayer remained unaltered with the addition of either BPA or DCF to the LUVs. These anisotropic data disagree with the conclusions derived from laurdan's GP data for BPA. This might evidence the existence of an indirect relationship between the laurdan's spectral changes and the effect of BPA at the glycerol backbone level where laurdan is located.¡**Error! Marcador no definido.** Consequently, the penetration of BPA throughout the lipid bilayer cannot be unequivocally identified from the analysis of the fluorescent spectral shifts of laurdan. It should be also noted that laurdan's anisotropy serves as a better *in-vitro* indicator for discrimination of the strongest membranotropic effects of xenobiotics as compared to GP measurements because statistically different anisotropy values against laurdan alone are obtained only for two out of the four contaminants investigated.

To shed light on the discrepancies between the GP and the anisotropic data for BPA as a target contaminant, the potential effect of BPA on the fluorescence emission spectrum of laurdan embedded in the vesicles was explored. Hence, fluorescence quenching effects were analyzed by the Stern-Volmer equation (Eq. 1), [33]

$$F_0/F = 1 + K_{sv}[C] \qquad \text{(Eq. 1)}$$

where F_0 and F are the emission intensities of laurdan at 490 nm in PC vesicles without and with individual quenchers (contaminants), respectively; K_{SV} the Stern-Volmer quenching constant; and C the concentration of the contaminant. Our findings (Figure S5) reveal that BPA and DCF do induce a negligible quenching effect of the fluorescence intensity of laurdan (K_{SV} < 0.025 μmol L^{-1}), whereas TCS and CPF seem to induce a subtle quenching effect, which would involve a dynamic and static process as suggested by their non-lineal Stern-Volmer plots. Consequently, the disagreement between the anisotropic and GP data for BPA is most likely a consequence of molecular effects other than fluorescent quenching.

^{1}H NMR mapping of the PC liposome-binding regions upon interaction with contaminants

Our results clearly demonstrate that the fluorescent data provided by membrane probes should be analyzed carefully because the specific chemical nature of the contaminant, as well as direct or indirect effects onto the lipid assembly and/or on the fluorescent probe, might induce to misleading interpretations. Therefore, fluorescence data necessarily needs to be supplemented by high resolution experimental techniques. Consequently, NMR spectroscopy has been employed to get insight at the atomic level on the specific architecture of the interactions occurring between soy PC LUVs and each contaminant (see SI for experimental methodology).

The ^{1}H-NMR assignment of 1,2-dilinoleoyl-sn-glycero-3-phosphocholine (PC 18:2, DLPC) was obtained at pD 7.4 and 37ºC using standard 1D and 2D NMR experiments. Despite the significant signal broadening as a result of the low molecular tumbling of the LUVs, the ^{1}H-NMR assignment could be accomplished for all of the protons, except for H5 (Figure 2), which likely appears under the suppressed water signal.

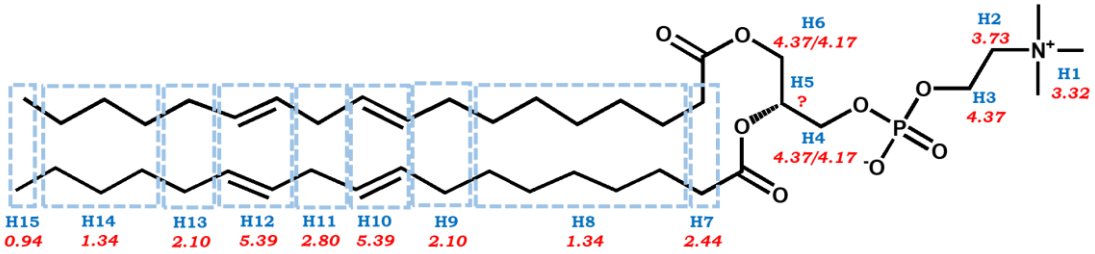

Figure 2. Chemical structure of 1,2-dilinoleoyl-sn-glycero-3-phosphocholine (DLPC, PC-18:2). C-H groups that displayed indistinguishable chemical shifts have been grouped in square dashed blue boxes. In addition, C-H moieties have been arbitrarily labelled as H_n (*blue*), and their ^{1}H chemical shifts are given in ppm (*red*).

The NMR assignment allowed us to map the interaction region between the PC 18:2 (DLPC) molecules that constitute the LUVs and each contaminant (Figure 3). The addition of DCF only induced significant chemical shift perturbation on the signals

corresponding to H1 and H2 at pD 7.4 (Figures 4A, B), which indicates that DCF mainly interacts with the outer polar moieties of PC (Figure 3A). This might occur through an electrostatically driven process as a result of the binding between the $–CH_2$-$N(CH_3)^+$ moiety of the PC 18:2 and the carboxylate moiety of DCF. However, the appearance of NOEs between the aromatic protons of DCF and the H1 protons of PC-18:2 (Figure 4C) suggested that a cation-π interaction is occurring between the choline group and the DCF that would position the aromatic rings perpendicular to the LUV surface. On the other hand, the DOSY spectra revealed that the relative diffusion coefficient (*D*) of DCF (Figure 4D) was notably different to that displayed by the soy PC LUVs, which indicates that DCF in solution does not interact with the liposomes to a large extent. Consequently, our results demonstrated that the binding between DCF and soy PC LUVs only occurs on the vesicle surface, although this process seems not to be thermodynamically favored.

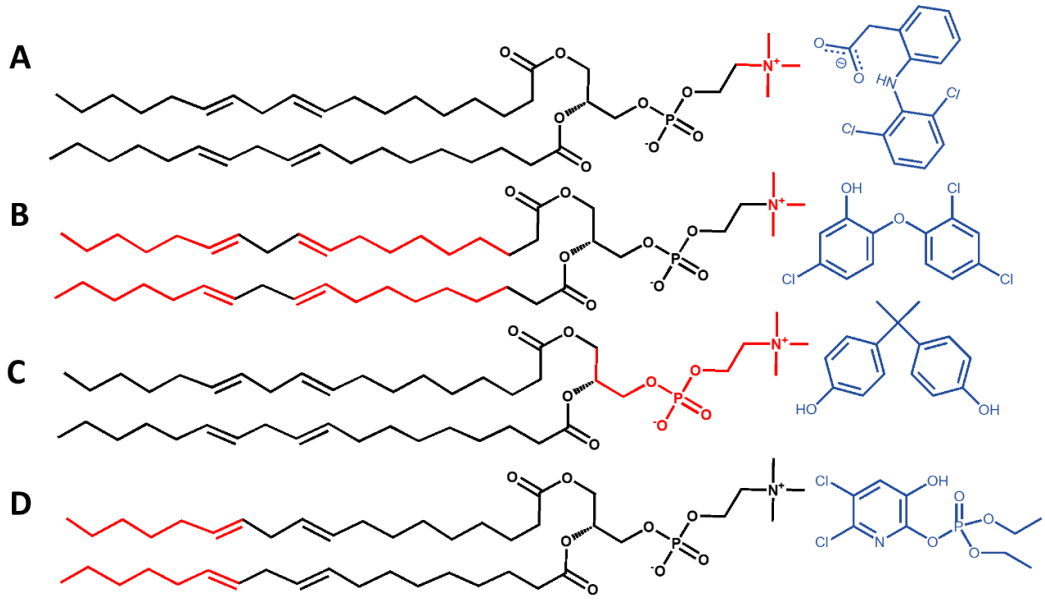

Figure 3. Chemical structures of PC-18:2 **(A-D)**, DCF **(A)**, TCS **(B)**, BPA **(C)** and CPF **(D)**. The chemical structure of the different contaminants (ligands) are shown in blue, whereas the C-H groups of PC-18:2 displaying chemical shift perturbations and/or intermolecular NOE with each contaminant at pD 7.4 (in 20mM phosphate buffer) are colored in red.

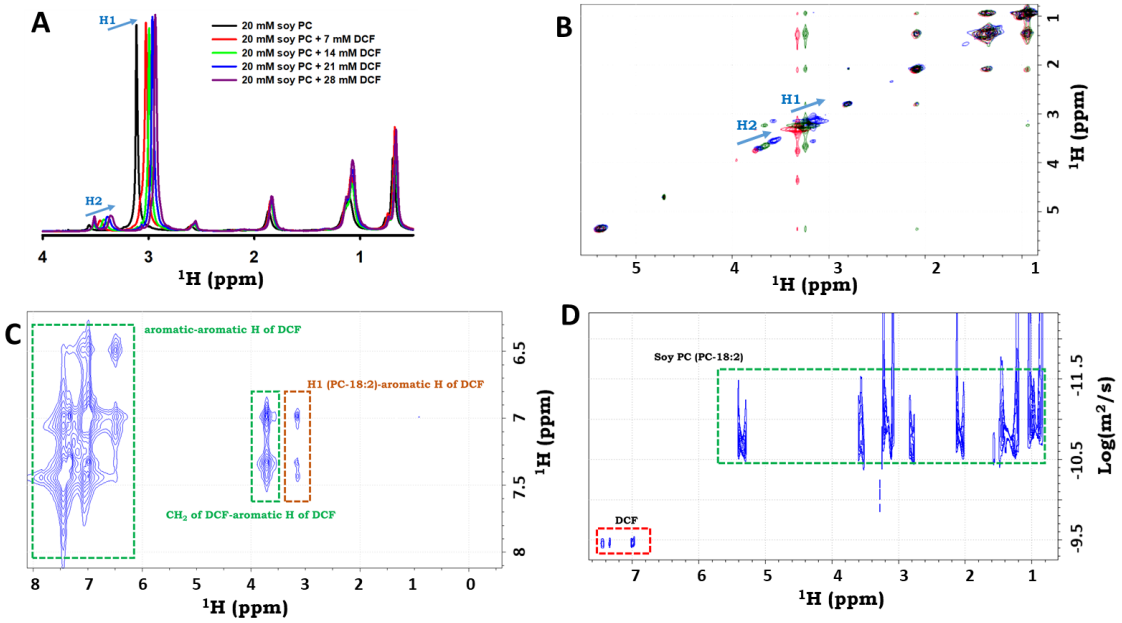

Figure 4. NMR study of the interaction between soy PC vesicles and DCF. **(A)** Overlapping of the aliphatic region of the ^{1}H-NMR spectra of soy PC LUVs with increasing concentrations of DCF at pD 7.4. The signals displaying higher chemical shift perturbations as a result of the DFC addition, are labeled according to the numbering given in Figure 2. **(B)** Overlapping of the ^{1}H,^{1}H-NOESY spectra of soy PC LUVs alone (*red*) and with DCF at 7mM (*green*) and 28mM (*blue*). The cross-peaks displaying a higher chemical shift perturbation as a result of the DFC addition, are labeled according to the numbering given in Figure 2. **(C)** Aromatic region of the ^{1}H-^{1}H NOESY spectrum of a mixture containing soy PC LUVs (20mM) and DFC (28mM). The aromatic-aromatic cross-peaks of DCF, as well as their intramolecular NOEs are squared in a green dashed box. The intermolecular NOEs between the aromatic protons of DCF and the H1 protons of PC-18:2 are squared in a brown dashed box. **(D)** 2D-DOSY spectrum of a mixture containing soy PC vesicles (20mM) and DFC (28mM). The ^{1}H signals of the soy PC LUVs have been squared in a dashed green box, whereas those corresponding to DFC has been squared in a dashed red box.

With respect to TCS, its low solubility in water (~35µM at 20ºC) might jeopardise the NMR interaction studies. However, the solubility of TCS was notably increased with the addition of vesicles. For instance, TCS at 17 mM concentration was completely dissolved in a 20mM liposome-containing solution. The DOSY spectrum of the TCS-liposome mixture suggest that TCS is embedded in the LUVs, because both TCS and LUVs displayed the same *D* value (Figure 5A). This observation was additionally confirmed by the ^{1}H,^{1}H-NOESY spectrum, which clearly showed intermolecular NOEs between the aromatic protons of TCS and the H10 and/or H12; H1; H13 and/or H9; H14 and/or H8; and H15 of PC-18:2 (Figure 5B). These results demonstrated that TCS is able to interact with the polar head groups of the PC vesicle surface, but most importantly with the hydrophobic core of the LUVs. To assess whether the surface binding was due to the interaction between the cationic choline of PC 18:2 and the phenolate form of TCS (its pK_a is ~7.9 and therefore, ~33% of TCS is under the phenolate form at pD 7.4), the ^{1}H,^{1}H-NOESY spectrum was also recorded at pD 4.7, for which the percentage of negatively charged TCS is negligible. Strong intermolecular NOEs involving H1 of PC 18:2 (Figure 5C) were still observed. This finding suggests that the LUV surface likely binds TCS through a cation-π interaction. The lack of NOEs involving the H10 and H12 groups indicates that TCS at this pD likely penetrates deeply across the fatty acid region of the LUV and it is tightly bound to the inner hydrophobic tail of the bilayer (Figure 3B).

As for BPA, the NMR DOSY spectrum revealed that this emerging contaminant is able to interact with soy PC LUVs at pD 7.4 (Figure 6A). The NMR titration of LUVs with BPA evidenced that NMR readouts corresponding to H1, H2 and H3 of PC 18:2 were the only ones that modified their chemical shifts upon adding BPA (Figure 6B). Consequently, BPA preferentially interacts with and accumulate at the polar head region of PC 18:2 (Figure 3C), and thus only minute amounts might penetrate into the hydrophobic core of the vesicle. This is likely occurring because the two phenol groups of BPA are tweezing the choline moiety through the anchoring of the hydroxyl group to the polar head group of PC. The unambiguous intermolecular ROE signals between the H1 of PC 18:2 and the *ortho*-position protons of BPA but not with those at *meta*-position nor with the methyl groups (Figure 6C) supported the hypothesized interaction mechanism. Accordingly, our results demonstrate that the supramolecular interaction of

PC liposomes with BPA exists but their binding is limited to the vesicle surface. This is fully supported by the NMR data reported by Malekar *et al.*[34]

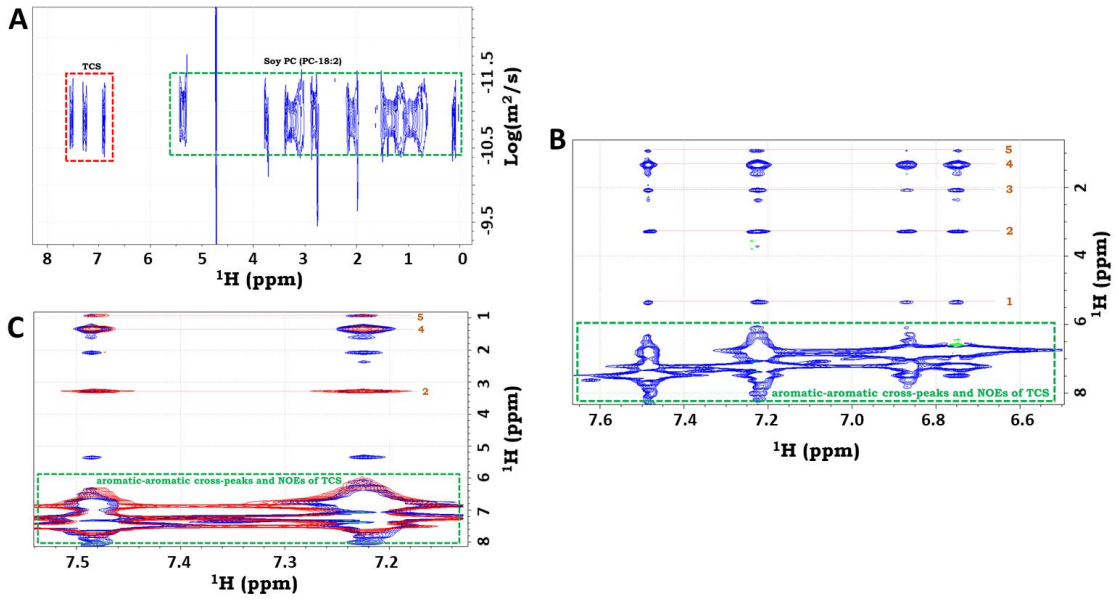

Figure 5. NMR study of the interaction between soy PC LUVs and TCS. **(A)** 2D-DOSY spectrum of a mixture containing soy PC LUVs (20mM) and TCS (17mM) in 20mM D_2O phosphate buffer at pD 7.4. The ^1H signals corresponding to the soy PC LUVs have been squared in a dashed green box, whereas those corresponding to TCS have been squared in a dashed red box. **(B)** ^1H,^1H-NOESY spectrum of a mixture containing soy PC LUVs (20mM) and TCS (17mM) prepared in 20mM D_2O phosphate buffer at pD 7.4. The ^1H-^1H cross-peaks of TCS and its intramolecular NOEs are squared in a dashed green box. The intermolecular NOEs detected between the aromatic protons of TCS and the protons of the soy PC LUVs are labelled as follows: i) the H10 and/or H12 of PC-18:2 (1); ii) the H1 of PC-18:2 (2); iii) the H13 and/or H9 of PC-18:2 (3); iv) the H14 and/or H8 of PC-18:2 (4); and v) the H15 of PC-18:2 (5). The numbering of each proton is given in Figure 2. **(C)** Overlapping of the ^1H,^1H-NOESY spectra of mixtures containing soy PC LUVs (20mM) and TCS (17mM) prepared at pD 7.4 (*blue*) and at pD 4.7 (*red*). The ^1H-^1H cross-peaks of TCS and its intramolecular NOEs are squared in a dashed green box. In addition, the intermolecular NOEs detected between the aromatic protons of TCS and the protons of the soy PC LUVs are labelled as described in the figure caption of panel (B).

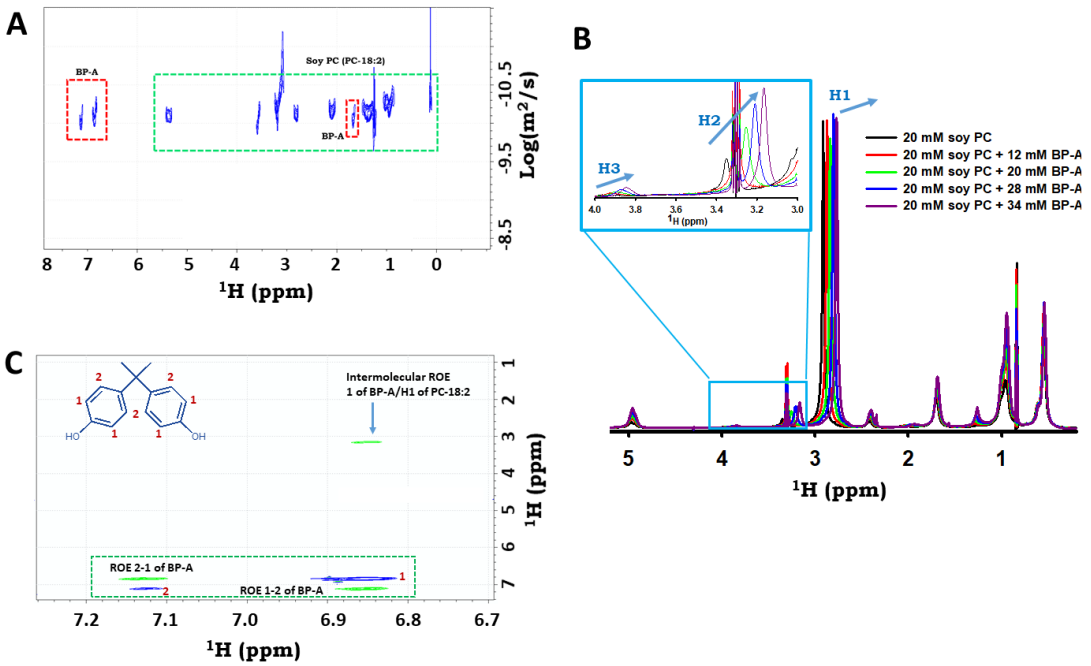

Figure 6. NMR study of the interaction between soy PC vesicles and BPA. **(A)** 2D-DOSY spectrum of a mixture containing soy PC vesicles (20mM) and BPA (34mM) in 20mM D_2O phosphate buffer at pD 7.4. The ^{1}H signals corresponding to the soy PC LUVs have been squared in a dashed green box, whereas those corresponding to TCS have been squared in a dashed red boxes. **(B)** Overlapping of the aliphatic region of the ^{1}H-NMR spectra of soy PC with increasing concentrations of BPA. The signals displaying a higher chemical shift perturbation as a result of the BPA addition are labeled according to the numbering given in Figure 2. The insert shows a zoom of the region between 3 and 4ppm. **(C)** ^{1}H,^{1}H-ROESY spectrum of a mixture containing soy PC LUVs (20mM) and BPA (34mM) in 20mM D_2O phosphate buffer at pD 7.4. The blue signals correspond to the aromatic cross-peaks of BPA, whereas the green signals correspond to the intramolecular BPA ROEs (squared in a green box), and to the intermolecular BPA/PC-18:2 ROE observed between the H1 protons of PC-18:2 and the protons at the *ortho* position of BPA.

Elucidation of the degree of penetration of CPF across the cellular lipid barrier was also investigated. The addition of CPF to a solution containing PC LUVs afforded supramolecular interactions, as both the contaminant and LUVs displayed similar *D* values (Figure 7A). In fact, CPF induced chemical shift perturbations on the ^{1}H-NMR signals that are characteristic of the hydrophobic core of the LUV (i.e. H12, H13, H14 and H15) (Figure 7B). The binding between CPF and the hydrocarbonated tail of the PC 18:2 was additionally confirmed by the identification of intermolecular NOEs between the H15 and H14 moieties of the PC 18:2 and the aromatic proton of CPF (Figure 7C), thus confirming that CPF is capable of entering into the lipid bilayer and remain predominantly at the inner hydrophobic region. Moreover, the ^{1}H,^{1}H-NOESY spectrum revealed that intramolecular NOEs between the aromatic proton of CPF and methyl moieties do occur. This observation suggests that CPF inside the PC liposomes might adopt a tripod-like conformation, where the aromatic ring and the two methyl groups would form the hypothetical tripod base. Consequently, our data demonstrate that CPF strongly interacts with soy PC liposomes as a highly bioaccumulable organic compound (Figure 3D).

Molecular dynamics of the different contaminants embedded in the lipid bilayer

The binding process between individual contaminants and the soy PC LUVs can be understood better if the elucidation of the interaction regions is supplemented with dynamical information on the most probable locations of the bilayer in which the contaminant is situated once inserted into the LUVs. In this context, molecular dynamic (MD) simulations have become a powerful tool. Because soy PC LUVs are mainly composed of unsaturated fatty acid chains, a computational model (see SI for further details) was built using a fully hydrated palmitoyl-linoleylphosphatidylcholine C18:2/C16:0 (PLPC) phospholipid. Initially, all the studied compounds were embedded in the water layer that solvates the aminophospholipid biomembrane surrogate and the entire system was allowed to equilibrate.

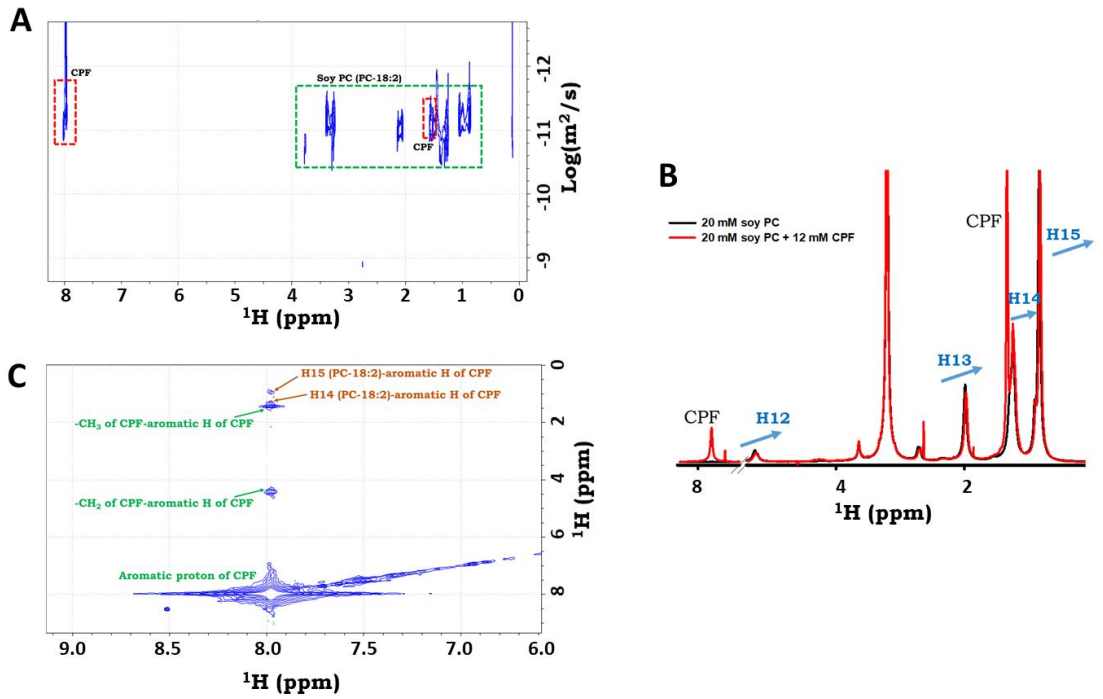

Figure 7. NMR study of the interaction between soy PC vesicles and CPF. **(A)** 2D-DOSY spectrum of a mixture containing soy PC vesicles (20mM) and CPF (12mM) in 20mM D_2O phosphate buffer at pD 7.4. The ^{1}H signals corresponding to the soy PC vesicles have been squared in a dashed green box, whereas those corresponding to CPF have been squared in dashed red boxes. **(B)** Overlapping of the ^{1}H-NMR spectra of soy PC LUVs without and with CPF at the 12mM level. The signals displaying a higher chemical shift perturbation as a result of the CPF addition are labeled according to the numbering given in Figure 2. **(C)** ^{1}H,^{1}H-NOESY spectrum of a mixture containing soy PC vesicles (20mM) and CPF (12mM) in 20mM D2O phosphate buffer at pD 7.4. Intramolecular NOEs detected for CPF are labelled in green. Intermolecular NOEs observed between CPF and PC-18:2 are labelled in brown.

The average area per lipid (A_{PLPC}) is a useful parameter to describe the packing of the lipid molecules within the bilayer, and to evaluate the stability of the bilayer during the MD simulations. The A_{PLPC} values and the bilayer thickness (h) for PLPC are similar to those previously reported by Wong-ekkabut *et al.*[35] In addition, the A_{PLPC} and h values were highly homogeneous across the different models (probes and contaminants), and were in good agreement with values reported for similar membranes (*e.g.*, areas spanning from 0.62 to 0.68 nm^2 for DPPC)[36] (see Table 2). The lateral diffusion

coefficients (D_{lat}) of the lipid bilayer for every contaminant were obtained by the Einstein relation, from the slope of the average mean square displacement after equilibration.[37] The computed values agreed well with experimental neutron scattering diffusion coefficients ((5–100)×10^{-8} cm^2/s).[38,39] This serves to demonstrate that the MD methodology herein proposed is fully validated.

Table 2. Average area per lipid (A_{PLPC}), average thickness (h) of the lipid bilayer and the lateral diffusion coefficient of the bilayer for each of the four contaminants and the membrane probes.

Compound	**A_{PLPC} (nm^2)**	**h (nm)**	**D_{lat} PLPC (cm^2/s)**
Laurdan	0.649±0.002	3.74	(9.2±6.0) × 10^{-8}
Prodan	0.645±0.005	3.64	(10.7±6.7) × 10^{-8}
Chlorpyrifos	0.659±0.003	3.75	(5.9±2.0) × 10^{-8}
Triclosan	0.658±0.004	3.73	(7.4±5.6) × 10^{-8}
Bisphenol A	0.657±0.005	3.72	(8.0±1.0) × 10^{-8}
Diclofenac	0.659±0.002	3.70	(19.2±12.2) × 10^{-8}

The evaluation of the data in Table 2 gives us invaluable information regarding the most favorable location of the probes/contaminants within the bilayer. For example, the D_{lat} value of PLPC in the presence of DCF is larger than that observed for laurdan or prodan. This finding suggests that DCF interacts with the phospholipid head groups of the lipid bilayer, mostly with the choline moiety, which agrees with our fluorescence and NMR data and previous data in the literature.[40] In contrast, the D_{lat} value of CPF is smaller than those of the probes, thus indicating that CPF increases the packing of the lipids, likely due to the non-covalent van der Waals interactions that necessarily should be stronger than those between lipids. The hindrance of the lateral diffusion of PLPC with the addition of CPF is in excellent agreement with both laurdan's GP and anisotropy data that indicate lipid ordering and rigidity, respectively, and also with NMR measurements for which NOEs are identified at the hydrophobic tail of the fatty acid chain.

Further insight into the ease of penetration of the contaminants and probes across the bilayer can be obtained throughout the mass density profile. Figure 8 illustrates the most

likely position of the xenobiotic/probe with respect the center of the bilayer (apolar–apolar interface) in the time course of the MD simulation. The naphthalene group of laurdan is predominately located at the polar head of the biomembrane (Figure 8), according with its expected behavior in previous DOPC bilayers,[41,42] yet prodan is mainly positioned below the glycerol region, in accordance with previous MD simulations on a DLPC bilayer.[43] Neutral and anionic charge states of TCS were simulated to understand the effect of the protonation on the degree of penetration. The anionic TCS mostly remains interacting with the polar head group, whereas the neutral TCS is inserted into the bilayer, which qualitatively agrees with our NMR data. MD simulations additionally revealed that BPA akin to neutral TCS is mainly located at the hydrophilic-hydrophobic interface of the PLPC, which is in good agreement with previous theoretical studies using DPPC bilayers.[44] Remarkably, TCS and BPA showed equal behavior across the PC lipid bilayer notwithstanding the dissimilar log P values. However, the dipole moments and Van de Waals volumes for both molecules are on a par, and thus the two molecular features seem to work as good indicators to elucidate compound permeability across lipid bilayers. On the other hand, CPF rapidly penetrates into the bilayer interface and, once located there, it is free to move through the two leaflets of the membrane. According to the NMR and MD data, the most likely location of CPF is at the hydrocarbon tails of lipids. Thus, CPF is expected to be highly bioaccumulated, which correlates well with its log P value close to 5 (see Table 1). In contrast, DCF is mostly displaced on the membrane-water interface, and thus is less prone to cross the lipid membrane, as already suggested by the NMR and molecular fluorescence data.

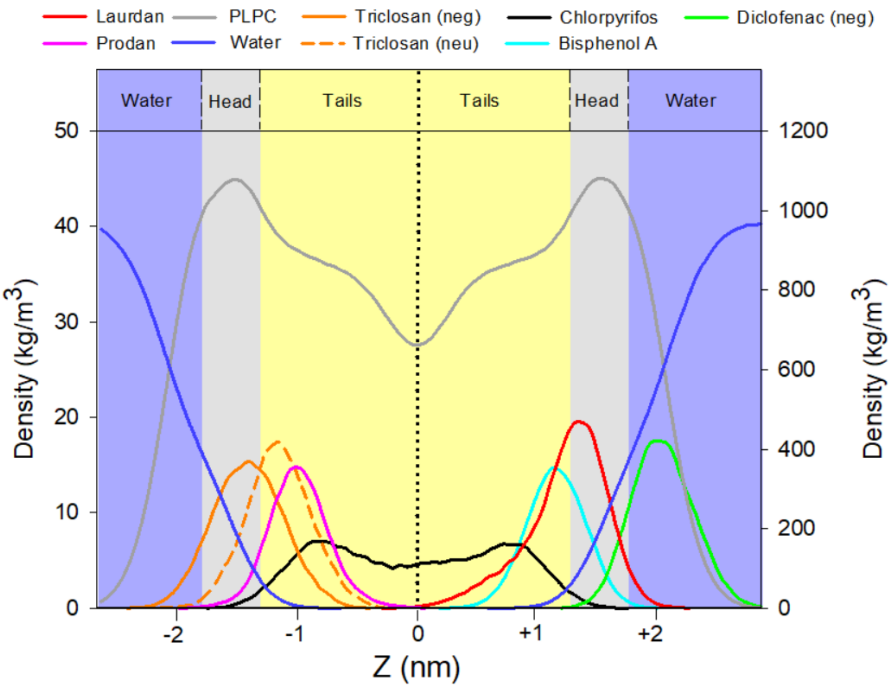

Figure 8. The average density profiles of water (blue line), PLPC lipid (gray line) in the right y-axis; triclosan-neg (negatively charged, orange solid line), triclosan-neu (uncharged, orange dashed line), Prodan (pink line), chlorpyrifos (black line), bisphenol-A (cyan line), laurdan (red line), diclofenac (green line) in the left y-axis as a function of the distance from the center of the lipid bilayer (Z).

CONCLUSIONS

In this study, the interaction regions and the membrane distribution of two probes and four contaminants into an elaborated model of phospholipid bilayer have been thoroughly investigated. Unprecedentedly, a new multidisciplinary approach involving a combination of empirical data based on ^{1}H-NMR and molecular fluorescence experiments using membrane probes along with MD simulations is proposed to predict *in-vitro* contaminant bioaccumulation based on passive diffusion. The MD simulations have corroborated the fact that the lipid bilayer is a highly dynamic structure and that the contaminants might move freely within a wider or restricted region of the membrane. Our holistic approach has demonstrated that DCF is not prone to penetrate into the lipid bilayer at physiological pH to a large extent, whereas CPF has the ability

to do so and move rapidly across the hydrophobic region. While the results for DCF and CPF are somehow unambiguous, some uncertainties (at atomic level of resolution) are identified regarding the binding of TCS or BPA to the LUVs. In any case, all the results herein reported have pointed out that TCS binds to the cationic choline group of the LUVs but at the same time is able to easily penetrate deeply along the hydrophobic region. On the other hand, BPA seems to be preferentially interacting with the polar head group of the LUV. All these observations reinforce the idea that a multidimensional approach that is able to tackle the complexity of lipid bilayers mimicking eukaryotic cell membranes and explore contaminant distribution and bioaccumulation across membranes is needed.

Supporting information (SI)

Detailed description of (i) materials, reagents and synthesis of liposomes, (ii) experimental methods based on the fluorescence detection of membrane probes embedded in liposomes and ^{1}H NMR assignment of signals from liposomes, (iii) fluorescence emission spectra of laurdan embedded in liposomes after addition of individual contaminants, (iv) ^{1}H NMR study of the interaction between contaminants and liposomes, and (iv) molecular dynamic exploration of the mobility of contaminants across lipid bilayers.

Acknowledgments

Manuel Miró acknowledges financial support from the FEDER/Spanish Ministry of Science, Innovation and Universities (MCIU)-Spanish State Research Agency (AEI) through projects CTM2017-84763-C3-3-R (MCIU/AEI/FEDER, EU) and CTM2017-90890-REDT (MICIU/AEI/FEDER, EU). Antonio Frontera extends his appreciation to AEI for the funding of project CTQ2017-85821-R (MICIU/AEI/FEDER, EU). Miquel Oliver thanks the Government of the Balearic Islands, Conselleria d'Educació, Cultura i Universitats, and the European Social Fund for PhD fellowship allocation (no. FPI/1681/2014).

REFERENCES

(1) Ebele, A. J.; Abou-Elwafa Abdallah, M.; Harrad, S. Pharmaceuticals and personal care products (PPCPs) in the freshwater aquatic environment. *Emerging Contaminants* **2017**, *3*, 1-16.

(2) Fairbairn, D. J.; Arnold, W. A.; Barber, B. L.; Kaufenberg, E. F.; Koskinen, W. C.; Novak, P. J.; Rice, P. J.; Swackhamer, D. L. Contaminants of emerging concern: mass balance and comparison of wastewater effluent and upstream sources in a mixed-use watershed. *Environ. Sci. Technol.* **2016**, *50*, 36−45.

(3) Reemtsma, T.; Berger, U.; Arp, H. P. H.; Gallard, H.; Knepper, T. P.; Neumann, M.; Quintana, J. B.; de Voogt, P. Mind the gap: persistent and mobile organic compounds water contaminants that slip through. *Environ. Sci. Technol.* **2016**, *50*, 10308−10315.

(4) Lohmann, R.; Muir, D.; Zeng, E. Y.; Bao, L.-J.; Allan, I. J.; Arinaitwe, K.; Booij, K.; Helm, P.; Kaserzon, S.; Mueller, J. F.; Shibata, Y.; Smedes, F.; Tsapakis, M.; Wong C. S.; You, J. Aquatic Global Passive Sampling (AQUA-GAPS) revisited: first steps toward a network of networks for monitoring organic contaminants in the aquatic environment. *Environ. Sci. Technol*. **2017**, *51*, 1060−1067.

(5) Schnoor, J. L. Re-emergence of emerging contaminants. *Environ. Sci. Technol.* **2014**, *48*, 11019−11020.

(6) Richardson, S. D.; Ternes, T. A. Water analysis: Emerging contaminants and current issues. *Anal. Chem*. **2018**, *90*, 398−428.

(7) Commission implementing decision (EU) 2015/495 of 20 March 2015 establishing a watch list of substances for Union-wide monitoring in the field of water policy pursuant to Directive 2008/105/EC of the European Parliament and of the Council, *Off. J. Eur.* **2015**, *L 78*, 40-42.

(8) Commission Implementing Decision (EU) 2018/840 of 5 June 2018 establishing a watch list of substances for Union-wide monitoring in the field of water policy pursuant to Directive 2008/105/EC of the European Parliament and of the Council, *Off. J. Eur.* **2018**, *L 141*, 9-12.

(9) Wild, C.P. Complementing the genome with an "exposome": The outstanding challenge of environmental exposure measurement in molecular epidemiology. *Cancer Epidemiol. Biomarkers Prev.* **2005**, *14*, 1847-1850.

(10) Vrijheid, M. The exposome: A new paradigm to study the impact of environment on health. *Thorax* **2014**, *69*, 876-878.

(11) Simpson, M.J.; McKelvie, J.R. Environmental metabolomics: new insights into earthworm ecotoxicity and contaminant bioavailability in soil. *Anal. Bioanal. Chem.* **2009**, *394*, 137–149.

(12) Schoeters, G. The REACH perspective: Toward a new concept of toxicity testing. *J. Toxicol.Environ. Health B Crit. Rev.* **2010**, *13*, 232-241.

(13) Semple, K.T.; Doick, K.J.; Burauel, P.; Craven, A.; Harms, H. Defining bioavailability and bioaccessibility of contaminated soil and sediment is complicated. *Environ. Sci. Technol.* **2004**, *38*, 228A–231A.

(14) Fedotov, P. S.; Kördel, W.; Miró, M.; Peijnenburg, W. J. G. M.; Wennrich, R.; Huang, P.-M. Extraction and fractionation methods for exposure assessment of trace metals, metalloids and hazardous organic compounds in terrestrial Environments. *Crit. Rev. Environ. Sci. Technol.* **2012**, *42*, 1117-1171.

(15) International Organization for Standardization. ISO 17402:2008. Soil quality: Requirements and guidance for the selection and application of methods for the assessment of bioavailability of contaminants in soil and soil materials. Geneva, Switzerland, 2008.

(16) Janoff, A.S., Ed. *Liposomes: rational design*. Marcel Dekker: New York, 1999.

(17) Lasic, D. D.; Barenholz, Y., Eds. *Handbook of nonmedical applications of liposomes*, vol. I-IV, CRC Press: Boca Raton, FL, 1996.

(18) Li, J.; Wang, X.-L.; Zhang, T.; Wang, C.-L.; Huang, Z.-J.; Luo, X.; Deng, Y.-H. A review on phospholipids and their main applications in drug delivery systems. *Asian J. Pharm. Sci.* **2014**, *10*, 81–98.

(19) Först, G.; Cwiklik, L.; Jurkiewicz, P.; Schubert, R.; Hof, M. Interactions of beta-blockers with model lipid membranes: Molecular view of the interaction of acebutolol, oxprenolol, and propranolol with phosphatidylcholine vesicles by time-dependent fluorescence shift and molecular dynamics simulations. *Eur. J. Pharm. Biopharm.* **2014**, *87*, 559–569.

(20) Kovács, E.; Savopol, T.; Iordache, M. M.; Săplăcan, L.; Sobaru, I.; Istrate, C.; Mingeot-Leclercq, M. P.;Moisescu, M. G. Interaction of gentamicin polycation with model and cell membranes. *Bioelectrochemistry* **2012**, *87*, 230–235.

(21) Directive 2013/39/EU of the European Parliament and of the Council of 12 August 2013 amending Directives 2000/60/EC and 2008/105/EC as regards priority substances in the field of water policy. *Off. J. Eur. Union* **2013**, *L 226*, 1-17.

(22) Wesołowska, O.; Gąsiorowska, J.; Petrus, J.; Czarnik-Matusewicz, B.; Michalak, K. Interaction of prenylated chalcones and flavanones from common hop with phosphatidylcholine model membranes. *Biochim. Biophys. Acta - Biomembr.* **2014**, *1838*, 173–184.

(23) Ghazaryan, N. A.; Ghulikyan, L.; Kishmiryan, A.; Andreeva, T. V.; Utkin, Y. N.; Tsetlin, V. I.; Lomonte, B.; Ayvazyan, N. M. Phospholipases A2 from Viperidae snakes: differences in membranotropic activity between enzymatically active toxin and its inactive isoforms. *Biochim. Biophys. Acta - Biomembr.* **2015**, *1848*, 463–468.

(24) Kużdżał, M.; Wesołowska, O.; Strancar, J.; Michalak, K. Fluorescence and ESR spectroscopy studies on the interaction of isoflavone genistein with biological and model membranes. *Chem. Phys. Lipids* **2011**, *164*, 283–291.

(25) Vequi-Suplicy, C.C.; Benatti, C.R.; Lamy, M.T. Laurdan in fluid bilayer: position and structural sensitivity. *J. Fluoresc.* **2006**, *16*, 431-439.

(26) Wu, D.-H.; Chen, A.; Johnson Jr, C.S. An improved diffusion-ordered spectroscopy experiment incorporating bipolar-gradient pulses. *J. Magn. Reson., Ser. A*, **1995**, *115*, 260-264.

(27) Khajeh, A.; Modarress, H. Effect of cholesterol on behavior of 5-fluorouracil (5-FU) in a DMPC lipid bilayer, a molecular dynamics study. *Biophys. Chem.* **2014**, *187-188*, 43-50.

(28) Lebecque, S.; Lins, L.; Dayan, F. E.; Fauconnier, M.-L.; Deleu, M. Interactions between natural herbicides and lipid bilayers mimicking the plant plasma membrane. *Front. Plant Sci.* **2019**, *10*, 329. DOI: 10.3389/fpls.2019.00329.

(29) Viard, M.; Gallay, J.; Vincent, M.; Meyer, O.; Robert, B.; Paternostre, M. Laurdan solvatochromism: solvent dielectric relaxation and intramolecular excited-state reaction. Biophys. *J*. **1997**, *73*, 2221–2234.

(30) Sachl, R.; Stepánek, M.; Procházka, K. Fluorescence study of the solvation of fluorescent probes prodan and laurdan in poly(ε-caprolactone)-block-poly(ethylene oxide) vesicles in aqueous solutions with tetrahydrofurane. *Langmuir* **2008**, *24*, 288-295

(31) Suwalsky, M.; Manrique, M.; Villena, F.; Sotomayor, C.P. Structural effects in vitro of the anti-inflammatory drug diclofenac on human erythrocytes and molecular models of cell membranes. *Biophys. Chem.* **2009**, *141*, 34-40.

(32) Oliver, M.; Bauzá, A.; Frontera, A.; Miró, M. Fluorescent lipid nanoparticles as biomembrane models for exploring emerging contaminant bioavailability supported by density functional theory calculations. *Environ. Sci. Technol.* **2016**, *50*, 7135-7143.

(33) Lakowicz, J.R., Ed. *Principles of Fluorescence Spectroscopy*, 3rd, ed.; Springer Science + Business Media: New York, 2006.

(34) Malekar, S. A.; Sarode, A. L.; Bach II, A. C.; Worthen, D. R. The localization of phenolic compounds in liposomal bilayers and their effects on surface characteristics and colloidal stability. *AAPS Pharm. Sci. Tech.* **2016**, *17*, 1468-1476.

(35) Wong-ekkabut, J.; Xu; Z.; Triampo W.; Tang I.-M.; Tieleman, D.P.; Monticelli, L. Effect of lipid peroxidation on the properties of lipid bilayer: a molecular dynamics study. *Biophys. J.* **2007**, *93*, 4225-4236.

(36) Nagle, J. F.; Tristam-Nagle, S. Structure of lipid bilayers. *Biochem. Biophys. Acta* **2000**, *1469*, 159-195.

(37) Martínez-Seara, H.; Róg, T. Molecular dynamics simulations of lipid bilayer: simple recipe of how to do it. In *Biomolecular Simulations: Methods and Protocols;* Monticelli, L.; Salonen, E., Eds.; Springer Science + Business Media: New York, Vol. 924, 2013, pp. 407-429.

(38) Tabony, J.; Perly, B. Quasielastic neutron scattering measureaments of fast local translational diffusion of lipid molecules in phospholipid bilayer. *Biochim. Biophys. Acta* **1990**, 1063, 67-72.

(39) Almeida, P. F. F.; Vaz, W. L. C.; Thompson, T. E. Lateral diffusion in the liquid phases of dimyristoylphosphatidylcholine/cholesterol lipid bilayers: a free volume analysis. *Biochem.* **1992**, *31*, 6739-6747.

(40) Ferreira, H.; Lúcio, M.; Lima, J.L.F.C.; Matos, C.; Reis, S. Effects of diclofenac on EPC liposome membrane properties. *Anal. Bional. Chem.* **2005**, *382*, 1256–1264.

(41) Jurkiewicz, P.; Sýkora, J.; Olzyńska, A.; Humpolíckvá, J.; Hof, M. Solvent relaxation in phospholipid bilayers: principles and recent applications. *J. Fluoresc.* **2005**, *15*, 883-894.

(42) Jurkiewicz, P.; Cwiklik, L.; Jungwirth, P.; Hof, M. Lipid hydration and mobility: an interplay between fluorescence solvent relaxation experiments and molecular dynamics simulations. *Biochimie* **2012**, *94*, 26-32.

(43) Nitschke, W. K.; Vequi-Suplicy, C.C.; Coutinho, K.; Stassen, H. Molecular dynamics investigations of prodan in DLPC bilayer. *J. Phys. Chem. B* **2012**, *116*, 2713-2721.

(44) Chen, L.; Chen, J.-L.; Zhou, G.-Q.; Wang, Y.; Wang, X.-G. Molecular dynamics simulations of the permeation of bisphenol A and pore formation in a lipid membrane. *Sci. Rep.* **2016**, *6*, 33399.

4.2.1. Información suplementaria (supplementary information)

A continuación, se detalla la información relativa al artículo original enviado para su publicación.

Supporting information for STOTEN

A holistic approach for the *in-vitro* elucidation of the bioaccumulation of organic emerging contaminants in lipid bilayers

Miquel Oliver[a], Miquel Adrover[b], Antonio Frontera[c], Joaquín Ortega-Castro[b], Manuel Miró[a*†]

[a]*FI-TRACE group, Department of Chemistry, University of the Balearic Islands, Carretera de Valldemossa km 7,5, E-07122 Palma de Mallorca, Spain.*

[b]*REACMOL group, Department of Chemistry, University of the Balearic Islands, Carretera de Valldemossa km 7,5, E-07122 Palma de Mallorca, Spain.*

[c]*SUPRAMOL group, Department of Chemistry, University of the Balearic Islands, Carretera de Valldemossa km 7,5, E-07122 Palma de Mallorca, Spain.*

11 pages

5 figures

* Corresponding authors: Manuel Miró (manuel.miro@uib.es); Miquel Adrover (miquel.adrover@uib.es); Joaquín Ortega-Castro (joaquin.castro@uib.es); Antonio Frontera (toni.frontera@uib.es)

Reagents and target species

Natural soybean L-α-phosphatidylcholine, LIPOID S100, was purchased from LIPOID Gmb (Ludwigshafen, Germany) with a concentration of L-α-phosphatidylcholine not less than 94% and a lipid tail distribution of linoleic acid (C18:2, (9Z,12Z)-octadeca-9,12-dienoic acid) as the main fatty acid, followed by palmitic acid (C16:0, n-hexadecanoic acid) and oleic acid (C18:1, cis-9-octadecenoic acid) with percentages of ca. 63, 15 and 11%, respectively. The target molecules in this work, *viz.*, triclosan (Irgasan), diclofenac sodium salt, bisphenol A and chlorpyrifos were purchased from Sigma-Aldrich/Merck KGaA (Darmstadt, Germany). The fluorescent membrane probes 6-dodecanoyl-N,N-dimethyl-2-naphthylamine (laurdan) and N,N-dimethyl-6-propionyl-2-naphthylamine (prodan) were also obtained from Sigma-Aldrich/Merck KGaA.

Synthesis of large unilamellar vesicles (LUV)

An initial phospholipid stock solution was prepared by dissolving 50 mg of soy phosphatidylcholine (PC) in chloroform. The solvent was then removed in a rotary evaporator under reduced pressure (290 mbar) and at 30 ºC during 2 h, and then followed by 2 extra hours under vacuum. Afterwards, the lipid film formed on the walls of a round bottomed flask was hydrated with PBS at final concentration of PC ~12.4 mM. The solution was then vortexed for 1 min each 5 min during 1 h to ensure the complete resuspension of the lipid in the aqueous saline medium. Then, the obtained multilamellar vesicles (MLV) were stored at 4ºC overnight for stabilization. Large unilamellar vesicles (LUV) were synthesized by extruding the milky suspension of MLV 29 times through a 100 nm pore size polycarbonate filter. The quality of the final product was evaluated by the NanoBrook 90Plus Particle Size Analyzer (Brookhaven, Holtsville, New York). The hydrodynamic diameter of the liposomes, known as Z-Average, and polydispersity index (PdI) were 129 nm and 0.076, respectively. The protocol used to synthetize LUV destined to NMR assays included some minor changes. In that case, the PBS was replaced by a 20mM phosphate buffer prepared in D_2O (pD 7.4), and the final concentration of PC was increased to 21.5 mM.

Fluorescence study of the membranotropic disturbing effects of the contaminants

Modification of the medium polarity at the surrounding of glycerol and polar group of the phospholipid bilayer of LUVs were investigated using fluorescent membrane probes (laurdan and prodan) at 37ºC for which the PC liposomes are encountered in the liquid crystalline phase.[1]

To this end, the stock solution of liposomes (12.4 mM PC) was diluted to 100 μM in PBS and stored in a brown glass vial. Then, a metered volume of laurdan or prodan from the 1 mM stock prepared in DMSO was added to the liposomal suspension at a final concentration of 1 μM and kept in darkness and at room temperature for at least 75 min for laurdan, and 10 min for prodan to obtain constant fluorescent values that indicate steady-state conditions for the fluorescent probe between the liposomal membrane and the external aqueous medium. An additional incubation time of 15 min was deemed necessary after incorporating the appropriate amount of contaminant to the liposomal mixture (final concentrations of 50, 100, 150 and 200 μM from a methanolic 50 mM stock) to reach the partition equilibrium.

Steady-state fluorescent assays were performed using a Varian Cary Eclipse fluorescence spectrometer (Agilent technologies, Mulgrave, Victoria). The solutions including the lipid suspension and the fluorescent probe at a molar ratio of 100:1 were divided in four aliquots of 1 mL in quartz cuvettes and incubated at 37 ºC in a peltier multicell holder for 5 min prior to measure. Fluorescence emission spectra were recorded from 400 to 600 nm by setting the excitation wavelength to 360 nm, and the photomultiplier detector voltage to 550 V with slit widths of 10 nm. The modification of lipid packing and ordering upon the addition of the organic contaminants was measured by the Generalized Polarization (GP) equation (Eq. 1):

$$GP = \frac{I_B - I_R}{I_B + I_R} \qquad \text{(Eq. 1)}$$

where I_B and I_R stand for the fluorescence emission intensities at 440 nm and 490 nm, respectively, corresponding to the maximum emission of the membrane probes in nonpolar media and aqueous solutions, respectively. Theoretically GP values range from -1 to +1. Negative values refer to a liquid-crystalline phase, and the gel phase, which is characterized by a more ordered and dehydrated membrane, provides positive values of GP.

Contaminant-dependent alteration of the fluidity of the membrane was also investigated by laurdan anisotropy detection using the fluorimeter polarizers. Samples were prepared as described previously. Steady state anisotropy (r_{ss}) was carried out in L-format at excitation and emission wavelengths of 350 nm and 440 nm, respectively. The photomultiplier voltage and slits were fixed to 600V and 10 nm, respectively. The r_{ss} values were obtained from the manufacturer's software using the following equation (Eq. 2):

$$r_{ss} = \frac{I_{VV} - GI_{VH}}{I_{VV} + 2GI_{VH}} \qquad \text{(Eq.2)}$$

where I_{VV} and I_{VH} stand for the fluorescence emission intensities at the vertical and the horizontal emission polarizers, respectively, with the excitation light in vertical mode. The *G* factor provided by the fluorimeter is used as a monochromator correction.

Assignment of NMR signals to PC liposomes

A solution containing soy PC (~20 mM) was prepared in 20 mM D_2O phosphate buffer at pD 7.4. PC LUV were synthesized by extrusion of a lipid film following the procedure described above. The resulting solution was supplemented with 5 mM of 4,4-dimethyl-4-silapentane-1-sulfonic acid (DSS) used as internal standard. 1D-^{1}H, 2D-^{1}H,^{1}H-NOESY (100 ms) and 2D-^{1}H,^{1}H-ROESY spectra were acquired by using a water suppression pulse sequence (Watergate pulse sequence[2]). These experiments were used to assign the observed ^{1}H-NMR signals to 1,2-dilinoleoyl-sn-glycero-3-phosphocholine (DLPC), because this is the main compound (~63%) of soy PC liposomes. Proton chemical shifts were referenced to the DSS signal at 0 ppm and 37ºC. All the spectra were acquired at 37ºC on a Bruker Avance III operating at 600 MHz and equipped with a 4mm MAS BB/^{1}H probe. All the spectra were processed and analysed by the TOPSPIN software.

NMR studies of the interaction of contaminants with PC liposomes

To map the interaction region between the PC-based LUVs and the individual contaminants, 500 µL of 20 mM PC liposomes in 20 mM D_2O phosphate buffer at pD 7.4 were titrated with different aliquots of stock solutions containing each contaminant. These were: i) a DCF solution (400 mM) prepared in 20 mM D_2O phosphate buffer at pD 7.4; ii) a TCS solution (349 mM) prepared in DMSO-d_6; iii) a BPA solution (1 M)

prepared in DMSO-d_6; and iv) a CPF solution (350 mM) prepared in DMSO-d_6. Additionally, soy PC solutions (~20 mM) prepared in 20 mM D_2O tartrate buffer at pD 4.7 were also titrated with different aliquots of a stock solution containing triclosan (1.4 M) in DMSO-d_6. The titrations involving the use of DMSO-d_6 were only carried out up to volumes of DMSO-d_6 lower than 4% of the total volume to have a negligible effect on the media surrounding the LUVs. The corresponding ^{1}H-NMR spectra were collected at each titration point. Moreover, 2D ^{1}H,^{1}H-NOESY (100 ms) and ^{1}H,^{1}H-ROESY spectra were also collected at specific titration points. The diffusion coefficients (*D*) of the mixtures containing soy PC LUVs and each contaminant were measured at the final titration point by the pulse field gradient spin echo (PGSE) using a standard ledbpgp2s experiment.[3] *D* is a good indicator of the relative molecular mobility that is dependent on the viscosity and the molecular size. All the NMR data were acquired at 37ºC on a Bruker Avance III operating at 600 MHz and equipped with a 4 mm MAS BB/^{1}H probe. All the spectra were processed and analysed by the TOPSPIN software.

Molecular dynamics studies

Molecular dynamics (MD) simulations were performed by the GROMACS 5.0.5 package and the united-atom GROMOS 53a6 force field.[4] MD calculations were conducted on a fully hydrated palmitoyl-linoleylphosphatidylcholine (C18:2/C16:0, PLPC) topology derived from Berger Lipids force fields[5] and developed by Tieleman's group.[6] The lipid bilayer includes 128 PLPC lipid molecules, which are arranged in a bilayer of 64 lipid molecules per leaflet, parallel to the x-y plane with three-dimensional periodic boundary conditions. Following the insertion of one molecule (*viz*., laurdan, prodan, chlorpyrifos, diclofenac, bisphenol A or triclosan) at the outer polar region of the lipid membrane, all systems were neutralized with the addition of Na^+, if needed, and then the unit cell was filled with SPC water model.[7] Partial charges for the laurdan, prodan, chlorpyrifos, diclofenac, bisphenol A and triclosan molecules were obtained using the restrained electrostatic fit (RESP) scheme. Electrostatic potentials were computed using the ab initio HF/6-31G(d) calculations using the Gaussian03 package.[8] All parameters of these molecules were taken from the general amber force field (GAFF)[9] using the antechamber software[10].

Each system was initially minimized using the steepest descent algorithm. The Particle Mesh Ewald (PME) summation method with a direct space cutoff of 1.2 nm, a grid spacing of 0.16 nm, and an interpolation order of 4 were used to compute long-range electrostatic interactions. A 100 ps NVT equilibration followed by a 1 ns NPT equilibration was carried out. Bond lengths and angles throughout the systems were constrained with the LINCS algorithm.[11] Finally, 200 ns production runs were performed, from which the first 40-70 ns were considered as equilibration time and discarded for data analyses. For the production runs, temperature was maintained to an average value of 310 K by using the Nose-Hoover thermostat[12,13] with a coupling time of 0.5 ps. Semi-isotropic pressure (1 bar) was maintained by using the Parrinello-Rahman barostat[14] with a coupling time of 2 ps. Trajectories were analyzed with GROMACS tools together with the scripts provided by Martinez-Seara and Róg[15], GridMAT software,[16] and VMD software package.

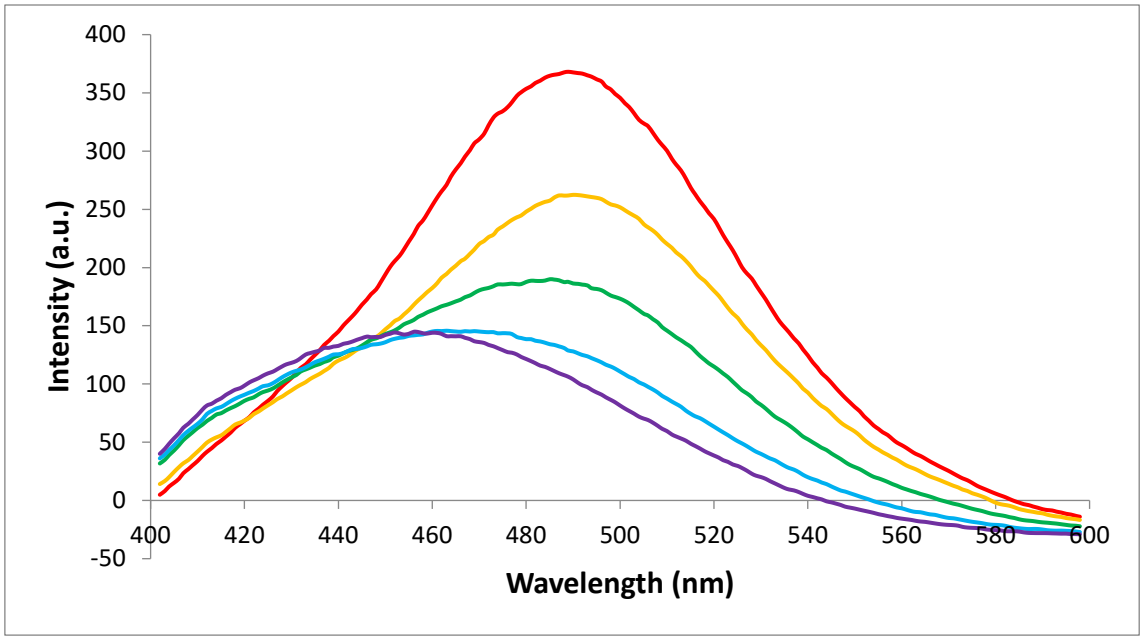

Figure S1. Fluorescence emission spectra (λ_{exc}=360 nm) at 37ºC of a solution containing 1µM laurdan and 100µM PC LUVs in the presence of 0 (*red*), 50 (*yellow*), 100 (*green*), 150 (*cyan*) and 200µM (*violet*) of triclosan.

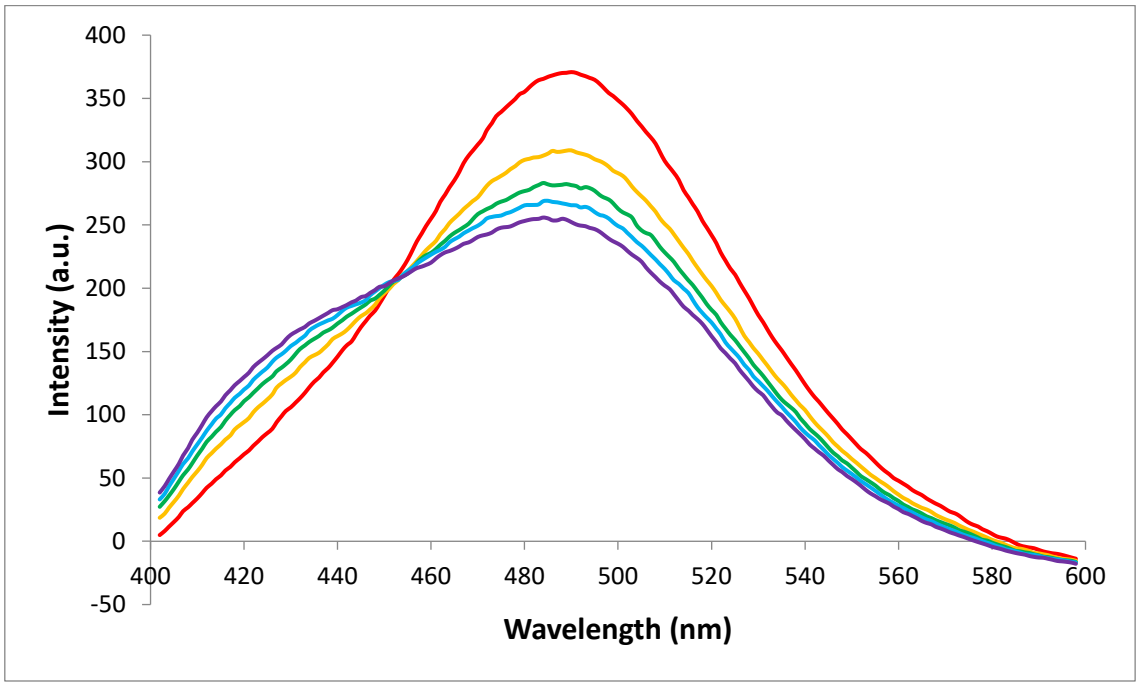

Figure S2. Fluorescence emission spectra (λ_{exc}=360 nm) at 37ºC of a solution containing 1µM laurdan and 100µM PC LVs in the presence of 0 (*red*), 50 (*yellow*), 100 (*green*), 150 (*cyan*) and 200µM (*violet*) of bisphenol A.

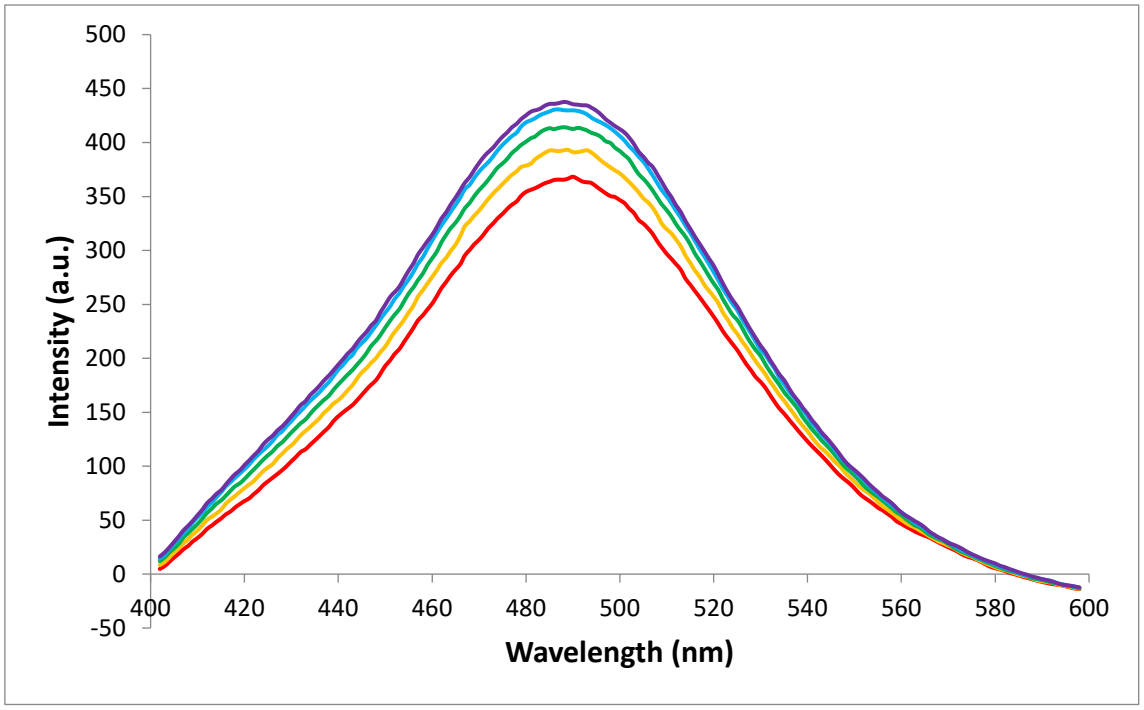

Figure S3. Fluorescence emission spectra (λ_{exc}=360 nm) at 37ºC of a solution containing 1µM laurdan and 100µM PC LUVs in the presence of 0 (*red*), 50 (*yellow*), 100 (*green*), 150 (*cyan*) and 200µM (*violet*) of diclofenac.

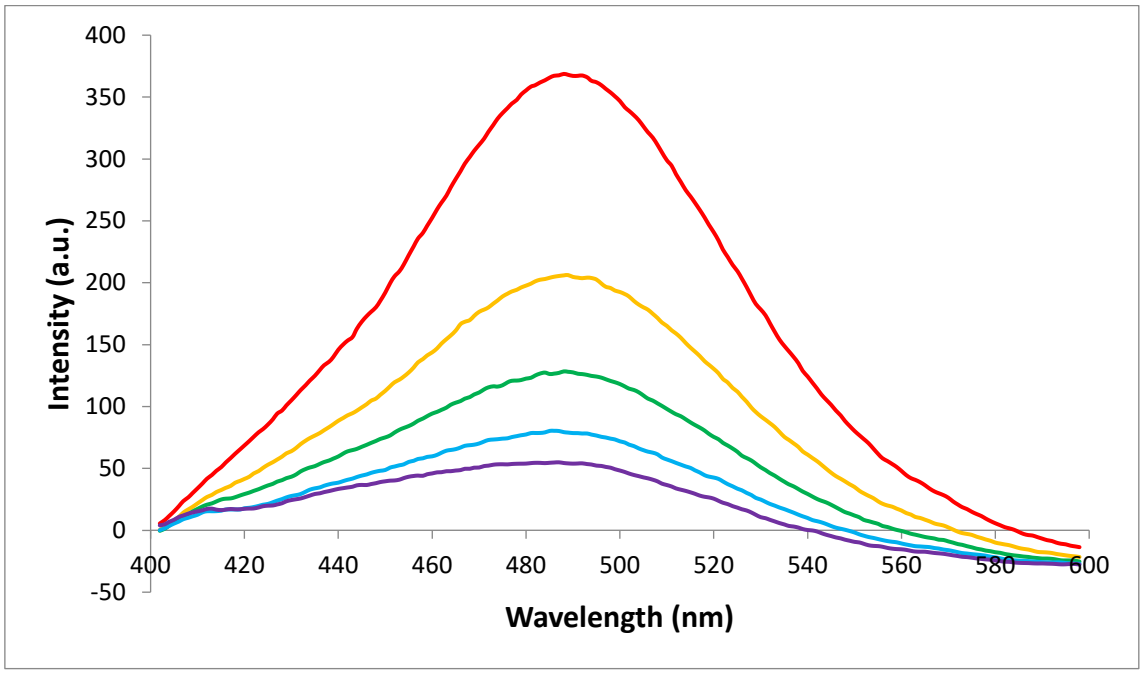

Figure S4. Fluorescence emission spectra (λ_{exc}=360 nm) at 37ºC of a solution containing 1µM laurdan and 100µM PC LUVs in the presence of 0 (*red*), 50 (*yellow*), 100 (*green*), 150 (*cyan*) and 200µM (*violet*) of chlorpyrifos.

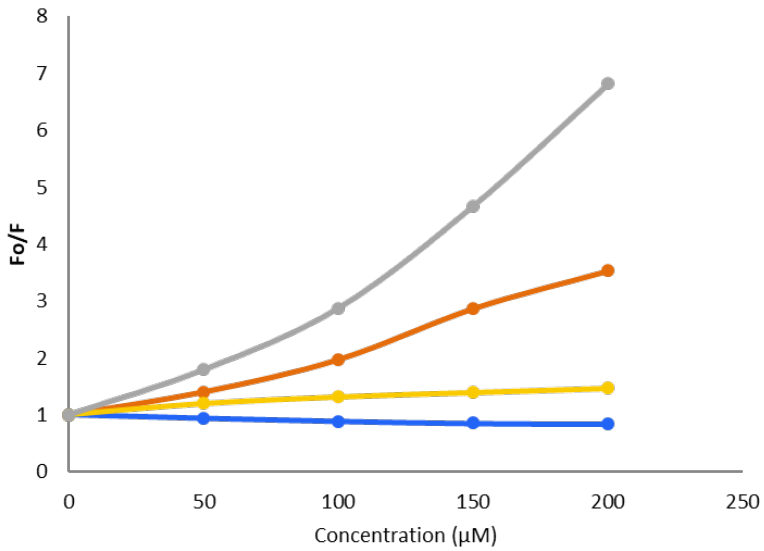

Figure S5. Stern–Volmer plots for a solution containing 100µM soy PC LUVs and 1µM of laurdan with increasing concentrations of individual contaminants (λ_{exc}=360 nm; λ_{em}=490nm). Data corresponding to TCS is shown in *blue*, that of DCF is shown in *orange*, that of BPA in *grey* and that of CPF in *yellow.* All the data was obtained at 37ºC.

REFERENCES

(1) Oliver, M.; Bauzá, A.; Frontera, A.; Miró, M. Fluorescent lipid nanoparticles as biomembrane models for exploring emerging contaminant bioavailability supported by density functional theory calculations. *Environ. Sci. Technol.* **2016**, *50*, 7135-7143.

(2) Piotto, M.; Saudek, V.; Sklenár, V. Gradient-tailored excitation for single-quantum NMR spectroscopy of aqueous solutions. *J. Biomol. NMR* **1992**, *2*, 661-666.

(3) Wu, D.; Chen, A.; Johnson Jr, C.S. An improved diffusion-ordered spectroscopy experiment incorporating bipolar-gradient pulses. *J. Magn. Reson., Ser. A* **1995**, *115*, 260-264.

(4) Oostenbrink, C.; Villa, A.; Mark, A. E.; van Gunsteren, W. F. A biomolecular force field based on the free enthalpy of hydration and solvation: the GROMOS force-field parameter sets 53A5 and 53A6. *J. Comput. Chem.* **2004**, *25*, 1656–1676.

(5) Berger, O.; Edholm, O.; Jähnig, F. Molecular dynamics simulations of a fluid bilayer of dipalmitoylphosphatidylcholine at full hydration, constant pressure, and constant temperature. *Biophys. J.* **1997**, *72*, 2002–2013.

(6) Bachar, M.; Brunelle, P.; Tieleman, D. P.; Rauk, A. Molecular dynamics simulation of a polyunsaturated lipid bilayer susceptible to lipid peroxidation. *J. Phys. Chem. B* **2004**, *108*, 7170–7179.

(7) Berendsen, H. J. C.; Postma, J. P. M.; van Gunsteren, W. F.; Hermans, J. Interaction models for water in relation to protein hydration. In: *Intermolecular Forces*; Pullman B., Ed.; Reidel Publ. Company: Dordrecht, The Netherlands, 1981, pp. 331-342.

(8) Frisch, M. J.; Trucks, G.W.; Schlegel, H. B.; Scuseria, G.E.; Robb, M. A.; Cheeseman, J. R.; Montgomery Jr, J.A.; Vreven, T.; Kudin, K.N.; Burant, J. C.; Millam, J. M.; Iyengar, S. S.; Tomasi, J.; Barone, V.; Mennucci, B.; Cossi, M.; Scalmani, G.; Rega, N.; Petersson, G.A.; Nakatsuji, H.; Hada, M.; Ehara, M.; Toyota, K.; Fukuda, R.; Hasegawa, J.; Ishida, M.; Nakajima, T.; Honda, Y.; Kitao, O.; Nakai, H.; Klene, M.; Li, X.; Knox, J. E.; Hratchian, H. P.; Cross, J. B.; Bakken, V.; Adamo, C.; Jaramillo, J.; Gomperts, R.; Stratmann, R. E.; Yazyev, O.; Austin, A. J.; Cammi, R.; Pomelli, C.; Ochterski, J. W.; Ayala, P. Y.; Morokuma, K.; Voth, G. A.; Salvador, P.; Dannenberg, J. J.; Zakrzewski, V. G.; Dapprich, S.; Daniels, A. D.; Strain, M. C.; Farkas, O.; Malick, D. K.; Rabuck, A. D.; Raghavachari, K.; Foresman, J. B.; Ortiz, J. V.; Cui, Q.; Baboul, A. G.; Clifford, S.; Cioslowski, J.; Stefanov, B. B.; Liu, G.; Liashenko, A.; Piskorz, P.; Komaromi, I.; Martin, R. L.; Fox, D. J.; Keith, T.; Al-Laham, M. A.; Peng, C. Y.; Nanayakkara, A.; Challacombe, M.; Gill, P. M. W.; Johnson, B.; Chen, W.; Wong, M. W.; Gonzalez, C.; Pople, J. A. Gaussian 03, Revision C.02. Gaussian Inc: Wallingford, UK, 2004.

(9) Wang, J.; Wolf, R. M.; Caldwell, J. W.; Kollman, P. A.; Case, D. A. Development and testing of a general AMBER force field. *J. Comput. Chem.* **2004**, *25*, 1157–1174.

(10) Wang, J.; Wang, W.; Kollman, P. A.; Case, D. A. Automatic atom type and bond type perception in molecular mechanical calculations. *J. Mol. Graph. Model* **2006**, *25*, 247–260.

(11) Hess, B.; Bekker, H.; Berendsen, H. J.; Fraaije, J. G. LINCS: a linear constraint solver for molecular simulations. *J. Comput. Chem*. **1997**, 18, 1463–1472.

(12) Nosé, S. A molecular dynamics method for simulations in the canonical ensemble. *Mol. Phys.* **1984**, *52*, 255–268.

(13) Hoover, W.G. Canonical dynamics: equilibrium phase-space distributions. *Phys. Rev. A* **1985**, *31*, 1695–1697.

(14) Parrinello, M.; Rahman, A. Polymorphic transitions in single crystals: A new molecular dynamics method. *J. Appl. Phys.* **1981**, *52*, 7182-7190.

(15) Martínez-Seara, H.; Róg, T. Molecular dynamics simulations of lipid bilayer: simple recipe of how to do it. In *Biomolecular Simulations: Methods and Protocols;* Monticelli, L.; Salonen, E., Eds.; Springer Science + Business Media: New York, Vol. 924, 2013, pp. 407-429.

(16) Allen, W.J.; Lemkul, J.A.; Bevan, D.R. GridMAT-MD: A grid-based membrane analysis tool for use with molecular dynamics. *J. Comput. Chem.* **2009**, *30*, 1952-1958.

Capítulo 5. Estudios Membranotrópicos de Fluorescencia Empleando un Método Fluídico Inteligente

5.1. Resumen

En este trabajo, se propone un sistema completamente automatizado para evaluar posibles mecanismos de interacción de xenobióticos con las membranas celulares, los llamados efectos membranotrópicos, utilizando liposomas y sondas fluorescentes de membrana. El método fluídico inteligente presenta la adquisición en tiempo real de lecturas de fluorescencia, procesamiento de datos y retroalimentación de forma no supervisada. Como prueba de la aplicabilidad del concepto, se investigó el comportamiento de los liposomas sintetizados con distintas concentraciones de colesterol y la acción potencialmente tóxica del bisfenol A y el diclofenaco como modelo de contaminantes emergentes, en un formato de flujo continuo. El método resultó tener una excelente precisión y reveló que el diclofenaco afecta muy levemente al orden e hidratación de la bicapa lipídica, independientemente de la concentración de colesterol, ya que interacciona a un nivel superficial de la membrana; mientras que el efecto membranotrópico del bisfenol A fue más pronunciado a niveles bajos de colesterol ya que el aumento de ese esterol provoca una disminución de la permeabilidad de la membrana.

5.2. Artículo original

A continuación, se adjunta el artículo original “In quest of effect directed analysis at the smart laboratory: Automated system for flow-through evaluation of membranotropic effects of emerging contaminants” de Miquel Oliver, Marc Roca-Jiménez, Manuel Miró, y David J. Cocovi-Solberg, enviado el 19 de septiembre de 2019 para su publicación en *Talanta*.

Talanta 209 (2020) 120600

Contents lists available at ScienceDirect

Talanta

journal homepage: www.elsevier.com/locate/talanta

In quest of effect directed analysis in the smart laboratory: Automated system for flow-through evaluation of membranotropic effects of emerging contaminants

Miquel Oliver[a], Marc Roca-Jiménez[a], Manuel Miró[a,**], David J. Cocovi-Solberg[b,*]

[a] FI-TRACE Group, Department of Chemistry, University of the Balearic Islands, Carretera de Valldemossa, Km 7.5, E-07122, Palma de Mallorca, Spain
[b] University of Natural Resources and Life Sciences, Muthgasse 18, Vienna, Austria

ARTICLE INFO

Keywords:
Exposomics
Emerging contaminants
Membrane effects
Smart system
Fluidics

ABSTRACT

The rate-determining step of the human exposome workflow is the acquisition of physiologically relevant data (e.g., effect directed analysis), which can be performed retrospectively or with ad hoc experiments. In this contribution, an automated system is proposed for evaluating potential interaction mechanisms of xenobiotics across cell membranes, the so-called membranotropic effects, using liposomes as a mimicry of biological membranes, and fluorescent membrane probes. The smart fluidic method features real-time acquisition of fluorescence readouts, data processing and feedback in a fully unsupervised mode. As a proof of concept applicability, the behavior of newly synthesized cholesterol-laden biomimetic liposomes, and the *in-vitro* potential toxicant action of bisphenol A and diclofenac as model of emerging contaminants on cell membrane surrogates were investigated in a flow-through format. Unattended operation resulted in excellent intermediate precision (< 1.5%) and unveiled that diclofenac affected the liposomal bilayer order very slightly, regardless of the cholesterol concentration, because it accumulates at a superficial level, while the membranotropic effect of bisphenol A was more pronounced at low concentration levels of cholesterol because at increased levels, the membrane reduces its permeability.

1. Introduction

Exposome evaluation determines or fingerprints the overall chemical composition of complex samples to which humans are exposed by resorting to a plethora of analytical techniques that yield huge amounts of data in a holistic format under increasingly unattended workflows [1,2]. The other side of the exposomic coin, that is, the biological assays applied to fractionated complex samples still remains a cumbersome task that is normally carried out manually [3]. Because of current regulations that pose concerns and limitations of the experimentation with living beings [4], the number of assays encompassing superior animals is minimized in favor of cell or surrogates testing, which constitute a unique opportunity for developing miniaturized and automatic methods due to the ease of manipulation of cellular entities by e.g. flow approaches. In this context, toxicologic effects that aim for the cell membrane as the biological target can be studied *in-vitro* using artificial membrane surrogates, such as liposomes [5,6], that is, nanovesicles with chemical composition and structure that mimics the phospholipid bilayer of eukaryotic living cells. While liposomes are easily synthesized with pure phospholipids, such as phosphatidylcholine, the variation of the precursor composition with the introduction of different phospholipid classes extracted from biological sources [7–9], surfactants or other additives can tune the physicochemical properties of the liposomes and endow them with varied flexibility, permeability, surface charge or affinity to different tissues to name a few. For example, human cells can contain up to 40% in weight of cholesterol, which changes or controls the order and fluidity of the membrane, thus altering the morphology, lipid packing and permeability of the bilayer [10]. Among the different analytical techniques for studying the effects of selected xenobiotics or mixtures in the liposomal membrane, fluorometric measurements using polarity-sensitive membrane probes constitute a gold standard methodology that benefits of low-cost, slight invasiveness and simplicity. The fluorescent membrane probe used in this work, Laurdan, is a hydrophobic molecule with a lauryl chain and naphthalene fluorescent moiety that locates at the level of the glycerol backbone of the lipid bilayer [11]. The emission spectrum of Laurdan exhibits a continuous red shift from 440 to 490 nm when changing from a hydrophobic (e.g., lipid phase) to polar medium due to the so-called

* Corresponding author.
** Corresponding author.
E-mail addresses: manuel.miro@uib.es (M. Miró), david.cocovi-solberg@boku.ac.at (D.J. Cocovi-Solberg).

https://doi.org/10.1016/j.talanta.2019.120600
Received 19 September 2019; Received in revised form 22 November 2019; Accepted 28 November 2019
Available online 29 November 2019
0039-9140/

dipolar relaxation phenomenon. The reorientation of solvent's dipoles in the surrounding of the probe requires energy and hence, decreasing the energy of Laurdan's excited state. The higher the number of molecules of water (or another polar molecule) around the probe, the higher the red shift of the emission spectrum of the fluorescent dye. To quantify this shift, the so-called generalized polarization (GP) [12] is often exploited (Eq. (1)):

$$GP = \frac{I_B - I_R}{I_B + I_R} \quad (1)$$

Where I_B and I_R are the fluorescence emission intensities at the blue and red spectral components of the emission spectrum respectively, that is, at 440 nm and 490 nm. The returned value is related to the lipid order and packing, hydration and fluidity, and thus depends on the membrane phase state; when the membrane is composed of well packed phospholipids, GP values are positive, contrariwise, if the membrane is disordered and hydrated, GP becomes negative [13].

In GP assays, the fluorescent membrane probe is incubated with the liposomes until a constant emission spectrum is obtained. Then, the xenobiotic is added to the mixture, and again the analyst waits until the fluorescence spectrum stabilizes. The spectrum shift, and the ΔGP values calculated from the emission intensities obtained after and before the addition of the target compound account for membranotropic effects. The time required for the probe to stabilize varies greatly with the composition of the liposomes, the target species to be studied and the temperature, and thus, experimental conditions must be optimized whenever a single parameter of the batch analysis is altered. Some combinations of factors may yield incubation times of more than a working day but setting extreme long incubation delays compromises the sample throughput since other combinations may stabilize very fast. To the best of our knowledge the GP assays have until now being always developed in a supervised batch format, even if the procedure is simple and does not resort to biological entities. This manual operation jeopardizes the required throughput in the exposomics field.

Among the various techniques available for automating those analysis, fluidic methods, that is, those which resort to the pressure driven manipulation of liquids in closed manifolds through the use of pumps and valves are very appealing candidates to automate the GP measurements [14,15] because of the simple components required, and the possibility of assembling dedicated manifolds. Those systems usually work in a mechanized regime: computer-controlled pumps and valves manipulate the fluids in a reproducible way for every sample without analyst intervention. A performance enhancement is achieved through the use of the so called 'automated methods' according to IUPAC definition, where the computer does not only control the mechanical part of the system, but also receives an analytical feedback allowing it to take decisions at real time.

In this contribution, we present a fluidic system capable of developing GP tests for investigation of membranotropic effects in an unattended manner by resorting to a smart method of data processing and treatment. The smart system provides continuous feedback and thus, this should be regarded as a unique example of liposome-based *automated* system. As a proof of concept, our fluidic automated system has been applied to liposomes containing different cholesterol levels aiming at simulating varied membrane cells, using Laurdan as a fluorescent probe, and the plastic additive bisphenol A and the nonsteroidal anti-inflammatory drug (NSAID) diclofenac as models of potentially emerging contaminants, the latter included in the First EU Watch list of emerging water pollutants.

2. Experimental

2.1. Reagents

Natural soybean L-α-phosphatidylcholine (PC), LIPOID S100, was purchased from LIPOID GmbH (Ludwigshafen, Germany) with a concentration of L-α-phosphatidylcholine not less than 94% and a lipid tail distribution of linoleic acid (C18:2, (9Z, 12Z)-octadeca-9,12-dienoic acid) as the main fatty acid, followed by palmitic acid (C16:0, n-hexadecanoic acid) and oleic acid (C18:1, cis-9-octadecenoic acid) with percentages of ca. 63, 15 and 11%, respectively. Cholesterol and the target xenobiotics in this work, *viz.*, diclofenac sodium salt (DCF), and bisphenol A (BPA) were purchased from Sigma-Aldrich/Merck KGaA (Darmstadt, Germany). The fluorescent membrane probe 6-dodecanoyl-N,N-dimethyl-2-naphthylamine (Laurdan) was also obtained from Sigma-Aldrich/Merck KGaA.

Stock solutions of pollutants, BPA and DCF, were prepared in methanol at a final concentration of 50 mM. The fluorescent probe Laurdan, 1 mM, was prepared in DMSO and cholesterol was dissolved in chloroform to a final stock solution of 12 mM.

The phosphate-buffered saline (PBS) 10X was prepared by dissolving 1.2 g of potassium phosphate monobasic, 7.2 g of disodium phosphate, 40 g of sodium chloride and 1 g of potassium chloride in 500 mL of water. Working solution (PBS 1X, pH 7.4) was prepared by a 10-fold dilution of the stock solution in water.

2.2. Synthesis of liposomes

Liposomes were prepared by lipid film hydration [16] followed by extrusion for unilamellar liposome formation [17]. To this end, 50 mg of soybean phosphatidylcholine (PC, LIPOID S100, average molecular weight of 787 g/mol) was dissolved in chloroform in a round bottom flask without or with cholesterol. Chloroform was then removed in a rotary evaporator under low pressure (290 mbar) and 30 °C for 2 h followed by vacuum pumping at room temperature for at least 2 h to obtain a uniform dried lipid film on the flask bottom wall without any organic solvent traces. Next, the lipid was hydrated with a given volume of PBS (pH 7.4) at room temperature to afford a fixed lipid concentration of 12.7 mM for PC, while that of cholesterol was 10, 20 or 30% mol of cholesterol per mol of PC. The solution was then vortexed for 1 h (1 min every 5 min) to obtain multilamellar vesicles (MLVs). The milky suspension was stored at 4 °C overnight for stabilization. Later, large unilamellar vesicles (LUVs) were obtained by extruding the MLVs solution 29 times through a 100 nm pore size polycarbonate filter [18]. Liposomal quality was evaluated by dynamic light scattering (DLS) using Zetasizer Nano ZS90 (Malvern Panalytical, Malvern, UK). The hydrodynamic diameter (Z-Average) was in all cases about 130 nm and Polydispersity Index (PdI) no more than 0.08.

While other procedures have been described for incorporating of the fluorescent probes during the synthesis of liposomes [19–21], the herein described procedure was chosen because of the simplicity for mixing of the liposomes and Laurdan. In fact, when the combination of more than one kind of liposome, as is the case in this work, and more than one probe must be evaluated, our fluidic system does necessitate a smaller number of ports of the selection valve (see the fluidic system section below).

2.3. Fluidic system

The fluidic system and components thereof are depicted in Fig. 1. It consists of a bi-directional Cavro XCalibur (Männedorf, Switzerland) syringe pump furnished with a 50 μL-syringe (Hamilton, Bonaduz, Switzerland) and a 3-position ceramic stream selector, a 14-port C25Z-31814EMH Cheminert stream selector (VICI AG International, Schenkon, Switzerland) and a Minipuls 3 bidirectional peristaltic pump (Gilson Incorporated, Middleton, USA) furnished with 1.3 mm i. d. Tygon tube. The mixing chamber is a glass barrel from a Ruthe syringe of 5 mL covered with aluminum foil for preventing the photodegradation of the labile fluorescent probe. The flow-through fluorimeter used as a detector is a Jasco FP-4025, configured to excite at 360 nm and monitor the emission at 440 nm and 490 nm simultaneously using the double wavelength mode. Data acquisition was carried out using a

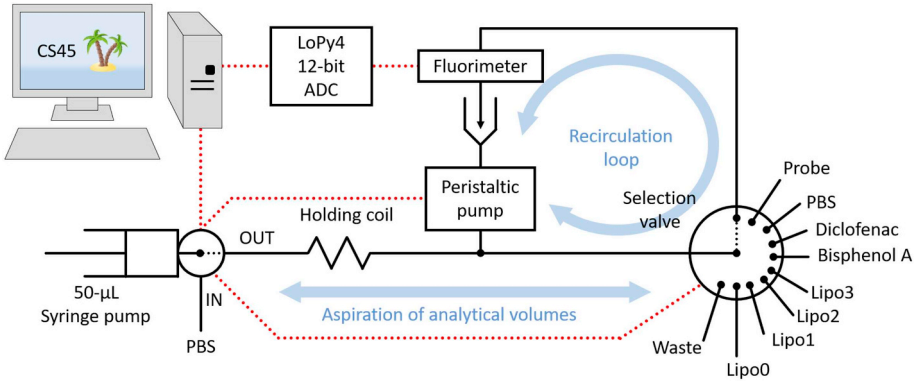

Fig. 1. Schematic depiction of the fully automated flow system for in-vitro investigation of the effect of emerging contaminants on membrane surrogates. Lipo0-3 stands for liposomes with 0, 10, 20 and 30% mol of cholesterol per mol of PC.

Taylor made 12-bit ADC converter with USB data transmission based on the Lopy4 chip (Pycom, London, UK). The internal reference voltage for the ADC is not calibrated from the factory and may vary with e.g. temperature changes. For this reason, a two-point calibration was implemented in the firmware based on the measurement of regulated voltage dividers and executed before every biochemical measurement. Additional information on the wiring, as well as the firmware can be found in the ESI and Fig. S1. All the tubing was 1/16″ o. d., 1/32″ i. d. fluorinated ethylene propylene (FEP) (IDEX Health and Science, Lake forest, Illinois, USA), except the tubes that connected the VICI stream selector to the reagents reservoir, that were 1/64" i. d. to minimize void volumes. The total volume of the recirculation loop was 1000 µL including the tube of the peristaltic pump, tube from the peristaltic pump to the valve, valve rotor, tube towards the fluorimeter, flow-through cell and tube towards the mixing chamber. The syringe pump and the stream selector were controlled in a multipoint RS232 bus (the selector in simplex), while the contact closure outputs of the syringe pump were used to control the activation/stop as well as the flow direction of the peristaltic pump. The flow-rate of the syringe pump was set to 50 µL/min in all analytical cycles, and to 600 µL/min for priming. The flow-rate of the peristaltic pump was fixed to 1750 µL/min, and thus, the volume aspirated or dispensed is proportional to the time the pump is activated. The ambient temperature was set to 23 °C throughout in order to minimize variations in GP values through batches of experiments.

A smart automated method was executed through the CocoSoft 4.5 freeware [22] for (i) controlling the entire fluidic instrumentation, (ii) acquiring and processing the bioanalytical data at real time and (iii) ultimately to modify the execution according to the data processing results, as described in the next section. Fig. 2 shows the CocoSoft window in experimental runtime. The instrumental method is running in the right hand of the screen, while emission at 440 and 490 nm are acquired through the Lopy4 adapter and plotted at real time in the top left of the screen. The GP value is calculated and appears in the bottom left part of the screen. In this window, x axis units are the number of measurements, that will be converted *a posteriori* to minutes.

2.4. Fundamentals of the automated flow method

The working principle of the proposed smart fluidic system is to prepare *in-situ* an appropriate composite solution of liposomes with Laurdan in PBS buffer into the mixing chamber. To this end, large volumes of PBS (ca. 2.5 mL) will be aspirated by the peristaltic pump from the multiposition valve. Reagents that are needed in much smaller amounts, such as the liposomes (20 µL), probe (2.54 µL) and xenobiotic (2.54 µL) are added at given times by the syringe pump because of its enhanced resolution (16 nL/step) by aspirating the required amount of a given solution or target species towards the holding coil, dispensing it to the mixing chamber via the flow-cell by reversed flow, and activating the peristaltic pump for mixing the composite liposome/probe/xenobiotic plug with PBS and homogenizing the mixture by the recirculation in the fluorimeter loop. The fluorescence signal is captured by CocoSoft 4.5 at regular times through the Lopy4 adapter and the GP is then calculated and stored at real time. Then, two time-windows are defined, and the average GP is calculated in each window: the first one was the average GP [from now to now-x minutes], and the second one [from now-x minutes to now-2x minutes]. Fig. 3 illustrates a graphical explanation of this algorithm.

If the absolute difference of both GP time-averaged values is smaller than a preset tolerance the GP is deemed constant, which indicates that the probe is stabilized within the lipid bilayer, and thus, the circulation is halted. At this time and without the analyst intervention, the syringe pump adds a minute volume of xenobiotic (viz., 2.54 µL) to the mixture of Laurdan and PC liposomes and the monitoring procedure is resumed unsupervised. In case that the absolute difference is higher than the tolerance, the circulation continues because this indicates that the GP value has varied significantly during the last two time-windows (2x minutes) and thus the probe is not yet stabilized into the lipid structure (Fig. 2). At the end of this protocol, the steady GP values, before and after the xenobiotic addition, are exported and the whole procedure is repeated with the next combination of liposomes, probe and xenobiotic after a cleaning program. Any combination of factors can be programed at will, and the 14-port count of the VICI selector allows the variation of several parameters through the biochemical assay without human intervention.

The length of the time windows and the tolerance allowed for the comparison of average GP values were optimized for a high-performance method with minimum dead time and no type II errors in the identification of steady state conditions of the incubation mixture.

The CocoSoft method is available in the SI, including the detailed control program, with description of flow-rates and volumes, as well as the real-time GP calculations of the smart system.

2.5. Study of the cholesterol influence in lipid membrane packing

To demonstrate the unattended capabilities of the designed fluidic system, the effect of modifying experimental conditions by addition of cholesterol to the LUVs was undertaken. Liposomes were synthesized according to the above described procedure. However, their composition was modified with 0, 10, 20 and 30% mol of cholesterol per mol of PC. In the automatic system, 20 µL of modified liposomes (12.7 mM PC) were diluted in 2.47 mL of PBS buffer (final concentration of 100 µM PC), incubated with 2.54 µL of Laurdan stock (final concentration of 1 µM) and the GP values were recorded and reported continuously by the smart method. The differences of GP values across different cholesterol concentrations will be related to the effects of

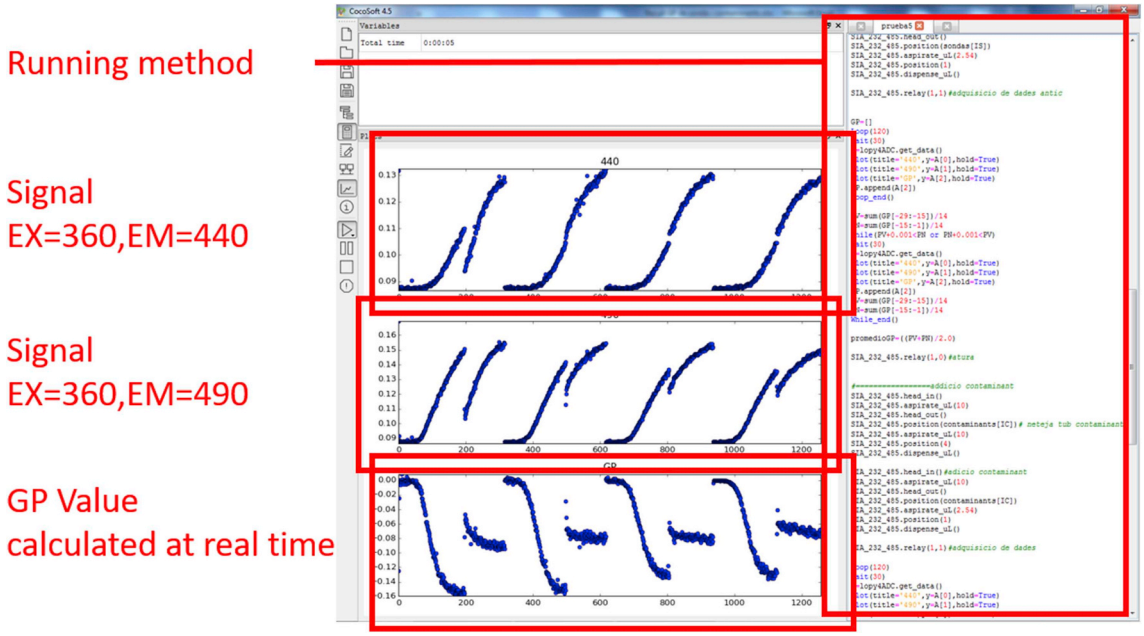

Fig. 2. Screenshot of CocoSoft program during unsupervised system execution. The fluidic method is executed in the right column of the screen, the 440 and 490 nm emission intensities are acquired at real time and the GP value is calculated in-situ as seen at the left side of the image.

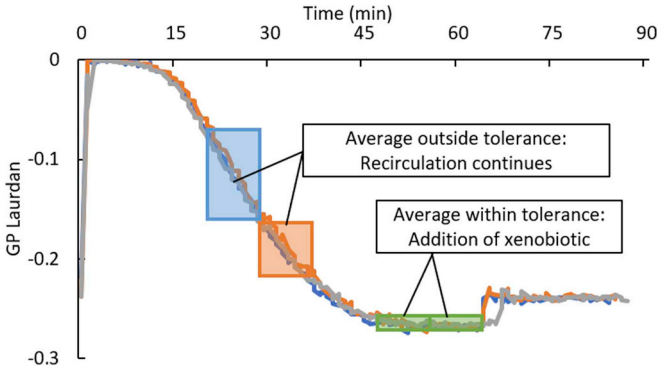

Fig. 3. Overlap of three consecutive replicates of the same mixture of Laurdan-laden liposomes and diclofenac. After stabilization of the liposomes and the Laurdan probe for 65 min, diclofenac is added. GP increased steeply, and the smart method identify steady-state regime after ca. 20 min.

cholesterol on the membrane packing, hydration of the bilayer and lipid ordering, and ultimately, on the facility of the xenobiotic to penetrate across the lipidic vesicle. After the GP reached a constant level, the fluidic system was automatically flushed by discarding the content of the recirculation loop through the waste port and cleaned 5 times with 1.3 mL of PBS buffer for 1 min. All this procedure was carried out in quadruplicate for every cholesterol level.

2.6. Study of membranotropic effects of selected xenobiotics

In a fully automatic mode, 20 μL of the synthesized liposomes with varying concentrations of cholesterol (0–30% mol of cholesterol per mol of PC) were diluted into 2.47 mL of PBS buffer (final concentration 100 μM PC) and incubated with 2.54 μL of Laurdan (final concentration 1 μM). When the smart method identified a steady GP value, a 2.54 μL aliquot of bisphenol A or diclofenac stock solution was added to a final concentration in the mixture of 50 μM, and the GP monitored again until reaching the next constant value. The used concentrations are in the same range as those reported elsewhere [23–27] for this kind of assays, as a tradeoff between sensitivity and representativity of expected concentrations. The GP variation before and after addition of the xenobiotic was calculated by subtraction, and this value along with the individual GPs and the entire temporal profiles for kinetic exploration were exported in a .txt file as plain text. The fluidic system was finally flushed and rinsed according to the same procedure described in the previous section. All experiments were carried out in quadruplicate (programmed by the user-friendly software).

For comparing the absolute value of GP obtained by the proposed method with the standard manual methodology, this last one was also applied [12], and the values obtained were compared with a *t*-test. In brief, in the manual method, the same proportion between buffer, probe, liposomes and contaminants was maintained, but carried out in a semimicro quartz cuvette format with a benchtop fluorescence spectrophotometer (Cary Eclipse, Varian). 992 μL of buffer were mixed in the cuvette with 8 μL of liposomes and 1 μL of Laurdan probe and incubated for 1 h protected from ambient light. Then, the cuvette was inserted in the spectrofluorimeter, the temperature was stabilized for 10 min to 23 °C, and the emission spectrum was acquired at excitation = 360 nm, 10 nm/s, with PMT voltage = 600 V, both slits set to 10 nm and the cuvette facing the excitation source with the 4 mm side, and the 10 mm side facing the detector system. 1.0 μL of contaminant were added, and emission spectra were acquired every minute until they were constant. This required in average ca. 15 min, which is in good agreement with the online obtained data.

3. Results and discussion

3.1. Investigation of the crucial parameters of the smart method

Data acquisition rate, tolerance and length of time windows are key parameters for the method to perform properly. Data acquisition rate was set to 30 s and maintained throughout the remaining study. Higher time resolution was not necessary because of the hour-scale of these incubation-based assays. Tolerance was set to 0.001 for being this the maximum resolution of the fluorimeter. Decreasing this number had no physical sense, and increasing it only boosted the false detection of stability (type II error), unless unpractically high time windows are to set. The time window length should be as minimum as possible yet preventing false stability detection. The time window was increased from the minimum value (equal to the data acquisition rate) and

increased in 1-min intervals between trial and error experiments. This value was finally set to 7.5 min because this was the minimum value that did not afford false negatives. Smaller values detected stability prematurely because the noise associated to the signal was not effectively dampened with the averaging procedure. Fig. 3 shows the overlap of 3 consecutive replicates of the assay with liposomes (0% cholesterol), probe (Laurdan) and xenobiotic (diclofenac) along with the fundamental principles of the smart algorithm.

It should be considered that the human analyst also requires some time after the stabilization in order to detect steady-state regime, so as can be seen in Fig. 3, the smart algorithm detects the stabilization of the incubating probe and LUV mixture approximately at a similar time than the human analyst would have needed. The time per assay is about 15 min longer than that explicitly required for the incubating mixture (Fig. 3) to stabilize in best case for tests involving a single GP measurement (as in the case of liposome/probe characterization), and 30 min for tests requiring two GP measurements (effect of xenobiotics), yet all the steps of the assays are performed fully unattended and the experimental results are *in-situ* obtained. It should be stressed that the incubation time of the probe with liposomes is *a priori* unknown and thus, in the supervised counterpart, the analyst must either monitor the fluorometric data continuously or at least at a given time, probably every 5–10 min, and this period must be summed to the time required for detecting the steady state.

As per Eq. (1), the GP range is [-1,1], making the Coefficient of Variation unsuitable for assessing repeatability and intermediate precision of measurements. Instead, the following dispersion statistics (Eq. (2)) was used for every quadruplicates of a given assay:

$$Dispersion = \frac{\max(x) - \min(x)}{dynamic\ range} = \frac{range\ (x)}{(1-(-1))} = \frac{1}{2} range(x) \quad (2)$$

The relative dispersion parameter was in all cases < 1.5% for up to 28 different assays in different days (each one in quadruplicate), showing the excellent precision of the designed smart method algorithm that allowed the unattended performance over weekend of up to 8 different membranotropic tests (each one quadruplicated).

In order to compare not only the time required for detecting the stabilization of the signals before and after addition of the xenobiotic, but also the absolute value obtained by the flow method, a *t*-test of comparison of means was performed between the ΔGP obtained by the herein proposed smart setup, and that of the standard manual method in order to assess the trueness of the proposed method [12]. The obtained p value of 0.060 ($p > 0.05$, $N = 3$) indicates that the results obtained with the proposed method do not differ statistically from those of the manual counterpart and thus, the fluidic setup does not introduce a significant bias onto the biochemical assays.

3.2. Influence of the cholesterol concentration on lipid ordering

As seen in Fig. 4 the higher the concentration of cholesterol up to 30% mol of cholesterol per mol of PC in LUVs the greater is the GP value recorded. It is known that the role of cholesterol in a hydrated and disordered lipid membrane is to enhance the lipid order by disturbing the mobility of the phospholipid's tails [28]. Our results agree with previous results in the literature because soy PC liposomes have a transition temperature from gel to liquid-crystalline phase lower than 0 °C [11] due to the high concentration of 18:2 fatty acids, thereby soy PC liposomes are at room temperature encountered in a highly fluid state. In fact, the degree of unsaturation of lipids affect the stiffening effect of cholesterol [29]. Phospholipids containing two unsaturated hydrocarbon chains, as is the case with natural PC, compared to one or none, are expected to cause a weakening effect of cholesterol on the membrane bending modulus [30,31]. The increase of the GP values caused by the addition of cholesterol (see Fig. 4) implies a decrease of the membrane phase polarity that could be explained by the extrusion

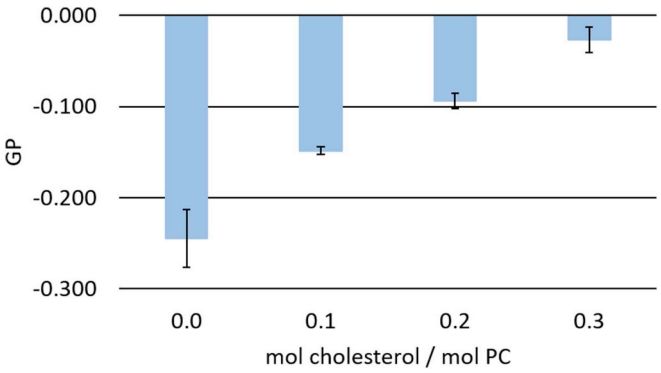

Fig. 4. Laurdan generalized polarization at increasing concentrations of cholesterol up to 30% mol of cholesterol per mol of PC.

of water outward the liposomal bilayer due to the interaction of cholesterol with the unsaturated phospholipid tails [32].

3.3. Membranotropic effects of diclofenac

The addition of the NSAID diclofenac into the liposomal solution caused a small yet significant ΔGP towards more positive values, thus implying a slight increase of lipid order (See Fig. 5). Similar results were obtained regardless of the concentration of cholesterol, from ΔGP = 0.028 for 0% cholesterol to ΔGP = 0.024 for 30% mol of cholesterol per mol of PC, thus indicating that the sterol did not disturb the effect of diclofenac over the membrane (Table 1). At pH 7.4, diclofenac molecules are mostly ionized ($pK_a = 3.97$) and thus the anti-inflammatory drug would at physiological pH interact preferably with the polar head of the phospholipids on the surface of the liposomal membrane [33], which would explain the low disturbing effect at the level of glycerol group where the Laurdan fluorophore is predominantly located. This hypothesis is in accordance with other studies of molecules whose polarity is pH dependent [34]. Nevertheless, the lack of any enthalpic contribution seen by Manrique-Moreno and coworkers suggests that there might not be strong electrostatic interactions between diclofenac and the choline group of PC, and that the interaction process might be mediated by only entropic processes at the lipid/water interface [35]. Similar results were obtained by Fernandes et al. [36] supporting the entropic rather than electrostatic effects.

3.4. Membranotropic effects of bisphenol A

The effect of BPA on the liposomal membrane polarity was very acute (See Fig. 6, Table 1), increasing the value of ΔGP more than two times

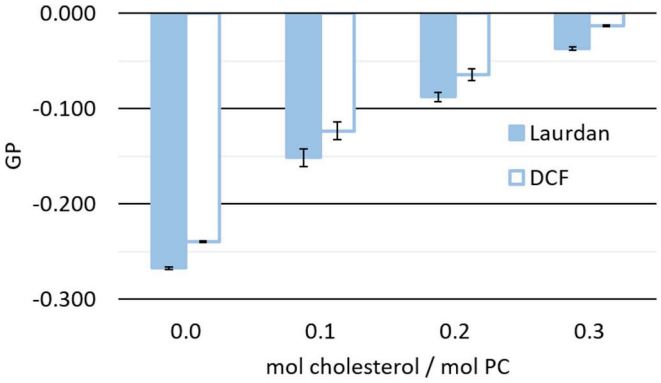

Fig. 5. Laurdan generalized polarization values at increasing concentrations of cholesterol (mol of cholesterol per mol of PC) in soy PC liposomes (blue bars) with the addition of DCF at the 50 μM level (white bars). Error bars stand for standard deviation (n = 4).

Table 1
Increment of GP values for Diclofenac and Bisphenol A for different concentrations of cholesterol.

Mol cholesterol per mol of PC (%)	Diclofenac	Bisphenol A
0	0.028	0.115
10	0.028	0.066
20	0.023	0.074
30	0.024	0.052

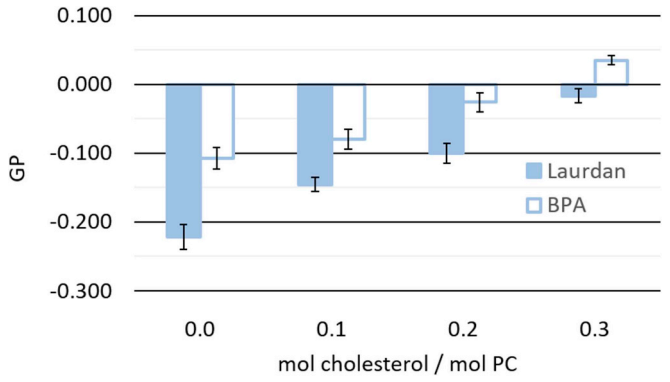

Fig. 6. Laurdan generalized polarization at increasing concentrations of cholesterol (mol of cholesterol per mol PC) in soy PC liposomes (blue bars) with the addition of BPA at the 50 μM level (white bars). Error bars stand for standard deviation (n = 4).

compared to that of DCF ($\Delta GP_{BPA}/\Delta GP_{DCF}$ = 4.12 for 0% cholesterol and 2.17 for 30% mol of cholesterol per mol of PC) and thus, causing a high impact on the order of the phospholipids. The difference observed for the GP values of the Laurdan in Figs. 5 and 6 in the absence of contaminant but with different concentrations of cholesterol is attributed to the small temperature changes in the laboratory environment. Nevertheless, a paired *t*-test of the Laurdan GP values in the various sets of experiments unveils no significant differences ($p = 0.052 > 0.05$).

The presence of cholesterol at increasing concentrations lessened the effect of this pollutant on the liposomal bilayer as indicated by the decrease of ΔGP. This phenomenon could be a consequence of the change of the liposome-water partition coefficient. A highly ordered membrane promoted by cholesterol onto the saturated acyl chains is less permeable to compounds due to the high degree of packing [37] and consequently, minimal interspaces between phospholipids do exist. Thermal data, NMR studies [38], and molecular dynamics simulations [39] agree with this observation and suggested that the preferable location of BPA is close to the lipid head group at the vicinity of the glycerol region wherein Laurdan is located. This fact would explain the strong effect on the medium polarity at the hydrophobic-hydrophilic interface, and thus onto Laurdan's emission fluorescence, caused by BPA, which dehydrates the liposomal bilayer. In fact, BPA is expected to be orientated in such a way that the hydroxyl moieties are directed towards the phosphate group forming hydrogen bonds while the main body of BPA is immersed into the PC tails.

4. Conclusions

This paper reports the first fully automated fluidic system that allows the unattended investigation of membranotropic effects of emerging contaminants on liposomes as membrane surrogates. The flow setup features a high degree of intermediate precision (< 1.5%) as a result of the smart algorithm implemented in CocoSoft 4.5 user-friendly freeware. Its performance has been exemplified by characterizing the membrane packing of natural PC liposomes with varying amounts of cholesterol, and investigation of the interaction of liposomes with two model examples of emerging water contaminants.

Declaration of competing interest

None.

Acknowledgements

Manuel Miró, Miquel Oliver and David J. Cocovi-Solberg acknowledge financial support from the Spanish Ministry of Science, Innovation and Universities (MCIU) and the Spanish State Research Agency (AEI) through projects CTM2017-84763-C3-3-R (MCIU/AEI/FEDER, EU) and CTM2017-90890-REDT (MCIU/AEI/FEDER, EU). David J. Cocovi-Solberg acknowledges also the Austrian Science Fund (FWF) for the economic support through the Lise-Meitner stipendium M02579.

Appendix A. Supplementary data

Supplementary data to this article can be found online at https://doi.org/10.1016/j.talanta.2019.120600.

References

[1] M. Vrijheid, The exposome: a new paradigm to study the impact of environment on health, Thorax 69 (2014) 876–878, https://doi.org/10.1136/thoraxjnl-2013-204949.
[2] C.P. Wild, Complementing the genome with an "exposome": the outstanding challenge of environmental exposure measurement in molecular epidemiology, Cancer Epidemiol. Biomark. Prev. 14 (2005) 1847–1850, https://doi.org/10.1158/1055-9965.EPI-05-0456.
[3] W. Brack, Effect-directed analysis: a promising tool for the identification of organic toxicants in complex mixtures? Anal. Bioanal. Chem. 377 (2003) 397–407, https://doi.org/10.1007/s00216-003-2139-z.
[4] G. Schoeters, The REACH perspective: toward a new concept of toxicity testing, J. Toxicol. Environ. Heal. B Crit. Rev. 13 (2010) 232–241, https://doi.org/10.1080/10937404.2010.483938.
[5] S. Ong, H. Liu, C. Pidgeon, Immobilized-artificial-membrane chromatography: measurements of membrane partition coefficient and predicting drug membrane permeability, J. Chromatogr., A 728 (1996) 113–128.
[6] S. Lin, X. Yang, H. Liu, Development of liposome/water partition coefficients predictive models for neutral and ionogenic organic chemicals, Ecotoxicol. Environ. Saf. 179 (2019) 40–49, https://doi.org/10.1016/J.ECOENV.2019.04.036.
[7] A.A. Khan, M. Jabeen, A.A. Khan, M. Owais, Anticancer efficacy of a novel propofol–linoleic acid-loaded escheriosomal formulation against murine hepatocellular carcinoma, Nanomedicine 8 (2013) 1281–1294, https://doi.org/10.2217/nnm.12.166.
[8] S.-K. Ruokonen, F. Duša, A.H. Rantamäki, A. Robciuc, P. Holma, J.M. Holopainen, M. Abdel-Rehim, S.K. Wiedmer, Distribution of local anesthetics between aqueous and liposome phases, J. Chromatogr., A 1479 (2017) 194–203, https://doi.org/10.1016/J.CHROMA.2016.12.005.
[9] Y.-C. Kuo, H.-C. Wu, D. Hoang, W.E. Bentley, W.D. D'Souza, S.R. Raghavan, Colloidal properties of nanoerythrosomes derived from bovine red blood cells, Langmuir 32 (2016) 171–179, https://doi.org/10.1021/acs.langmuir.5b03014.
[10] S.-T. Yang, A.J.B. Kreutzberger, J. Lee, V. Kiessling, L.K. Tamm, The role of cholesterol in membrane fusion, Chem. Phys. Lipids 199 (2016) 136–143, https://doi.org/10.1016/j.chemphyslip.2016.05.003.
[11] M. Oliver, A. Bauzá, A. Frontera, M. Miró, Fluorescent lipid nanoparticles as biomembrane models for exploring emerging contaminant bioavailability supported by density functional theory calculations, Environ. Sci. Technol. 50 (2016) 7135–7143, https://doi.org/10.1021/acs.est.6b00772.
[12] T. Parasassi, G. De Stasio, G. Ravagnan, R.M. Rusch, E. Gratton, Quantitation of lipid phases in phospholipid vesicles by the generalized polarization of Laurdan fluorescence, Biophys. J. 60 (1991) 179–189, https://doi.org/10.1016/S0006-3495(91)82041-0.
[13] T. Parasassi, F. Conti, E. Gratton, Time-resolved fluorescence emission spectra of Laurdan in phospholipid vesicles by multifrequency phase and modulation fluorometry, Cell. Mol. Biol. 32 (1986) 103–108.
[14] M. Trojanowicz, K. Kołacińska, Recent advances in flow injection analysis, Analyst 141 (2016) 2085–2139, https://doi.org/10.1039/c5an02522b.
[15] M. Trojanowicz, Advances in Flow Analysis, Wiley, 2008.
[16] A.D. Bangham, J. De Gier, G.D. Greville, Osmotic properties and water permeability of phospholipid liquid crystals, Chem. Phys. Lipids 1 (1967) 225–246, https://doi.org/10.1016/0009-3084(67)90030-8.
[17] M.J. Hope, M.B. Bally, G. Webb, P.R. Cullis, Production of large unilamellar vesicles by a rapid extrusion procedure. Characterization of size distribution, trapped volume and ability to maintain a membrane potential, Biochim. Biophys. Acta Biomembr. 812 (1985) 55–65, https://doi.org/10.1016/0005-2736(85)90521-8.
[18] M. Li, C. Du, N. Guo, Y. Teng, X. Meng, H. Sun, S. Li, P. Yu, H. Galons, Composition design and medical application of liposomes, Eur. J. Med. Chem. 164 (2019) 640–653, https://doi.org/10.1016/J.EJMECH.2019.01.007.
[19] D. Bonarska-Kujawa, H. Pruchnik, H. Kleszczyńska, Interaction of selected

anthocyanins with erythrocytes and liposome membranes, Cell. Mol. Biol. Lett. 17 (2012) 289–308, https://doi.org/10.2478/s11658-012-0010-y.
[20] G. Först, L. Cwiklik, P. Jurkiewicz, R. Schubert, M. Hof, Interactions of beta-blockers with model lipid membranes: molecular view of the interaction of acebutolol, oxprenolol, and propranolol with phosphatidylcholine vesicles by time-dependent fluorescence shift and molecular dynamics simulations, Eur. J. Pharm. Biopharm. 87 (2014) 559–569, https://doi.org/10.1016/J.EJPB.2014.03.013.
[21] C. Pereira-Leite, C. Nunes, J.L.F.C. Lima, S. Reis, M. Lúcio, Interaction of celecoxib with membranes: the role of membrane biophysics on its therapeutic and toxic effects, J. Phys. Chem. B 116 (2012) 13608–13617, https://doi.org/10.1021/jp304037v.
[22] D.J. Cocovi-Solberg, M. Miró, CocoSoft: educational software for automation in the analytical chemistry laboratory, Anal. Bioanal. Chem. 407 (2015) 6227–6233, https://doi.org/10.1007/s00216-015-8834-8.
[23] O. Wesołowska, M. Kużdżał, J. Štrancar, K. Michalak, Interaction of the chemopreventive agent resveratrol and its metabolite, piceatannol, with model membranes, Biochim. Biophys. Acta Biomembr. 1788 (2009) 1851–1860, https://doi.org/10.1016/j.bbamem.2009.06.005.
[24] K. Cieślik-Boczula, R.M. Petrus, G. Köhler, T. Lis, A. Koll, Interaction of piperidin derivative of mannich base with DPPC liposomes, J. Phys. Chem. B 117 (2013) 2938–2946, https://doi.org/10.1021/jp311825h.
[25] A.R. Neves, C. Nunes, S. Reis, New insights on the biophysical interaction of resveratrol with biomembrane models: relevance for its biological effects, J. Phys. Chem. B 119 (2015) 11664–11672, https://doi.org/10.1021/acs.jpcb.5b05419.
[26] M. Suwalsky, M. Benites, F. Villena, F. Aguilar, C.P. Sotomayor, The organochlorine pesticide heptachlor disrupts the structure of model and cell membranes, Biochim. Biophys. Acta Biomembr. 1326 (1997) 115–123, https://doi.org/10.1016/S0005-2736(97)00019-9.
[27] M. Suwalsky, M. Manrique, F. Villena, C.P. Sotomayor, Phospholipid bilayers as molecular models for drug-cell membrane interactions, The Case of the Antiinflamatory Drug Diclofenac, Macromol. Symp. 296 (2010) 436–445, https://doi.org/10.1002/masy.201051059.
[28] A.A. Jovanović, B.D. Balanč, A. Ota, P.A. Grabnar, V.B. Djordjević, K.P. Šavikin, B.M. Bugarski, V.A. Nedović, N.P. Ulrih, Comparative effects of cholesterol and β-sitosterol on the liposome membrane characteristics, Eur. J. Lipid Sci. Technol. 120 (2018) 1800039, https://doi.org/10.1002/ejlt.201800039.
[29] W. Zhang, M.L. Coughlin, J.M. Metzger, B.J. Hackel, F.S. Bates, T.P. Lodge, Influence of cholesterol and bilayer curvature on the interaction of PPO–PEO block copolymers with liposomes, Langmuir 35 (2019) 7231–7241, https://doi.org/10.1021/acs.langmuir.9b00572.
[30] J. Pan, T.T. Mills, S. Tristram-Nagle, J.F. Nagle, Cholesterol perturbs lipid bilayers nonuniversally, Phys. Rev. Lett. 100 (2008) 198103, https://doi.org/10.1103/PhysRevLett.100.198103.
[31] D. Bochicchio, L. Monticelli, The membrane bending modulus in experiments and simulations: a puzzling picture, Adv. Biomembr. Lipid Self-Assembly. 23 (2016) 117–143, https://doi.org/10.1016/BS.ABL.2016.01.003.
[32] H.A. Pérez, A. Disalvo, M. de los Á Frías, Effect of cholesterol on the surface polarity and hydration of lipid interphases as measured by Laurdan fluorescence: new insights, Colloids Surfaces B Biointerfaces 178 (2019) 346–351, https://doi.org/10.1016/J.COLSURFB.2019.03.022.
[33] H. Ferreira, M. Lúcio, J.L.F.C. Lima, C. Matos, S. Reis, Effects of diclofenac on EPC liposome membrane properties, Anal. Bioanal. Chem. 382 (2005) 1256–1264, https://doi.org/10.1007/s00216-005-3251-z.
[34] M. Di Foggia, S. Bonora, A. Tinti, V. Tugnoli, DSC and Raman study of DMPC liposomes in presence of ibuprofen at different pH, J. Therm. Anal. Calorim. 127 (2017) 1407–1417, https://doi.org/10.1007/s10973-016-5408-8.
[35] M. Manrique-Moreno, P. Garidel, M. Suwalsky, J. Howe, K. Brandenburg, The membrane-activity of ibuprofen, diclofenac, and naproxen: a physico-chemical study with lecithin phospholipids, Biochim. Biophys. Acta Biomembr. 1788 (2009) 1296–1303, https://doi.org/10.1016/J.BBAMEM.2009.01.016.
[36] E. Fernandes, T. Soares, H. Gonçalves, S. Bernstorff, M.R. Oliveira, C. Lopes, M. Lúcio, A molecular biophysical approach to diclofenac topical gastrointestinal damage, Int. J. Mol. Sci. 19 (2018) 3411, https://doi.org/10.3390/ijms19113411.
[37] H. Yamamoto, H.M. Liljestrand, Partitioning of Selected Estrogenic Compounds between Synthetic Membrane Vesicles and Water: Effects of Lipid Components, Environ. Sci. Technol. 38 (4) (2004) 1139–1147.
[38] S.A. Malekar, A.L. Sarode, A.C. Bach, D.R. Worthen, The localization of phenolic compounds in liposomal bilayers and their effects on surface characteristics and colloidal stability, AAPS PharmSciTech 17 (2016) 1468–1476, https://doi.org/10.1208/s12249-016-0483-5.
[39] L. Chen, J. Chen, G. Zhou, Y. Wang, C. Xu, X. Wang, Molecular dynamics simulations of the permeation of bisphenol A and pore formation in a lipid membrane, Sci. Rep. 6 (2016) 33399, https://doi.org/10.1038/srep33399.

5.2.1. Información suplementaria (supplementary information)

A continuación, se detalla la información relativa al artículo original enviado para su publicación.

Electronic Supplementary Information

In quest of effect directed analysis at the smart lab: Automated system for flow-through evaluation of membranotropic effects of emerging contaminants

Miquel Oliver[a], Marc Roca-Jimenez[a], Manuel Miró*[a], David J. Cocovi-Solberg*[a]

[a]*FI-TRACE group, Department of Chemistry, University of the Balearic Islands, Carretera de Valldemossa, km 7.5, E-07122 Palma de Mallorca, Spain*

**Corresponding author.*

Email addresses: dj.cocovi.solberg@gmail.com (David J. Cocovi-Solberg), manuel.miro@uib.es (Manuel Miró)

DJCS present address: University of Natural Resources and Life Sciences, Muthgasse 18, 1190 Vienna, Austria.

9 pages

1 Smart method

1 Firmware of the taylor made ADC

1 Image: connection of the ADC

Detailed description of the automated workflow: Smart Cocosoft algorithm

```
#Initialization and set of reagent related variables

liposomes=[6] #positions of all liposomes to be tested

probes=[8] #positions of all probes to be tested

xenobiotics=[10,11] #position of all xenobiotics to be tested

name_xenobiotics=['BPA','DCF'] #name of the xenobiotics of each position. For the reporting

replicates=4#number of replicates for each combination of liposome, probe, xenobiotic

SIA_232_485.initialize()

SIA_232_485.set_flowrate_uL_min(600)


#Fill holding coil

Loop(5)

SIA_232_485.head_in() #syringe pump

SIA_232_485.fill()

SIA_232_485.head_out() #syringe pump

SIA_232_485.position(4) #Waste (in selection valve)

SIA_232_485.empty()

Loop_end()

# Aspirating PBS (Conditioning step)

SIA_232_485.position(3) #aspirate PBS (in selection valve)

SIA_232_485.relay(2,1) #Peristaltic pump (PP) clockwise

SIA_232_485.relay(1,1) #PP turns on
```

```
Wait(60)

SIA_232_485.relay(1,0) #PP stops

SIA_232_485.relay(2,0) #PP counterclockwise

#Autozero

SIA_232_485.position(1) #towards mixing chamber

SIA_232_485.relay(1,1) #PP turns on

Wait('autozero') ) #Wait until the analyst activates the autozero button of the fluorimeter

SIA_232_485.relay(1,0) #PP stops

#emptying and rinsing of the system

SIA_232_485.position(4) #Waste

SIA_232_485.relay(1,1) #PP turns on

Wait(90)

SIA_232_485.relay(1,0) #PP stops

SIA_232_485.set_flowrate_uL_min(50)


#this section provies the loop over all possible combinations of liposomes, probes and xenobiotics

IL=-1 #will keep track of the current liposome

Loop(len(liposomes)) #the method will be repeated for any liposome

IL+=1 #IL is initialized

IP=-1#will keep track of the current probe

Loop(len(probes)) #the method will be repeated for any probe

IP+=1 #IP is initialized
```

```
IX=-1 #will keep track of the current xenobiotic

Loop(len(xenobiotics)) #the method will be repeated for any xenobiotic

IX+=1 #IX is initialized


#START REPLICATES

Loop(replicates) #replicates for every combination

SIA_232_485.position(3) #Aspirate PBS

SIA_232_485.relay(2,1) #PP clockwise

SIA_232_485.relay(1,1) #PP turns on

Wait(87)

SIA_232_485.relay(1,0) #PP turns off

SIA_232_485.relay(2,0) #PP counterclockwise


#Addition of liposomes and probe

SIA_232_485.head_in() #syringe pump

SIA_232_485.aspirate_uL(10)#Aspirates PBS

SIA_232_485.head_out() #syringe pump

SIA_232_485.position(liposomes[IL]) #cleaning of liposomes tube

SIA_232_485.aspirate_uL(10)

SIA_232_485.position(4) #Waste

SIA_232_485.empty()


#addition liposomes
```

```
SIA_232_485.head_in() #Sets head valve to IN position

SIA_232_485.aspirate_uL(10) # Aspirates PBS

SIA_232_485.head_out() #syringe pump

SIA_232_485.position(liposomes[IL]) #cleaning of liposomes tube

SIA_232_485.aspirate_uL(20)

SIA_232_485.position(1)  #towards mixing chamber

SIA_232_485.empty()


SIA_232_485.position(1)  #towards mixing chamber

SIA_232_485.relay(1,1) #PP turns on

Wait(300)

SIA_232_485.relay(1,0) #PP turns off


SIA_232_485.head_in()

SIA_232_485.aspirate_uL(10) #Aspirates PBS

SIA_232_485.head_out()

SIA_232_485.position(sondas[IP]) #cleaning the probe tube

SIA_232_485.aspirate_uL(10)

SIA_232_485.position(4) #Waste

SIA_232_485.empty()


#addition probe

SIA_232_485.head_in()
```

```
SIA_232_485.aspirate_uL(10)#Aspirates PBS

SIA_232_485.head_out()

SIA_232_485.position(probes[IP])

SIA_232_485.aspirate_uL(2.54)

SIA_232_485.position(1) #towards mixing chamber

SIA_232_485.empty()

SIA_232_485.relay(1,1) #PP turns on


#Data acquisition

GP=[]

Loop(60) #Initially will take 60 points, every 30 seconds

Wait(30) #take a point every 30 seconds

A=lopy4ADC.get_data()#Acquire point

Plot(title='440',y=A[0],hold=True) #Plot fluorescence and GP

Plot(title='490',y=A[1],hold=True)

Plot(title='GP',y=A[2],hold=True)

GP.append(A[2]) #Adds the corrent GP value to the log

Loop_end()


OA=sum(GP[-29:-15])/14#Old average(average in old time window)

NA=sum(GP[-15:-1])/14#New average(average in new time window)

While(OA+0.001<NA or NA+0.001<OA) #If the difference is higher than the
tolerance, the recirculation continues
```

```
Wait(30)

A=lopy4ADC.get_data()

Plot(title='440',y=A[0],hold=True)

Plot(title='490',y=A[1],hold=True)

Plot(title='GP',y=A[2],hold=True)

GP.append(A[2])

OA=sum(GP[-29:-15])/14

NA=sum(GP[-15:-1])/14

While_end()#otherwise the pump stops and xenobiotic is added


averageGP=((OA+NA)/2.0)


SIA_232_485.relay(1,0) #PP turns off


#contaminant addition

SIA_232_485.head_in()

SIA_232_485.aspirate_uL(10) #PBS

SIA_232_485.head_out()

SIA_232_485.position(xenobiotics[IX]) #cleaning of contaminant tube

SIA_232_485.aspirate_uL(10)

SIA_232_485.position(4) #Waste

SIA_232_485.empty()
```

```
SIA_232_485.head_in()

SIA_232_485.aspirate_uL(10) #PBS

SIA_232_485.head_out()

SIA_232_485.position(xenobiotics[IX])

SIA_232_485.aspirate_uL(2.54)

SIA_232_485.position(1) #towards mixing chamber

SIA_232_485.empty()


SIA_232_485.relay(1,1) #PP turns on


#Data acquisition

Loop(60)

Wait(30)

A=lopy4ADC.get_data()

Plot(title='440',y=A[0],hold=True)

Plot(title='490',y=A[1],hold=True)

Plot(title='GP',y=A[2],hold=True)

GP.append(A[2])

Loop_end()


OA=sum(GP[-29:-15])/14

NA=sum(GP[-15:-1])/14

While(OA+0.001<NA or NA+0.001<OA)
```

```
Wait(30)

A=lopy4ADC.get_data()

Plot(title='440',y=A[0],hold=True)

Plot(title='490',y=A[1],hold=True)

Plot(title='GP',y=A[2],hold=True)

GP.append(A[2])

OA=sum(GP[-29:-15])/14

NA=sum(GP[-15:-1])/14

While_end()


#Exporting experimental GP data to .txt file as plain text

tempdata=open('Valors.txt','a')

tempdata.write(name_xenobiotics[IC]+',\t'+str(averageGP).replace('.',',')+'\t'+str((OA+NA)/2.0).replace('.',',')+'\r')

tempdata.close()


#Save the whole curve

tempdata=open('Curves.txt','a')

tempdata.write(str(GP).replace(', ','\t').replace('.',',').replace('[','').replace(']','')+'\r')

tempdata.close()


SIA_232_485.relay(1,0) #PP turns off
```

```
#Emptying the flow system

SIA_232_485.position(4) #Waste

SIA_232_485.relay(1,1) #PP turns on

Wait(110)

SIA_232_485.relay(1,0) #PP turns off


#Cleaning the flow system

Loop(5)


SIA_232_485.position(3) #Aspirates PBS

SIA_232_485.relay(2,1) #PP clockwise

SIA_232_485.relay(1,1) #PP turns on

Wait(45)

SIA_232_485.relay(1,0) #PP turns off

SIA_232_485.relay(2,0) #PP counterclockwise


#recirculation

SIA_232_485.position(1)  #towards mixing chamber

SIA_232_485.relay(1,1) #PP turns on

Wait(60)

SIA_232_485.relay(1,0) #PP turns off


#emptying
```

```
SIA_232_485.position(4)  #Waste

SIA_232_485.relay(1,1) #PP turns on

Wait(60)

SIA_232_485.relay(1,0) #PP turns off

Loop_end()

Loop_end()

Loop_end()

Loop_end()

Loop_end()

#End of method
```

LoPy4 firmware

```
import pycom #Imports required libraries
import time
import machine


pycom.heartbeat(False) #Deactivates the default blue flicker
while True:
    pycom.rgbled(0xFF0000)  # Turn on red led
    time.sleep(0.05) # The ADC stabilizes
    meanADC3=0 #Variable is initiated
    adc = machine.ADC(0)
    adcread = adc.channel(attn=0, pin='P16') #ADC channel is selected (1 point of the calibration)
    for i in range(1024):
        meanADC3+=adcread()#1024 measures are added
    meanADC3/=1024#and averaged
    meanADC3/=4096#and normalized to the ADC resolution


    pycom.rgbled(0xFF0000)  # Red
    time.sleep(0.05)
    meanADC4=0
    adc = machine.ADC(0)
    adcread = adc.channel(attn=0, pin='P15') #ADC channel is set (second point of the calibration)
```

```
    for i in range(1024):
        meanADC4+=adcread()
    meanADC4/=1024
    meanADC4/=4096


    pycom.rgbled(0x00FF00)  # Green
    time.sleep(0.05)
    meanADC1=0
    adc = machine.ADC(0)
    adcread = adc.channel(attn=0, pin='P17') #ADC channel is set (first fluorometric measurement)
    for i in range(1024):
        meanADC1+=adcread()
    meanADC1/=1024
    meanADC1/=4096
    meanADC1=(0.692-0.233)/(meanADC4-meanADC3)*(meanADC1-meanADC3)+0.233 #first fluorescence value is interpolated in the calibration


    pycom.rgbled(0x0000FF)  # Blue
    time.sleep(0.05)
    meanADC2=0
    adc = machine.ADC(0)
    adcread = adc.channel(attn=0, pin='P18') #ADC channel is set (second fluorometric measurement)
```

```
    for i in range(1024):
        meanADC2+=adcread()
    meanADC2/=1024
    meanADC2/=4096
    meanADC2=(0.692-0.233)/(meanADC4-meanADC3)*(meanADC2-
meanADC3)+0.233 #second fluorescence value is interpolated in the calibration


    print('F'+str(meanADC1)+'G'+str(meanADC2)) #The two fluorescence readings are
send through RS232
```

LoPy4

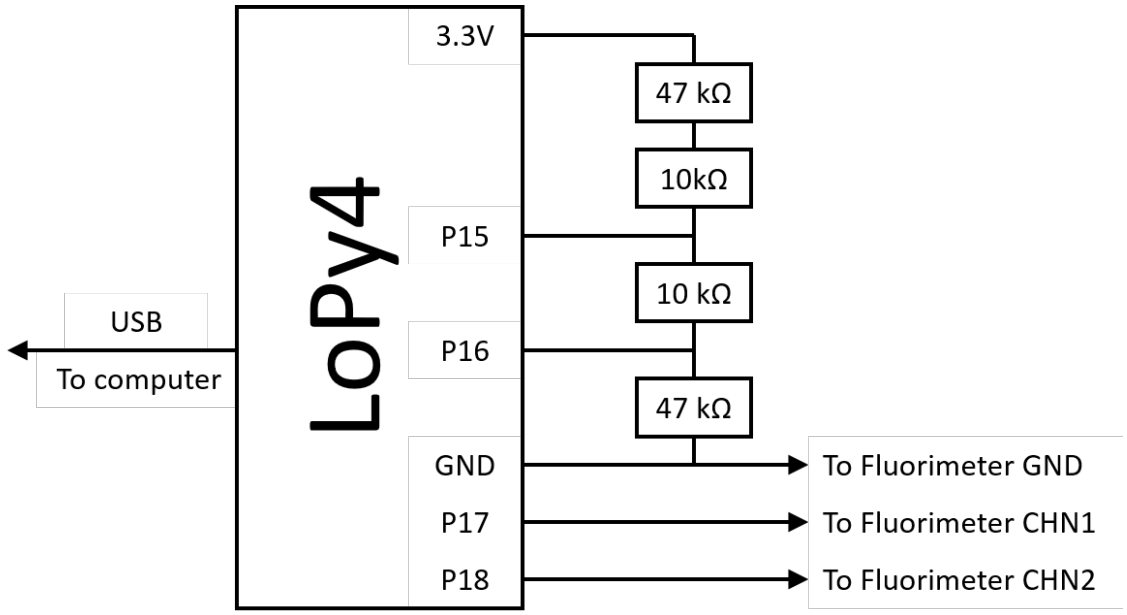

Figure SI1. Connection of the LoPy4 for calibration and temperature compensation for fluorimetric data acquisition

Capítulo 6. Estudios Membranotrópicos de Fluorescencia y su Correlación con Ensayos de Ecotoxicidad y Citotoxicidad

6.1. Resumen

En la actualidad, se carece de información relativa al impacto toxicológico recíproco de algunos compuestos químicos que se encuentran formando mezclas binarias o más complejas. En este trabajo, se ha estudiado el impacto del butilparabeno, metilparabeno y diclofenaco en el comportamiento toxicológico y propiedades del triclosán (a diferentes niveles de concentración) por medio de diversos bioensayos ecotoxicológicos como Microtox, XenoScreen YES/YAS y citotóxicos en Caco-2 y HEPG2, y sistemas liposómicos. Los estudios analíticos y biológicos se realizaron mediante dos metodologías de modelización: adición de concentración (CA) y acción independiente (IA), y tres niveles de concentración diferentes de cada uno de los compuestos estudiados. Se demostró que la actividad de triclosán a elevadas concentraciones fue afectada en presencia de pequeñas cantidades de metilparabeno y butilparabeno en la prueba Microtox. De la misma forma, el diclofenaco influye en la actividad de triclosán cuando este se encuentra en concentraciones bajas (utilizando el modelo CA). Las propiedades agonísticas estrogénicas de triclosán fueron influidas por los dos parabenos estudiados de una forma antagonista. Se comprobó que la actividad antagonista estrogénica de triclosán estaba afectada ligeramente por los parabenos y diclofenaco en las mezclas binarias, causando efectos antagonistas y sobreestimación. Las células HepG2 mostraron ser las más resistentes a los efectos tóxicos de las mezclas a las concentraciones estudiadas y no se detectó ninguna prueba significativa de sinergia o antagonismos con el ensayo MTT. Los ensayos liposómicos en las mezclas binarias siguieron las mismas tendencias obtenidas que el ensayo MTT con células Caco-2, confirmando la validez del modelo *in vitro* empleado en este estudio. Dado que los estudios de toxicidad de mezclas de contaminantes emergentes son escasos, este estudio representa una clave importante en confirmar la utilidad y versatilidad de la modelización de contaminantes emergentes en toxicología medioambiental.

6.2. Artículo original

A continuación, se adjunta el artículo original “Ecotoxicological equilibria of triclosan in Microtox, XenoScreen YES/YAS, Caco2, HEPG2 and liposomal systems are affected by the occurrence of other pharmaceutical and personal care emerging contaminants”de Miquel Oliver, Błażej Kudłak, Monika Wieczerzak, Salette Reis, Sofia Lima, Marcela Segundo, y Manuel Miró, enviado el 4 de septiembre de 2019 para su publicación en *Science of the Total Environment*.

Elsevier Editorial System(tm) for Science of the Total Environment

Manuscript Draft

Manuscript Number: STOTEN-D-19-13573R1

Title: Ecotoxicological equilibria of triclosan in Microtox, XenoScreen YES/YAS, Caco2, HEPG2 and liposomal systems are affected by the occurrence of other pharmaceutical and personal care emerging contaminants

Article Type: Research Paper

Keywords: triclosan toxicity; parabens; diclofenac; endocrine potential; genotoxicity; liposomes

Corresponding Author: Dr. Błażej Kudłak, Ph.D. Eng.

Corresponding Author's Institution: Gdańsk University of Technology

First Author: Błażej Kudłak, Ph.D. Eng.

Order of Authors: Błażej Kudłak, Ph.D. Eng.; Miquel Oliver; Monika Wieczerzak; Salette Reis; Sofia A Lima; Marcela A Segundo; Manuel Miro

Abstract: Contaminants of emerging concern may be considered as any chemicals or factors whose unintended continuous release and persistence in the environment may lead to any observable undesirable response of living beings. Still not much is known on reciprocal toxicological impact of given chemicals when present in binary or more complex mixtures. In this work, an attempt was thus undertaken to study the impact of butylparaben, methylparaben and diclofenac on toxicological behavior and properties of triclosan (at varying concentration levels) with respect to Microtox, XenoScreen YES/YAS, Caco-2, HEPG2, and liposomal systems. Having performed analytical and biological studies modelling was done using two modelling approaches, viz., concentration addition (CA) and independent action (IA) at three concentration levels of each chemical studied. The effect of the highest concentration of triclosan studied was impacted by even small amounts of methylparaben and butylparaben in Microtox while diclofenac preferably affected triclosan activity at its lowest concentration level (with CA model). Estrogenic agonistic properties of triclosan were severely impacted by both parabens in an antagonistic way; diclofenac showed in all cases underestimation or synergy at the lowest triclosan concentration studied. Estrogenic antagonistic activity of triclosan was also slightly affected by parabens and by diclofenac in binary mixtures, showing overestimation and antagonist effects. HepG2 cells appeared to be the most resistant to the toxic effect of the mixtures at the concentrations tested and no significant proof of synergy or antagonism could be detected with the MTT assay. The liposome assays on the mixtures followed the same trends obtained with the MTT assay with Caco-2 cells, confirming the validity of the in vitro model used in this research. As studies on emerging contaminants mixtures toxicity are still scarce, research presented here constitute an important part in confirming utility and versatility of emerging contaminants modelling in environmental toxicology.

Ecotoxicological equilibria of triclosan in Microtox, XenoScreen YES/YAS, Caco2, HEPG2 and liposomal systems are affected by the occurrence of other pharmaceutical and personal care emerging contaminants

Miquel Oliver [1], Błażej Kudłak[2*], Monika Wieczerzak[2], Salette Reis[3], Sofia Lima[3], Marcela Segundo[3], Manuel Miro[1]

[1] FI-TRACE group, Department of Chemistry, University of the Balearic Islands, Carretera de Valldemossa km 7,5, E-07122 Palma de Mallorca, Illes Balears, Spain

[2] Department of Analytical Chemistry, Faculty of Chemistry, Gdańsk University of Technology, 11/12 Narutowicza Str., Gdańsk 80-233, Poland

[3] LAQV, REQUIMTE, Department of Chemistry, Faculty of Pharmacy, University of Porto, R Jorge Viterbo Ferreira, 228, 4050-313 Porto, Portugal

**Corresponding Author: blakudla@pg.edu.pl, ORCID 0000-0002-2237-2927*

Abstract

Contaminants of emerging concern may be considered as any chemicals or factors whose unintended continuous release and persistence in the environment may lead to any observable undesirable response of living beings. Still not much is known on reciprocal toxicological impact of given chemicals when present in binary or more complex mixtures. In this work, an attempt was thus undertaken to study the impact of butylparaben, methylparaben and diclofenac on toxicological behavior and properties of triclosan (at varying concentration levels) with respect to Microtox, XenoScreen YES/YAS, Caco-2, HEPG2, and liposomal systems.

Having performed analytical and biological studies modelling was done using two modelling approaches, viz., concentration addition (CA) and independent action (IA) at three concentration levels of each chemical studied. The effect of the highest concentration of triclosan studied was impacted by even small amounts of methylparaben and butylparaben in Microtox while diclofenac preferably affected triclosan activity at its lowest concentration level (with CA model). Estrogenic agonistic

properties of triclosan were severely impacted by both parabens in an antagonistic way; diclofenac showed in all cases underestimation or synergy at the lowest triclosan concentration studied. Estrogenic antagonistic activity of triclosan was also slightly affected by parabens and by diclofenac in binary mixtures, showing overestimation and antagonist effects. HepG2 cells appeared to be the most resistant to the toxic effect of the mixtures at the concentrations tested and no significant proof of synergy or antagonism could be detected with the MTT assay. The liposome assays on the mixtures followed the same trends obtained with the MTT assay with Caco-2 cells, confirming the validity of the *in vitro* model used in this research. As studies on emerging contaminants mixtures toxicity are still scarce, research presented here constitute an important part in confirming utility and versatility of emerging contaminants modelling in environmental toxicology.

Keywords: triclosan toxicity, parabens, diclofenac, Microtox, endocrine potential, genotoxicity, liposomes

1. Introduction

Contaminants of emerging concern, or emerging contaminants, comprise both inorganic and organic species that are known to be persistent in the environment and are continuously introduced as a result of anthropogenic activities, either as replacements of banned chemical counterparts or owing to their positive attributes in human consumables (Schnoor 2014, Richardson and Kimura 2017). Moreover, some new chemicals of increased polarity can slip through wastewater treatment plants because of incomplete removal and ultimately enter marine settings (Reemtsma et al. 2016). The European Commission is aware of increasing amounts of unregulated chemical species in the environment, which have potential deleterious effects on wildlife, and thus recently published the "Updated Watch List of Substances for Union-wide Monitoring in the Field of Water Policy Pursuant to Directive 2008/105/EC" (EU 2018/840). The number of chemical classes categorized as environmentally relevant emerging contaminants is steadily increasing, as highlighted by a series of comprehensive reviews (Richardson and Ternes 2018, Richardson and Kimura 2016, Richardson and Ternes 2014) and authoritative reviews (La Farre et al. 2008, Lorenzo et al. 2018, Ebele et al. 2017; Bletsou et al. 2015). These scientists are major contributors to improving the

monitoring and analysis of the influence of pharmaceutical and personal care products present in natural waters, including (i) antimicrobial agents (e.g., triclosan), (ii) preservatives (e.g., alkyl esters of phthalic acid, better known as parabens), (iii) ultraviolet filters, (iv) stimulants, (v) insect repellants, (vi) artificial sweeteners, and (vii) several antibiotics, along with anti-inflammatory, anti-depressant, anti-diabetic, and anti-helminthic drugs.

Indeed, such pharmaceuticals and personal care products are among the most frequently detected pollutants in environmental settings, and their pervasiveness and continuous introduction into the trophic chain remain a major concern given their biologically active nature (Richmond et al. 2017). For example, diclofenac is a popular painkiller from the non-steroidal anti-inflammatory group, and its frequent use, especially in veterinary medicine, has led to the extinction of vultures grazing in Asian countries. The diclofenac concentration in environmental matrices varies from the nanogram to microgram per liter range (Lonappan et al. 2016). Triclosan is another common environmental contaminant, which has antifungal and antibacterial properties and is thus widely used in cosmetics, antibacterial soaps, patches, and hygienic products in hospitals. Recent studies have shown that triclosan contributes to the growth of cancer cells and can penetrate breast milk (Lee et al. 2014, Bever et al. 2018). According to studies carried out on women of different age groups, triclosan was found to accumulate in the adipose tissue, and the highest concentration was detected in women in their 30s and 40s, which is attributed to the more frequent use of cosmetics and cleaning products in these groups. Triclosan in the environment is often detected at similar levels as diclofenac, ranging from nanograms to micrograms per liter (Allmyr et al. 2008; Petrie et al. 2016; Perez et al. 2013). In addition, methylparaben and butylparaben have been detected at the same levels in environmental samples, which are used as preservatives in cosmetics, drugs, and foods. Some studies showed that parabens have endocrine-disrupting properties and are weak estrogen receptor agonists (butyl being a stronger agonist due to its higher lipophilicity) (Okubo et al. 2001). Further details of these compounds are provided in Table 1, and their concentrations alone and in mixtures (i.e., plausible combined toxicity) in biotic and abiotic samples are given in Table 2.

Table 1. Concentrations of emerging contaminants in natural waters, wastewaters and biological samples confirming their co-presence under real environmental conditions.

Analyte / Mw [g/mol] / LogP	**Sample**	**Concentration**	**Detection technique**	**Reference**
Triclosan / 289.54 / 4.98-5.53 (Drugbank, 2019d)	13 species of fishes from Spanish Mediterranean River Basins.	nd-17.41 ng/g dw	LC-MS/MS	Pico et al. 2019
Diclofenac/ 318.13 /0.6-0.8 experimental at the pH≥10 (Ingram et al. 2011) 4.26-4.75 (Drugbank 2019a)		nd-15.35 ng/g dw		
Methylparaben / 152.15 / 1.67-2.17 (Drugbank 2019b)		nd-84.69 ng/g dw		
Triclosan	Yangtze River surface water (China)	nd-65.6 ng/L	UPLC-QqQ-MS	Ma et al. 2018
Methylparaben		0.23-42.1 ng/L		
Butylparaben / 194.23 / 3-3.82 (Drugbank, 2019c)		Nd-0.16 ng/L		
Triclosan	Wastewater from Meknes city and its surrounding (Morocco)	1.6-13.9 pg/mL	DPV/EIS/ Spectrophotometry	Motia et al. 2019
Diclofenac	Surface water (River Isar and lake Wörthsee)	0.031 µg/L	ELISA/LC-MS	Huebner et al. 2015
	Waste water	2.5 µg/L		
Diclofenac	Water from Taihu lake, China	nd-26 ng/L	UPLC-QqQ-MS	Xie et al. 2017
	Sediment from Taihu Lake	nd-7.3 ng/g dw		
	Fishes from Taihu Lake	0.8-68 ng/g dw		
	Plankton from Taihu Lake	nd-31 ng/g dw		
	Molluscs from Taihu Lake	1.2-31 ng/g dw		

Table 1. (continued)

Analyte / Mw [g/mol] / LogP	**Analyte / Mw [g/mol] / LogP**	**Analyte / Mw [g/mol] / LogP**	**Analyte / Mw [g/mol] / LogP**	**Analyte / Mw [g/mol] / LogP**
Triclosan	*S. latissima, L. digitata* (Macroalgae from Fureholmen Solund, Norway)	nd	UPLC-QqQ-MS	Alvarez-Munoz et al. 2015
	M. galloprovincialis, C. gallina (bivalves from Ebro delta, Spain)	1.3-2 ng/g dw		
	L. aurata and P. flesus (Fishes from Tagus and Scheldt stuaries, Portugal and Netherlands, respectively)	Detected but lower than quantification limit (LOQ) (0.75ng/g dw)		
Methylparaben	*S. latissima, L. digitata* (Macroalgae from Fureholmen Solund, Norway)	nd		
	Mytilus spp., M. galloprovincialis (bivalves from Tagus estuary, Portugal, and Po delta, Italy)	4.2-12 ng/g dw		
	M. galloprovincialis, C. gallina (bivalves from Ebro delta, Spain)	Detected but lower than LOQ (0.01 ng/g dw)		
	L. aurata and P. flesus (Fishes from Tagus and Scheldt stuaries, Portugal and Netherlands, respectively)	0.9-18.1 ng/g dw		
Triclosan	*S. latissima, L. digitata* (Macroalgae from Fureholmen Solund, Norway)	nd	UPLC-QqQ-MS	Alvarez-Munoz et al. 2015
	M. galloprovincialis, C. gallina (bivalves from Ebro delta, Spain)	1.3-2 ng/g dw		
	L. aurata and P. flesus (Fishes from Tagus and Scheldt stuaries, Portugal and Netherlands, respectively)	Detected but lower than quantification limit (LOQ) (0.75ng/g dw)		
Methylparaben	*S. latissima, L. digitata* (Macroalgae from Fureholmen Solund, Norway)	nd		
	Mytilus spp., M. galloprovincialis (bivalves from Tagus estuary, Portugal, and Po delta, Italy)	4.2-12 ng/g dw		
	M. galloprovincialis, C. gallina (bivalves from Ebro delta, Spain)	Detected but lower than LOQ (0.01 ng/g dw)		
	L. aurata and P. flesus (Fishes from Tagus and Scheldt stuaries, Portugal and Netherlands, respectively)	0.9-18.1 ng/g dw		

Table 1. (continued)

Analyte / Mw [g/mol] / LogP	**Analyte / Mw [g/mol] / LogP**	**Analyte / Mw [g/mol] / LogP**	**Analyte / Mw [g/mol] / LogP**	**Analyte / Mw [g/mol] / LogP**
Triclosan	*Tursiops truncates (*bottlenose dolphins) Charleston, South Carolina and the Indian River Lagoon, Florida Effluent from WWTPs in Charleston Charleston's rivers	0.025 to 0.270 ng/g ww 190 ng/L 4.9-13.7 ng/L	HRGC/HR-MS	Fair et al. 2009
Diclofenac	Water from Zivny stream (a tributary of Blanice River, Czech Republic) *Erpobdella octoculata* (worm)	2-146 ng/L 8-46 ng/g	SPE/LC-MS/MS	Grabicova et al. 2015
Methylparaben Diclofenac Methylparaben Diclofenac	Waste Water effluent from three Slovenian and three Croatian WWTPs Surface Water from Sava River	11.8-1910 ng/L (average 379 ng/L) 113-812 ng/L (average 480 ng/L) 14.8-139.5 ng/L (average 26.3 ng/L) 0.065-4.6 ng/L (average 2.3 ng/L)	GC-MS	Cesen et al. 2019
Triclosan Methylparaben Butylparaben	Shellfish eight species (*Buccinidae, Veneridae, Haliotidae, Mytilidae, Pectinidae, Ostreidae, Corbiculidae* and *Pteriidae*) collected from Shenzhen, China	<LOQ–6.5 × 10^3 pg/g ww 1.29 × 10^2–2.48 × 10^4 pg/g ww <LOQ–359 pg/g ww	HPLC-MS/MS	Lu et al. 2019
Methylparaben	Small cetaceans from Korean costs: Common dolphins (*Delphinus capensis*) Finless porpoises (*Neophocaena asiaeorientalis*)	1.3-224 ng/g ww 6.4-569 ng/g ww	HPLC-MS/MS	Jeong et al. 2019
Methylparaben Butylparaben Methylparaben Butylparaben	Surface water from Yellow River and Huai River (Henan province, China) Surface sediment from Yellow River and Huai River (Henan province, China)	1.92-154 ng/L 0.04-0.99 ng/L 7.07-27.6 ng/g 0.96-7.61 ng/g	UHPLC-MS/MS	Feng et al. 2019
Triclosan Methylparaben Butylparaben	Costal water from Kenting National Park (Taiwan)	1.52 ± 0.81 ng/L 34.9 ± 30 ng/L 0.2 ± 0.6 ng/L	LC–MS/MS	Kung et al. 2018

To gain a better understanding of the actual risk posed by these chemicals in the environment, in the present study, we assessed the toxicity of binary mixtures of triclosan, methylparaben, butylparaben, and diclofenac at varying concentrations (confirmed with data presented in Table 1 but also to set the rationale behind studies on higher order mixture and chronic toxicity studies) against organisms belonging to different trophic levels and artificial membranes. The selected organisms and organelle-like systems used as models were the bacterium *Vibrio fischeri* (Microtox®), genetically modified *Saccharomyces cerevisiae* yeasts (XenoScreen YES/YAS), Caucasian colon adenocarcinoma (Caco-2) and HepG2 human cell lines, and liposomes. Such approach is justified if one gets a closer look at data collected in table 2, which confirms impact of these chemicals to organisms belonging to all trophic levels and their organelles.

This battery of assays includes basic low-level organisms, which can be primary targets of pollutants in the environment. The gram-negative bacterium *V. fischeri* can be found in salt and brackish waters, and the change in the bioluminescence of the bacterial suspension after a period of incubation with contaminated samples forms the basis of the so-called Microtox® test. The XenoScreen YES/YAS test involves genetically modified yeasts harboring human androgenic (hERα) and estrogenic (hARα) receptors, making them sensitive to the presence of substances with endocrine properties (Marugán et al., 2012, Wieczerzak et al. 2016a). This test allows for assessments of the agonistic and antagonistic properties of chemicals in various types of samples. The human colon Caco-2 cell line is widely used in studies on the intracellular invasion of numerous chemicals and biological species; the transport of lipids, drugs, and nanoparticles; and in viral infection evaluations. HepG2 cells are an immortal cell line used to model polarized hepatocytes and their response to genotoxic, cytotoxic (including cytoprotective, anti-genotoxic, and cogenotoxic) chemicals and their toxicity (Mersch-Sundermann et al. 2004). A minimalistic *in vitro* eukaryotic cell model based on the use of large unillamelar phosphatidylcholine liposomes was also included in the present study for comparison against ecotoxicological and *in vitro* cellular assays.

Predicting the overall toxicity of mixtures containing organic chemicals, especially those with biological activity, is a very complicated task, and currently available models are associated with respective drawbacks and do not always reflect reality. Moreover, experimental studies that could provide an unambiguous answer are not always possible since it is impracticable to study all possible mixtures on various species at different

concentrations to obtain actual data (Kudłak et al. 2019; Wieczerzak et al. 2016b). Among the numerous methods to assess the total impact of chemical mixtures, two main models should be differentiated: (i) the concentration addition (CA) model and (ii) the independent action (IA) model. The CA model assumes that all of the mixture components have similar modes of action (MOAs). Alternatively, in the IA model, individual components have different MOAs. These models are most often used to predict the toxicity of chemical mixtures in the field of environmental toxicology (Abendroth et al. 2011; Backhaus and Faust 2012; Belden et al. 2007; EU 2012; Gao et al. 2018; Hadrup et al. 2013; Liu et al. 2015).

As shown in Table 2, our individual target analytes appear to have multiple effects on biota. However, their combined mode of ecotoxicity toward organisms of different trophic levels assessed with the above-mentioned modeling approaches has not been attempted to date.

Therefore, the aims of this work were as follows: (i) to determine the basic toxicity levels of analytes of interest on different biological systems and the membranotropic effects on liposomes, and (ii) evaluate the toxicological impact of the analytes when present in mixtures with two mathematical models - IA and CA. Utilizing the same standardized methodology for all assays enables obtaining reliable insights for assessing the actual risk that these mixtures pose to organisms.

2. Materials and methods

2.1. Test materials

The model compounds, namely, diclofenac sodium salt (CAS no. 15307-79-6), triclosan (CAS no. 3380-34-5, HPLC purity ≥97%), methyl 4-hydroxybenzoate (methylparaben, CAS no. 99-76-3, purity ≥99%), and butyl 4-hydroxybenzoate (butylparaben, CAS no. 94-26-8, purity ≥99%), were purchased from Sigma-Aldrich/Merck KGaA (Darmstadt, Germany). For liposome assays, 200 mM stock solutions of individual contaminants were prepared in MeOH. Binary mixtures were prepared 1000-fold concentrated in MeOH with respect to working solutions. Laurdan stock solution was 1 mM in DMSO (1000 times concentrated compared to working solutions).

For Caco2 and HepG cell assays 100 mM stock solutions of individual contaminants were prepared in a mixture of DMSO/water in order to avoid large volumes of DMSO (lower than 2% of final volume) in inhibitory curves due to the intrinsic cell toxicity of this solvent. Binary mixtures at different concentration levels were prepared in DMEM buffer from stock solutions. Although the weighted amount of every substance differed, all solutions were prepared so as to not exceed the respective solubility limits.

2.2. Microtox®

The Microtox® reagents and methodology is given in Wieczerzak et al. 2016a and in details in electronic supplementary material.

2.3. XenoScreen YES/YAS

The XenoScreen YES/YAS reagents and methodology is given in Kudłak et al. 2019 and in details in electronic supplementary material.

2.4. *Citotoxicity tests*

For cell culture experiments, dimethyl sulfoxide (≥ 99.9 %), Dulbecco's phosphate buffered saline (PBS) at pH 7.4, Triton X-100, thiazolyl blue tetrazolium (MTT) and trypan blue powder were purchased from Sigma-Aldrich/Merck KGaA. Dulbecco's modified eagle media (DMEM; ref: 31966-021), heat inactivated fetal bovine serum (FBS), penicillin-streptomycin (PenStrep) and trypsin-EDTA were purchased from Thermo Fisher Scientific (Waltham, MA, US). Lactate dehydrogenase (LDH) Cytotoxicity Detection Kit was acquired from Takara Bio Inc. (Shiga, Japan). Caco-2 and HepG2 cell lines were purchased from the American Type Culture Collection (ATCC, LGC Standards GmbH, Wesel, Germany) and used after a passage number of 35-42, and 29-40, respectively. Absorbance readings were performed using a Synergy™ HT Multi-mode microplate reader (BioTek Instruments Inc., Winooski, VT, USA).

Table 2. Summarized information on confirmed ecotoxicological impact of analytes studied.

Analyte	Effect	Organism	Concentration levels tested	Detection technique	Reference
Triclosan	Induced significant biochemical changes, including histidine, amide II, left-handed helix DNA and stretching C-O deoxyribose. This suggests structural alterations to proteins and DNA.	*Limnodrilus hoffmeisteri* (worm)	8 µg/g (28 days of exposition)	FTIR spectroscopy	Peng et al. 2019
	Seriously affected the secondary structure of proteins by protein aggregation. Fatty acids in membrane were nearly destroyed or blocking of fatty acid and lipid synthesis.	*Chlorococcum* sp. (green algae)	96-h acute test at concentrations ≥ 28.9 mg/L	FTIR spectroscopy	Xin et al. 2017
	Caused accelerated erratic movement in larvae. Delayed hatch was observed at 72 hpf (hours post fertilization) following embryonic exposure.	Zebrafish	0.1 µg/L 1µg/L for 48h 48 h LC_{50} value of 1.5±0.5 mg/l for zebrafish embryos	Imaging	Zhou et al. 2019
	Decrease of the metabolic capacity. Activity of SOD and CAT enhanced.	*Mytilus galloprovincialis* (mussels)	1 µg/L for 28 days	Biochemical parameters	Freitas et al. 2019
Diclofenac	Decrease of the metabolic capacity and lipid damage increased at 21°C. Activity of SOD and CAT enhanced.	*Mytilus galloprovincialis* (mussels)	1 µg/L for 28 days	Biochemical parameters	Freitas et al. 2019
	Respiration rate decreased, which may be a result of metabolism reduction.	*Mytilus edulis trossulus* (Baltic sea blue mussel)	100 and 1000 µg/L	Physiological indicators	Ericson et al. 2010
	Increased total chlorophyll. Increased carotenoids content. Levels of anthocyanins decreased.	*Lemna minor* and *L.gibba* (aquatic plant) *L.gibba* *L.gibba*	20-100µg/L for 96h 20-100µg/L for 96h 0.16-100µg/L for 96h	Biochemical markers with spectrophoto-metric detection	Alkimin et al. 2019

Table 2. (continued)

Analyte	Effect	Organism	Concentration levels tested	Detection technique	Reference
Diclofenac	Carbohydrate and fatty acid metabolic pathway promoted. Metabolomics pathway disturbed.	*Chlorella pyrenoidosa* (green algae)	<30 mg/L for 8 days >100 mg/L for 8 days	GC-MS and biochemical markers with spectrophoto-metric detection	Zhang et al. 2019
	Ability to consume food weakened AChE activity and MDA contents increased. SOD, CAT, GR and GST activities decreased.	*Daphnia magna* (planktonic crustacean)	5-100 µg/L for 2-7 days of exposure	Diagnostic reagent kits with spectrophoto-metric detection	Nkoom et al. 2019
	Blocking of the enzyme cyclooxygenase, which catalyzes arachidonic acid degradation during prostaglandin production Increased LPX.	*Cyprinus carpio* (common carp)	7.1 mg/L for 12, 24, 48, 72 and 96 h	Biomarkers	Islas-Flores et al. 2013
Methyl and butyl-paraben	Increased activity of SOD, GPx and GR and GSH-t levels in gills and live.	*Oreochromis niloticus* (Nile tilapia)	4 mg/L for 6-12 days	Biochemical analysis	Silva et al. 2018
Butyl-paraben	Reduced fertility of F1 female rats due to impaired steroidogenesis and folliculogenesis (anti-estrogenic effect).	*Holtzman* rat	10, 100 and 1000 mg/kg bw/day for 21 days	Hormone assays, fertility assessments and PCR	Maske et al. 2018
	Down-regulated transcription factor *pdx1*, as well as genes involved in GSH synthesis, while upregulating GSH-disulfide reductase. Intestinal effusion, pericardial edema, and accelerated yolk utilization.	*Danio rerio* (zebrafish)	250, 500, 1,000 or 3,000 nM from 3 hpf to 7 days	RNA and PCR analysis, HPLC and morphologic parameters	Brown et al. 2018

Table 2. (continued)

Analyte	Effect	Organism	Concentration levels tested	Detection technique	Reference
Methyl-paraben	Pericardial edema, pigmentation, and tail defect and decreased locomotor activity. Overexpression of *myca* and *ccnd1* oncogenes. Increased MDA, which is used as an index of LPO and decreased GST activity and nitric oxide. Increase of apoptosis.	Zebrafish	50 mg/L (LC50) from 4 hpf to 72 hours	RNA and PCR analysis, morphologic and biochemical parameters	Ates et al. 2018
	Decrease of ChE and CAT activity. Survival and growth not significantly affected by chronic exposure.	*Artemia franciscana* (aquatic crustacean)	0.05 and 0.1 mg/L for 48h 0.05 and 0.1 mg/L for 9 days 24 h-LC50 value of 36.7 mg/L	Biochemical and physiological parameters	Comeche et al. 2017

Acronyms:
SR: Synchrotron radiation, SOD: Superoxide dismutase, CAT: Catalase, ChE: Cholinestarase, AChE: Acetylcholinestarase, GST: Gluthathion-S-transferase, MDA: Malondialdehyde, GR: Glutathione reductase, LPX/LPO: Lipid peroxidation, GPx: Glutathione peroxidase, GSH-t: Total glutathione

The thiazolyl blue tetrazolium reduction (MTT) assay was used to evaluate cellular metabolic activity, and the lactate dehydrogenase (LDH) assay was conducted to evaluate cell viability based on changes in membrane integrity. Caco-2 and HepG2 cells (American Type Culture Collection, LGC Standards GmbH, Wesel, Germany) were used after passages 35–42 and 29–40, respectively, and cultured in Dulbecco's modified Eagle medium (DMEM; ref: 31966-021) supplemented with 10% (v/v) heat-inactivated fetal bovine serum and 1% (v/v) penicillin-streptomycin (all from ThermoFisher Scientific, Waltham, MA, USA). The cells were maintained in a humidified chamber at 37 °C and 5% (v/v) CO_2 and were detached using 0.25 % (w/v) trypsin/ethylenediaminetetraacetic acid (EDTA; ThermoFisher Scientific) when reaching 80% confluence.

Prior to the assays, each cell line was cultured in 96-well plates by adding 4×10^5 cells/mL (4×10^4 cells/well) and left to grow overnight. The supernatant was removed and replaced by 100 µL of the test solution (containing individual species or binary mixtures thereof) and incubated for 24 h. Thereafter, the supernatant (100 µL) was removed for further LDH assays, and 100 µL of MTT (Sigma-Aldrich/Merck KGaA) dissolved in a fresh culture medium (0.5 mg/mL) was added to the plate. The microplate was incubated at 37 °C for 3 h and the resulting formazan crystals were solubilized

using 100 µL of dimethyl sulfoxide (DMSO; ≥99.9%, Sigma-Aldrich/Merck KGaA) after removal of the MTT aqueous medium. Absorbance measurements were then taken at 570 nm against 630 nm on a Synergy™ HT multi-mode microplate reader (BioTek Instruments Inc., Winooski, VT, USA). The absence of cytotoxicity (100% metabolic activity) was evaluated by replacing the test sample with the culture medium, while using 1% (v/v) Triton X-100 solution (Sigma-Aldrich/Merck KGaA) in DMEM as positive control for a cytotoxic effect. Statistical calculations were performed on the basis of the percentage of metabolic activity.

For the LDH assay (LDH Cytotoxicity Detection Kit, Takara Bio Inc., Shiga, Japan), 100 µL of the test solutions collected over the time course of the MTT assay were centrifuged, and the supernatant was mixed with 100 µL of the reagent mixture from the kit, comprising the catalyst (diaphorase), NAD^+, and tetrazolium salt. After incubation for 30 min at room temperature in the dark, absorbance values were read at 490 nm and 690 nm. The absence of cell viability (100% cytotoxicity) was evaluated by replacing the test sample by 1% (v/v) Triton X-100 solution in DMEM. Statistical calculations were performed on the basis of the percentage of cytotoxicity.

The negative control for the MTT/LDH assays was performed in DMEM buffer, without any compound, showing viability values of 100 ± 5%. For the positive control, 1% Triton X-100 surfactant in DMEM buffer was proven to induce cell death with viabilities of 1.00 ± 0.05%. The viability values are the average of several tests and do not normally exceed 5% deviation. The toxicity of DMSO employed in the preparation of stock solutions was also evaluated. Cell viability was above 90% for the maximum concentration of DMSO in standards of individual compounds. The concentration of DMSO in binary mixtures was in all instances lower than that of the inhibition curves and thus, the solvent effect onto the toxicity is negligible.

2.5. Liposomes assay

Liposomes were prepared by lipid film hydration (Bangham et al. 1967) followed by extrusion (Hope et al. 1985). To this end, 10 mg of soybean phosphatidylcholine (PC; LIPOID S100, average molecular weight 787 g/mol) was solubilized in 1.0 mL of chloroform. The solvent was first removed in a rotary evaporator at low pressure (290

mbar) and 30 °C for 2 h and then under vacuum for approximately 2 h or more so as to obtain a uniform dried lipid film without any organic solvent traces. The lipid was then reconstituted in 1 mL phosphate buffered saline (PBS, pH 7.4; Sigma) at room temperature to afford a final lipid concentration of approximately 12.7 mM PC, which was then vortexed for 1 h (1 min every 5 min) to obtain multilamellar vesicles (MLVs). The milky suspension was maintained overnight at 4 °C to allow the MLVs to become sufficiently hydrated for stabilization. Subsequently, the solution was extruded 29 times through polycarbonate filters (100-nm pores) to generate highly homogeneous large unilamellar vesicles with a hydrodynamic diameter (Z-average) of 129 nm and a polydispersity index as low as 0.076. Liposomal characterization was performed by dynamic light scattering using a Zetasizer Nano ZS90 system (Malvern Panalytical, Malvern, UK).

The effect of the individual contaminants and mixtures on the lipid packing and ordering of liposomes was investigated by a membrane fluorescence probe, *v*6-dodecanoyl-N,N-dimethyl-2-naphthylamine (Laurdan). The Laurdan fluorescence emission spectrum is strongly dependent on the polarity of its surrounding medium once inserted into the lipid membrane; the higher the concentration of water (or another polar solvent) in the vicinity of the probe, the higher the red shift of the spectrum from 440 nm towards 490 nm will be. This effect is caused by the so-called dipolar relaxation phenomenon and is a consequence of the decrease of the probe's excited state energy due to reorientation of the molecules of the polar solvent around the probe's dipole (Parasassi et al. 1986). This phenomenon is measured by the generalized polarization (GP) parameter that correlates well with the phase state of the membrane (Parasassi et al. 1991). In the gel phase, the membrane is more ordered and thus less hydrated, and the GP takes on positive numbers; otherwise, for a disordered and hydrated membrane, the so-called liquid-crystalline phase (as is the case in this work), the GP values are negative. GP values were obtained using the following equation:

$$GP = \frac{I_{440} - I_{490}}{I_{440} + I_{490}} \text{ (eq. 1.)}$$

where I_{440} and I_{490} represent the emission intensities of the liposome-embedded Laurdan at 440 nm and 490 nm, respectively. GP values range from +1 to -1.

For experimental GP measurements, liposomes, obtained as described above, were diluted in PBS (pH 7.4) at a final concentration of 100 μM PC. The membrane probe (stock solution of 1 mM in DMSO) was added to the liposomal solution at a final concentration of 1 μM Laurdan and kept in the dark at room temperature for 2 h to allow for equilibration of the probe into the membrane (Oliver et al. 2016). The liposomal solution was then divided into 1-mL aliquots. One microliter of the emerging contaminants, alone or as binary mixtures in methanol, was added to the 1-mL aliquots of the Laurdan-embedded liposomes. Samples were incubated for 30 min at room temperature and placed in a 96-well white microplate with a solid bottom (Cat. No. 30196, SPL Life Sciences) for further fluorescence detection. Fluorescence data were recorded by a Varian Cary Eclipse fluorescence spectrometer (Agilent technologies, Mulgrave, Victoria) at room temperature. The emission intensity was measured at 440 nm and 490 nm (excitation wavelength was fixed to 360 nm). Operational parameters were set to 10-nm slit widths and a 600-V photomultiplier detector voltage.

The $GP_{contaminant}/GP_{Laurdan}$ ratio was used as the analytical parameter for statistical calculations. Using the Laurdan GP as a control, $GP_{contaminant}/GP_{Laurdan}$ percentage ratios close to 100% indicated the lack of effects of contaminants on the morphology and structural characteristics of the liposomes (i.e., absence of membrane toxicity). However, lower or higher GP percentages indicated a greater membranotropic effect, serving as a marker of the potential toxicity of the contaminant and/or binary mixture. The negative control for liposome assays was carried out only with the fluorescent probe Laurdan to get the initial fluorescence signal or GP value that serves as a reference. We assigned the value of 100% “viability” or 100% of no effect to this signal. There is no positive control in this case because the value of 0% does not make sense as all the experimental values are relative to the GP of Laurdan alone. Methanol in the working solution not exceeded 0.1% so solvent control was not considered as relevant in terms of liposome stability.

2.6. Apoptosis and CYP450-based assays for HepG2 cells

The apoptotic effect of the different chemicals on HepG2 cells was evaluated using FITC Annexin V Apoptosis Detection Kit I (BioLegend, San Diego, CA, USA) according to the manufacturer instructions. In brief, after incubation with the

contaminant mixtures for 24 h, the cells were washed twice with PBS, detached with 0.25% trypsin-EDTA, and centrifuged for 5 min. Subsequently, the supernatant was discarded, the cells were resuspended in 50 □L of binding buffer with Annexin V-FITC and 7-AAD reagents, and incubated 15 min prior to analysis using a BD Accuri C6 flow cytometer (BD Biosciences, Erembodegem, Belgium). For each sample, a minimum of 20 events were recorded.

The effect of the different chemicals on expression of the CYP450 family was also assessed by flow cytometry. HepG2 cells were labeled with cytochrome P450 1A2-Alexa Fluor 647 and cytochrome P450 3A4-FITC antibodies (Novus Biologicals, Centennial, CO, USA) according to manufacturer instructions, and then analyzed with the BD Accuri C6 flow cytometer.

2.7. Model deviation ratio (MDR) analysis

The IA and CA models were used to calculate the actual toxic effect of the tested binary mixtures. These two approaches serve to assess the combined toxicological effect of chemicals assuming a similar MOA (CA) or dissimilar MOA (IA). CA models are more frequently applied for environmental risk assessments because they are slightly more conservative than IA models. The combined toxicological effect of a mixture assessed by the CA model is given by equation 2:

$$ECx_{mix} = \left(\sum_{i=1}^{n} \frac{p_i}{ECx_i}\right)^{-1} \qquad \text{(eq. 2.)}$$

where ECx_{mix} is the x_{mix} effect caused by the total concentration of the mixture of studied chemicals (components) (Expected value), p_i indicates the proportion of component *i* in the mixture calculated based on the concentration of component *i* in the mixture, *n* indicates the number of components in the mixture, and ECx_i indicates the x_i effect caused by component *i* at a given studied concentration in the mixture.

The CA model does not account for possible interactions between different chemicals in the mixture, and deviations of the tested mixture toxicity from the predicted values could be evidence of synergistic or antagonistic interactions between chemicals.

By contrast, IA models assume independent action from the combined chemicals, and were calculated using equation 3:

$$E(C_{mix}) = 1 - \prod_{i=1}^{n}(1 - E(c_i)) \quad \text{(eq. 3.)}$$

where EC_{mix} is the overall effect expressed as a fraction of the maximal possible effect of a mixture of chemical *i* in a mixture with *n* chemicals (expected value), c_i indicates the concentration of component *i* in the mixture, *n* indicates the number of components in the mixture, and $E(c_i)$ indicates the effect of component *i*, applied separately.

To confirm/deny the presence of synergy/antagonism, the MDR coefficient was used to compare predicted and observed values (Kudłak et al. 2016, Wieczerzak et al. 2015). MDR is defined as shown in equation 4:

$$\text{MDR} = \frac{\text{Expected}}{\text{Observed}} \quad \text{(eq. 4.)}$$

where *Expected* is the effective toxicity of the mixture predicted by the CA or IA models, and *Observed* is the effective toxicity of the mixture obtained during the toxicity assessments.

Mixtures with MDR > 2.0 are considered to exhibit a high probability of antagonism, while those with values below 0.5 show a synergistic characteristic. Here, we arbitrarily assumed that an MDR falling within 0.50–0.71 and 1.40–2.00 indicates possible under- and overestimation of the models, respectively.

3. Results and discussion

Inhibition curves were performed in a concentration range based on previous experiments and the know-how of our group. After obtaining IC50 values of every single compound, triclosan exhibited the major toxicity, with the lower IC50, namely, ten times lower than butylparaben, the second most toxic compound of our selected contaminants. In this way, it was decided to evaluate the effect of the other contaminants on the toxicity of triclosan throughout binary mixtures using the IC20 value of triclosan at 100% IC20, 66% IC20 and 33% IC20. IC20 was chosen instead of

IC50 for different reasons: i) to diminish working concentrations of pollutants, thus being closer to environmental values; ii) to avoid high levels of dead cells, as the effect of binary mixtures on cell viability is unknown due to possible synergistic effects that could increase the toxicity to close 100%, and thus discrimination of the effects of different binary mixtures would be impracticable.

3.1. Microtox®

The results of CA modeling with bioluminescent bacteria demonstrated intriguing trends. The highest concentration of triclosan was impacted by methylparaben to the greatest extent with a decreasing content of methylparaben; the same behavior was evident in the case of the mixture of triclosan with butylparaben, showing synergistic toxicity effects. The trend of the diclofenac impact was similar but with a much lower magnitude. In the case of mixtures containing the lowest concentrations of triclosan, the CA model with methylparaben indicated no synergism or antagonism and suggested underestimation for butylparaben and diclofenac. IA models showed that in most cases, the analytes have independent MOAs because there is a good agreement between theoretical and experimental data.

In fact, independent MOAs have also been observed indirectly for Mytilus galloprovincialis mussels exposed to triclosan and diclofenac in different salinity conditions (Freita et al. 2019). The metabolic capacity and oxidative status were changed in all tested conditions, but triclosan had effect over glutathione peroxidase activity while exposure to diclofenac enhanced catalase response.

Table 3 shows the variations in MDR values depending on triclosan concentrations for solutions of selected parabens and diclofenac evaluated with Microtox. Overestimation of the IA model was only detected for mixtures of triclosan and methylparaben at the lowest concentrations tested for these compounds.

Table 3. MDR values depending on the triclosan concentration for solutions of selected parabens and diclofenac studied with Microtox (MDR values >2.0 exhibit antagonism, MDRs <0.5 show synergism, MDR values within 0.50-0.71 and 1.40-2.00 values mean, respectively, under- and overestimation of presented models; for values of particular concentrations C1, C2 and C3 of all analytes please refer to the table below)

CA						**IA**		
Triclosan[a]						**Triclosan[a]**		
C1	**C2**	**C3**				**C1**	**C2**	**C3**
0.71	0.87	1.01	**C1**	**[b]Methyl-paraben**	**C1**	1.08	1.18	1.16
0.60	0.79	1.01	**C2**		**C2**	1.09	1.25	1.23
0.40	0.69	1.00	**C3**		**C3**	1.17	1.64	1.50
0.68	0.93	0.65	**C1**	**[c]Buthyl-paraben**	**C1**	1.05	1.36	0.91
0.59	0.66	0.47	**C2**		**C2**	1.11	1.15	0.72
0.27	0.31	0.51	**C3**		**C3**	0.74	0.78	0.93
0.85	0.83	0.71	**C1**	**[d]Diclofenac s.**	**C1**	1.15	1.15	1.07
0.72	0.78	0.57	**C2**		**C2**	1.09	1.21	0.91
0.66	0.72	0.70	**C3**		**C3**	1.07	1.22	1.21

[a]Triclosan			[b]Methylparaben			[c]Butylparaben			[d]Diclofenac sodium salt			
C1	C2	C3	C1	C2	C3	C1	C2	C3	C1	C2	C3	
1.180	0.778	0.389	51.90	34.30	17.10	3.94	2.60	1.30	73.0	48.2	24.1	µM

3.2. XenoScreen

3.2.1. XenoScreen YES+

The estrogenic agonistic behavior of analytes can confirm behavior related to the endocrine disruption potential of mixtures. As shown in Table 4, both the CA and IA models confirmed an antagonistic impact of methyl- and butylparaben on triclosan. Moreover, a concentration-dependent impact was noticeable in which reducing the concentration (down to the 1-micromolar level) of substances in the mixtures enhanced the antagonistic impact concerning their interactions. . In this context, considering a recent study concerning prenatal exposure to certain xenobiotics, including triclosan and methyl-, butyl- and propyl-paraben, adverse birth outcomes have been associated with these compounds. Triclosan was positively associated with gestational age among males, and negatively associated with gestational age among females. Methyl-, butyl- and propyl-paraben were associated with decreased odds of small-for-gestational age infants, thus showing, in a population-based study context, that these compounds may have different endocrine effect (Aker et al. 2019). This topic has also been summarized

in a review concerning the impact of environmental exposure to endocrine disrupting chemicals on the reproductive potential among women (Karwacka et al. 2019), measured by ovarian reserve and by assisted reproductive technology outcomes. Exposure to triclosan decreased the oocyte quality and the embryo quality while exposure to parabens decreased the antral follicle count and the rate of clinical pregnancy and live births. A recent study also evaluated the associations between repeated measures of several chemicals and their mixtures with reproductive hormones in women (Pollack et al. 2018). Parabens were associated with increased estradiol while phenols (including triclosan) were associated with decreased estradiol, luteinizing hormone, and follicle stimulating hormone, showing also here an antagonistic effect.

The observed impact of diclofenac on the endocrine potential of triclosan was even more interesting from an environmental point of view in which increasing concentrations of diclofenac (while keeping the concentration of triclosan constant) suggested a possible synergistic impact of the mixtures (MDR values reached down to 0.71).

Table 4. MDR values depending on the triclosan concentration for solutions of selected parabens and diclofenac studied with XenoScreen YES+ (MDR values >2.0 exhibit antagonism, MDRs <0.5 show synergism, MDR values within 0.50-0.71 and 1.40-2.00 values mean, respectively, under- and overestimation of presented models; for values of particular concentrations C1, C2 and C3 of all analytes, please refer to the table below)

CA						**IA**		
Triclosan[a]						**Triclosan[a]**		
C1	C2	C3				C1	C2	C3
3.87	3.20	2.52	C1	**[b]Methyl-paraben**	C1	7.02	6.28	5.43
2.71	2.64	1.83	C2		C2	4.70	4.89	3.47
2.64	2.38	1.03	C3		C3	4.90	4.65	1.91
2.91	3.27	2.08	C1	**[c]Buthyl-paraben**	C1	8.06	9.11	6.90
3.33	2.95	1.95	C2		C2	7.26	6.71	5.14
2.61	2.93	0.87	C3		C3	5.34	6.40	2.20
0.62	0.71	0.59	C1	**[d]Diclofenac sodium salt**	C1	1.70	1.48	1.21
0.60	0.59	0.59	C2		C2	1.70	1.27	1.25
0.42	0.58	0.58	C3		C3	1.26	1.33	1.30

[a]Triclosan			[b]Methylparaben			[c]Butylparaben			[d]Diclofenac sodium salt			
C1	C2	C3	C1	C2	C3	C1	C2	C3	C1	C2	C3	
12.5	31.3	50.0	0.45	1.13	1.81	0.039	0.097	0.155	5.8	14.4	23.0	µM

3.2.2. XenoScreen YES-

The estrogenic antagonistic effect (XenoScreen YES-) of triclosan was only slightly impacted by the co-presence of the other analytes tested (Supplementary Table S1). Interestingly, some behavioral trends were noted in which butylparaben moderately impacted the endocrine potential of triclosan at low and medium concentrations based on CA models. IA calculations however showed a tendency of diclofenac to exhibit a certain antagonistic impact, especially at higher concentrations of the drug. Taking into account the most plausible scenario of the independent MOAs of these analytes, it can be concluded that diclofenac does mitigate the YES- based triclosan toxicity.

3.2.3. XenoScreen YAS+

The androgenic agonistic behavior of triclosan mixtures with methyl- and butylparaben were very well modeled with the CA approach, whereas IA modeling values showed antagonistic action for many of these mixtures (MDR values > 2.0) or overestimation (Supplementary Table S2). Interestingly, in the mixture of triclosan with diclofenac, synergy was observed more often with CA modeling (and underestimation), which was confirmed by IA mathematical calculation. At the lowest concentration of triclosan tested, potentiation of synergy with diclofenac was observed, confirming the great threat of these chemicals when present in the environment in combination at concentrations that would otherwise be considered non-toxic on their own.

3.2.4. XenoScreen YAS-

The antagonistic androgenic behavior of triclosan was barely affected by methyl- and butylparabens. No such activity was confirmed in the MDR analysis (Supplementary Table S3), although IA modeling indicated some overestimation results. By contrast, for diclofenac, both overestimation and antagonism were observed in almost all mixtures with triclosan based on the CA model and in all cases calculated with the IA model. This result is of particular interest considering the plausible synergy of such mixtures from the YES+ analysis, demonstrating that triclosan-diclofenac mixtures at environmentally stated levels showed both anti-androgenic and pro-estrogenic activities.

3.3. MTT and LDH assays of Caco-2 and HepG2 cells

Prior to the cytotoxicity testing of xenobiotic mixtures, inhibition curves of each compound were constructed after 24 h of exposure. In accordance with our previous findings summarized above, triclosan again emerged as the most toxic pollutant for both cell lines, with 20% inhibitory concentration (IC_{20}) values of 150 μM and 72 μM for Caco-2 and HepG2 cells, respectively. Based on the IC_{20} value for the discrimination of potential toxic effects and the reliable measurement of potential synergy across mixtures, three triclosan concentrations were defined as C3, C2, and C1, corresponding to 100%, 66%, and 33% of the IC_{20} at 150, 100, and 50 μM for Caco-2 cells, and 72, 48, and 24 μM for HepG2 cells. The inhibition curves revealed non-toxic effects for the other contaminants at the concentrations chosen for triclosan. Therefore, the effects of methylparaben, butylparaben, and diclofenac on triclosan were evaluated in all cases at the same C3, C2, and C1 levels (see the SI) with all possible combinations to determine how these xenobiotics may interact and alter the toxic action of triclosan. HepG2 cells appeared to be the most resistant to the toxic effect of the mixtures at the tested concentrations of xenobiotics (Supplementary Table S4). None of the concentration mixtures showed significant indices of synergy or antagonism based on the MTT assay. Only the binary mixtures of triclosan with butylparaben or diclofenac, all at the highest level (C3), showed a trend towards synergic effects on these cells. This finding is in good agreement with previous results of Rudzok et al. (2010) who reported synergism for the combination of triclosan and diclofenac by MTT assays using both the IA and CA models.

Results of the MTT assay for Caco-2 cells confirmed lack of a clear impact of the parabens studied on the toxicity of triclosan in a binary mixture. In both the CA and IA models, there were no indications of synergy or antagonism (Supplementary Table S5). There was only one case of strong synergy observed when the highest concentrations of triclosan and butylparaben were tested. However, further validation of this result in subsequent studies with a larger number of intervals within the studied range is warranted, as the trends of both the IA and CA models suggest that this behavior is plausible but the abrupt change from lack-of-impact to synergy appears too strong under the tested intervals. Moreover, there were interesting results found for the mixture of triclosan with diclofenac with both the CA and IA models, demonstrating evident cases of underestimation and synergy for the highest concentration of triclosan in combination

with C2 and C3 levels of diclofenac. This further justifies the need of additional studies of the impact of triclosan on these pharmaceuticals at environmentally relevant levels in risk assessment explorations. In fact, a recent study targeting the evaluation of the delayed toxicity during the developmental stage on zebrafish embryos showed that a mixture of 8 pharmaceuticals at their highest environmental concentration levels had an adverse effect on larval behaviour during embryonic development (Zhou et al. 2019). Experiments using each compound alone did not elicit this negative response, stressing the importance of evaluating combinations of compounds.

LDH assays were performed only for the most cytotoxic mixtures according to the previous MTT results; that is, C3 of triclosan mixed with C1, C2, and C3 of both butylparaben and diclofenac. While the MTT test is indicative of cell metabolic activity, the LDH assay can be used as a cell death marker because this cytoplasmic enzyme is released into the surrounding environment when the cell membrane is damaged. For Caco-2 cells, binary mixtures of triclosan and butylparaben showed a strong synergistic effect on cytotoxicity (cell death) as the concentration of the latter pollutant increased, which was in line with the results of the MTT assay (see above). Further, there was no appreciable change of cytotoxicity for mixtures of triclosan with diclofenac at any concentration level of both contaminants. These differences further suggest that the mechanisms of the interaction of butylparaben or diclofenac with triclosan on live cells are somewhat different. Environmental concentrations of diclofenac, methylparaben and butylparaben did not show any effect on the cell toxicity of triclosan at the IC20 value (100%, 66% and 33%). Environmental concentrations were in the range of ng/L (pM) against the IC20 triclosan at the mg/L (μM) level. The range of environmental concentrations selected for the studies is based on the following references: 5.7-62ng/L MP (Jonkers et al. 2010), 0.2-7.1ng/L BP (Jonkers et al. 2010), 60-460ng/L DCF (McEneff et al. 2014).

The combination of triclosan with butylparaben or diclofenac did not show any trend in cell death for the hepatocytes, thus indicating that the behavior of the contaminant mixtures on HepG2 cells is entirely different than that on Caco-2 cells. The experimental results demonstrated a low degree of cell damage for the mixtures of PPCPs, which is in good agreement with the detoxifying ability of hepatocytes towards xenobiotics.

3.4. Liposome tests

The three concentration levels of each of the four investigated xenobiotics were set at 24, 48, and 72 μM, according to the data used above for the cytotoxicity tests, wherein the IC20 value of triclosan for the hepatocyte cell line was 72 μM. Notably, the liposome tests on the mixtures followed the same trends obtained with the MTT assay with Caco-2 cells (Supplementary Table S6), thus indicating the validity of the *in vitro* model. Methyl- and butylparaben showed a negligible impact on the toxicity of triclosan at any of the concentration levels studied (although butylparaben seemed to have a slightly higher relative impact on the toxicity of triclosan than methylparaben). As shown in Table S6, the toxicity of triclosan was strongly affected by diclofenac, mathematically confirming that synergy of such a binary mixture occurs at the highest concentration levels studied.

3.5. CYP expression and apoptosis

Metabolism determines the fate of a compound upon entry in the human body. Among the various drug metabolizing enzymes, cytochrome P450s (CYP450) constitute an important protein family acting in xenobiotic metabolism, which usually converts xenobiotics into safe metabolites. This activity can be detected by an increase in the gene and protein expression. As CYP 450 xenobiotic-metabolizing enzymes are primarily expressed in the liver, HepG2 cells were studied (Burkina et al. 2017). No enhancement in the expression of CYP450 3A4 and CYP450 1A2 was observed for HepG2 cells under the selected experimental conditions (highest concentrations of triclosan, diclofenac, and butylparaben; mixtures of triclosan and diclofenac; and mixtures of triclosan and butylparaben at the levels specified above for HepG2 cells), indicating that the occurrence of these pollutants and their mixtures did not cause the induction of CYP expression. This finding is in good agreement with previous studies demonstrating no effect of triclosan on CYP-mediated metabolism in either HepG2 cells or HepG2/vector cells (Wu et al. 2017).

Apoptosis was observed in some conditions, namely in the presence of the highest concentration of triclosan (46.4% apoptotic cells with triclosan at C3). The presence of butylparaben in combination with triclosan seemed to inhibit apoptosis in an inverse-

concentration-dependent manner. Specifically, similar values for apoptotic cells were found for the highest concentration of butylparaben (46.6%), and the apoptosis frequency decreased when lower concentrations of butylparaben (C1 and C2) were concomitantly present with the highest concentration of triclosan (C3) in the reaction medium (40.1% for C2 butylparaben and 28.4% for C1 butylparaben).

4. Conclusions

Environmental toxicity testing has traditionally mainly focused on the effects of single pollutants only (Wieczerzak et al. 2016b); however, the combinations of common contaminants in a given environment can have very different effects than their independent impacts. The presents study contributes to and expands recent efforts in this field to find the best modeling approaches for describing the impact of compounds (when present in mixtures) in selected bioassays. The need for such comprehensive analyses is becoming increasingly apparent in modern ecotoxicological studies. In the present work, we confirmed a significant impact of selected paraben compounds with varied log P values and diclofenac on the ecotoxicological potential of triclosan, a common antimicrobial agent used in numerous applications. As shown by the MDR analysis of CA and IA models, the type of interaction (or its lack) is mainly dependent on the concentration levels of the various contaminants tested. This justifies the importance of considering results from mixtures in ecotoxicological studies when describing and assessing the environmental impact of chemicals, whereas the majority of previous cytotoxicity tests of triclosan have not considered its impacts in mixtures (Zhang et al. 2019a, Ma et al. 2013, Wang et al. 2019). In fact, such ecotoxicity data of mixtures should be also considered by policy makers and authorities issuing admissible concentration levels of different substances found in everyday products or medications.

Based on our results and a review of the relevant literature, it is clear that ecotoxicity assessments require testing a wide range of concentration levels of various chemicals (e.g., BPA analogues, heavy metals, PPCPs, PAHs) in both their binary mixtures and higher-order combinations. Indeed, mixtures of chemicals clearly behave differently on biological systems than each of the components individually. However, more research is needed in this regard, focusing not only at the levels recorded in different environmental or biological settings but also at lower levels for which no toxicological response would

be theoretically expected within a given timeframe (different for acute or chronic toxicity studies A current trend in this field is the development of fast and accurate online screening methodologies to shorten the response times of currently used bioassays and enable the rapid confirmation of the existence/lack of synergy/antagonism between mixture constituents (and also their degradation products).

The most reliable approach to tackle this problem should involve the development of fast and accurate online screening methodologies to shorten the response times of currently used bioassays and enable the rapid confirmation of the existence/lack of synergy/antagonism between mixture constituents (and their degradation products). The present study provides clear confirmation of the impact of diclofenac, methylparaben, and butylparaben on the toxicity of triclosan to almost all organisms and systems studied, demonstrating that even low concentrations of these contaminants may trigger undesirable effects on organisms of different trophic levels.

Acknowledgments:

Błażej Kudłak is grateful to the National Science Center, Poland, for funding (grant no. 2017/01/X/ST4/00474). Manuel Miró acknowledges financial support from the Ministry of Science, Innovation and Universities (MCIU)-Spanish State Research Agency (AEI) through projects CTM2017-84763-C3-3-R (MCIU-AEI/FEDER, EU) and CTM2017-90890-REDT (MCIU-AEI/FEDER, EU). Miquel Oliver thanks the Government of the Balearic Islands, Conselleria d'Educació, Cultura i Universitats, and the European Social Fund for PhD fellowship allocation (no. FPI/1681/2014). Salette Reis, Sofia Lima, and Marcela Segundo acknowledge funding from FCT/MCTES through PT national funds (UID/QUI/50006/2019).

Polish authors dedicate this work to Prof. Jacek Namieśnik, who unexpectedly passed away on 14.04.2019 and who strongly supported Polish-Spanish scientific cooperation.

References

Abendroth, J.A., Blankenship, E.E., Martin, A.R., Roeth, F.W. 2011. Joint Action Analysis Utilizing Concentration Addition and Independent Action Models. Weed Technology, 25: 436-446. DOI: 10.1614/WT-D-10-00102.1

Aker AM, Ferguson KK, Rosario ZY, Mukherjee B, Alshawabkeh AN, Cordero JF, Meeker JD. The associations between prenatal exposure to triclocarban, phenols and parabens with gestational age and birth weight in northern Puerto Rico. Environ Res. 2019;169:41-51. doi:10.1016/j.envres.2018.10.030.

Alkimin G.D., Daniel D., Frankenbach S., Serodio J., Soares A.V.M.V., Barata C., Nunes B., 2019. Evaluation of pharmaceutical toxic effects of non-standard endpoints on the macrophyte species *Lemna minor* and *Lemna gibba*. Sci. Tot. Environ 657: 926-937.

Allmyr, M., Harden, F., Toms, L. M. L., Mueller, J. F., McLachlan, M. S., Adolfsson-Erici, M., Sandborgh-Englund, G. 2008. The influence of age and gender on triclosan concentrations in Australian human blood serum. Sci. Tot. Environ., 393: 162-167.

Alvarez-Munoz, D., Rodriguez-Mozaz, S., Maulvault, A.L., Tediosi, A., Fernandez-Tejedor, M., van den Huewel, F., Kotterman, M., Marques, A., Brcelo, D. 2015. Occurrence of pharmaceuticals and endocrine disrupting compounds in macroalgaes, bivalves, and fish from coastal areas in Europe. Environ. Research, 143:56-64.

Ates P.S., Unal I., Ustundag U.V., Alturfan A.A., Yigitbasi T., Emekli-Alturfan E., 2018. Methylparaben induces malformations and alterations on apoptosis, oxidant–antioxidant status, *ccnd1* and *myca* expressions in zebrafish embryos. J. Biochem. Mol. Toxicol. 32: 22036.

Backhaus, T., Faust, M., 2012. Predictive environmental risk assessment of chemical mixtures: a conceptual framework. Environ. Sci. Technol. 46: 2564-2573.

Bangham, A. D., De Gier, J., Greville, G. D. 1967. Osmotic properties and water permeability of phospholipid liquid crystals. Chem. Physics Lipids, 1: 225–246.

Belden, J.B., Gilliom, R.J., Lydy, M.J., 2007. How well can we predict the toxicity of pesticide mixtures to aquatic life? Integr. Environ. Assess. 3, 364-372.

Bever, C. S., Rand, A. A., Nording, M., Taft, D., Kalanetra, K. M., Mills, D. A., Breck M.A, Smilowitz J.T., German J.B., Hammock, B. D. 2018. Effects of triclosan in breast milk on the infant fecal microbiome. Chemosphere, 203:467-473.

Bletsou A. A., Jeon J., Hollender J., Archontaki E., Thomaidis N. S. 2015. Targeted and non-targeted liquid chromatography-mass spectrometric workflows for identification of transformation products of emerging pollutants in the aquatic environment. TrAC-Trends Anal. Chem., 66:32-44.

Brown S.E., Sant K.E., Fleischman S.M., Venezia O., Roy M.A., Zhao L., Timme-Laragy A.R. 2018. Pancreatic beta cells are a sensitive target of embryonic exposure to butylparaben in zebrafish (*Danio rerio*). Birth Defects Research, 110:1-16.

Burkina V., Rasmussen M.K., Pilipenko N., Zamaratskaia G., 2017. Comparison of xenobiotic-metabolising human, porcine, rodent, and piscine cytochrome P450. Toxicology, 375: 10-27.

Cesen, M., Ahel, M., Terzic, S., Heath, D.J., Heath, E., 2019. The occurrence of contaminants of emerging concern in Slovenian and Croatian wastewaters and receiving Sava River. Sci. Tot. Environ. 650:2446-2453.

Comeche, A., Martin-Villamil, M., Pico, Y., Varo, I., 2017. Effect of methylparaben in *Artemia franciscana*. Compar. Biochem. Physiol. Part C: Toxicology & Pharmacology 199:98-105.

COMMISSION IMPLEMENTING DECISION (EU) 2018/840 of 5 June 2018 establishing a watch list of substances for Union-wide monitoring in the field of water policy pursuant to Directive 2008/105/EC of the European Parliament and of the Council and repealing Commission Implementing Decision (EU) 2015/495 (Official Journal EU L 141, 7.6.2018, 9-12).

Drugbank, 2019a, https://www.drugbank.ca/salts/DBSALT000466, accessed on 17.03.19

Drugbank, 2019b, https://www.drugbank.ca/drugs/DB14212, accessed on 17.03.19

Drugbank, 2019c, https://www.drugbank.ca/drugs/DB14084, accessed on 17.03.19

Drugbank, 2019d, https://www.drugbank.ca/drugs/DB08604 accessed on 17.03.19

Ericson, H., Thorsen, G., Kumblad, L. 2010. Physiological effects of diclofenac, ibuprofen and propranolol on Baltic Sea blue mussels. Aquatic Toxicol. 99:223–231.

Freitas, R., Coppola, F., Costa, S., Pretti, C., Intorre, L., Meucci, V., Amadeu, A.M.V.M., Sole, M. 2019. The influence of temperature on the effects induced by Triclosan and Diclofenac in mussels. Sci. Tot. Environ. 663:992-999.

Ebele, A.J., Abdullah, M. A-E., Harrad, S., 2017. Pharmaceuticals and personal care products (PPCPs) in the freshwater aquatic environment. Emerging Contaminants, 3: 1-16.

EU 2012, report "Toxicity and Assessment of Chemical Mixtures" of DG Health & Consumers, ISBN 978-92-79-30700-3,doi:10.2772/21444

Fair, P.A., Lee H.-B., Adams, J., Darling, C., Pacepacivius, G., Alaee, M., Bossart, G.D., Henry, N., Muir, D. 2009. Occurrence of triclosan in plasma of wild Atlantic bottlenose dolphins (*Tursiops truncatus*) and in their environment. Environ. Poll. 157: 2248-2254.

Feng, J., Zhao, J., Xi, N., Guo, W., Sun, J. 2019. Parabens and their metabolite in surface water and sediment from the Yellow River and the Huai River in Henan Province: Spatial distribution, seasonal variation and risk assessment. Ecotoxicol. Environ. Saf. 172:480-487.

Freitas R, Coppola F, Costa S, Manzini C, Intone L, Meucci V, Soares A, Pretti C, Sole M. Does salinity modulates the response of Mytilus galloprovincialis exposed to triclosan and diclofenac? Environ Pollut. 2019;251:756-65. doi:10.1016/j.envpol.2019.04.115.

Gao, Y., Feng, J., Kang, L., Xu, X., Zhu, L. 2018, Concentration addition and independent action model: Which is better in predicting the toxicity for metal mixtures on zebrafish larvae, Sci. Tot. Environ. 610-611, 442-450.

Grabicova, K., Grabic, R., Blaha, M., Kumar, V., Cerveny, D., Fedorova, G., Randak, R. 2015. Presence of pharmaceuticals in benthic fauna living in a small stream affected by effluent from a municipal sewage treatment plant. Wat. Research, 72: 145-153.

Hadrup, N., Taxvig, C., Pedersen, M., Nellemann, C. L., Hass, U., & Vinggaard, A. M. (2013). Concentrationaddition, independent action and generalized concentration addition models for mixture effect prediction of sexhormone synthesis in vitro. PloS One, 8(8) https://doi.org/10.1371/journal.pone.0070490

Hope, M. J., Bally, M. B., Webb, G., Cullis, P. R. 1985. Production of Large Unilamellar Vesicles by a Rapid Extrusion Procedure Characterization of Size Distribution, Trapped Volume and Ability to Mantain a Membrane-Potential. Biochim. Biophys. Acta, Biomembr. 812: 55−65.

Huebner, M., Weber, E., Niessner, R., Boujday, S., Knopp, D. 2015. Rapid analysis of diclofenac in freshwater and wastewater by a monoclonal antibody-based highly sensitive ELISA. Anal. Bioanal. Chem. 407:8873–8882.

Islas-Flores, H., Gomez-Olivan, L.M., Galar-Martinez, M., Colin-Cruz, A., Neri-Cruz, N., Garcia-Medina, S. 2013. Diclofenac-induced oxidative stress in brain, liver, gill and blood of common carp (*Cyprinus carpio*). Ecotoxicol. Environ. Saf. 92:32–38.

Jeong, Y., Xue, J., Park, K.J., Kannan, K., Moon, H.-B., 2019. Tissue-specific accumulation and body burden of parabens and their metabolites in small cetaceans. Environ. Sci. Technol. 53:475−481.

Jonkers, N., Sousa, A., Galante-Oliveira, S., Barroso, C.M., Kohler, H.-P.E., Giger, W., 2010. Occurrence and sources of selected phenolic endocrine disruptors in Ria de Aveiro, Portugal. 17: 834-843.

Karwacka A, Zamkowska D, Radwan M, Jurewicz J. Exposure to modern, widespread environmental endocrine disrupting chemicals and their effect on the reproductive potential of women: an overview of current epidemiological evidence. Hum Fertil. 2019;22(1):2-25. doi:10.1080/14647273.2017.1358828.

Kudłak, B., Wieczerzak, M., & Namieśnik, J. 2019. Bisphenols (A, S, and F) affect the basic hormonal activity determined for pharmaceuticals–Study of *Saccharomyces cerevisiae*. Environ. Poll. 246: 914-920.

Kung, T.A., Lee, S.H., Yang, T.C., Wang, W.H. 2018. Survey of selected personal care products in surface water of coral reefs in Kenting National Park, Taiwan. Sci. Tot. Environ. 635:1302-1307.

La Farre, M., Perez, S., Kantiani, L., Barcelo, D., 2008. Fate and toxicity of emerging pollutants, their metabolites and transformation products in the aquatic environment. TrAC – Trends Anal. Chem., 27:991-1007.

Lee, H. R., Hwang, K. A., Nam, K. H., Kim, H. C., Choi, K. C. 2014. Progression of breast cancer cells was enhanced by endocrine-disrupting chemicals, triclosan and octylphenol, via an estrogen receptor-dependent signaling pathway in cellular and mouse xenograft models. Chem. Res. Toxicol., 27: 834-842.

Liu, L., Liu, S.-S., Yu, M., Zhang, J., Chen, F. 2015. Concentration addition prediction for a multiple-component mixture containing no effect chemicals. Anal. Methods. 23: 9912–9917.

Lonappan, L., Brar, S. K., Das, R. K., Verma, M., Surampalli, R. Y. 2016. Diclofenac and its transformation products: environmental occurrence and toxicity-a review. Environ. Int., 96:127-138.

Lorenzo M., Campo J., Pico Y., 2018. Analytical challenges to determine emerging persistent organic pollutants in aquatic ecosystems. TrAC Trends in Analytical Chemistry, 103:137-155.

Lu, S., Wang, N., Ma, S., Hu, X., Kang, L., Yu, Y. 2019. Parabens and triclosan in shellfish from Shenzhen coastal waters: Bioindication of pollution and human health risks. Environ. Poll. 246:257-263.

Ma, H., Zheng, L., Li, Y., Pan, S., Hu, J., Yu, Z., Zhang, G., Sheng, G., Fu J. 2013. Triclosan reduces the levels of global DNA methylation in HepG2 cells. Chemosphere 90:1023-1029.

Ma, X., Wan, Y., Wu, M., Xu, Y., Xu, Q., He, Z., Xia W., 2018. Occurrence of benzophenones, parabens and triclosan in the Yangtze River of China, and the implications for human exposure, Chemosphere 213: 517-525.

Marugán, J., Bru, D., Pablos, C., Catalá, M. 2012. Comparative evaluation of acute toxicity by Vibrio fischeri and fern spore based bioassays in the follow-up of toxic chemicals degradation by photocatalysis. J. Haz. Mat., 213:117-122.

Maske, P., Dighe, V., Vanage, G. 2018. n-butylparaben exposure during perinatal period impairs fertility of the F1 generation female rats. Chemosphere, 213:114-123.

Mersch-Sundermann, V., Knasmüller, S., Wu, X. J., Darroudi, F., Kassie, F. 2004. Use of a human-derived liver cell line for the detection of cytoprotective, antigenotoxic and cogenotoxic agents. Toxicol. 198: 329–340.

McEneff, G., Barron, L., Kelleher, B., Paull, B., Quinn, B., 2014. A year-long study of the spatial occurrence and relative distribution of pharmaceutical residues in sewage effluent, receiving marine waters and marine bivalves. Sci. Tot. Environ. 476-477:317-326.

Motia, S., Tudor, I. A., Ribeiro, P. A., Raposo, M., Bouchikhi, B., El Bari, N., 2019. Electrochemical sensor based on molecularly imprinted polymer for sensitive triclosan detection in wastewater and mineral water, Sci. Tot. Env. 664: 647-658.

Nkoom, M., Lu, G., Lui, J., Dong, H., Yang, H. 2019. Bioconcentration, behavioral, and biochemical effects of the non-steroidal anti-inflammatory drug diclofenac in *Daphnia magna*. Environ. Sci. Poll. Res. 26:5704–5712.

Okubo, T., Yokoyama, Y., Kano, K., & Kano, I. 2001. ER-dependent estrogenic activity of parabens assessed by proliferation of human breast cancer MCF-7 cells and expression of ERα and PR. Food Chem. Toxicol., 39:1225-1232.

Oliver, M., Bauzá, A., Frontera, A., and Miró, M. 2016. Fluorescent lipid nanoparticles as biomembrane models for exploring emerging contaminant bioavailability supported by density functional theory calculations. Environ. Sci. Technol., 50:7135-7143.

Parasassi, T., F. Conti, and E. Gratton. 1986. Time-resolved fluorescence emission spectra of Laurdan in phospholipid vesicles by multifrequency phase and modulation fluorometry. Cell. Mol. Bio. 32: 103-108.

Parasassi, T., De Stasio, G., Ravagnan, G., Rusch, R. M., Gratton, E., 1991. Quantitation of lipid phases in phospholipid vesicles by the generalized polarization of Laurdan fluorescence. Biophys. J. 60: 179−189.

Peng, F.-J., Hu, L.-X., Pan, Ch.-G., Ying, G.-G., van den Brink, P.J. 2019. Insights into the sediment toxicity of personal care products to freshwater oligochaete worms using Fourier transform infrared spectroscopy. Ecotox. Env. Safety. 172: 296-302.

Perez, A. L., Sylor, D., Anderle, M., Slocombe, A. J., Lew, M. G., Unice, K. M., & Donovan, E. P., 2013. Triclosan occurrence in freshwater systems in the United States (1999–2012): A meta-analysis. Environ. Toxicol. Chem., 32: 1479-1487.

Petrie, B., Youdan, J., Barden, R., Kasprzyk-Hordern, B. (2016). Multi-residue analysis of 90 emerging contaminants in liquid and solid environmental matrices by ultra-high-performance liquid chromatography tandem mass spectrometry. J. Chrom. A, 1431:64-78.

Pico, Y., Belenguer, V., Corcellas, C., Diaz-Cruz, MS., Eljarrat, E., Farré, M., Gago-Ferrero, P., Huerta, B., Navarro-Ortega, A., Petrovic, M., Rodríguez-Mozaz, S., Sabater, L., Santín, G., Barcelo, D. 2019. Contaminants of emerging concern in freshwater fish from four Spanish Rivers. Sci. Tot. Env. 659: 1186-1198.

Pollack AZ, Mumford SL, Krall JR, Carmichael AE, Sjaarda LA, Perkins NJ, Kannan K, Schisterman EF. Exposure to bisphenol A, chlorophenols, benzophenones, and parabens in relation to reproductive hormones in healthy women: A chemical mixture approach. Environ Int. 2018;120:137-44. doi:10.1016/j.envint.2018.07.028.

Reemtsma, T.; Berger, U.; Arp, H. P. H.; Gallard, H.; Knepper, T. P.; Neumann, M.; Quintana, J. B.; de Voogt, P. 2016. Mind the gap: persistent and mobile organic compounds water contaminants that slip through. Environ. Sci. Technol. 50:10308−10315.

Richardson, S.D., Ternes, T.A., 2014. Water analysis: emerging contaminants and current issues. Anal. Chem., 86: 2813-2848.

Richardson, S. D., Kimura, S. Y. 2016. Water Analysis: Emerging Contaminants and Current Issues. Anal. Chem. 88:546−582.

Richardson, S. D., Kimura, S. Y. 2017. Emerging environmental contaminants: Challenges facing our next generation and potential engineering solutions. Environ. Technol. Innovation, 8: 40−56.

Richardson, S. D., Ternes, T. A. 2018. Water analysis: Emerging contaminants and current issues. Anal. Chem. 90:398−428.

Richmond, E. K., Grace, M. R., Kelly, J. J., Reisinger, A. J., Rosi, E. J., Walters, D. M. (2017). Pharmaceuticals and personal care products (PPCPs) are ecological disrupting compounds (EcoDC). Elem. Sci. Anth., 5:66.

Rudzok, S., Schlink U., Herbarth O., Bauer M., 2010. Measuring and modeling of binary mixture effects of pharmaceuticals and nickel on cell viability/cytotoxicity in the human hepatoma derived cell line HepG2. Toxicol. App. Pharmacol., 244: 336-343.

Schnoor, J. L. 2014. Re-emergence of emerging contaminants. Environ. Sci. Technol. 48: 11019−11020.

Silva, D.C., Serrano, L., Oliveira, T.M.A., Mansano, A.S., Almeida, E.A., Vieira, E.M. 2018. Effects of parabens on antioxidant system and oxidative damages in Nile tilapia (*Oreochromis niloticus*). Ecotoxicol. Environ. Saf. 162:85–91.

Wang, L., Mao, B., He, H., Zhong, Y., Yu, Z., Yang, Y., Li, H., An, J. 2019. Comparison of hepatotoxicity and mechanisms induced by triclosan (TCS) and methyl-triclosan (MTCS) in human liver hepatocellular HepG2 cells. Toxicol. Res. DOI: 10.1039/C8TX00199E

Wieczerzak, M., Kudłak, B., Yotova, G., Nedyalkova, M., Tsakovski, S., Simeonov, V., Namieśnik, J., 2016a. Modeling of pharmaceuticals mixtures toxicity with deviation ratio and best-fit functions models. Sci. Tot. Environ., 571:259-268.

Wieczerzak, M., Namieśnik, J., Kudłak, B., 2016b, Bioassays as one of the Green Chemistry tools for assessing environmental quality: A review, Env. Int., 94:341-361.

Wu, Y., Chitranshi, P., Loukotková, L., da Costa, G.G., Beland, F.A., Zhang, J., Fang J.-L., 2017. Cytochrome P450-mediated metabolism of triclosan attenuates its cytotoxicity in hepatic cells. Archives of Toxicol., 91: 2405–2423.

Xie, Z., Lu, G., Yan, Z., Liu, J., Wang, P., Wang, Y., 2017. Bioaccumulation and trophic transfer of pharmaceuticals in food webs from a large freshwater lake. Environ. Poll., 222:356-366.

Xin, X., Huang, G., Liu, X., An, Ch., Yao, Y., Weger, H., Zhang, Chen X., 2017. Molecular toxicity of triclosan and carbamazepine to green algae Chlorococcum sp.: A single cell view using synchrotron-based Fourier transform infrared spectromicroscopy. Environ. Poll., 226: 12-20.

Zhang, H., Shao, X., Zhao, H., Li, X., Wei, J., Yang, Ch., Cai, Z. 2019a. Integration of Metabolomics and Lipidomics Reveals Metabolic Mechanisms of Triclosan-Induced Toxicity in Human Hepatocytes. Environ. Sci. Technol. 53:5406-5415.

Zhang, Y. Guo, J., Yao, T., Zhang, Y., Zhou, X., Chu, H. 2019b. The influence of four pharmaceuticals on *Chlorella pyrenoidosa* culture. Scientific Reports 9:1624.

Zhou, S., Chen, Q., di Paolo, C., Shao, Y., Hollert, H., Seiler, T.-B., 2019. Behavioral profile alterations in zebrafish larvae exposed to environmentally relevant concentrations of eight priority pharmaceuticals. Sci. Tot. Environ. 664: 89-98.

6.2.1. Información suplementaria (supplementary information)

A continuación, se detalla la información relativa al artículo original enviado para su publicación.

Supporting information for article

Ecotoxicological equilibria of triclosan in Microtox, XenoScreen YES/YAS, Caco2, HEPG2 and liposomal systems are affected by the occurrence of other pharmaceutical and personal care emerging contaminants

Miquel Oliver [1], Błażej Kudłak[2*], Monika Wieczerzak[2], Salette Reis[3], Sofia Lima[3], Marcela Segundo[3], Manuel Miró[1]

[1] Department of Chemistry, University of the Balearic Islands, Carretera de Valldemossa km 7,5, E-07122 Palma de Mallorca, Illes Balears, Spain

[2]Department of Analytical Chemistry, Faculty of Chemistry, Gdańsk University of Technology, 11/12 Narutowicza Str., Gdańsk 80-233, Poland

[3] LAQV, REQUIMTE, Department of Chemistry, Faculty of Pharmacy, University of Porto, R Jorge Viterbo Ferreira, 228, 4050-313 Porto, Portugal

**Corresponding Author: blakudla@pg.edu.pl, ORCID 0000-0002-2237-2927*

1. Data for XenoScreen YES/YAS

Concentration levels of analytes studied during research with XenoScreen YES/YAS assay												
Triclosan[a]			Methylparaben[b]			Butylparaben[c]			Diclofenac sodium salt[d]			
C1	C2	C3	C1	C2	C3	C1	C2	C3	C1	C2	C3	
12.5	31.3	50.0	0.45	1.13	1.81	0.039	0.097	0.155	5.8	14.4	23.0	µM

Supplementary Table 1. MDR values variations depending on triclosan concentration change for solutions of selected parabens and diclofenac studied with XenoScreen YES- (MDR values >2.0 exhibit antagonism, MDRs < 0.5 show synergism, MDR values within 0.50-0.71 and 1.40-2.00 values mean, respectively, under- and overestimation of presented models, for values of particular concentrations C1, C2 and C3 of all analytes please refer to table above)

CA						**IA**		
[a]Triclosan						**[a]Triclosan**		
C1	C2	C3				C1	C2	C3
0.80	0.81	0.92	C1	**[b]Methyl-paraben**	C1	1.45	1.51	1.74
0.88	0.90	1.00	C2		C2	1.56	1.62	1.84
0.79	0.91	0.85	C3		C3	1.42	1.65	1.57
0.70	0.79	0.86	C1	**[c]Buthyl-paraben**	C1	1.48	1.64	1.72
0.70	0.82	0.98	C2		C2	1.48	1.76	2.06
0.84	0.86	0.93	C3		C3	1.78	1.83	1.92
0.94	1.17	1.01	C1	**[d]Diclofenac sodium salt**	C1	1.65	1.97	1.74
1.23	1.18	1.23	C2		C2	2.28	2.10	2.23
1.18	1.29	0.94	C3		C3	2.09	2.18	1.62

Supplementary Table 2. MDR values variations depending on triclosan concentration change for solutions of selected parabens and diclofenac studied with XenoScreen YAS+ (MDR values >2.0 exhibit antagonism, MDRs <0.5 show synergism, MDR values within 0.50-0.71 and 1.40-2.00 values mean, respectively, under- and overestimation of presented models, for values of particular concentrations C1, C2 and C3 of all analytes please refer to table above)

CA						**IA**		
[a]Triclosan						**[a]Triclosan**		
C1	C2	C3				C1	C2	C3
1.19	0.91	0.76	C1	**[b]Methyl-paraben**	C1	2.33	1.88	1.52
1.09	1.01	0.92	C2		C2	1.94	2.00	1.80
1.03	0.96	1.06	C3		C3	1.80	1.90	2.05
0.87	1.08	0.74	C1	**[c]Buthyl-paraben**	C1	1.84	2.05	1.44
0.98	0.94	0.78	C2		C2	2.02	1.83	1.56
0.79	0.86	1.01	C3		C3	1.57	1.67	1.95
0.19	0.55	0.55	C1	**[d]Diclofenac sodium salt**	C1	0.51	1.07	1.08
0.36	0.58	0.32	C2		C2	1.00	1.18	0.64
0.37	0.62	0.62	C3		C3	1.15	1.38	1.38

Supplementary Table 3. MDR values variations depending on triclosan concentration change for solutions of selected parabens and diclofenac studied with XenoScreen YAS- (MDR values >2.0 exhibit antagonism, MDRs <0.5 show synergism, MDR values within 0.50-0.71 and 1.40-2.00 values mean, respectively, under- and overestimation of presented models, for values of particular concentrations C1, C2 and C3 of all analytes please refer to table above)

CA						**IA**		
[a]Triclosan						**[a]Triclosan**		
C1	C2	C3				C1	C2	C3
0.99	0.96	0.92	C1	**[b]Methyl-paraben**	C1	1.88	1.88	1.81
0.99	0.99	0.96	C2		C2	1.79	1.85	1.82
1.01	0.98	1.00	C3		C3	1.84	1.82	1.88
0.95	0.97	0.91	C1	**[c]Buthyl-paraben**	C1	1.90	2.00	1.88
0.95	0.93	0.92	C2		C2	1.84	1.95	1.91
0.93	0.96	1.18	C3		C3	1.75	1.96	2.40
1.16	1.25	1.18	C1	**[d]Diclofenac sodium salt**	C1	2.32	2.36	2.28
1.31	1.41	1.32	C2		C2	2.38	2.43	2.31
1.93	2.23	2.12	C3		C3	3.11	3.34	3.17

2. Data for MTT assay with HEPG2 cells

Supplementary Table 4. MDR values variations depending on triclosan concentration change for solutions of selected parabens and diclofenac studied with MTT of HEPG2 cells (MDR values >2.0 exhibit antagonism, MDRs <0.5 show synergism, MDR values within 0.50-0.71 and 1.40-2.00 values mean, respectively, under- and overestimation of presented models, for values of particular concentrations C1, C2 and C3 of all analytes please refer to table below)

CA						**IA**		
Triclosan						**Triclosan**		
C1	C2	C3				C1	C2	C3
1.01	0.95	0.93	C1	**Methylparaben**	C1	0.99	0.89	0.78
1.01	0.92	0.91	C2		C2	1.00	0.88	0.78
0.99	0.91	0.89	C3		C3	0.98	0.88	0.79
0.96	0.97	0.85	C1	**Buthylparaben**	C1	0.97	0.91	0.80
0.98	0.93	0.81	C2		C2	0.99	0.89	0.78
0.98	0.89	0.76	C3		C3	0.99	0.86	0.73
0.98	0.99	1.00	C1	**Diclofenac sodium salt**	C1	0.99	0.93	0.94
1.00	0.97	0.79	C2		C2	1.01	0.93	0.92
0.98*	0.93*	0.77*	C3		C3	0.99	0.90	0.87

* - data inconclusive, studies to be repeated in more split ranges.

Triclosan			Methylparaben			Butylparaben			Diclofenac sodium salt			
C1	C2	C3	C1	C2	C3	C1	C2	C3	C1	C2	C3	
24,0	48.0	72.0	24,0	48.0	72.0	24,0	48.0	72.0	24,0	48.0	72.0	µM

3. Data for MTT assay with Caco2 cells

Supplementary Table 5. MDR values variations depending on triclosan concentration change for solutions of selected parabens and diclofenac studied with MTT of Caco2 cells (MDR values >2.0 exhibit antagonism, MDRs <0.5 show synergism, MDR values within 0.50-0.71 and 1.40-2.00 values mean, respectively, under- and overestimation of presented models, for values of particular concentrations C1, C2 and C3 of all analytes please refer to table below)

CA						**IA**		
Triclosan						**Triclosan**		
C1	C2	C3				C1	C2	C3
1.04	1.02	0.99	C1	**Methyl-paraben**	C1	1.05	0.96	0.94
1.06	1.00	0.95	C2		C2	1.08	0.96	0.91
1.05	1.00	0.89	C3		C3	1.03	0.95	0.85
0.99	0.94	1.01	C1	**Buthyl-paraben**	C1	0.99	0.88	0.95
1.10	0.90	0.92	C2		C2	1.05	0.84	0.86
1.05	0.95	0.38*	C3		C3	1.00	0.88	0.35*
0.93	1.05	0.74	C1	**Diclofenac sodium salt**	C1	0.95	0.99	0.70
1.05	1.06	0.51	C2		C2	1.06	1.01	0.49
1.02	0.95	0.25	C3		C3	1.04	0.92	0.24

* - data inconclusive. studies to be repeated in more split ranges to confirm the trend to synergy

Triclosan			Methylparaben			Butylparaben			Diclofenac sodium salt			
C1	C2	C3	C1	C2	C3	C1	C2	C3	C1	C2	C3	
49.5	99.0	150.0	49.5	99.0	150.0	49.5	99.0	150.0	49.5	99.0	150.0	µM

4. Data for lyposomes studies

Supplementary Table 6. MDR values variations depending on triclosan concentration change for solutions of selected parabens and diclofenac studied with lyposomes (MDR values >2.0 exhibit antagonism. MDRs <0.5 show synergism. MDR values within 0.50-0.71 and 1.40-2.00 values mean, respectively, under- and overestimation of presented models, for values of particular concentrations C1, C2 and C3 of all analytes please refer to table below)

CA						**IA**		
Triclosan						**Triclosan**		
C1	C2	C3				C1	C2	C3
0.90	0.91	1.02	C1	**Methyl-paraben**	C1	0.82	0.79	0.78
0.85	0.87	0.89	C2		C2	0.80	0.78	0.73
0.89	0.87	0.91	C3		C3	0.85	0.80	0.77
0.89	0..92	0.91	C1	**Buthyl-paraben**	C1	0.80	0.77	0.71
0.91	0.86	0.89	C2		C2	0.82	0.74	0.73
0.86	0.88	0.87	C3		C3	0.78	0.77	0.73
0.88	0.82	0.69	C1	**Diclofenac sodium salt**	C1	0.80	0.70	0.53
0.85	0.74	0.59	C2		C2	0.79	0.65	0.48
0.80	0.75	0.47	C3		C3	0.74	0.68	0.40

Triclosan			Methylparaben			Butylparaben			Diclofenac sodium salt			
C1	C2	C3	C1	C2	C3	C1	C2	C3	C1	C2	C3	
24.0	48.0	72.0	49.5	99.0	150.0	49.5	99.0	150.0	49.5	99.0	150.0	µM

5. Methodology and reagents of performing:

5.1. Microtox® assay

The Microtox® test acute reagent (lyophilized bacterium *Vibrio fischeri*), OAS - osmotic adjustment solution (22% solution of sodium chloride), RS - reconstitution solution and diluent (2% solution of sodium chloride) were purchased from Modern Waters (USA). The study was conducted using Microtox® analyzer model 500 (M500). Apparatus is equipped with 30 incubation wells, reagent (bacterial suspensions) well and read well. Temperatures are assigned to the corresponding type of performed test and the internally maintained at 5.5 ± 1.0 °C for reagent well and 15.0 ± 0.5 °C for both the incubation part and the read well.

To determine effective concentration (e.g. EC_{50}, EC_{20} or NOEC) for each model compound, a range screening test was performed first. Each of the solutions of model compounds ware tested in fourteen serial dilution of the original stock and in duplicate for every compound using standard protocol 81.9% basic acute Microtox® test. Lyophilized reagent with *Vibrio fischeri* bacteria was hydrated with 1 mL of RS and maintained at 5.5 ± 1.0 °C to make a primary stock suspension of bacteria. Subsequently, 100 µL of the bacterial suspension (150 µL of the primary bacterial stock diluted in 1500 µL of diluent) and a pre-made samples of standard dissolved in distilled water were added to the first vial. To produce a suitable osmotic pressure (above 2%), OAS was added to the vial with the highest concentration, and proper dilutions were prepared. The incubation time of the samples with bacteria for all of the tests was 30 min according to the Microtox® basic test protocol.

After range finding tests (narrowing the concentration range studied) the effective concentration were determine using early mentioned protocol with the difference that test was performed in four serial dilutions for each original stock in three replicates for each compound. EC_{50} parameter for diclofenac (sodium salt), triclosan, methylparaben, butylparaben were calculated based on the dose-response plot equation.

In order to determine whether the addition of one substance to solution of another one would change the toxic effect, concentrated solutions of the compounds were prepared. Test mixtures were prepared in such a way that the compounds were present in an appropriate ratio respectively 100% 66% or 33% of effective concentration of first model substance and the second substance with a 100%, 66% and 33% of its

EC_{50} in different ratios. Incubation time of samples with bacteria for all of the tests was 30 min according to the test protocol. Every batch of Microtox acute reagent was studied against reference chemicals (namely, phenol, copper sulphate, 3,5-dichlorophenol) and in all cases the toxicity values were within the range of certificates provided by the manufacturer.

5.2.XenoScreen YES/YAS

A set of XenoScreen YES/YAS reagents was purchased from Xenometrix AG (Allschwil, Switzerland), namely, a vial with hERα (YES) yeasts (to determine oestrogenic activity) and hARα (YAS) *Saccharomyces cerevisiae* yeasts (to determine androgenic activity) immobilized on the filtration paper, basal medium, vitamin solution, L-aspartic acid solution, L-threonine solution, CuSO4 solution, 5α-dihydrotestosterone (DHT, YAS+ (agonist) control), 4-hydroksytamoxyphene (HT, YES- (antagonist) control), and flutamide (FL, YAS- (antagonist) control). 17β-estradiol (E2, YES+ (agonist) (CAS no. 50-28-2), dimethyl sulphoxide (DMSO, biological purity (CAS no. 67-68-5)) and chlorophenol red-β-D-galactopyranoside dye (CPRG, biological purity (CAS no. 99792-79-7)) were purchased from Sigma Aldrich (Darmstadt, Germany). Measurements of OD_{690} cell density (wavelength 690 nm) and of the intensity of the CPRG transformation product OD_{570} (wavelength 570 nm) were performed with a TECAN Infinite M200 spectrophotometer. OD values of yeasts cultures exposed to reference materials (controls) were used to determine regularity and stability of cultured media containing yeasts and subsequently diluted to perform studies.

A slightly modified protocol for XenoScreen YES/YAS® has been utilized for the investigation of the endocrine potential of binary mixtures. The yeast cells were cultured from the filter papers in growth medium (basic medium with a vitamin solution and a solution of L-threonine, L-aspartic acid and copper (II) sulphate (VI)). Then, 5 mL of growth medium was transferred to labelled culture bottles with caps with a gas permeable filter. Afterwards, the yeast disks were sterilely transferred and placed on an orbital shaker set at 32 °C and 100 rpm for 48 hours. Test plates were prepared in such a way that the controls were in duplicate in eight serial dilutions of E2, HT, DHT and FL for YES+, YES-, YAS+ and YAS-, respectively for calculation of EC_{50} values:

- YES agonist (YES+) plate E2 in DMSO (min. concentration $1x10^{-11}$ M, max. concentration $1x10^{-8}$ M),

- YES antagonist (YES-) plate HT in DMSO (min. concentration $1x10^{-8}$ M, max. concentration $1x10^{-5}$ M; additionally, in the entire plate, E2 was kept at a constant concentration of $1x10^{-9}$ M),

- YAS agonist (YES+) plate DHT in DMSO (min. concentration $1x10^{-9}$ M, max. concentration $1x10^{-6}$ M),

- YAS antagonist (YAS-) plate FL in DMSO (min. concentration $1x10^{-7}$ M, max. concentration $1x10^{-4}$ M; additionally, in the entire plate, DHT was kept at a constant concentration of $3x10^{-8}$ M).

The addition of E2 or DHT present at the same concentration as the entire YES or YAS antagonist plate, respectively, is intended to examine (confirm/deny) the andro- and estrogenic antagonistic activity of samples. A substance with the antagonist properties competes with E2 or DHT present on the plate and binds to the receptor without inducing the expression of β-galactosidase. Without the enzyme, substrate staining does not occur. However, if the test sample does not contain antagonistic substances, then E2 or DHT available in the wells bind the receptor, and express β-galactosidase. Thus, the staining of the substrate occurs. To determine whether the addition of selected substances to the triclosan solutions would affect the endocrine potential, preconcentrated solutions of analytes were prepared. The study of the effects of analytes on the toxicity of the triclosan was carried out at three concentration levels (listed for each substance at the bottom of Table 4 of main text and at the beginning of subchapter 1 of this electronic supplement).

20 µL of binary mixtures and 80 µL of 20 mM CRPG dye were added to each assay well. Studied pharmaceuticals, parabens and hormones were mixed in three concentration ratios in such a way as to detect a broad range of possible interactions. All of the studies on mixtures were performed in triplicate; furthermore, controls were made for pure substances in duplicate, YES and YAS suspensions of yeast cultures (100 µL; yeast cell density >0.3 OD_{690}) were added into agonist and antagonist YES and YAS plates, respectively. Assay plates were sealed with semi-permeable membranes and placed in the bag zipper moistened with watered gauze on an orbital shaker for 48 h at

32 °C and 100 rpm. After 48 h of incubation, a cell density determined by OD was read at a wavelength of 690 nm and the colour intensity at a wavelength of 570 nm was determined. Afterwards, the activity of β-galactosidase was calculated as the ratio of $\frac{(OD_{570}-OD_{690})}{OD_{690}}$.

CAPÍTULO 7. CONCLUSIONES

.

In this work, several analytical tools have been established in order to evaluate the membranotropic effects, potential bioavailability and toxicity of recurrent emerging contaminants (ECs) in environmental samples and foodstuff. The use of liposomes, as biorelevant surrogates of eukaryotic cells, has been the driving force of the entire thesis.

The interaction regions within the membrane and the degree of penetration and distribution across the lipid bilayer of two membrane fluorescent probes and several ECs have been investigated into a natural model of phospholipid bilayer constituted of soy phosphatidylcholine. In particular, we have selected model compounds that are representative of four different classes of emerging contaminants in environmental compartments with distinct physicochemical properties: (i) parabens group as a model of preservatives; (ii) triclosan (TCS) as an anti-microbial agent; (iii) diclofenac (DCF) as a model of non-steroidal anti-inflammatory drug; and (iv) bisphenol A as a plastic additive, and compared with chlorpyrifos (CPF) as a legacy overused insecticide.

Unprecedentedly, a new multidisciplinary approach involving a combination of empirical data based on molecular fluorescence using membrane probes and ^{1}H-NMR experiments along with molecular dynamic simulations and Density Functional Theory (DFT) calculations is proposed to predict *in-vitro* contaminant distribution across membranes and related parameters as bioaccumulation and toxicity. Our simple, fast and cost-effective *in vitro* method based on fluorescence generalized polarization or anisotropy measurements for testing membranotropic effects offers a suitable proxy for end points of concern with no need of laborious and time-consuming *in vivo* testing protocols informing about membrane changes including phospholipid order, lipid packing and fluidity. The molecular dynamic simulations have corroborated the fact that the lipid bilayer is a highly dynamic structure and that the contaminants might move freely within a wider or restricted region of the membrane. ^{1}H-NMR assignment allowed us to map the interaction region between the 18:2 phospholipid molecules that constitute the liposomes and each contaminant at the atomic level. Furthermore, DFT calculations could evaluate both the interaction energies and the geometries of the complexes between each compound and contiguous phospholipids within the membrane.

Our holistic approach carried out on chapters 3 and 4 has demonstrated that ionic compounds, such as DCF at physiological pH, are not able to penetrate into the lipid bilayer at a large extent, whereas CPF has the ability to do so and move rapidly across the hydrophobic region. While the results for some xenobiotics are somehow unambiguous among all different theoretical and empirical approximations, some uncertainties appear with certain ECs – liposome interactions. An interesting issue is that the interaction with the alkyl chains of the phospholipids induces a coplanarity of the aromatic rings in TCS, thus facilitating the permeability across the lipid membrane and thus is able to compensate the energy required to separate the chains of two contiguous phospholipids. But at the same time, TCS seems to bind partially to the choline polar group of the phosphatidylcholine.

Despite the versatility and facility of obtaining fluorescence data for the two-state assumption of the membrane phase state (gel or liquid crystalline phase), the selection of a suitable maximum emission wavelength for each membrane probe is difficult, because the emission spectra is dependent on both the lipid species and membrane morphology. In addition, the multiple excitation states of Laurdan and many factors that do affect the heterogeneity of Laurdan complicate the analysis and the interpretation of data. RMN experiments are very accurate but have limited sensitivity and need long time of operation and data processing; hence large concentrations of analytes and also sophisticated instrumentation are required. Molecular dynamic simulations provide interesting information about the most probable location of every individual compound into the bilayer, but the model is in fact a simplification of the real soy phosphatidylcholine liposome because only one type of phospholipid with two different chains was used. Therefore, the properties of the computational membrane would be not exactly the same than those of the experimental liposome membrane. In the case of DFT calculations, reliable information on energy interactions is obtained but the huge amount of data that the computational program has to manage limits the actual number of atoms to be included in the simulation, thus hampering the realistic mimic of a bilayer fragment. Calculations of non-covalent 1:1 complexes are quite far from real interactions into the membrane.

All these observations reinforce the idea that a multidimensional approach to tackle the complexity of lipid bilayers that mimic cell membranes is needed in order to avoid

misleading interpretations of membranotropic effects of ECs when only one approach is used.

The data provided by generalized polarization and anisotropy fluorescent measurements confirmed that the level of hydration and fluidity were higher for those liposomes used in the chapter 3 compared to those in the chapter 4. In fact, liposomes in chapter 3, known as transfersomes, kindly provided by Enoc Solutions, were synthetized with additional ingredients such as ethanol and surfactants, apart from soy phosphatidylcholine, for increasing the permeability through intact skin thanks to the highly deformable membrane. Liposomes from chapter 4 however were simple lipid vesicles constituted of only one component, that is, soy phosphatidylcholine.

The idea behind building an intelligent flow methodology for investigation of liposome-EC interactions was to set a rugged method for high-throughput assays. The fully automated fluidic system allowed the unattended investigation of membranotropic effects of ECs on different liposomes and the *in-vitro* potential toxicant action of these xenobiotics on the cell membrane. The performance of the flow setup was exemplified by characterizing the phospholipid packing and order of soy PC liposomes with varying amounts of cholesterol, and the changes induced on the membrane by the incorporation of different contaminants. For this purpose, on-line fluorescence measurements were acquired in order to calculate the generalized polarization in a flow-through format. The smart fluidic method featured real-time acquisition of fluorescence readouts, data processing and feedback in a fully unsupervised mode with a high degree of reproducibility (<1.5%) as a result of the smart algorithm implemented in the CocoSoft user-friendly freeware.

In spite of the good analytical features of the system, some drawbacks still have to be solved. Little fluctuations of the temperature in the laboratory throughout the day and the heating of the fluorimeter caused slight variations on the generalized polarization values between consecutive samples. It becomes clear that the requirement of a device for temperature modulation is the next step for ensuring reliable data. A concern about acquisition of fluorescence measurements was observed at the beginning of the experiments due to the small range of the reference voltage for the analog to digital converter (ADC) calibration. Although these issues had no substantial significance on

the kinetic study, they might be inspected again for the sake of reliable unmanned analysis in the long term.

The presence of concomitant contaminants in a given environmental compartment can impact biota quite differently than that expected from individual doses. In order to study the interaction of binary mixtures of ECs, in the chapter 6, different bioassays were selected using a diversity of organisms, cells and artificial membranes to investigate eco/cytotoxic effects. In the mentioned chapter, the type of interaction (synergism or antagonism) of different parabens and diclofenac on the toxicity of TCS was estimated through two modelling approaches viz., concentration addition (CA) and independent action (IA) at three concentration levels of each chemical studied. Results evidenced that the impact of TCS on biota was strongly influenced by the level of concentration of each compound demonstrating that even low concentrations of these contaminants, below their toxicity individual effect, may trigger undesirable effects on organisms of different trophic levels, from bacteria to mammalian cells. One more appreciation can be done related to liposomes, the driving force of the present dissertation: notably, the liposome tests on the mixtures followed the same trends obtained with the viability (MTT) assay with Caco-2 cells, thus indicating the validity of the *in vitro* model using membrane surrogates as an alternative to human gut living cells.

To sum up, liposomes are versatile tool for investigation of the effect of ECs on lipid bilayers and offer a valuable alternative to avoid experimentation with living beings or cell testing. The ease of synthesis and manipulation of lipid vesicles also allow the automation of these assays via flow approaches, thus simplifying experimental work and giving new and useful applications in the field of exposomics, such as effect direct analysis of bioavailable fractions in an untargeted fashion.

Capítulo 8. Trabajo Futuro

A lo largo de la tesis he cometido muchos errores, ya fuera a la hora de abordar un problema, de enfocar una idea, de llevar a cabo un experimento o de resolver un contratiempo. Han sido todos esos errores, sin embargo, que me han permitido avanzar y ver de otra forma cómo funciona la investigación de nuevos conceptos, y que sin ellos ahora volvería fallar allí mismo donde fallé tiempo atrás. Mi formación durante estos años me ha permitido llegar a la conclusión de que una idea por simple que parezca pueda estar asociada a una complejidad experimental inesperada y que la planificación del trabajo es clave en el buen desarrollo del proyecto. No solo de los errores se aprende, también hay que saber parar a tiempo y ser perseverante hasta cierto punto. Ahora soy consciente de que cuando una idea no sale tras varios intentos la solución no es la obstinación que solo puede entorpecer la investigación y repercutir en la eficiencia del trabajo experimental, sin embargo, recular y buscar una nueva alternativa o idea resulta más eficaz. "*Cuando una batalla está perdida, solo los que han huido pueden combatir en otra*" (Demóstenes)

La investigación llevada a cabo estos años ha aportado a nuestro grupo tanto conceptos básicos para la compresión del uso de los liposomas como modelo sintético de membrana biológica como el desarrollo de nuevos conceptos e ideas originales en el campo de la exposómica ambiental. El trabajo conjunto multi-disciplinar con investigadores de otros ámbitos, desde química física, química teórica, toxicología, bioquímica y farmacología nos ha proporcionado un punto de vista holístico de la interacción xenobiótico-membrana permitiendo una mayor comprensión del comportamiento y papel de las membranas biológicas en presencia de un fármaco o contaminante. A raíz de este conocimiento adquirido han surgido nuevas ideas para profundizar en el concepto de biodisponibilidad en un futuro próximo.

La elección de la fosfatidilcolina de soja, como lípido natural en la síntesis de nuestros liposomas, nos ha permitido un acercamiento más realista a la membrana biológica comparado al uso de lípidos puros al contener una mezcla de cadenas de longitud e insaturaciones variadas. En trabajos posteriores se pretende elaborar liposomas con un mayor grado de complejidad y que incluyan mezclas de fosfolípidos y colesterol en distintas proporciones con el objetivo de simular membranas celulares de distintos

tejidos y órganos. Estos liposomas nos darán una información más fidedigna de la interacción de contaminantes con la membrana y permitirán la comparación de posibles diferencias de los efectos membranotrópicos en función del tipo de célula emulada.

Siguiendo con la misma idea de la síntesis de liposomas organomiméticos se llevará a cabo la elaboración de matrices de colágeno y ácido hialurónico con la intención de formar una red tridimensional proteica gelatinosa donde se retendrán liposomas. Estas vesículas estarán formadas con fosfolípidos característicos del estrato córneo donde abunda la fosfatidilcolina hidrogenada, colesterol y ceramidas, que dan rigidez a las membranas, con el objetivo de estudiar fenómenos de permeación y la biodisponibilidad de diversos xenobióticos aplicados por vía tópica a través de piel artificial. Dentro de la misma temática se pretende imitar, en la medida de lo posible, la mucosa intestinal usando la misma matriz proteica, o similar, usada para la piel, pero incluyendo en ella liposomas constituidos por lípidos presentes en las membranas plasmáticas propias de enterocitos y colonocitos. Los resultados se compararán con estudios *in vitro* en piel sintética obtenida por impresión 3D a partir de fibrina y fibroblastos, y en mucosas sintéticas con células vivas. Para hacer posible estos estudios comparativos se buscará la colaboración universidad-empresa con el grupo BioDan, "una innovadora compañía de bioingeniería especializada en medicina regenerativa con un enfoque particular en la piel".

El desarrollo y la optimización de un sistema automático inteligente nos ha permitido la experimentación de distintas formulaciones liposomales con diversos xenobióticos de forma consecutiva y la obtención de un gran número de datos sin supervisión y reduciendo al máximo la intervención humana. En base a esta prueba de concepto se añadirán mejoras al sistema que nos darán la opción de investigar efectos membranotrópicos a distintas temperaturas mediante la incorporación de un módulo Peltier con termostato acoplado cuyos parámetros podrán ser controlados desde CocoSoft. Este dispositivo adicional permitirá la elaboración de curvas sigmoideas elaboradas a partir de los valores de GP adquiridos en un amplio rango de temperaturas cuyo punto de inflexión informará de la temperatura de transición de la membrana de los liposomas de estudio. Además, el sistema en flujo nos da la posibilidad de la inyección de pequeñas alícuotas de contaminante a nivel de microlitros o nanolitros en la disolución liposomal permitiendo la opción de realizar estudios de quenching

aportando información adicional sobre el tipo de interacción entre el xenobiótico y la sonda de membrana.

El conocimiento adquirido nos ha alertado de cómo compuestos a concentraciones por debajo de su toxicidad dada por IC_{50} pueden incrementar la toxicidad de otros compuestos por medio de sinergias por lo que resulta de interés realizar estudios membranotópicos no solo con xenobióticos individuales sino también con mezclas binarias.

Los liposomas tienen multitud de posibilidades y sus aplicaciones siguen creciendo desde su descubrimiento hace más de 50 años. Una particularidad de los liposomas es su capacidad de incrementar la solubilidad de compuestos apolares gracias a las características anfipáticas de los fosfolípidos que componen su membrana. Así, un compuesto poco soluble en un medio acuoso, en presencia de liposomas, tendrá la posibilidad de interaccionar con las membranas en mayor o menor medida, lo que se denomina coeficiente de partición membrana-agua, aumentando de este modo la cantidad disuelta en el medio y disminuyendo a su vez la cantidad precipitada o en suspensión. Con esta idea en mente, los liposomas podrían emplearse en metodologías medioambientales para evaluar la biodisponibilidad de uno o varios contaminantes presentes, por ejemplo, en el suelo usando estas vesículas lipídicas como extractantes suaves. Esta aplicación nos podría dar información por tanto de parámetros como la bioacumulación o biodegradación de contaminantes en organismos de subsuelo como microorganismos o lombrices de tierra, especie clave para la salud de la tierra y muy sensible a la presencia de contaminantes, pero sin necesidad de tests *in-vivo*. De este modo, la agitación suave de cierta cantidad de suelo en suspensión en un medio acuoso liposomal durante un tiempo determinado y ajustando diversos parámetros podría mimetizar en cierto modo la biota del medio y su capacidad fisiológica de extraer o degradar contaminantes presentes en su hábitat. Análogamente se podría preparar una disolución liposomal con área superficial similar a la del promedio del intestino delgado humano (unos 30 m^2) para simular la biodisponibilidad gastrointestinal. Esta aplicación demuestra que los liposomas no solo son útiles dentro del campo de la farmacia, medicina y otras disciplinas destinadas al bienestar del ser humano, sino que tienen un hueco en el campo medioambiental y de la ecotoxicidad.

ANEXO

A reliable sensing platform for plasmonic ELISA based on automatic flow-based methodology

Natcha Kaewwonglom[a], Miquel Oliver[b], David J. Cocovi Solberg[b,c], Katharina Zirngibl[d], Dietmar Knopp[d], Jaroon Jakmunee[a], Manuel Miró[b]

[a]*Research Center on Chemistry for Development of Health Promoting Products from Northern Resources, Department of Chemistry, Faculty of Science, Chiang Mai University, Chiang Mai 50200, Thailand.*

[b]*FI-TRACE Group, Department of Chemistry, Faculty of Sciences, University of the Balearic Islands, E-07122 Palma de Mallorca, Illes Balears, Spain.*

[c]*University of Natural Resources and Life Sciences (BOKU), Muthgasse 18, 1190 Vienna, Austria.*

[d]*Institute of Hydrochemistry and Chemical Balneology, Chair of Analytical Chemistry and Water Chemistry, Technische Universität München, Marchioninistrasse 17, 81377 München, Germany*

Published in Analytical Chemistry

Resumen

La detección colorimétrica mediante el uso de nanopartículas de oro (AuNPs) se basa en la propiedad de resonancia plasmónica de superficie localizada (LSPR) propia de dichas NPs. Los métodos de detección basados en esta característica ofrecen ventajas significativas como la aplicación a una amplia gama de analitos, facilidad de uso, eliminación de disolventes orgánicos tóxicos, aplicaciones en el sitio de cuidado (point-of-care), así como alta sensibilidad de detección frente a cromóforos orgánicos.

Cuando un haz de luz interacciona con nanopartículas metálicas mucho menores que la longitud de onda incidente tienen lugar excitaciones dipolares de los electrones libres en la superficie metálica que presentan una oscilación coherente y se acoplan con los fotones absorbidos de una determinada frecuencia [1]. Este fenómeno da lugar a una resonancia localizada que en el caso de metales nobles absorbe luz visible. La frecuencia y ancho de banda del espectro de absorción del LSPR dependen de la forma y tamaño de las NPs pero también de su índice de refracción y estado de agregación. Otro punto importante es que el LSPR depende de la constante dieléctrica del disolvente (ε_m) por lo que el color de la disolución cambiará en función de este parámetro.

Por ejemplo, la agregación de las AuNPs inducida por un analito resulta en la alteración del color de la disolución y por tanto del espectro de absorción, pasando de un color de tono rosado en el caso de pequeñas AuNPs a un color violeta grisáceo para AuNPs agregadas. En la figura 1 se muestra un ejemplo donde el tripéptido glutatión (GSH) altera el LSPR de las AuNPs debido a los grupos tiol de este compuesto capaces de interaccionar con el oro [2] provocando un desplazamiento batocrómico del máximo del espectro de absorbancia debido a la agregación de las AuNPs.

Las moléculas incapaces de inducir cambios en las AuNPs pueden ser medidos de forma indirecta. Por ejemplo, en este trabajo la cuantificación de diclofenaco se realiza por medio de un ELISA* competitivo plasmónico usando un anticuerpo monoclonal primario (mAb) para el diclofenaco y un anticuerpo policlonal secundario unido covalentemente a la enzima glucosa oxidasa (GOx). A menor concentración de diclofenaco en la muestra real, mayor será la cantidad de mAb y Ab secundario presentes en la prueba lo que a una concentración fija de glucosa generará mayor concentración de peróxido de hidrógeno. En medio ácido este peróxido de hidrógeno actuará como reductor de Au (III) a AuNP pudiendo visualizar cambios en base a las

diferencias en la velocidad de nucleación y crecimiento de las AuNPs provocadas por las distintas concentraciones de peróxido de hidrógeno resultantes del ELISA.

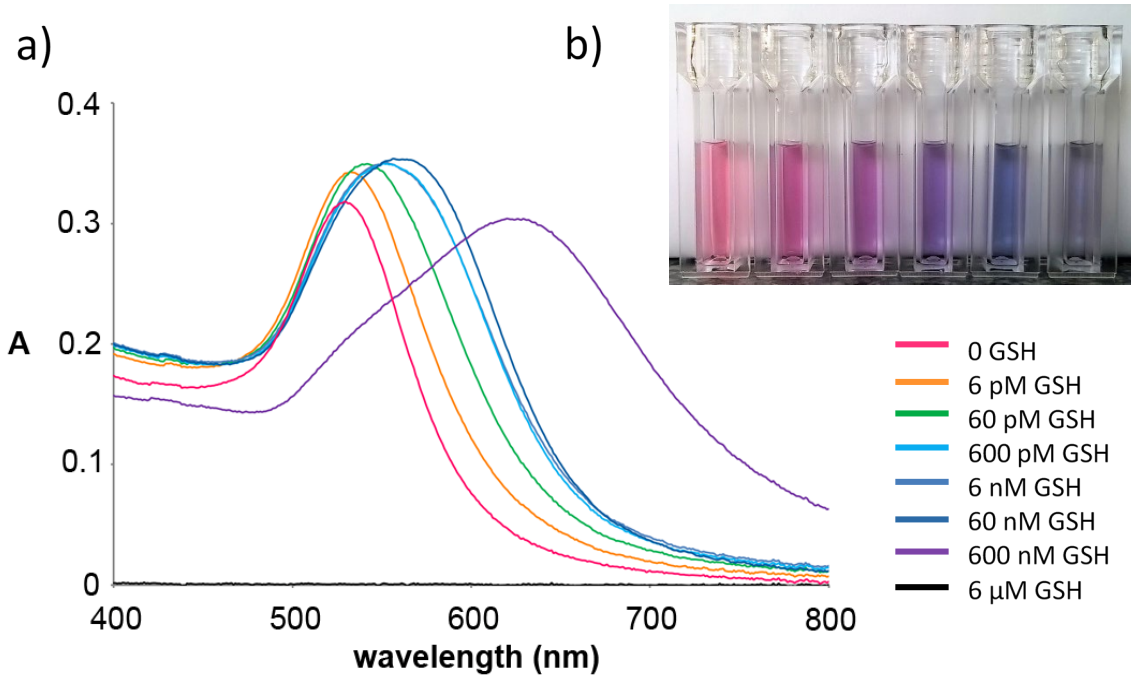

Figura 1. a) Espectros UV-Vis del LSPR para diferentes concentraciones de GSH en el crecimiento de AuNPs. b) Tonalidades de AuNPs en función de la concentración de GSH. De izquierda a derecha: 0, 6 pM, 60 pM, 600 pM, 60 nM y 600 nM GSH.

Sin embargo, la síntesis *in situ* de las AuNPs en placas ELISA es afectada por una multitud de factores (temperatura, agitación, concentraciones de reactivos, presencia de impurezas, etc.) que dificultan la reproducibilidad de los ensayos manuales debidos a la variabilidad de la velocidad de la formación de las AuNPs. Para compensar este problema, en este trabajo se ha optimizado un ELISA competitivo acoplado a un sistema en flujo automático capaz de monitorear a tiempo real los espectros de LSPR registrando, a intervalos de tiempo definidos, las cinéticas de crecimiento de las AuNPs mediante el uso de un fotómetro USB miniaturizado. Esto nos permite elegir para cada ensayo el tiempo de análisis más apropiado para obtener la mejor sensibilidad del método evitando de ese modo errores causados por la naturaleza tan caprichosa de las AuNPs durante su nucleación, crecimiento y agregación. Este nuevo enfoque ha sido

utilizado en este trabajo para la determinación de diclofenaco en agua de mar a concentraciones por debajo del nivel establecido por la Comisión de la Unión Europea sin pretratamiento de la muestra con unas características de sensibilidad, repetibilidad y precisión mayores que el ELISA convencional y el ELISA plasmónico en microplaca.

* ELISA: (acrónimo del inglés Enzyme-Linked ImmunoSorbent Assay) es una técnica de inmunoensayo basada en placas, normalmente de poliestireno con 96 pocillos de 400 µL, diseñada para determinar y cuantificar proteínas, anticuerpos, hormonas y otras biomoléculas. En estos ensayos, participan uno o más anticuerpos y antígenos, uno de los cuales, en función del tipo de ELISA, debe ser inmovilizado en una superficie sólida. La molécula fijada, normalmente un antígeno, formará un complejo con el anticuerpo el cual a su vez está unido a un enzima. La determinación se lleva a cabo mediante la actividad enzimática con su sustrato correspondiente generando un producto cuantificable. La clave en estos ensayos es la interacción específica antígeno-anticuerpo. En función del tipo de estrategia usada tanto para la captura como la determinación del analito, el ELISA se divide en distintos tipos (los más comunes son directo, indirecto, sándwich y competitivo), siendo posible también variar la composición de la propia placa originando así una gran diversidad de metodologías cada una con sus ventajas y desventajas.

Referencias

1. Willets, K. A.; Van Duyne, R. P. Localized Surface Plasmon Resonance Spectroscopy and Sensing. *Annu. Rev. Phys. Chem*. **2007**, *58*, 267–97. https://doi.org/10.1146/annurev.physchem.58.032806.104607

2. Gobbo, P.; Biondi, M. J.; Feld, J. J.; Workentin, M. S. Arresting the time-dependent H_2O_2 mediated synthesisof gold nanoparticles for analytical detection and preparative chemistry. *J. Mater. Chem. B*, **2013**, *1*, 4048–4051. https://doi.org/10.1039/c3tb20913j

analytical chemistry

Article

Cite This: Anal. Chem. 2019, 91, 13260−13267

pubs.acs.org/ac

Reliable Sensing Platform for Plasmonic Enzyme-Linked Immunosorbent Assays Based on Automatic Flow-Based Methodology

Natcha Kaewwonglom,[†] Miquel Oliver,[‡] David J. Cocovi-Solberg,[‡] Katharina Zirngibl,[∥] Dietmar Knopp,[∥] Jaroon Jakmunee,[†] and Manuel Miró*[,‡]

[†]Research Center on Chemistry for Development of Health Promoting Products from Northern Resources, Department of Chemistry, Faculty of Science, Chiang Mai University, Chiang Mai 50200, Thailand

[‡]FI-TRACE Group, Department of Chemistry, Faculty of Sciences, University of the Balearic Islands, E-07122 Palma de Mallorca, Illes Balears, Spain

[∥]Institute of Hydrochemistry and Chemical Balneology, Chair of Analytical Chemistry and Water Chemistry, Technische Universität München, Marchioninistrasse 17, 81377 München, Germany

Supporting Information

ABSTRACT: Plasmonic enzyme-linked immunosorbent assays (ELISA) using the localized surface plasmon resonance (LSPR) of metal nanoparticles has emerged as an appealing alternative to conventional ELISA counterparts for ultrasensitive naked-eye detection of biomolecules and small contaminants. However, batchwise plasmonic ELISA involving end-point detection lacks ruggedness inasmuch as the generation or etching of NP is greatly dependent on every experimental parameter of the analytical workflow. To tackle the above shortcomings, this paper reports on an automatic flow methodology as a reliable detection scheme of hydrogen peroxide related enzymatic bioassays for ultrasensitive detection of small molecules. Here, a competitive ELISA is combined with the in-line generation of plasmonic gold nanoparticles (AuNPs) followed by the real-time monitoring of the NP nucleation and growth rates and size distribution using a USB miniaturized photometer. Glucose oxidase was labeled to the secondary antibody and yielded hydrogen peroxide that acted as the measurand and the reducing agent of the Au(III)/citrate system in the flow network. High-throughput plasmonic assays were feasible by assembling a hybrid flow system composed of two microsyringe pumps, a perfluoroalkoxy alkane reaction coil, and a 26-port multiposition valve and operated under computer-controllable flow conditions. The ultratrace determination of diclofenac in high matrix samples, e.g., seawater, without any prior sample treatment was selected as a proof-of-concept application of the flow-based platform for determination of emerging contaminants via plasmonic ELISA. The detection limit (0.001 μg L^{-1}) was 1 order of magnitude lower than that endorsed by the first EU Watch List for diclofenac as a potentially emerging contaminant in seawater and also than that of a conventional colorimetric ELISA, which in turn is inappropriate for determination of diclofenac in seawater at the levels endorsed by the EU regulation. The proposed automatic fluidic approach is characterized by the reproducible timing in AuNPs nucleation and growth along with the unsupervised LSPR absorbance detection of AuNPs with a dynamic range for diclofenac spanning from 0.01 to 10 μg L^{-1}. Repeatability and intermediate precision (given as normalized signal readouts) in seawater were <4% and <14%, respectively, as compared to RSDs as high as 30% as obtained with the batchwise plasmonic ELISA counterpart.

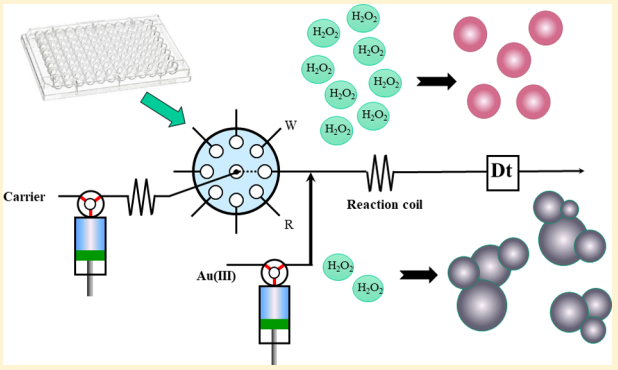

Enzyme-linked immunosorbent assays (ELISA) adapted to different formats, e.g., direct, indirect, sandwich, and competitive ELISA are routine biochemical assays involving antigen−antibody binding for high-throughput and ultrasensitive detection of low and high molecular mass compounds in a variety of research fields including clinical,[1] environmental,[2,3] and food analysis.[4] In fact, recent trends geared toward the development of ELISA tests for emerging organic pollutants, e.g., pharmaceuticals, personal care products, and endocrine-disrupting chemicals, in environmental waters.[5,6] The standard ELISA protocol involves the colorimetric detection of the biochemical product of the prior enzymatic reaction, e.g., hydrogen peroxide, by resorting to organic chromophores, such as 3,3′,5,5′-tetramethylbenzidine (TMB), *o*-phenylenediamine

Received: August 22, 2019
Accepted: September 9, 2019
Published: September 9, 2019

DOI: 10.1021/acs.analchem.9b03855
Anal. Chem. 2019, 91, 13260−13267

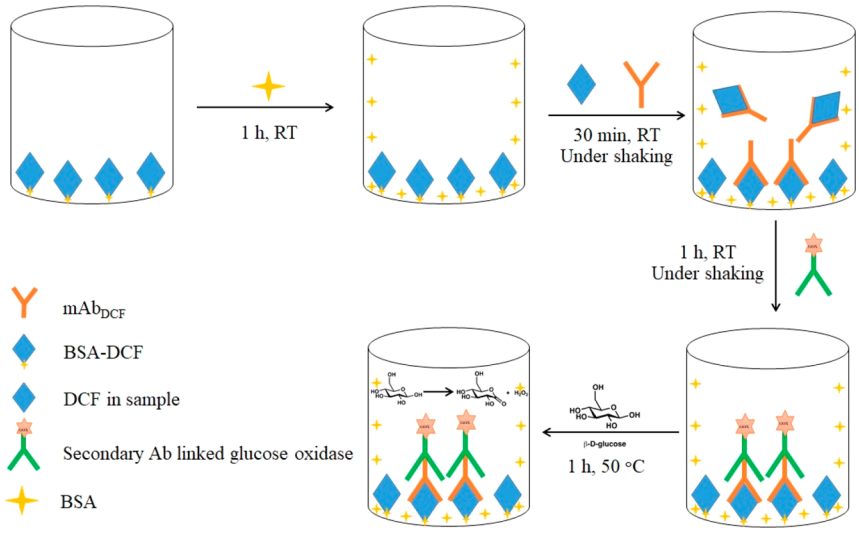

Figure 1. Schematic illustration of the microtiter plate-based competitive ELISA protocol for DCF prior to flow-through LSPR detection of AuNP

(OPD), and 2,2′-azino-bis(3-ethylbenzthiazoline-6-sulfonic acid) (ABTS).[1,2,4−7] However, colorimetric competitive and sandwich ELISA sensing platforms may have limited sensitivity for determination of low-molecular mass pollutants at environmentally relevant levels because the detection is merely based on the color measurement of the resulting solution by conventional photometric analysis. Especially, this comes true for detecting pollutants in marine ecosystems that are found at low ng L^{-1} (ppt) levels. For that reason, sample treatment, e.g., sample clean-up, or preconcentration stages using solid-phase extraction are quite often indispensable to achieve the required concentration range for appropriate detectability.[8,9]

Plasmonic ELISA using the localized surface plasmon resonance (LSPR) absorption of metal nanoparticles (NP) has emerged as an appealing alternative to conventional ELISA counterparts for ultrasensitive naked-eyed detection of small molecules.[10−13] This is because of the higher molar absorptivity of plasmonic AuNPs and AgNPs as compared to organic dyes[14,15] that ameliorates the detection sensitivity of the biochemical assays, and the unique optical properties of plasmonic nanomaterials. Interest has grown in recent years toward exploiting analyte-induced shifts of the LSPR absorption bands of NPs, that is, variation of particle size distribution, shape, and composition, as analytical readouts.[5,12,14] This is demonstrated by a plethora of analytical methods combining ELISA with nanotechnology which capitalized on the aggregation, etching, nucleation, or growth of metal NP.[13−19]

However, plasmonic ELISA assays based on end-point measurements lack ruggedness inasmuch as the visualized results are greatly dependent on the majority of the experimental conditions, including (i) mixing time, (ii) reaction temperature, (iii) concentration and purity of reagents, (iv) competing side reactions with redox agents, (v) order of reagent addition, and most importantly (vi) agitation mode (also in the course of optical detection through the plate reader), thus jeopardizing the repeatability of the assays because of variable reaction rates for nanoparticle growth and etching.[13,19,20] Efforts toward halting further reaction development via addition of ancillary chemicals, such as glutathione or thiosulfate[17−22] do not offset changes in kinetic constants. In addition, the temporal resolution of naked eye protocols or conventional plate readers[14] might be insufficient for reliable monitoring of the reaction rates and detection under well-defined NP growth/etching conditions. For example, a variation of the concentration of hydrogen peroxide from a mere 119.95 μM to 120.00 μM under given reaction conditions[19] is reported to induce AuNP nucleation and lead to profound changes of the LSPR absorption bands, yet the reliability of the analytical protocol in a batchwise mode is deemed questionable. In fact, the experimental results reported in some papers dealing with batch plasmonic ELISA have been the subject matter of open debate in scientific forums (e.g., Pubpeer posts),[23] and a potential case of unethical publishing behavior.[24]

To tackle the above shortcomings, the various generations of flow analysis and miniaturized systems thereof spanning from microfluidic to millifluidic devices[25] offer viable platforms for (i) accommodation of NP-mediated assays,[26] (ii) kinetic discrimination reactions,[26] and (iii) in-line synthesis of AuNP/AgNP[26−30] on account of the controllable laminar diffusion/dispersion and reproducible timing for NP nucleation and growth as compared to batch counterparts. In contrast to standard well-plate assays, interfering effects from bovine serum albumin, along with primary and secondary antibodies immobilized on the plates onto the nucleation of AuNP/AgNP are entirely circumvented by resorting to bespoke fluidic approaches for reliable localized LSPR absorbance detection.[31]

In this work, an automatic flow platform inspired by the principles of flow chemistry[32] is proposed to offset the high variability in nucleation and growth kinetics of AuNP throughout plasmonic ELISA in batch format. The mesofluidic device is able to take advantage of metallic nanoprobes for reliable optical detection following monoclonal antibody-based ELISA by in-line monitoring of the time-dependent AuNP nucleation and growth unsupervised. The determination of diclofenac in waters at realistic environmental concentrations[33,34] and below the Environmental Quality Standards (EQS) endorsed by the First Watch List of the European Union[35] to identify potential emerging contaminants, that is, 0.1 μg L^{-1} in fresh and drinking waters and 0.01 μg L^{-1} in marine waters, is herein proposed as a proof-of-concept study. The feasibility of the combination of competitive ELISA with online plasmonic detection of hydrogen peroxide-triggered AuNP for tackling complex samples is demonstrated by the analysis of seawater without any prior sample treatment.

DOI: 10.1021/acs.analchem.9b03855
Anal. Chem. 2019, 91, 13260−13267

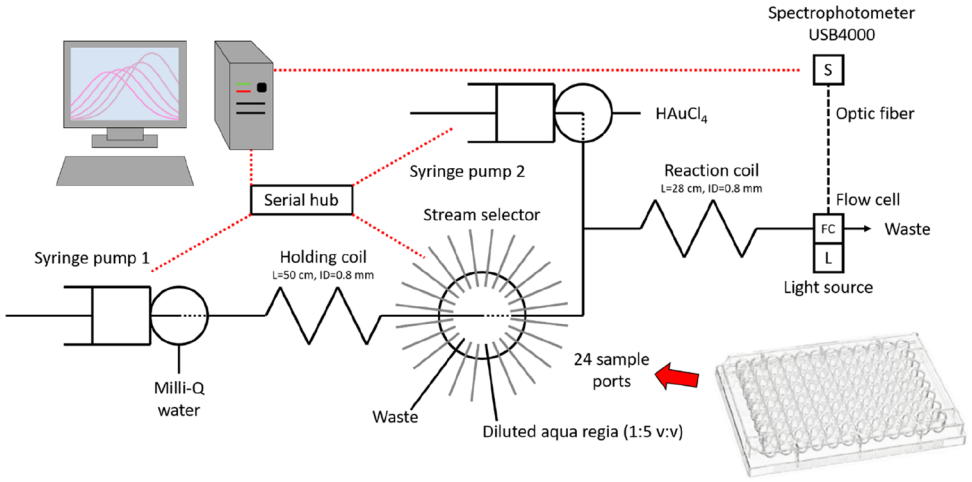

Figure 2. Schematic diagram of the automatic flow-through system for high-throughput ultrasensitive detection of DCF in seawater using plasmonic NP probes following competitive ELISA. FC (UV−vis flow-through cell), L (Light source) and S (Spectrophotometer).

EXPERIMENTAL SECTION

Detailed description of reagents, samples, and synthesis of the BSA-DCF conjugates is given in the Supporting Information.

Competitive ELISA Protocols for DCF. A diagrammatic description of the competitive ELISA protocol prior to online plasmonic NP detection is illustrated in Figure 1. Initially, the microtiter plate was coated overnight at 4 °C with 200 μL of 0.5 μg mL^{-1} BSA-DCF according to Huebner et al.[6] at a pH 9.6 (0.1 mol L^{-1} $NaHCO_3$ adjusted with dilute NaOH). Then, the plate was rinsed 3 times with 400 μL of 0.05% Tween in PBS and blocked with 400 μL of 1 g L^{-1} BSA in PBS for 1 h at room temperature (RT). Afterward, the plate was again washed with 400 μL of PBS-Tween thrice. The competitive ELISA was carried out by adding 100 μL of DCF standard solution within the range of 0.0001 to 100 μg L^{-1} or seawater sample, whereupon 100 μL of 400 ng mL^{-1} mAb_{DCF} in PBS was added to the plate followed by incubation for 30 min at RT under gentle mixing at 100 rpm using a plate shaker. After three washing steps with PBS-Tween, 200 μL of 1:1000 diluted Ab_{GOx} from the stock solution in 1 g L^{-1} BSA in PBS was added to the well plate and incubated for 1 h at RT while shaking at 100 rpm. After incubation, the plate was washed with 400 μL of PBS-Tween three times to overcome unspecific binding followed by two additional rinsing steps with sodium citrate buffer (10 mM, pH 6.5) to remove PBS salt prior to the LSPR detection. Then, 200 μL of 400 mM glucose in 20 mM sodium citrate (pH 6.5) was added to each well and incubated for 1 h at 50 °C. Finally, 150 μL aliquots of each well after the enzymatic reaction were stored in 1.5 mL-amber vials (Thermo Fisher Scientific) equipped with a 300 μL-polyspring insert (Thermo Fisher Scientific, Waltham, MA), which were nested to the multiposition valve of the flow system (see below) for automatic high-throughput hydrogen-peroxide mediated plasmonic NP detection.

For comparison, a competitive microtiter plate ELISA for DCF was performed following the protocol described above but using an HRP-labeled secondary antibody (0.2 μg/mL in PBS; 200 μL/well) and colorimetric readout (TMB assay).[6] After final washing, the substrate solution (200 μL/well) was added, and the plates were shaken for about 15 min for color development. Finally, the enzyme reaction was stopped with 5% H_2SO_4 (100 μL/well) and the absorbance was read at 450 nm with a microplate reader (Synergy HT, Bio-Tek, Bad Friedrichshall, Germany). For construction of the calibration curves, diclofenac standard solutions to cover the concentration range between 0.0001 to 100 μg L^{-1} were prepared in 3.5 % (w/v) sea-salt (S9883, Merck, Germany) and also in tap water for comparison.

Fluidic Setup for In-Line LSPR Detection Using AuNP Probes. The bespoke fluidic platform for in-line monitoring of the hydrogen-peroxide dependent generation of plasmonic AuNP is schematically illustrated in Figure 2. It consists of (i) a 26-position low pressure stream selector C35Z-31826D (MPV) mounted on a microelectric actuator (VICI AG International, Schenkon, Switzerland), (ii) two bidirectional microsyringe pumps (SP, Cavro Xcalibur, Tecan Group Ltd., Männedorf, Switzerland) each furnished with a 1 mL gastight glass syringe (Hamilton, Bonaduz, Switzerland) containing Milli-Q water (SP1) as a carrier, and 20 mM $HAuCl_4$ (SP2), respectively, and with a three-way head valve to either communicate with the flow system or aspirate reagent/carrier, (iii) a 10 mm path-length flow-through quartz cell (18 μL, Hellma GmbH, Müllheim, Germany), and (iv) a miniaturized USB4000 UV−vis spectrometer (Ocean Optics, Largo, FL). The spectrometer is connected via a 300 μm optical fiber (QP300-1-SR-BX, Ocean Optics) to the ISS UV−vis integrated sampling system (Ocean Optics) equipped with the light source and a direct attach cuvette holder. SP2 was covered by aluminum foil to prevent photochemical reactions of $HAuCl_4$. The flow manifold (including the holding coil, HC) was built from fluorinated ethylene propylene (FEP) tubing of 1/32 in. i.d. and 1/16 in. o.d., except that the reaction coil that was made of perfluoroalkoxy alkane (PFA, 1/32 in. i.d. and 1/16 in. o.d.) with lengths shown in Figure 2. The MPV was furnished with 10−32 nuts for connecting tubes, while other fluidic connections were made with 1/4−28 in. nuts with appropriate ferrules.

CocoSoft freeware[36] was selected as a user-friendly software for programming the motion and flow rates of the SP1 and SP2 and selection of the ports of the MPV throughout the flow method. SpectraSuite software (2008 Ocean Optic, 64-bit version 1.6.0.11) was used for control of the spectrometer detection parameters and data acquisition. Both software packages were synchronized for the sake of the unsupervised operation by CocoSoft proxying user's mouse clicks in pixels and times defined throughout the fluidic method as described below.

DOI: 10.1021/acs.analchem.9b03855
Anal. Chem. 2019, 91, 13260−13267

Automatic Flow Method for High-Throughput DCF Determination Based on LSPR Detection of AuNPs. After completion of the competitive ELISA for DCF in a well plate format, the resulting solution of the enzymatic reaction of glucose with GOx to yield hydrogen peroxide was transferred to the flow-based system by inserting the samples in Eppendorf tubes that were nested to ports 1−24 of the MPV, while the two remaining ports were used for aspiration of 1:5 (v/v) diluted aqua regia (as a rinsing solution of the flow manifold) and waste, respectively. The plasmonic gold nanoparticles were generated by in-line merging of 50 μL of hydrogen-peroxide and 20 mM citrate buffer containing sample solution (after aspiration from a given MPV port into the HC by SP1) with 50 μL of 0.6 mM $HAuCl_4$ in 0.5 mM HNO_3 from SP2 in a T-confluence by simultaneous activation of the two syringe pumps followed by pumping of the mixture toward the flow cell at 1.0 mL min^{-1} (see Figure 2). The dispersed zone was then brought to the flow-through spectrophotometric cell to fill the chamber volume (the remainder of the zone was kept in the PFA tubing) where it remained halted for a maximum of 10 min to yield plasmonic AuNPs. The LSPR spectra of AuNPs were recorded every 30 s with an integration time of 60 ms and a boxcar smoothing of 5 (11 pixels). The absorbance (Abs) was monitored continuously at 540 nm against a reference wavelength of 800 nm. To this end, virtual clicks from CocoSoft software opened the SpectraSuite window, clicked on the "convert active spectrum to overlay" button, and minimized again the SpectraSuite program. This three-click procedure was repeated every 30 s during the stopped-flow time of 10 min, thus accumulating a total number of 20 spectra that were recovered and processed anytime subsequently. After data acquisition, the nanoparticle-containing plug was discarded, and the flow-through cuvette and tubing were flushed with 220 μL of 1:5 (v/v) diluted aqua regia at 1.0 mL min^{-1} by SP1 for dissolving potentially adsorbed nanoparticles and thus preventing fouling and cross contamination effects. The flow method ended by washing the reaction coil with 8000 μL of Milli-Q water at 1.0 mL min^{-1} from SP1. After automatic analysis of 24 samples, cleaning of the reaction coil with aqua regia overnight is recommended for removal of remnants of AuNP attached to the tubing walls. For every sample cohort analysis, the reaction time that allowed discrimination of blank against the EQS of DCF in seawater was adopted as an experimental parameter for samples and calibrants. The ratio of absorbance (A) for a given measurement against the maximum absorbance signal (A_0) of the LSPR peak obtained in the absence of DCF was selected as analytical readout ($Abs_{A/A0}$). A four parameter logistic sigmoidal regression of $Abs_{A/A0}$ against [DCF] was used as a standard calibration curve, yet linearization of the plot against log [DCF] within a predefined working range of concentrations was also investigated.

RESULTS AND DISCUSSION

Investigation of Experimental Variables of the DCF Competitive Plasmonic Immunoassay. Of the several experimental variables influencing the hydrogen peroxide yield of the competitive ELISA, both mAb_{DCF} and Ab_{GOx} are crucial factors for discrimination of blank versus ultratrace DCF concentrations on the basis of the maximum absorbance of the LSPR band (A_0 at 540 nm minus 800 nm) and the tonality change of the ensuing AuNPs across the flow system. Preliminary batchwise detection was accomplished by the addition of 100 μL of 0.5 mM Au(III) (pH = 6.8) after the mAb_{DCF}/Ab_{GOX}-based ELISA. The mAb_{DCF} concentration was investigated within the range spanning from 100−1 000 ng mL^{-1}, i.e., 1:50 000 to 1:5 000 dilution under stagnant conditions for the plasmonic detection. The A_0 value along with the slopes obtained by linearization of the working range of the sigmoid curve (∼0.1−10 ng mL^{-1} DCF) increased with increasing the mAb_{DCF} concentration until 400 ng mL^{-1} (1:12 500 dilution) after which the surplus of mAb impaired the detection of ultratrace level concentration of DCF by the competitive ELISA and render poorer IC_{50} values (*viz.*, analyte concentration giving 50% curve inhibition).[6] Likewise, an ∼4-fold improvement of the slope of the linearized sigmoid curve and 2-fold enhanced A_0 were observed by increasing the Ab_{GOx} concentration from 1:10 000 up to 1:1 000 dilution, thus indicating the absence of excess Ab_{GOx} under the experimental concentrations assayed. Therefore, the mAb_{DCF} and Ab_{GOx} dilutions from the stocks were set to 1:12 500 and 1:1 000, respectively, for the remainder of the studies of the flow-through method.

The pH of the GOx catalyzed reaction after incubation with Ab_{GOx} is another yet critical parameter of the competitive ELISA, which will factor into the further development of the AuNPs and the particle size distribution thereof throughout the stopped-flow system (see next section). The pH range over which appropriate glucose turnover by GOx is reported in the literature[37,38] spans from 5.5 to 7.5, while Au(III) reduction by hydrogen peroxide with the subsequent NP nucleation necessitates pH values around 6.5 as indicated by Peng et al.[39] Hydrogen citrate/citrate buffer (pK_{a3} = 6.4) was selected for pH adjustment to 6.5 with the additional advantage of using citrate as a coreducing and stabilizing reagent of AuNPs in the flow system.[28,40,41] However, the concentration of the reducing buffer should be thoroughly investigated as a primary influent parameter on the morphology of AuNP. The absorbance of AuNPs at 540 nm increased with sodium citrate concentrations ranging from 2 mM up to 20 mM at a reaction time of 7 min, which most likely indicates faster nucleation rates and, thus, smaller NP sizes would be generated. On the other hand, the increase of citrate concentration (investigated up to 30 mM) favored NP stabilization whereby excessively long reaction times might be called for across the flow system for appropriate method sensitivity against DCF. Therefore, a 20 mM hydrogen citrate/sodium citrate buffer (pH = 6.5) was adopted for the enzymatic reaction and NP size control. The effect of glucose concentration and the enzymatic reaction time on the ELISA were also investigated from 50−800 mM and 15−90 min at 50 °C,[42] respectively. Glucose acts as the enzyme substrate, but the surplus of the enzymatic oxidation reaction might serve also as a coreductant of Au(III),[43] thus ameliorating the AuNP nucleation kinetics. The higher the concentration of glucose (up to 400 mM) the higher was the slope of the linearized sigmoid curve. The enzymatic incubation time was fixed to 60 min inasmuch as the increase of H_2O_2 yield was proven negligible afterward.

Investigation of Critical Parameters of the Fluidic System for AuNPs Nucleation and LSPR Detection. Throughout the competitive ELISA, the lower the DCF concentration the higher the yield of H_2O_2 and thus the faster the nucleation and growth of NP is expected. As a consequence, smaller NP will be generated under flow conditions, and the hypsochromic (blue) shift of the LSPR band toward 540 nm is to be monitored unsupervised by the CocoSoft freeware.

DOI: 10.1021/acs.analchem.9b03855
Anal. Chem. 2019, 91, 13260−13267

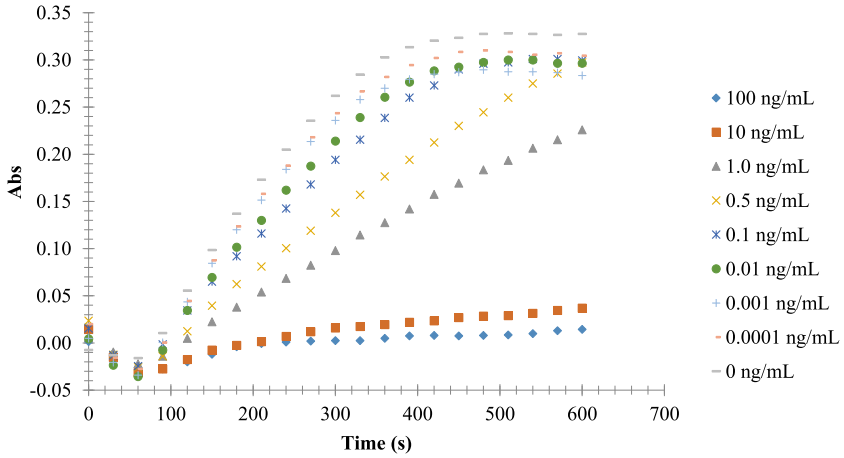

Figure 3. Monitoring of the in-line generation of hydrogen-peroxide mediated AuNP over time at varied DCF concentrations by resorting to the stopped-flow fluidic platform. Absorbance data are given as readouts at 540 nm (analytical wavelength) minus 800 nm (reference wavelength) up to 10 min.

Several flow configurations were initially investigated for the in-line formation of plasmonic NP under ultratrace concentrations of DCF (10−100 pg mL^{-1}). A simple on-line sequential injection system encompassing the sequential injection of 50 μL of solution from ELISA and 50 μL of Au(III) into the HC followed by pumping of the stacked zones by flow-reversal toward the flow-cell rendered poor sensitivity as a consequence of insufficient mutual penetration of the two plugs by axial dispersion in the way to the detection system. To surmount this problem, a hybrid fluidic configuration that in turn promotes radial mixing under laminar flow conditions was assembled instead by resorting to two simultaneously operating stand-alone microsyringe pumps (see Figure 2). The flow rate toward the flow-through detector was affixed to 1.0 mL min^{-1} to ensure a sufficient residence time to initiate nucleation across the reaction coil without excessive NP fouling onto the tubing walls.

The effect of critical parameters such as the Au(III) concentration and the tubing material of the reaction coil of the flow system on the plasmonic signals was studied in detail. Negatively charged tubing-solution interfaces are expected to offer enhanced nucleation rates of AuNP as signaled by Huang et al.[31] because the concentration of the initially positively charged citrate-Au(III) complexes generated in-line after the T-junction will increase locally on the reactor walls. Afterward, the negatively charged citrate-capped nuclei will be repelled from the tubing and will be transferred along with the neutral gold seeds back into the bulk solution, thus facilitating optical monitoring of the kinetics of AuNP nucleation and growth while minimizing carryover effects of NP attached irreversibly on the manifold tubing. A variety of tubing materials of 0.8 mm i.d. with varying Z potential values at pH 6.5, namely, polyetheretherketone (PEEK), polytetrafluoroethylene (PTFE), fluorinated ethylene propylene (FEP), and perfluoroalkoxyalkane (PFA) were assayed. Experimental results demonstrated that the two tubing materials with the most negative surface potential at pH 6.5, i.e., PFA and FEP,[31] yielded smaller AuNPs with narrower size distribution at a given reaction time as identified by the high values of A_0 and narrow LSPR bands. The relative roughness of the four fluorinated tubing materials was also explored by scanning electron microscopic (SEM) images and illustrated in Figure S1. The SEM micrographs revealed that compared to PEEK and PTFE, PFA, and FEP featured smoother inner surface, which is in good agreement with previous authors.[44,45]

Based on our experimental findings, PFA was selected as the tubing material of the in-line reactor for efficient generation of smaller nanoparticle sizes, and to circumvent interassay AuNP fouling onto the inner surfaces by in-line rinsing with diluted aqua regia.[31]

The effect of Au(III) concentration and the Au(III)/citrate ratio on the sensitivity of the flow-through plasmonic method and the dynamic range for DCF was investigated within the range of 0.3−0.7 mM Au(III) by in-line merging of the gold solution with the hydrogen peroxide containing standards obtained by calibration of the ELISA with distinct concentrations of DCF. The higher the Au(III) concentration (up to 0.6 mM) the smaller the relative nanoparticle size and the larger difference of Abs_A at 540 nm were obtained for 10 pg mL^{-1} against 10 ng mL^{-1} DCF (see Figure S2). The reagent concentration was affixed to 0.6 mM Au(III) that rendered a final citrate to gold molar ratio of ∼33 and a final concentration of Au(III) of 0.3 mM throughout the flow-through PFA reactor.

Under the aforementioned experimental physicochemical conditions of the flow method, the nucleation rates of plasmonic AuNP were monitored over time (up to 10 min) in a fully automatic mode (see spectra in Figure S3). The LSPR spectra obtained online at varied DCF concentrations at a fixed reading time of 5.5 min are illustrated in Figure S4. The difference between the LSPR absorbance at the maximum wavelength (λ_{max} = 540 nm) and reference wavelength (λ_{ref} = 800 nm) was used as an analytical readout to generate the signal-time curves at increasing concentrations of DCF as shown in Figure 3. The suitable time window of AuNPs nucleation and growth for discrimination and quantification of 10 pg mL^{-1} DCF in seawater against lower concentrations of DCF (1 pg mL^{-1} and below) corresponds to 4−7 min (see Figure 3). By processing of the recorded LSPR spectra obtained by the automatic flow system, the best reaction time for plotting of the calibration graph and undertake the ultrasensitive determination of DCF in seawater can be readily tuned intra- and interday unsupervised.

Analytical Performance of the Flow System and Real Sample Analysis. The analytical performance of the automatic flow-through LSPR absorbance method for ultratrace determination of DCF was studied in terms of dynamic range, sensitivity, intermediate precision, limits of detection and quantification, and application of real seawater samples. A 4-parameter logistic sigmoid curve of Abs(A/A_0) against DCF

DOI: 10.1021/acs.analchem.9b03855
Anal. Chem. 2019, 91, 13260−13267

concentration was plotted within the range of 0−100 ng mL^{-1} DCF using DCF-free seawater (as identified by HPLC−MS following solid-phase extraction)[6] for matrix-matched calibration. The sigmoid standard curve (see Figure 4) was fitted to

$$\mathrm{Abs}\left(\frac{A}{A_0}\right) = 0.044 + \frac{0.982}{1 + \left(\frac{\left[\mathrm{DCF}\left(\frac{\mathrm{ng}}{\mathrm{mL}}\right)\right]}{0.792}\right)^{0.710}}$$

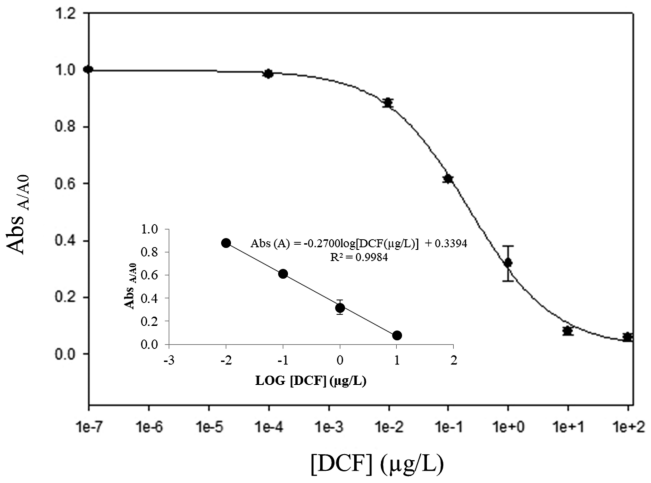

Figure 4. Logistic sigmoid calibration curve of LSPR absorbance of AuNP as obtained by the flow-through platform following the competitive ELISA under matrix matched conditions. The inset illustrates the dynamic linear range from 0.01 up to 10 $\mu g\ L^{-1}$ DCF at a stopped flow time of 7 min. Error bars are given as standard deviation (n = 3).

with a correlation coefficient of 0.9942, yet a dynamic linear range over a 3-decade log scale, namely, 0.01−10 $\mu g\ L^{-1}$ DCF using the equation $(\mathrm{Abs}(A/A_0) = -0.27 \times \log[\mathrm{DCF}\ (\mathrm{ng\ mL^{-1}})] + 0.34$ (R^2 = 0.9984) could be harnessed instead for the sake of rapid quantification of DCF (see inset in Figure 4). The linear range equates to a concentration range of 50−400 μM hydrogen peroxide as determined by external calibration with standard solutions of hydrogen peroxide. The limits of detection (LOD) and quantitation (LOQ) based on the $3s_b$ and $10s_b$ criteria (n = 7) were calculated from the normalized calibration as the concentrations equating to $1-3s_b$ and $1-10s_b$, respectively, which corresponded to 0.001 and 0.003 $\mu g\ L^{-1}$ DCF, respectively. For the sake of comparison, the analytical performances of the batchwise plasmonic ELISA and the conventional colorimetric ELISA have been also investigated. A linear range of 0.1−100 $\mu g\ L^{-1}$ and 0.03−0.16 $\mu g\ L^{-1}$ DCF along with an LOD of 0.08 $\mu g\ L^{-1}$ DCF and 0.018 $\mu g\ L^{-1}$ DCF have been obtained for the plasmonic and the colorimetric ELISA, respectively (see Figures S5 and S6). It should be noted that the LOD of the batchwise ELISA counterpart is about 1 order of magnitude above the maximum acceptable method detection limit specified by the EU Commission for DCF in seawater (viz., 0.01 $\mu g\ L^{-1}$ DCF). The LOD of the colorimetric ELISA is much closer to the critical value but the required detectability in seawater could not be reached as well. Further, the LOD and dynamic range of the flow-through SPR system are on a par with those reported in the literature for determination of DCF in seawater by HPLC/UHPLC−MS[46−48] but with no need of prior solid-phase preconcentration and matrix cleanup/desalting protocols (see Table S1 for details) and at least 1 order of magnitude better than most of the previous ELISA, immunosensors, or cell sensors for diclofenac,[6,49−53] which to the best of our knowledge have been merely applied to freshwaters and industrial waters but saline or hypersaline waters (see Table S2). This is most likely a consequence of high matrix interfering effects of saline matrixes in the detection scheme that can be overcome by using the flow-based kinetic-controlled detection system herein reported. It should also be stressed the fact that the reproducibility of manual immunoassays/biosensors might amount to RSD values as high as 23−100%.[6,49,50,54] Most importantly, the minimum spiked concentration level of DCF in all of the previous works spanned from 15 to 1000 ng/L,[6,49−52,54−56] again indicating that none of the immunoassays is suitable for detection of DCF at the environmental quality standard level set in seawater, that is, 10 ng/L.

The precision of the proposed fluidic method was studied at three distinct concentration levels of DCF in seawater that covered 3 orders of magnitude, viz., 0.01, 0.1, and 1.0 ng mL^{-1}. The intraday relative standard deviations (% RSD of normalized signal readouts, n = 5) at a reaction time of 7 min were 1.4%, 3.0%, and 3.2%, respectively, thus indicating a good repeatability in AuNP nucleation and growth under flow regime. The interday intermediate precision values at 0.01, 0.1, and 1.0 ng mL^{-1} levels in seawater increased up to 3.9, 13.6, and 10.8%, respectively, but were significantly better than those obtained with the batchwise counterpart with RSD values of 16.0, 14.3, and 30.0%, respectively.

The trueness (lack of bias) of the flow-through AuNP-based LSPR method was ascertained by direct analysis of spiked coastal seawater sampled at various beaches in Mallorca island, Spain (see the Experimental Section in Supporting Information) using the linear calibration curve. None of the real samples contained detectable DCF, *viz.*, [DCF] < 2 ng L^{-1}, as determined by solid phase extraction using Oasis HLB followed by reversed-phase (C18)-HPLC−MS detection according to the protocol by Huebner et al.[6] Every sample was spiked at two distinct concentration levels, viz., 0.01 ng mL^{-1} and 0.1 ng mL^{-1} DCF, the former being the maximum allowed concentration of DCF in seawater endorsed by the EU Watch List. The relative recoveries ranged in all instances from 90 to 106% (see Table 1), thus indicating the absence of multiplicative matrix interferences throughout the ELISA and the flow-through LSPR sensing method, making the use of the method of the standard additions unnecessary.

Table 1. Relative Recoveries of DCF in Seawater Samples As Determined by ELISA in Combination with On-Line LSPR Absorbance Detection of AuNP

sample	added (ng mL^{-1})	found ($\mu g\ L^{-1}$)	recovery (%)
S'Estanyol	0.01	0.009 ± 0.001	90 ± 10
	0.1	0.094 ± 0.005	94 ± 5
Port de Pollensa	0.01	0.010 ± 0.001	100 ± 10
	0.1	0.099 ± 0.003	99 ± 3
Santa Ponsa (winter)	0.01	0.0102 ± 0.0009	102 ± 9
	0.1	0.099 ± 0.010	99 ± 10
Santa Ponsa (spring)	0.01	0.0106 ± 0.0003	106 ± 3
	0.1	0.103 ± 0.002	103 ± 2

DOI: 10.1021/acs.analchem.9b03855
Anal. Chem. 2019, 91, 13260−13267

CONCLUSION

A bespoke flow-through system is herein proposed for the first time as a reliable platform for automatic monitoring of the nucleation and growth rates of AuNPs. The plasmonic NPs are used as nanoprobes for high-throughput LSPR determination of diclofenac, which is taken as a model of an environmental emerging contaminant. The flow manifold was built for unsupervised analysis of up to 24 samples containing varying levels of hydrogen peroxide from competitive ELISA. By using user-friendly software for programming of hydrodynamic variables and data recording, the proposed (meso)fluidic platform features (i) automatic injection of microliter volumes of sample and Au(III), (ii) controllable mixing of solutions and in-line generation of AuNP, and (iii) unsupervised recording of time-resolved LSPR absorption bands, thus overcoming the reported limitations of batchwise plasmonic ELISA for reliable quantitative analysis. Without any prior sample processing method, our fluidic approach is capable of determining diclofenac in troublesome samples (e.g., seawater) at concentrations down to 10 ng L^{-1}, that is, below those endorsed by the EU Watch List for potential emerging contaminants, and those detected by the conventional colorimetric ELISA. Current research work is underway in our lab to expand the scope of applicability of the fluidic LSPR absorbance platform to ultratrace determination of other emerging organic contaminants listed by the Watch List in combination with mAb-based highly sensitive ELISA using enzymes other than oxidases.

ASSOCIATED CONTENT

Supporting Information

The Supporting Information is available free of charge on the ACS Publications website at DOI: 10.1021/acs.analchem.9b03855.

Detailed description and information on (i) reagent and solutions; (ii) morphology of the inner walls of the flow-through reactor; (iii) effect of the Au(III) concentration on the size of the plasmonic gold nanoparticles and LSPR absorption bands; and (iv) time-resolved LSPR absorption spectra and influence of DCF concentration (PDF)

AUTHOR INFORMATION

Corresponding Author

*E-mail: manuel.miro@uib.es.

ORCID

Dietmar Knopp: 0000-0003-4566-9798

Manuel Miró: 0000-0002-8413-3008

Notes

The authors declare no competing financial interest.

ACKNOWLEDGMENTS

Manuel Miró, Miquel Oliver, and David J. Cocovi-Solberg acknowledge financial support from the Spanish Ministry of Science, Innovation and Universities (MCIU) and the Spanish State Research Agency (AEI) through Projects CTM2017-84763-C3-3-R (MCIU/AEI/FEDER, EU) and CTM2017-90890-REDT (MCIU/AEI/FEDER, EU). Technical assistance by Dr. de la Rica is greatly appreciated. The Thailand Research Fund (TRF), the Commission on Higher Education, Faculty of Science, and Chiang Mai University are acknowledged for funding support. The Royal Golden Jubilee (RGJ) Ph.D. Program is gratefully acknowledged for the scholarship to N. Kaewwonglom (N.K.). N.K. also thanks the FI-TRACE group at the University of Balearic Islands for scientific supervision and availability of instrumentation and the Graduate School of Chiang Mai University for financial support.

REFERENCES

(1) Drijvers, J. M.; Awan, I. M.; Perugino, C. A.; Rosenberg, I. M; Pillai, S. The Enzyme-Linked Immunosorbent Assay: The Application of ELISA in Clinical Research. In *Basic Science Methods for Clinical Researchers*; Jalali, M., Saldanha, F. Y. L., Jalali, M., Eds.; Academic Press:Boston, MA, 2017; Chapter 7, pp 119−133.

(2) Krall, A. L.; Elliott, S. M.; Erickson, M. L.; Adams, B. A. *Environ. Pollut.* **2018**, *234*, 420−428.

(3) Zhu, N.-F.; Zhu, Y.-Q.; Wang, J.; Gyimah, E.; Hu, X.-L.; Zhang, Z. *Talanta* **2019**, *199*, 72−79.

(4) González-Martínez, M. Á.; Puchades, R.; Maquieira, Á. Immunoanalytical Technique: Enzyme-Linked Immunosorbent Assay (ELISA). In *Modern Techniques for Food Authentication*, 2nd ed.; Sun, D.-W., Ed.; Academic Press: Boston, MA, 2018; Chapter 15, pp 617−657.

(5) Zhang, Z.; Zeng, K.; Liu, J.-F. *TrAC, Trends Anal. Chem.* **2017**, *87*, 49−57.

(6) Huebner, M.; Weber, E.; Niessner, R.; Boujday, S.; Knopp, D. *Anal. Bioanal. Chem.* **2015**, *407*, 8873−8882.

(7) Sogawa, R.; Saita, T.; Yamamoto, Y.; Kimura, S.; Narisawa, Y.; Kimura, S.; Shin, M. *J. Pharm. Anal.* **2019**, *9*, 49−54.

(8) Sanchis, A.; Bosch-Orea, C.; Salvador, J. P.; Marco, M. P.; Farré, M. *Anal. Bioanal. Chem.* **2019**, *411*, 5897−5907.

(9) Antunes, J.; Justino, C.; da Costa, J. P.; Cardoso, S.; Duarte, A. C.; Rocha-Santos, T. *Microchem. J.* **2018**, *138*, 465−471.

(10) Liang, Y.; Huang, X.-L.; Chen, X.-R.; Zhang, W.-J.; Ping, G.; Xiong, Y.-H. *Sens. Actuators, B* **2018**, *259*, 162−169.

(11) Xiong, Y.; Pei, K.; Wu, Y.-Q.; Duan, H.; Lai, W.-H.; Xiong, Y.-H. *Sens. Actuators, B* **2018**, *267*, 320−327.

(12) Ma, X.-M.; Chen, Z.-T.; Kannan, P.; Lin, Z.-Y.; Qiu, B.; Guo, L.-H. *Anal. Chem.* **2016**, *88*, 3227−3234.

(13) de la Rica, R.; Stevens, M. M. *Nat. Protoc.* **2013**, *8*, 1759−1764.

(14) Zhang, Z.-Y.; Wang, H.; Chen, Z.-P.; Wang, X.-Y.; Choo, J.; Chen, L.-X. *Biosens. Bioelectron.* **2018**, *114*, 52−65.

(15) Zhang, Y.-L.; McKelvie, I. D.; Cattrall, R. W.; Kolev, S. D. *Talanta* **2016**, *152*, 410−422.

(16) Liang, J.-J.; Yao, C.-Z.; Li, X.-Q.; Wu, Z.; Huang, C.-H.; Fu, Q.-Q.; Lan, C.-F.; Cao, D.-L.; Tang, Y. *Biosens. Bioelectron.* **2015**, *69*, 128−134.

(17) Lin, Y.; Xu, S.-H.; Yang, J.; Huang, Y.-J.; Chen, Z.-T.; Qiu, B.; Lin, Z.-Y.; Chen, G.-N.; Guo, L.-H. *Sens. Actuators, B* **2018**, *267*, 502−509.

(18) Zhan, L.; Wu, W. B.; Yang, L.; Huang, C. Z. *Anal. Chim. Acta* **2017**, *962*, 73−79.

(19) Cecchin, D.; de la Rica, R.; Bain, R. E. S.; Finnis, M. W.; Stevens, M. M.; Battaglia, G. *Nanoscale* **2014**, *6*, 9559−9562.

(20) De la Rica, R.; Stevens, M. M. *Nat. Nanotechnol.* **2012**, *7*, 821−824.

(21) Gobbo, P.; Biondi, M. J.; Feld, J. J.; Workentin, M. S. *J. Mater. Chem. B* **2013**, *1*, 4048−4051.

(22) Wang, X.; Niessner, R.; Knopp, D. *Analyst* **2015**, *140*, 1453−1458.

(23) *Pubpeer Publications*, comments on "Plasmonic ELISA for the ultrasensitive detection of disease biomarkers with the naked eye. Nat. Nanotechnol. 2012, 7, 821". https://pubpeer.com/publications/54AECF24E96162E3A563AED08BE0B3 (last accessed date August 21, 2019).

(24) Lévy, R. *Homeopathic Nanoparticles, In Three Little (Nano) Controversies and Their Morals*, https://raphazlab.wordpress.com/2017/09/20/three-little-nano-controversies-and-their-morals (last accessed date August 21, 2019).

(25) Miró, M.; Hansen, E. H. *Anal. Chim. Acta* **2007**, *600*, 46−57.

(26) Passos, M. L. C.; Pinto, P. C. A. G.; Santos, J. L. M.; Saraiva, M. L. M. F. S.; Araujo, A. R. T. S. *Anal. Chim. Acta* **2015**, *889*, 22−34.

(27) Passos, M. L. C.; Costa, D.; Lima, J. L. F. C.; Saraiva, M. L. M. F. S. *Talanta* **2015**, *133*, 45−51.
(28) Baber, M. R. *Synthesis of inorganic nanoparticles using microfluidic devices*. Ph.D. Thesis, University College London, London. U.K., 2017.
(29) Ftouni, J.; Girardon, J. S.; Penhoat, M.; Payen, E.; Rolando, C. *Microsyst.Technol.* **2012**, *18*, 151−158.
(30) Hao, N.; Nie, Y.; Zhang, J. X. J. *Int. Mater. Rev.* **2018**, *63*, 461−487.
(31) Huang, H.; Toit, H. D.; Besenhard, M. O.; Ben-Jaber, S.; Dobson, P.; Parkin, I.; Gavriilidis, A. *Chem. Eng. Sci.* **2018**, *189*, 422−430.
(32) Trojanowicz, M. *Talanta* **2016**, *146*, 621−640.
(33) Bonnefille, B.; Gomez, E.; Courant, F.; Escande, A.; Fenet, H. *Mar. Pollut. Bull.* **2018**, *131*, 496−506.
(34) Lonappan, L.; Brar, S. K.; Das, R. K.; Verma, M.; Surampalli, R. Y. *Environ. Int.* **2016**, *96*, 127−138.
(35) Commission Implementing Decision (EU) 2015/495 of 20 March 2015 establishing a watch list of substances for Union-wide monitoring in the field of water policy pursuant to Directive 2008/105/EC of the European Parliament and of the Council. *Off. J. Eur. L* **2015**, *78*, 40−42.
(36) Cocovi-Solberg, D. J.; Miró, M. *Anal. Bioanal. Chem.* **2015**, *407*, 6227−6233.
(37) Bankar, S. B.; Bule, M. V.; Singhal, R. S.; Ananthanarayan, L. *Biotechnol. Adv.* **2009**, *27*, 489−501.
(38) Odebunmi, E.; Owalude, S. *J. Appl. Sci. Environ. Manage.* **2007**, *11*, 95−100.
(39) Peng, C.-F.; Dan, X.-H.; Xie, Z.-J.; Liu, C.-L. *J. Nanomater.* **2014**, *2014*, 576082.
(40) Giri, B. Synthesis of gold nanoparticles on microchip. In *Laboratory Methods in Microfluidics*; Giri, B., Ed.; Elsevier: Amsterdam, The Netherlands, 2017; Chapter 16, pp 103−107.
(41) Ji, X.-H.; Song, X.-N.; Li, J.; Bai, Y.-B.; Yang, W.-S.; Peng, X.-G. *J. Am. Chem. Soc.* **2007**, *129*, 13939−13948.
(42) Yang, Y.-C.; Tseng, W.-L. *Anal. Chem.* **2016**, *88*, 5355−5362.
(43) Liu, J.-C.; Qin, G.-W.; Raveendran, P.; Ikushima, Y. *Chem. Eur. J.* **2006**, *12*, 2131−2138.
(44) McKeen, L. W. High-temperature and high-performance polymers, In *Permeability Properties of Plastics and Elastomers*, 3rd ed.; McKeen, L. W., Ed.; William Andrew Publishing: Oxford, U.K., 2012; Chapter 11, pp 233−250.
(45) Hecht, K. *Microreactors for gas/liquid reactions: The role of surface properties*. Ph.D. Dissertation, Karlsruhe Institute of Technology, Karlsruhe, Germany, 2013.
(46) Wu, J.-M.; Qian, X.-Q.; Yang, Z.-G.; Zhang, L. F. *J. Chromatogr. A* **2010**, *1217*, 1471−1475.
(47) Magnér, J.; Filipovic, M.; Alsberg, T. *Chemosphere* **2010**, *80*, 1255−1260.
(48) Pereira, C. D. S.; Maranho, L. A.; Cortez, F. S.; Pusceddu, F. H.; Santos, A. R.; Ribeiro, D. A.; Cesar, A.; Guimarães, L. L. *Sci. Total Environ.* **2016**, *548−549*, 148−154.
(49) Hlaváček, A.; Peterek, M.; Farka, Z.; Mickert, M. J.; Prechtl, L.; Knopp, D.; Gorris, H. H. *Microchim. Acta* **2017**, *184*, 4159−4165.
(50) Hlaváček, A.; Farka, Z.; Hübner, M.; Horňáková, V.; Němeček, D.; Niessner, R.; Skládal, P.; Knopp, D.; Gorris, H. H. *Anal. Chem.* **2016**, *88*, 6011−6017.
(51) Steinke, N.; Döring, S.; Wuchrer, R.; Kroh, C.; Gerlach, G.; Härtling, T. *Sens. Actuators, B* **2019**, *288*, 594−600.
(52) Shi, J.; Xu, M.-X.; Tang, Q.-H.; Zhao, K.; Deng, A.; Li, J.-G. *Spectrochim. Acta, Part A* **2018**, *191*, 1−7.
(53) Schirmer, C.; Posseckardt, J.; Schroder, M.; Glaser, M.; Howitz, S.; Scharff, W.; Mertig, M. *Talanta* **2019**, *203*, 242−247.
(54) Nguyen, T. T. K.; Vu, T. T.; Anquetin, G.; Tran, H. V.; Reisberg, S.; Noel, V.; Mattana, G.; Nguyen, Q. V.; Dai Lam, T.; Pham, M. C.; Piro, B. *Biosens. Bioelectron.* **2017**, *97*, 246−252.
(55) Wang, C.; Jiang, T.-X.; Zhao, K.; Deng, A.; Li, J.-G. *Talanta* **2019**, *193*, 184−191.
(56) Hu, L.-Y.; Zheng, J.; Zhao, K.; Deng, A.; Li, J.-G. *Biosens. Bioelectron.* **2018**, *101*, 260−267.

DOI: 10.1021/acs.analchem.9b03855
Anal. Chem. 2019, 91, 13260−13267

Supporting information

A reliable sensing platform for plasmonic ELISA based on automatic flow-based methodology

Natcha Kaewwonglom[a], Miquel Oliver[b], David J. Cocovi Solberg[b,c], Katharina Zirngibl[d], Dietmar Knopp[d], Jaroon Jakmunee[a], Manuel Miró[*b]

aResearch Center on Chemistry for Development of Health Promoting Products from Northern Resources, Department of Chemistry, Faculty of Science, Chiang Mai University, Chiang Mai 50200, Thailand.

bFI-TRACE Group, Department of Chemistry, Faculty of Sciences, University of the Balearic Islands, E-07122 Palma de Mallorca, Illes Balears, Spain.

cUniversity of Natural Resources and Life Sciences (BOKU), Muthgasse 18, 1190 Vienna, Austria

[d]Institute of Hydrochemistry and Chemical Balneology, Chair of Analytical Chemistry and Water Chemistry, Technische Universität München, Marchioninistrasse 17, 81377 München, Germany.

[*] Corresponding author. E-mail: manuel.miro@uib.es

Table of contents

Reagents, solutions, and samples

Solvents and reagents were of analytical grade. Milli-Q water with resistivity > 18 MΩ·cm was obtained by a Milli-Q® Advantage A10 Water Purification System (Merck-Millipore, Darmstadt, Germany). Diclofenac standard stock solution (DCF, 10 mg mL^{-1}) was prepared by dissolving diclofenac sodium salt (Merck KGaA, Darmstadt, Germany) in methanol. Glucose, bovine serum albumin (BSA, lyophilized powder), triethylamine (TEA), N-(3-dimethylaminopropyl)-N'-ethylcarbodiimide hydrochloride (EDC), and gold (III) chloride hydrate ($HAuCl_4$) were purchased from Merck. Tri-sodium citrate dihydrate and sodium hydrogen carbonate were purchased from Scharlau (Barcelona, Spain). The phosphate buffer saline (PBS) (10 mM, pH 7.4) was prepared by dissolving 0.12 g potassium phosphate monobasic, 0.69 g disodium phosphate, 4.0 g sodium chloride and 0.1 g potassium chloride in 400 mL of water. Then, the pH was adjusted to 7.4 and brought up to 500 mL with water.

Transparent microtiter plates with 96 flat-bottom wells and with high affinity to molecules containing mixed hydrophilic/hydrophobic domains (MaxiSorp™ wells, Thermo Fisher Scientific, Waltham, MA, USA), were selected for the competitive ELISA. A high affine monoclonal antibody (K_D of 1.5 x 10^{-10}) against diclofenac (mAb_{DCF}) was prepared, purified and characterized as described elsewhere (1). A mAb_{DCF} stock of 5000 mg L^{-1} was used throughout. Goat anti-mouse IgG H&L-conjugated glucose oxidase secondary antibody (Ab_{GOx}) was purchased from Abcam plc (Cambridge, UK). Horseradish peroxidase (HRP)-labeled anti-mouse IgG produced in horse was purchased from Axxora (Loerrach, Germany). The substrate buffer (pH 3.8) for the colorimetric ELISA was prepared with 46.0 g potassium dihydrogen citrate and 0.1 g potassium sorbate in 1 L of water. The substrate solution consisted of 25 mL substrate buffer, 500 μL TMB stock solution (375 mg of 3,3′,5,5′-tetramethylbenzidine dissolved in 30 mL of DMSO), and 100 μL 1% (v/v) hydrogen peroxide. The stop solution was 5% (v/v) H_2SO_4.

Coastal seawaters were sampled at varied locations of the island of Mallorca, Spain, *namely*, *S'Estanyol* (Latitude (N)= 39° 21′ 41.0′′, Longitude (E)= 2° 55′ 10.7′′), *Port de Pollença* (N=39° 54′ 28.6′′, E=3° 05′ 04.2′′) and *Santa Ponça* (N=39° 31′ 02.2′′; E= 2° 28′ 47.2′′) in spring (May 2018) and winter (February 2018). The collected samples were stored in amber glass bottles at 4 °C and filtered over nylon syringe filter

(25 mm, 0.22 µm pre-fil, NYP2520200, Scharlab SL) just before the competitive ELISA and analyzed without sample dilution and any other sample pretreatment procedure.

Preparation of DCF-BSA conjugates

BSA linked DCF (BSA-DCF) was synthesized according to De Medina *et al.* (2) as follows: Briefly, DCF (acid form) was dissolved in 2 mL of DMF/H_2O (1:4; v/v) at a final concentration of 15 mM. To this solution, TEA (10 eq) and EDC (10 eq) were added and the mixture was stirred at ambient temperature for 1 h. The activated hapten solution was added dropwise to the protein solution (12 mg mL^{-1} BSA, corresponding to 0.185 mM BSA) in 3.2 mL of 5 mM borax buffer at pH 8.5. The reaction mixture was stirred at ambient temperature for 24 h. The BSA-DCF conjugate was purified and concentrated by using 10 kDa cut-off filtration units (Vivaspin 20 -12 tubes, Sartorius AG, Göttingen, Germany) and centrifugation at 4500*g* for 20 min at 4°C. The final conjugate was lyophilized to yield a colorless solid and characterized by MALDI-TOF-MS (autoflexTM Speed MALDI-TOF(/TOF), Nd:YAG SmartBeam laser 355 nm, Bruker Daltonik GmbH, Bremen, Germany). A mean coupling density of 7 mol DCF per mol of BSA protein was determined. A 0.05% Tween in PBS was used as a washing buffer solution throughout the ELISA.

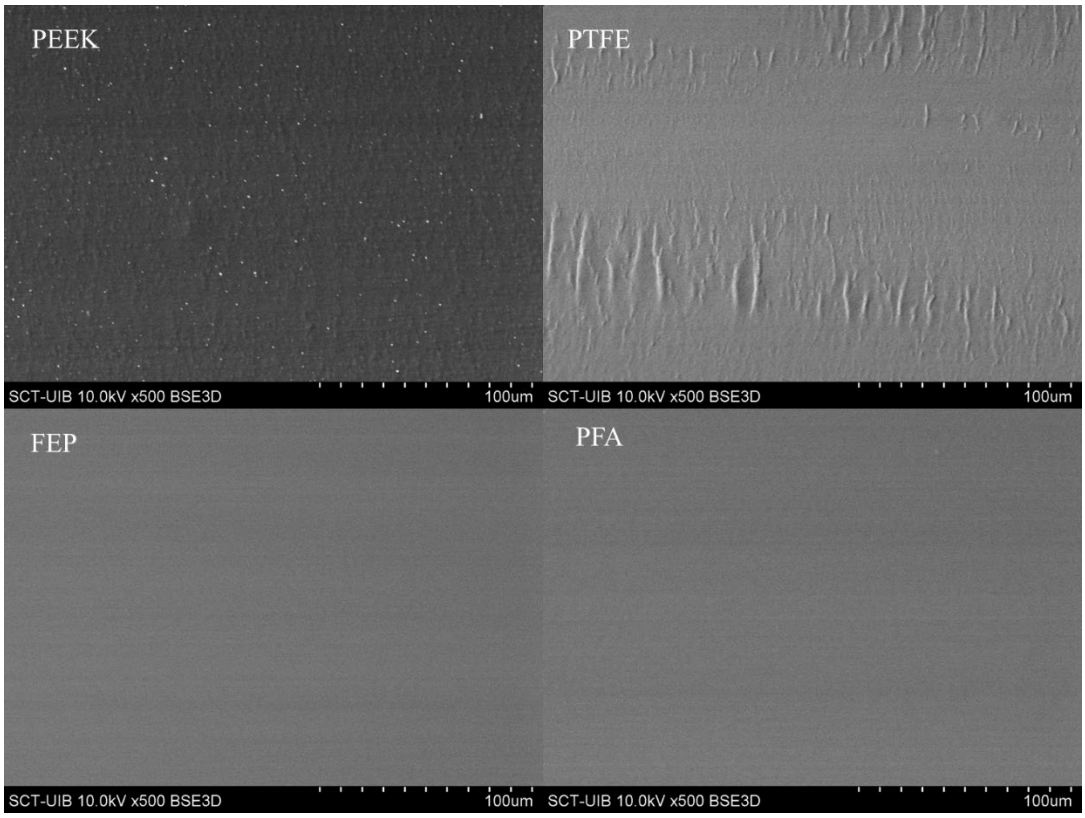

Figure S1. Scanning microscopic micrographs of the inner walls of polymeric tubing (PEEK, PTFE, FEP and PFA) of the flow network at a 500-fold magnification

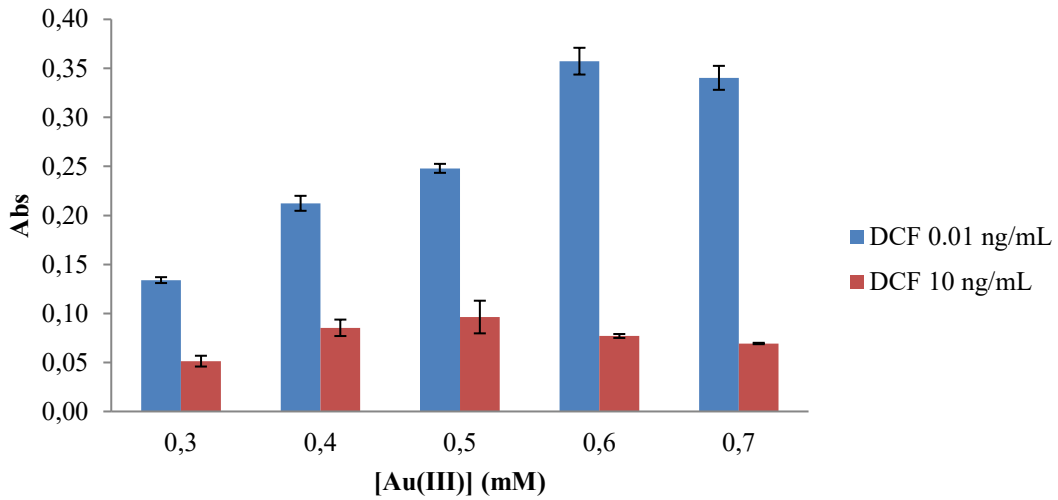

Figure S2. Effect of the Au(III) concentration on the size of the plasmonic AuNP as obtained by the automatic flow-through method using PFA tubing. Results are expressed as the average of three replicates ±standard deviation (n=3).

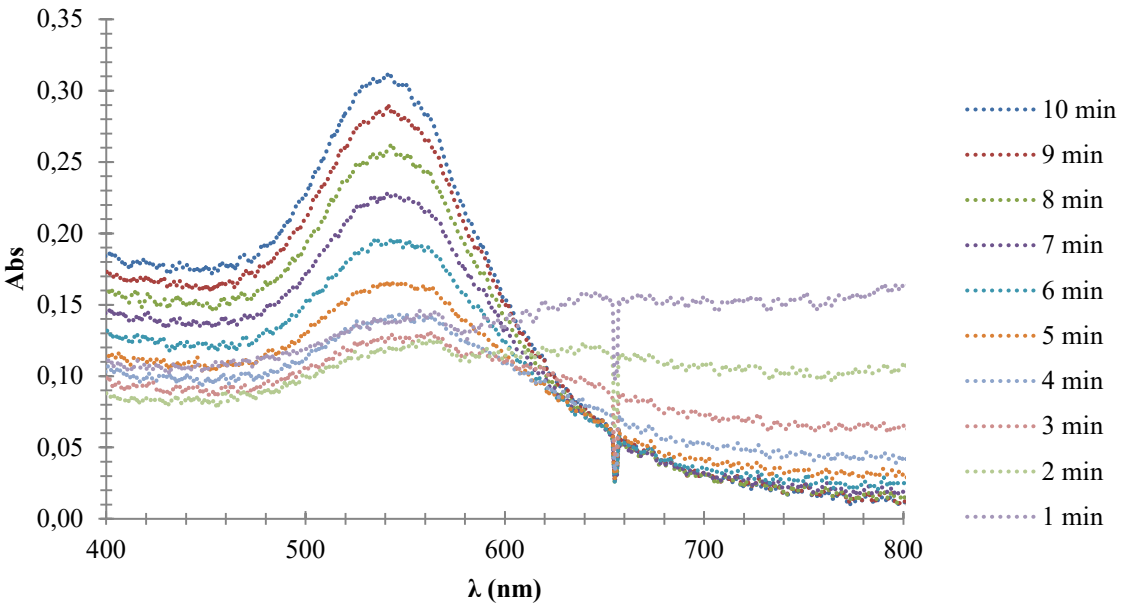

Figure S3. Localized surface plasmon resonance spectra of AuNPs under stopped-flow conditions at a DCF concentration level of 0.5 ng mL^{-1} and a total reaction time of 10 min (here recorded every 1 min) aimed at the automatic monitoring of the nucleation and growth rates of AuNP.

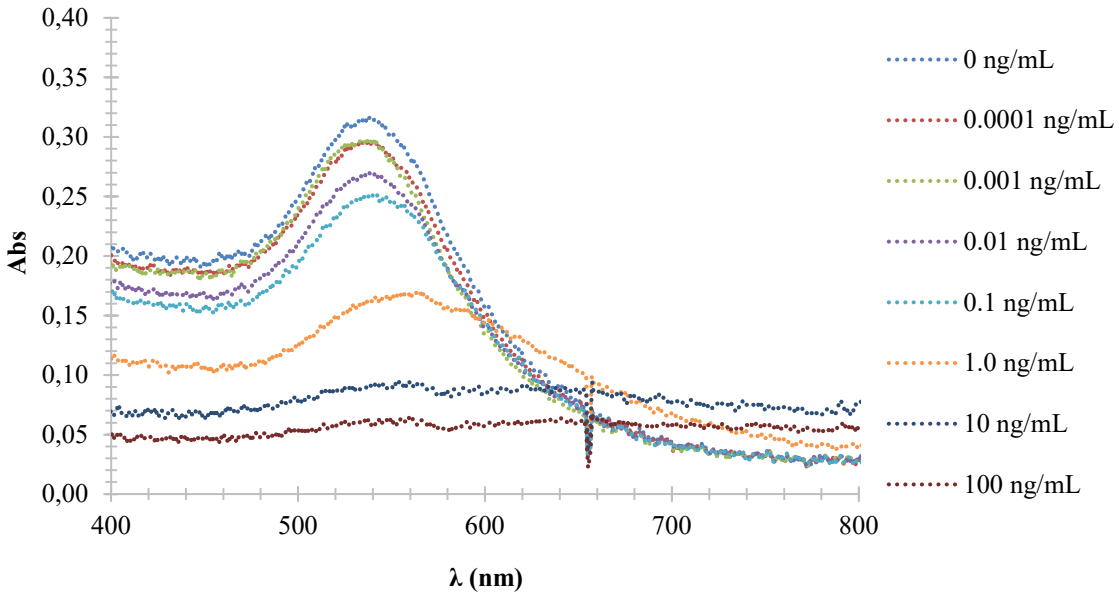

Figure S4. Localized surface plasmon resonance spectra of AuNPs under stopped-flow conditions at varied concentration levels of DCF for a total reaction time of 5.5 min.

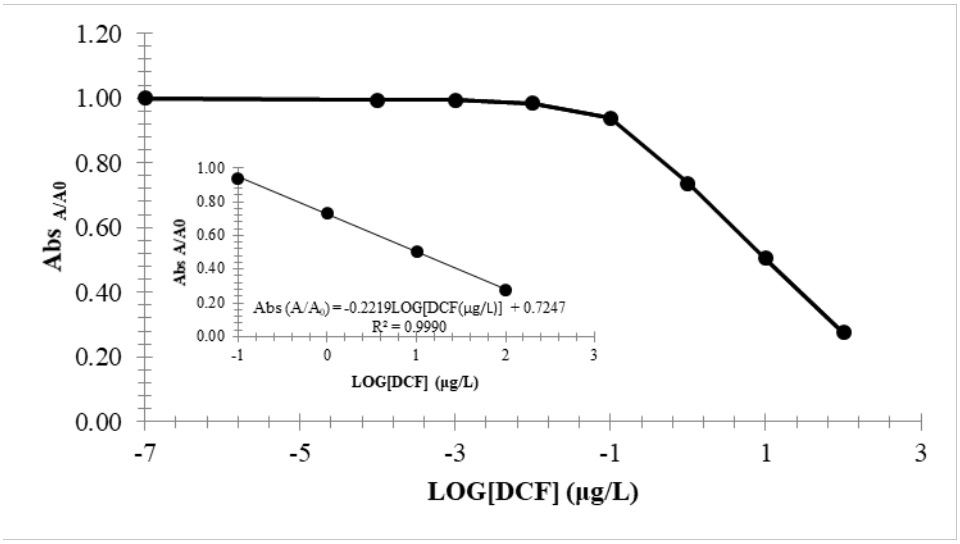

Figure S5. Linearized calibration graph of the batch plasmonic ELISA for a reaction time of 8 min. Experimental conditions: 400 ng/L mAb; 1:1000 diluted Ab_{GOx}; 400 mM glucose; 20 mM sodium citrate; 0.6 mM Au(III); and enzymatic reaction time of 60 min.

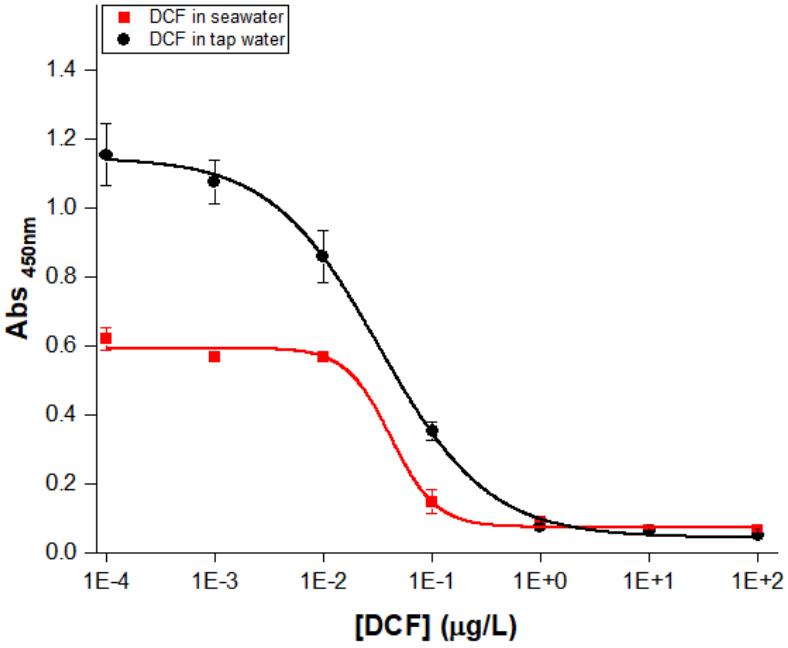

Figure S6. Dose-response curves of competitive ELISA for DCF performed on microtiter plate with tap water and seawater using an HRP-labelled secondary antibody (0.2 µg/mL in PBS; 200 µL/well) and colorimetric readout. Figures of merit: (a) tap water, IC_{50}: 39 ng/L; LOD: 8.5 ng/L; linear working range: 9 to 220 ng/L; (b) seawater, IC_{50}: 56 ng/L; LOD: 18 ng/L, linear working range: 30 to 160 ng/L. Error bar is given as SD. Note that the absorbance readouts are much lower in seawater than those of tap water as a result of matrix effects.

Table S1. Analytical performance of GC-MS and LC-MS methods for determination of DCF at trace level concentrations in seawater

Sample	Separation and detection techniques	Sample pretreatment	Dynamic range (ng L^{-1})	LOD (ng L^{-1})	RSD (%)	Ref.
Seawater	UHPLC–ESI-MS/MS	SPE (Oasis HLB cartridge)	>1.0	0.9	< 8.5	(3)
Seawater	UHPLC- QTOF-MS	Bag-SPE (XAD-2 resin)	10 – 800	4	7.2	(4)
Seawater	HPLC–QqQ-MS/MS	SPE (Chromabond HR-X cartridges)	>7.4	1.0	-	(5)
Surface and seawater	GC–Q-MS	SPE (Atlantic® HLB disks)	0.5 – 80	0.1	0.7 – 28.9	(6)
Seawater	UHPLC–QqQ-MS/MS	SPE (Strata-X cartridges)	1000 – 7500*	0.02	1.80 – 4.40	(7)
Seawater	Plasmonic ELISA combined with an automatic fluidic platform	No need of neither sorptive preconcentration/clean-up nor sample dilution	10 – 10,000	1.0	≤3.8	This work

UHPLC–MS/MS: Ultra-high performance liquid chromatography coupled to tandem mass spectrometry; GC-MS: Gas chromatography coupled to mass spectrometry; QTOF: quadrupole time-of-flight; QqQ: Triple quadrupole, * Before preconcentration

Table S2. Analytical performance of batchwise bioanalytical assays for determination of DCF in freshwaters and industrial waters

Sample	Immunoassay	Detection technique	Dynamic range (ng L^{-1})	LOD (ng L^{-1})	RSD (%)	Ref.
Lake, river and wastewater	Indirect competitive ELISA	Colorimetric (dye)	11-180	7.8	≤ 23	(8)
River water and drinking water	Direct competitive	Luminescence (Upconversion NP)	20 – 10,000	20	Up to 100	(9)
Lake, river and tap water	Indirect competitive	Luminescence (Upconversion NP)	50-1000	50	Up to 36	(10)
No real samples	Indirect competitive	Transmittance (near-surface refractive index changes)	1000-10,000	NR	ca. 6	(11)
Tap water and drinking water	Indirect competitive ELISA	Chemiluminescence	100-100,000	50	≤6.6	(12)

Table S2. (continued)

Sample	Immunoassay	Detection technique	Dynamic range (ng L^{-1})	LOD (ng L^{-1})	RSD (%)	Ref.
Tap water	Direct competitive	Voltammetry	0.025-25	0.025	Up to 46%	(13)
Lake and tap	Indirect competitive	Electrochemiluminescence	1-800,000	0.33	2.3	(14)
Lake, tap and wastewater	Indirect competitive	Electrochemiluminescence	5-100,000	1.7	≤5.5	(15)
No real sample	Genetically modified yeast	Fluorescence detection	3×10^6-15×10^6	ca. 1.5×10^6	NR	(16)
Seawater	Plasmonic ELISA combined with an automatic fluidic platform	Surface plasmon resonance of AuNP	10 – 10,000	1.0	≤3.8	This work

NP: Nanoparticle; NR: Not reported

REFERENCES

(1) Huebner, M.; Weber, E.; Niessner, R.; Boujday, S.; Knopp, D. Rapid analysis of diclofenac in freshwater and wastewater by a monoclonal antibody-based highly sensitive ELISA. *Anal. Bioanal. Chem.* **2015**, *407*, 8873-8882.

(2) De Medina, A.; Paillasse, M. R.; Segala, G.; Al Saati, T.; Boyes, J.; Delsol, G.; Allal, C.; Marsili, S.; Silvente-Poirota, S.; Poirot, M. Hapten synthesis, antibody production and development of an enzyme-linked immunosorbent assay for detection of the natural steroidal alkaloid Dendrogenin A. *Biochimie* **2013**, *95*, 482-488

(3) Wu, J.-M.; Qian, X.-Q.; Yang, Z.-G.; Zhang, L.-F. Study on the matrix effect in the determination of selected pharmaceutical residues in seawater by solid-phase extraction and ultra-high-performance liquid chromatography–electrospray ionization low-energy collision-induced dissociation tandem mass spectrometry. *J. Chromatogr. A* **2010***, 1217,* 1471-1475.

(4) Magnér, J.; Filipovic, M.; Alsberg, T. Application of a novel solid-phase-extraction sampler and ultra-performance liquid chromatography quadrupole-time-of-flight mass spectrometry for determination of pharmaceutical residues in surface sea water. *Chemosphere* **2010***, 80,* 1255-1260.

(5) Pereira, C. D. S.; Maranho, L. A.; Cortez, F. S.; Pusceddu, F. H.; Santos, A. R.; Ribeiro, D. A.; Cesar, A.; Guimarães, L.L. Occurrence of pharmaceuticals and cocaine in a Brazilian coastal zone. *Sci. Total Environ.* **2016**, *548-549*, 148-154.

(6) Česen, M.; Heath, E. Disk-based solid phase extraction for the determination of diclofenac and steroidal estrogens E1, E2 and EE2 listed in the WFD watch list by GC–MS. *Sci. Total Environ.* **2017***, 590-591*, 832-837.

(7) Paíga, P.; Lolić, A.; Hellebuyck, F.; Santos, L. H. M. L. M.; Correia, M.; Delerue-Matos, C. Development of a SPE–UHPLC–MS/MS methodology for the determination of non-steroidal anti-inflammatory and analgesic pharmaceuticals in seawater. *J. Pharm. Biomed. Anal*. **2015***, 106*, 61-70.

(8) Huebner, M.; Weber, E.; Niessner, R.; Boujday, S.; Knopp, D. Rapid analysis of diclofenac in freshwater and wastewater by a monoclonal antibody-based highly sensitive ELISA. *Anal. Bioanal. Chem.* **2015**, *407*, 8873-8882.

(9) Hlaváček, A.; Peterek, M.; Farka, Z.; Mickert, M.J.; Prechtl, L.; Knopp, D.; Gorris, H.H. Rapid single-step upconversion-linked immunosorbent assay for diclofenac. *Microchim. Acta* **2017**, *184*, 4159–4165.

(10) Hlaváček, A.; Farka, Z.; Hübner, M.; Horňáková, V.; Němeček, D.; Niessner, R.; Skládal, P.; Knopp, D.; Gorris, H.H. Competitive upconversion-linked immunosorbent assay for the sensitive detection of diclofenac. *Anal. Chem.* **2016**, *88*, 6011-6017.

(11) Steinke, N.; Döring, S.; Wuchrer, R.; Kroh, C.; Gerlach, G.; Härtling, T. Plasmonic sensor for on-site detection of diclofenac molecules. *Sens. Actuators, B: Chem.* **2019***, 288,* 594-600*.*

(12) Shi, J.; Xu, M.-X.; Tang, Q.-H.; Zhao, K.; Deng, A.; Li., J.-G. Highly sensitive determination of diclofenac based on resin beads and a novel polyclonal antibody by using flow injection chemiluminescence competitive immunoassay. *Spectrochim. Acta, A* **2018**, *191*, 1-7.

(13) Nguyen, T. T. K.; Vu, T. T.; Anquetin, G.; Tran, H. V.; Reisberg, S.; Noël, V.; Mattana, G.; Nguyen, Q. V.; Lam, T. D.; Pham, M. C.; Piro, B. Enzyme-less electrochemical displacement heterogeneous immunosensor for diclofenac detection*. Biosens. Bioelectron.* **2017**, *97*, 246-252.

(14) Wang, C.; Jiang,T.-X.; Zhao, K.; Deng, A.; Li., J.-G. A novel electrochemiluminescent immunoassay for diclofenac using conductive polymer functionalized graphene oxide as labels and gold nanorods as signal enhancers. *Talanta* **2019**, *193*, 184-191.

(15) Hu, L.-Y.; Zheng, J.; Zhao, K.; Deng, A.; Li., J.-G. An ultrasensitive electrochemiluminescent immunosensor based on graphene oxide coupled graphite-like carbon nitride and multiwalled carbon nanotubes-gold for the detection of diclofenac. *Biosens. Bioelectron.* **2018**, *101*, 260-267.

(16) Schirmer, C.; Posseckardt, J.; Schroder,M.; Glaser,M.; Howitz,S.; Scharff,W.; Mertig, M. Portable and low-cost biosensor towards on-site detection of diclofenac in wastewater. *Talanta* **2019**, *203*, 242-247.

Universitat
de les Illes Balears